INVESTIGATION OF KNUDSEN AND GAS-ATMOSPHERE EFFECTS ON EFFECTIVE THERMAL CONDUCTIVITY OF POROUS MEDIA

To the Faculty of Mechanical, Process and Energy Engineering
of the
Technische Universität Bergakademie Freiberg
approved

THESIS

to attain the academic degree of

Doktor–Ingenieur

Dr.–Ing.

Submitted

by **Dipl.-Ing. Khaled Raed**

born on the 24.07.1979 in Nabk

Reviewers: **Prof. Dr.-Ing. Ulrich Gross**
Editor in Chief, International Journal of Thermal Sciences (Elsevier Ltd.)
Institute of Thermal Engineering
Technische Universität Bergakademie Freiberg
Freiberg, Germany

Dr. Ulf Hammerschmidt
Member of ''Board of Governors'' of Int. Thermal Conductivity Conference
Special-Field Heat Transfer, Department Mechanics and Acoustic
Physikalisch-Technische Bundesanstalt
Braunschweig, Germany

Date of the award: June 7, 2013

PREFACE

Declaration

I hereby declare that I completed this work without any improper help from a third party and without using any aids other than those cited. All ideas derived directly or indirectly from other sources are identified as such.

In the selection and in the use of materials and in the writing of the manuscript I received support from the following persons:

Prof. Dr.-Ing. Ulrich Gross, (selection and evaluation of the materials)
Dr. Dave McElroy, (correcting the English writing)

Persons other than those above did not contribute to the writing of this thesis. I did not seek the help of a professional doctorate-consultant. Only persons identified as having done so received any financial payment from me for any work done for me.

This thesis has not previously been submitted to another examination authority in the same or similar form in Germany or abroad.

ACKNOWLEDGMENT

This thesis could not have been produced without the financial and technical support of the Deutsche Forshungsgemeinschaft (DFG) and the Institute of Thermal Engineering within the Faculty of Mechanical, Process and Energy Engineering at the ‘‘Techniche Universität Bergakademie Freiberg’’ in Germany.

I could not success to achieve the present work without the cumulated efforts of many people, who contributed to the successful completion of this work. Therefore, I would like to express my appreciation to everyone who contributes in any way towards the completion of my thesis.

To start, I would like to express my sincere gratitude to my supervisor Prof. Dr. Eng. Ulrich Gross, who gave me the chance to work in his department and to be a part of his research team. His valuable guidance, continuous support, and the freedom he gave me in the research helped to complete this work. Many thanks for his confidence and valuable discussions, which arisen in me the motivation to look from ‘‘different angle’’, to plan new experiments and to do extra research, which led finally to interesting research outcomes.

I am gratefully indebted to my second supervisor Dr. Ulf Hammerschmidt, who I met back in 2005 for the first time in Saint John, New Brunswick in Canada, where we had our first short discussion. Since that time, I had many inspiring discussions with him. I am so grateful for his willingness to become my supervisor. Thanks for his encouragements in the final phase of my thesis.

A special thank goes to my friend Dr. Dave McElroy in Tennessee, USA. I am very much grateful to his continuous support and valuable long-distance engorgements as well as the interesting discussions. Without his guidance, involvement, support, and help in correcting the writings, the compilation of this work would’ve been coupled with more difficulties. I will not forget the combined response of him and Hans Groot to my question ‘‘how to complete my thesis while I do research?’’, the answer was ‘‘GIVE UP SLEEPING AND WRITE!’’.

All experiments on characterization of the porous structure were performed at the department of Ceramic, Glass, and Construction Materials, in TU Freiberg. Therefore I would like to thank Prof. Dr. Eng. Christos G. Aneziris for his support in performance of the numerous experiments in his lab. A special thank for Mrs. Jana Hubálková for her valuable discussions about the experimental methods and the porous structure.

I would like to thank all my colleagues in our group ‘‘Thermodynamics and Heat transfer’’ for their support and encouragement to successfully complete this work, especially my colleagues Mr. Gerald Barth, Dr. Eng. Rhena Wulf. Many thanks to Rhena for her support and collaboration in the final phase of my thesis. A grateful thank for the main vein of our labs Mr. Andreas Wahl, Mr. Gerd Mardaus and Mrs. Almut Hegewald, I am really grateful for their technical support in performing the experiments and also having the patience in realizing my ideas in the experimental works.

Many thanks go to all my friends, especially to my friend Mr. Husam Wafai, he was a great help in correcting the English writings. Many thanks go to my best friend Ziad Mohieddin in USA for his support and long-distance interest. I would also like to thank Mrs. Hannelore Dombois, she was always a great help in giving me many advises in life.

My endless thank, love, and respect goes to my parents. I owe them a lot for their love, support, and long-distance encouragement. Without their belief in me, and without their prayers, I could not have achieved this work successfully. I am grateful to my siblings for their continuous support. At last, but not least, the upmost respect and appreciation goes to my lovely family (Natalie and Yasmin). Without the understanding and the great love of my wife Natalie, this work could not be completed. My sincere apology to my daughter Yasmin for being busy the last two years working on my thesis and research, and not spending much time with her. Thank you for your love.

March 2013, Freiberg, Germany
Khaled Raed

''*A thinker sees his own actions as experiments and questions-as attempts to find out something. Success and failure are for him answers above all*''

Friedrich Nietzsche (1844- 1900)

''*The seeker after the truth is not one who studies the writings of the ancients and, following his natural disposition, puts his trust in them, but rather the one who suspects his faith in them and questions what he gathers from them, the one who submits to argument and evidence, and not to the sayings of a human being whose nature is fraught with all kinds of imperfection and deficiency.*

Thus the duty of the man, who investigates the writings of scientists, if learning the truth is his goal, is to doubt all that he reads, and, applying his complete mind to analysis it from every side. He should also suspect the results of his study, so that he may avoid falling into either prejudice or impreciseness''

Alhazan Ibn al-Haytham (965- 1040)

TABLE OF CONTENTS

PART II: EXPERIMENTAL INVESTIGATIONS

PART IV: CONCLUSION

PART I: INTRODUCTION AND THEORETICAL BACKGROUND

1 General Introduction

1.1 Background

It is well known that fossil sources of energy are limited. In the recent years, this fact, in addition to the considerable permanent increase in the cost of fossil energy, gave policy makers and researchers the motivation to be more concerned about solving this problem. The solution lies in transforming our energy system, in Germany known as ''Energiewende''.

Germany's Energiewende (energy transformation) is a plan to transform the use of nuclear and fossil fuels to renewable energies. It started in the 1980s, became policy in 2000 and sped up after the Fukushima disaster in March 2011 (The Economist, 2012). Changing the energy use mix in Germany is a complicated process. More effective use of energy is a part of this planned transformation. Demonstration, Research and Development by the thermal insulation materials technical community in industrial, commercial, and residential applications is integral to this savings.

Heat transfer through high porosity insulation materials is a complicated process. This study is based on obtaining careful measurement and characterization of the thermo-physical properties of such materials. The intent is to create a basis for understanding and comparing the behavior of these materials, and to offer guidance to developing better thermal insulations.

1.2 Objectives and Scope of Research

The goal of this study is to find out and understand how the effective thermal conductivity of porous insulation materials will change, in relation to the characterized pore size distribution, when an exchange of the filling gas is made.

Industrial application of thermal insulation materials in furnaces and other high-temperature facilities with various gas atmospheres requires knowledge of the insulation thermal conductivity and it would be valuable to find formulations for prediction of the change in effective thermal conductivity due to exchanging the gas atmosphere. Heat transfer through such highly porous insulation materials is governed by the coupled processes of conduction through a solid matrix and a filling gas, and also through radiation. This implies that exchanging the gas atmosphere in the facility causes a change in the filling gas properties and consequently a change in the effective thermal conductivity of the porous material. On the other hand, the behavior of the filling gas is related to the characterized porous structure of the insulation material, this is known as Knudsen effect (Knudsen, 1911).

The objectives of this study are focused on studying and analyzing the combined influences of Knudsen and filling gas effects upon the effective thermal conductivity of porous insulation materials. Two kinds of investigations are performed to achieve these objectives: The first is experimental work with the available facilities at Institute for Thermal Engineering, TU Freiberg, in order to measure effective thermal conductivity of the

investigated materials under various gas atmospheres. The second is physical-mathematical modeling to predict the effect of the filling gas on the thermal conductivity of the porous materials based on the knowledge about the behavior of the filling gas in the porous structure of materials.

The experimental work is the major part of this study. Twelve different thermal insulations commercially available in Germany were chosen for this study. All of these materials are typical insulation materials that are used in high temperature facilities and all have different porous structures. The choosing criterion was the type of pore size distribution. Therefore, these materials belong to a wide range within the classes of insulation materials, from light fire-resistant bricks till super-insulators with very low thermal conductivity. Thus, they are different in porous structure, in thermal properties, and in chemical composition. The various porous structure control parameters: porosity, bulk density, and pore size distributions were experimentally determined for all investigated materials.

The effective thermal conductivity of all investigated materials in different gas atmospheres (krypton, argon, nitrogen and helium) are mainly measured using a radial heat flowmeter apparatus (RHFA) after implementing many improvements on the experimental facility. The improvements were required to ensure accurate measurement of thermal conductivity of the various investigated materials. In some cases, numerical modeling of the apparatus is additionally implemented to estimate some effects that produce various errors in the measurements. Evaluation of the effective thermal conductivity was limited for most materials in the temperature range between 300 °C and 700 °C. Validation of the results of thermal conductivity measurements performed in the radial heat flowmeter apparatus under nitrogen atmosphere is accomplished through comparative measurements of the same materials performed in the panel test facility (PTF) in air atmosphere.

By observing the results of effective thermal conductivity, many effects were analyzed and discussed. Some new effects were detected such as the coupling between radiation and Knudsen conduction. Confirming these effects was done through performing measurements of thermal diffusivity of the investigated materials using the laser flash method (LFM) in vacuum as well as in different gas atmospheres (argon, nitrogen and helium). However, applying the Laser Flash Method to porous materials was faced with many difficulties, e.g. transparency of materials to the laser beam. Self-developed series of experiments were implemented to overcome these difficulties. These experiments were focused on solving the problems by finding the appropriate surface coating. Thermal diffusivity is evaluated successfully for only four representative materials among all investigated materials after applying the appropriate surface coating.

Different models were tested in the light of Knudsen effect in order to predict the effect of the filling gas on the effective thermal conductivity of all investigated materials over a certain temperature range. A new improved model, which considers different physical effects, is introduced in this study based on the kinetic theory. Validation of the new improved model is done through applying it to the investigated materials and directly comparing with experimental results taking into account the uncertainty of the measurements

1.3 Outlines of this Thesis

The accomplished work in this study includes various sections in experiments as well as in modeling. Therefore, this thesis is structured in four parts for a better representation of the research study. Figure 1 shows a flowchart of the structure of this study. Each part includes the relevant chapters, as follows:

- Part I : Introduction and Theoretical Background (Chapter 1- 3)
- Part II: Experimental Investigations (Chapters 4-7)
- Part III: Analysis and Modeling (Chapters 8-9)
- Part IV: Conclusion (Chapter 10)

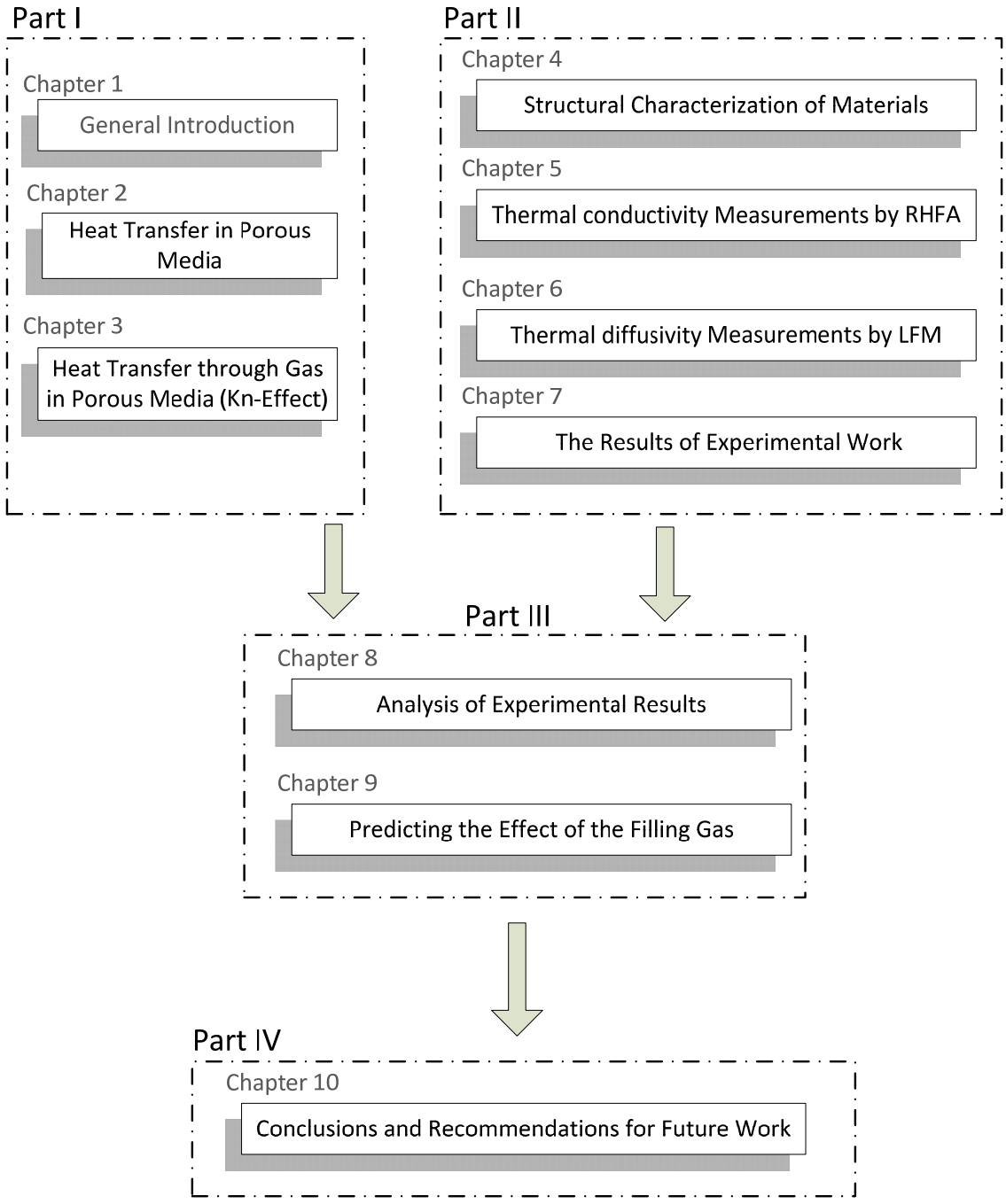

Figure 1: Flowchart of this thesis

In the first part of this thesis, the theoretical background of this study is explained with regard to heat transfer in porous media, see Chapter 2. A comprehensive description of Knudsen effect and new classification of models for evaluating gas thermal conductivity are presented in Chapter 3.

The second part describes the entire experimental work that is performed in the scope of this study. In this part, the applied experimental facilities and techniques are presented. A critical study about the principles and the evaluation models of these facilities is included in this part. It contains also the accomplished improvements on the experimental facilities in order to apply them to the investigated porous materials. Finally, the results of the entire experimental work are presented in the last chapter of this part, see Chapter 7.

The third part of this thesis contains the analysis and interpretation of the experiential results regarding different physical effects. The coupling factors between these effects are obviously detected and explained in this part, see Chapter 8. The results of testing the different models from literature and the new improved model are presented in Chapter 9. In this chapter, many comparisons are made between the calculated data and experimental results of effective thermal conductivity.

In the last part, i.e. Part IV, the conclusions of this study are presented. In addition to conclusions, the limitations of the applied methodology as well as many recommendations for further research in this area are presented in the last part of this thesis.

1.4 Copyrights and Notices regarding the Written Form of Thesis:

The included figures in this study, as long as without any citation, are done by the author with the consideration to be as accurate as possible. Thus, the author maintains the copyright of these figures, and any use or further publishing of these figures requires asking the author for permission before publishing. The recommendations for future work include new ideas, and the author of this thesis expects the courtesy of mentioning his name in case of applying any of these ideas.

2 Heat transfer in porous insulation materials

In general the insulation materials are classified into three categories: the first category is the reflective insulation, which are usually used in form of foils, to minimize the radiative heat flux. The second category is the evacuated form of insulation in which the evacuated gap plays a kind of insulation. A very common example here is the thermos Dewar bottle. The third category is the porous insulation materials (aka[1] porous media). Commonly used insulation materials (powders, fibers, aerogels, foams, and ceramics) have porous structure. They are classified as two-phase materials (gas-solid) and occasionally as three-phase materials (gas-solid-liquid) when they contain condensed vapors. The heat transfer phenomenon in such heterogeneous media is complex. This phenomenon has been the main focus for numerous of experimental and theoretical studies. In this chapter the basic principles of the heat transfer in porous media and the various factors which influence the heat transfer mechanisms will be explained.

2.1 Effective Thermal Conductivity

The French mathematician and physicist J. Fourier introduced in 1807 the first relation between heat flux and temperature difference based on experimental results (Wang, et al., 2008). The Fourier's Law defines the ***heat conduction*** in homogeneous and isotropic medium as:

$$\vec{q} = -\lambda \nabla T \tag{1}$$

The proportionality factor λ characterizes the medium and is known as the thermal conductivity. Heat transfer in porous insulation materials occurs mainly through coupled conduction in solid matrix and filler gas, as well as through radiation, and occasionally attended through convection (see Figure 2). The proportionality factor in Fourier's Law which describes the total ***heat transport*** in porous media will be called the effective thermal conductivity (aka apparent thermal conductivity). This could be written as a function of the different thermal conductivities:

$$\lambda_{eff} = f(\lambda_s, \lambda_{gas}, \lambda_{conv}, \lambda_{rad}) \tag{2}$$

Estimation of the effective thermal conductivity was the aim of numerous studies in literature. In most of them the conduction heat transfer in the two phases (gas and solid) was firstly evaluated based on geometry thermal resistance model and then radiation was added, e.g. for fibrous materials (Verschoor, et al., 1952b) for porous materials (Kamiuto, et al., 1984; Rath, et al., 1990). Many studies were done to compare the different models (Gorring and Chruchill, 1961; Lal Chaurasia, et al., 1978; Tsotsas and Martin, 1987b). The discrepancy between estimated and experimental data is due to the random distribution of phases, nonhomogeniety, anisotropic/directional properties and non-uniform shape of particles in real material, whereas the models are developed for idealized structure. Some correction factors were introduced later to the resistance model (Wonchala and Wynnyckyj,

[1] aka: also known as

1984; Singh, 2003; Fricke, et al., 2006). Other researchers investigated the interaction between conduction and radiation to estimate the effective thermal conductivity (Heinemann and Caps, 1996; Lee and Cunnington, 2000). A simple model for contributions acting in parallel is written as:

$$\lambda_{eff} = \lambda_s + \lambda_{gas} + \lambda_{rad} \tag{3}$$

where λ_s is the heat conduction of the solid matrix (i.e. it contains the geometric specification e.g. the porosity, as seen later in this chapter, see eq. (4) in section 2.2). The model by eq. (3) was applied to estimate the effective thermal conductivity of various porous insulation materials, (Woodside and Messmer, 1961; Zeng, et al., 1995a; Caps and Fricke, 2000a; Lee, et al., 2002). More about the effective thermal conductivity models will be discussed in chapter (9).

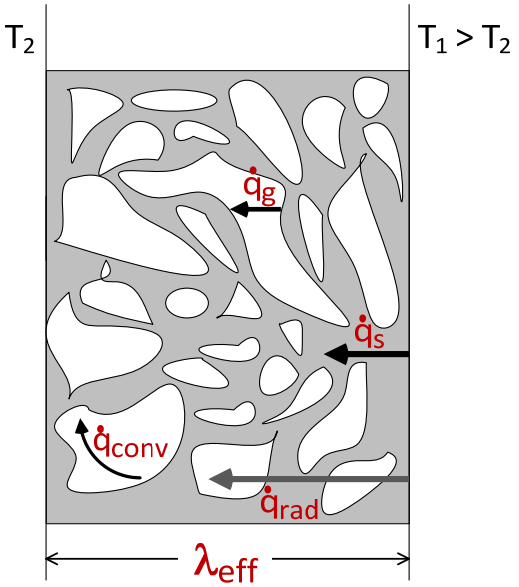

Figure 2: A rendering of the heat transfer mechanisms in porous media

In the following subsections each heat transfer mechanism will be presented and its dependency on the various parameters will be discussed.

2.2 Heat Transfer by Conduction

Heat conduction through porous media occurs as energy diffusion process specified in the solid skeleton (matrix) and in the gas residing within the pores (see q_s and q_g in Figure 2). The molecules in the gas filling the pores are energy carriers and transfer the heat in pores by collision with the solid surface inside the pores and by collision with each other. This will be described explicitly in the next chapter 3. Heat conduction in solids on the microscopic scale is primarily due to two energy transfer contributions: the lattice vibration and the translation motion of free electrons. In electrically conductive materials like metals, the free electron heat conduction mechanism dominates, whereas in non-metallic solid, such as silica or polymer, the lattice vibration mechanism dominates. However, heat conduction by lattice

vibration is very low comparing to heat conduction by free electron motion. Consequently, non-metallic or dielectric materials with low bulk thermal conductivity are usually chosen among solids to provide insulation (Tseng, et al., 1997). The specific properties of the solid that forms the matrix in the insulation material determine the heat conduction by the solid on a macroscopic scale. According to the kind of contact between the solid units, there are two types of solid matrices: matrix with loose particles (nonconsolidated) like fibrous materials, powders, and granulates, other matrix with bonded particles (consolidated) like ceramic, aerogel, and foam. The heat transfer by the solid phase in porous media depends on:

- Bulk Thermal conductivity of the solid material (Loeb, 1954)
- Solid volume fraction (porosity) (Bala, et al., 1990)
- Contact resistance between the nonconsolidated particles (Moore, et al., 1982)
- The extent of the continuity of the solid phase (Kaviany, 1995).

The distribution of the solid phase, e.g. in foams, is homogenous and well continuous, whereas in fibrous material with anisotropic distribution of fibers yields non-continuous solid phase in respect to the heat flux direction. This led to difficulties by the mathematical modeling the thermal conductivity of the solid phase for such porous media. A great amount of work has been done to estimate the heat transfer by conduction in porous media and resulted in a variety of different models. The concept of the developed models is to find out the distribution rate between the solid and gas phases, which is arranged in series, parallel or both. The existing models can be classified into two categories according to the concept of the constitutive model: the first category contains models that are based on estimating the collective heat conduction in the two phases (gas-solid) from one cell or one pore unit, (e.g. Wakao and Vortmeyer, 1971; Ogniewicz and Yovanovich, 1977; Litovsky and Shapiro, 1992b; Doermann and Sacadura, 1996). The second category contains models that deal separately with estimating the heat conduction in each phase, i.e. models for estimating the thermal conductivity of the filling gas (will be presented in details in chapter 3), and models for estimating the thermal conductivity of the solid matrix depend on physical properties (bulk thermal conductivity of the solid material) and geometric specifications of the porous material. Geometric specifications vary with the kind of the insulation material as follows:

- Fibrous materials: fiber size, fiber orientation and fibers volume fraction (Stark and Fricke, 1993; Lee and Cunnington, 2000)
- Aerogel: density of aerogel (Fricke, et al., 1992)
- Foam: foam porosity and geometry of the foam cell wall (Placido, et al., 2005)
- Porous ceramic materials: the microcrack thickness and the distance between the microcracks (Litovsky, et al., 2001)

In general estimating the thermal conductivity of the solid matrix describes as follows:

$$\lambda_s = f\left(\lambda_{bulk\ solid}, \psi, \chi_{cont}, \chi_{geo}\right) \tag{4}$$

where χ_{cont}, χ_{geo} are coefficients that depended on the contact resistance and the specified geometry of the insulation materials, respectively.

2.3 Heat Transfer by Convection:

Heat transfer by convection occurs in the gas in the pores due to two combined mechanisms: molecular diffusion and macroscopic gas motion. The porous structure of insulation materials partitions the gas into small units and thereby hinders a large scale motion of the gaseous phase, so the heat transfer by convection could be neglected. This has been confirmed by Skochdopole (Skochdopole, 1961), where he obtained that convection occurs in gaps bigger than 4 mm. Litovsky et al. (1996) accomplished a study on non-metallic insulation with Porosity exceeding 30%. They used the following equations to evaluate the heat transfer by convection:

$$\begin{aligned} &\lambda_{conv} = \lambda_0(Nu - 1) \\ &Nu \ \propto Ra \\ &Ra \ \propto Gr \,\mathrm{Pr}\, Da \\ &Da \ \propto Permeability \end{aligned} \tag{5}$$

Even though the gas permeability of porous ceramic increases with higher porosity, they concluded that no convection influence in such materials can be observed for atmospheric pressures lower than 30 MPa. An experimental study was done by Daryabeigi (Daryabeigi, 2003) to measured the thermal conductivity of highly porous fibrous insulation materials by changing the heat flux direction regarding to gravity force. This implies that steady state measurements were done with heat source located sometimes below the sample, another time above. The results of the thermal conductivity of the two kinds of measurements show good agreement within uncertainty of 7.5 %. All those mentioned above studies and others adduce that the contribution of convection to the total heat transfer in porous insulation materials is small enough to be neglected. However, all those studies are valid for insulation with covered top.

If the insulation materials have low density and open-cell porous structure and the heat flow crosses from the bottom face to the top face, the heat transfer by natural convection contributes possibly in the overall heat transfer rate. That was proofed by Fournier and Klarsfeld (Fournier and Klarsfeld, 1974). They measured the thermal conductivity and air flow permeability of many samples of glass fiber with different densities. They introduce a critical density for each given thickness and cold face temperature. For the materials which have density greater than the critical density (which is based on the Rayleigh number) the heat transfer by natural convection could be neglected. Developing the convection theory in porous media shows that it depends upon the thermal and mechanical boundary condition of the insulation (Graves, et al., 1993). Further experimental investigation was done on loose-fill fiber glass insulation under winter conditions in ORNL (Oak ridge National laboratory) with ‘‘open-top’’ like in attic insulation (Graves, et al., 1993; Wilkes, et al., 1993). The results show that the thermal resistance of the sample with open top decreases up to 30 % at same mean temperature compared with covered one by increasing the temperature difference across the sample over 60 °F. That was attributed to the initial natural convection. The result was later taken into consideration and included by ASTM (American Standard for Testing and Materials) in practical use to characterize material for building under simulated winter conditions (ASTM, 2009).

2.4 Heat Transfer by Radiation

Heat transfer by radiation occurs by electromagnetic waves (photons). Stefan-Boltzmann's law by eq. (6) shows that the total hemispherical emissive power (thermal radiation) of a body (black or gray) radiating into vacuum at a defined temperature is increased by the power of four of the absolute temperature (Siegel and Howell, 1992):

$$e = \sigma . \mathrm{T}^4 \tag{6}$$

Energy transfer by radiation in porous media is complicated. Porous media can absorb, emit and scatter the spectral radiation. Absorbing the radiation increases the internal energy of the medium. The absorption coefficient weighs the ability of the medium to absorb the thermal radiation. Scattering occurs by collision between photons and the solid particles, which leads the photons to change their direction and lose or gain energy. This could be expressed mathematically as scattering coefficient, which is the inverse of the mean free path of photons before undergoing scattering. Independent Scattering applies when the distance between the particles is large enough that radiation of each solid particle is not affected by neighboring particle. Scattering is considered isotropic when it is equal in every direction (Siegel and Howell, 1992). However, scattering in the case of insulation materials is usually direction dependent and thus anisotropic. Scattering can be evaluated by solving the Maxwell electromagnetic equation of the radiation field. The solution is based on one particle radiation model (sphere). There are many solutions in literature which vary with respect to the size parameter, which is the ratio of particle size (e.g. the diameter in case of spherical particles) to wavelength. There are several kinds of scattering solutions such as Mie Scattering, Rayleigh scattering and others. The Mie theory is applicable for a wide range of size parameter (Kaviany, 1995).

The sum of the absorption and scattering is called *extinction*. Bouguer-Lambert's Law (aka Beer's Law) shows that the intensity of spectral radiation attenuates exponentially while it passes an absorbing-scattering medium (Siegel and Howell, 1992):

$$\mathrm{I}_\Lambda(\mathrm{S}) = \mathrm{I}_\Lambda(0) . \mathrm{e}^{-\kappa_\Lambda(\mathrm{S})} \tag{7}$$

The exponent $\kappa_\Lambda(\mathrm{S})$ is equal to the integral of local extinction coefficient over the penetration length. This exponent is called the *optical thickness* or the opacity of the material. The optical thickness depends directly on the extinction properties and the thickness of material. Optical thickness has been also defined as the ratio of material thickness to the mean free path of photons. An *optically thick porous media* is one with a thickness that is large relative to the mean free path of the photon.

By considering radiation transfer as a local process, the heat transfer through radiation in optically thick porous media with isotropic scattering could be estimated by using the Rosseland diffusion equation (Siegel and Howell, 1992):

$$\dot{q}_{rad} = -\frac{16}{3a_R(\Lambda)}\sigma\, T^3 \frac{\partial T}{\partial Z} \tag{8}$$

Rosseland mean extinction coefficient $a_R(\Lambda)$, also called effective/specific extinction coefficient (Stark and Fricke, 1993) can be calculated from extinction coefficient and the spectral distribution of the emissive power (Siegel and Howell, 1992).

$$\frac{1}{a_R(\Lambda)} = \int_0^\infty \frac{1}{E_\Lambda}\frac{\partial e_{b\Lambda}}{\partial e_b} \tag{9}$$

For anisotropic scattering or extinction, the real extinction coefficient E_Λ in Rosseland equation will be substituted by weighted extinction coefficient E_Λ^* (Placido, et al., 2005).

By comparing the Rosseland equation by eq. (8) with Fourier's law by eq. (1), aka ''quasi radiation thermal conductivity'' λ_{rad} can be concluded:

$$\lambda_{rad} = \frac{16}{3a_R(\Lambda)}\sigma\, T^3 \tag{10}$$

Many studies in literature deal with porous media as continuum and use Rosseland diffusion equation to calculate the radiative component of heat transfer. Evaluation of the Rosseland mean extinction coefficient for aerogel was done by (Tseng, et al., 1997; Wu, et al., 1999) through Infra red optical measurement by using Fourier Transform Infra Red (FTIR) spectrometer. This has been obtained by using an integrating sphere to collate the transmission and reflection spectra (Linford, et al., 1974; Stark and Fricke, 1993). The radiative thermal conductivity is proportional to temperature to the power of three. The extinction properties of porous material could be determined by the measurement of the overall thermal conductivity in evacuated atmosphere and plotting it versus temperature to the power of three. The slope of the line compared with the eq. (10) gives the effective extinction coefficient (Fricke and Caps, 1988; Fricke, et al., 1991).

The above mentioned methods to evaluate quasi radiative thermal conductivity are based on Fourier's law. The thermal conductivity according to Fourier is independent of the sample thickness. However, the thickness of the sample is an important parameter in the radiative heat transfer. Since the heat transfer through porous media is not pure conduction, the sample thickness affects the overall heat transfer. The dependency of effective thermal conductivity of low density materials on the specimen thickness was discussed by Shirtliffe (Shirtliffe, 1980). He developed a three layer model as function of density and thickness. Hamaker (Hamaker, 1947) developed a two-flux model representing the radiation flux through the material:

$$\dot{q}_{rad} = \frac{8\sigma T^3}{E_\Lambda}\frac{dT}{dZ} + \frac{1}{A_{abs}E_\Lambda}\frac{d^2q}{dZ^2} - \frac{1}{A_{abs}^2E_\Lambda}\frac{dA_{abs}}{dZ}\frac{dq}{dZ} \tag{11}$$

The Hamaker's model differs from Fourier's Law. Both could be identical when the (A_{abs}) absorption cross-section and the first derivation of radiative flux (dq/dz) are constant. Stephenson (Stephenson, 2010) evaluated the Hamaker's model for fibrous material through

the iterative method and compared to Fourier's law. Hamaker's model gives accurate temperature gradient over the sample and reflects the edge effect.

Other researchers developed models of radiation heat transfer for the assessment of scattering/extinction behavior of one particle by using the diffraction theory, see e.g. for foam (Doermann and Sacadura, 1996) and for fiber (Marschall and Milos, 1997). In porous media with small pore size (e.g. Aerogel) comparing to wavelength the extinction consists merely of absorption (Fine, et al., 1980; Scheuerpflug, et al., 1991; Heinemann and Caps, 1996). Neglecting the inner scattering the absorption could be easily evaluated by measuring the FTIR-Spectrum with and without sample and applying the Bouguer-Lambert's Law (Syed, et al., 2008).

The heat transfer through radiation in porous media is affected by different parameter:

- Optical properties or opacity of solid material. Adding opacifier powder, such as carbon black, will increases the extinction coefficient strongly and thus decrease the radiative conductivity (Lee, et al., 1995; Zeng, et al., 1995b)
- Density/porosity. Increasing the density, such as increasing the solid portion of the media, will increase the absorption of radiation and reduce the penetration through porous medium, which will decrease the radiative conductivity (Lu, et al., 1995)
- Pore size. Decreasing the pore size, such as control the producing process to get small pore size as in producing aerogel or foam, the radiative conductivity will be decreased (Glicksman, 1994; Smith, et al., 1998)

2.5 Summary of Chapter 2:

As shown the heat transfer in porous media is governed by the contributions of conduction in solid and gas in addition to the contribution of radiation. There are many parameters, which affect each of these contributions. Analysis and study all these effects is combined with huge efforts. However, the center of the objectives of this study is the effect of the filling gas. Therefore, more theoretical background and various evaluation models for the heat conduction in gas will be presented in the following chapter.

3 Heat Conduction through Gas in Porous Media

The gas phase occupies a large part of insulation materials, which usually have more than 70 % porosity. Studying heat conduction through the filler gas is crucial to understanding and evaluating the overall heat transfer in porous media. In this chapter some theories and models are reviewed to understand the gas behavior and its role in heat flow in the porous structure.

3.1 Kinetic Theory of Gases

Gas kinetic theory is a very common theory that has its historical roots in ancient Greece. Gombosi noted it was applied by many scientists to explain and predict macroscopic properties, such as transport coefficients (viscosity, diffusion coefficient, thermal conductivity) in terms of the microscopic properties of the constituents (molecular properties). The Kinetic theory is based on the concept that each state of matter (solid, liquid and gas) is composed of finite particles which are continuously in motion. These particles are called molecules and their exact paths and velocities are difficult to describe; Gas kinetic theory deals with statistical results for estimating the molecular properties of gas. One of these results is Maxwell-Boltzmann distribution function which describes the probable velocities for the molecules of **still** gas (stagnant, non-flowing). Kennard (1938) showed the mean speed of molecules could be obtained based on the distribution function,

$$\bar{v} = 2\left(\frac{2kT}{\pi m_g}\right)^{1/2} \tag{12}$$

During its motion, each molecule undergoes many collisions with others molecules. From eq. (12) it could be seen that the mean velocity of molecules increase with the square root of temperature divided by mass. This relation determines the dependency of the bulk gas thermal conductivity on the temperature, as we will see later. Clausius has introduced the ‘‘mean free path’’, which is the average distance traveled by a molecule between two successive collisions. Considering the molecules as hard elastic spheres, the collision between two molecules could be mathematically described by determining the collision cross section (Kennard, 1938):

$$\Gamma = \pi d_m^2 \tag{13}$$

For an ideal gas with *n* molecules which have the same mean speed $\bar{v}$, the mean free path is evaluated as follows (Kennard, 1938):

$$\Lambda = \frac{1}{\sqrt{2} n \Gamma} = \frac{kT}{\sqrt{2}\pi d_m^2\, p} \tag{14}$$

The kinetic theory basically treats the heat transfer through conduction in a gas as a molecular phenomenon, where the kinetic energy is being transferred from a layer of molecules with higher energy to molecules with lower energy in another layer by intermolecular collisions with the motion of the molecules along the mean free path. The

kinetic theory provides a general physical model (e.g. Eucken's equation) for the conduction in gas, which is widely and effectively used to estimate the gas thermal conductivity. However, there are two critical factors limiting the validity of this model: (a) according to this model the gas thermal conductivity is independent of the gas pressure; (b) there are no considerations of the surrounding conditions (e.g. dimensions of the enclosure, surface-quality of the enclosure, etc.).

3.2 Knudsen Effect

3.2.1 Comprehension of Knudsen Effect

The gas at atmospheric pressure and room temperature that situated in a container, whose dimensions are much, much larger than the mean free path, has a bulk value of the gas thermal conductivity, which is described well through the above mentioned kinetic theory. Under these conditions the molecules interact with each other much more than with the walls of the container. If the gas pressure is low, or the gas is situated in certain geometry being relatively small in comparison with the mean free path of the gas, then we have the gas in the low density state (rarefied gas). In this state, from molecular aspect, the collisions between gas molecules and the container walls become more dominant than intermolecular collisions. In the end of the 19th century and the beginning of the 20th century, it was a challenge to find a theory for heat transfer in such rarefied gases (Smoluchowski, 1898; Knudsen, 1911; Smoluchowski, 1911b; Knudsen, 1934).

Knudsen (1911), by using the fundamental work of former researchers, founded a theory of heat transfer in rarefied gases by introducing and determining a very important parameter: the ‘‘accommodation coefficient’’, which describes the efficiency of energy transfer between gas molecules and the surface.

In the same year, Smoluchowski (1911) developed the so-called ‘‘temperature jump theory’’ by introducing a temperature slip near the wall for heat conduction in low density gases. Experiments by Knudsen (1911) on heat conduction by gas between parallel plates, separated by the distance L and made from various metals, were evaluated by the ratio of L to the mean free path:

$$\mathrm{Kn} = \frac{\Lambda}{\mathrm{L}} = \frac{kT}{\sqrt{2}\pi d_m^2 P\ \mathrm{L}} \tag{15}$$

This ratio became very common and later it came to be related to his name as the Knudsen number. The Kn defines the degree of rarefaction of a gas and shows the limit of the range where a gas behaves as a continuum characterized by the molecular interactions (Schaaf and Chambre, 1956; Springer, 1971). The gas as continuum fluid is called a ‘‘free gas’’ (Verschoor, et al., 1952a; Fricke, 1992), i.e. a gas inside a big sided enclosure with a characteristic length much larger than the mean free path of the gas molecules.

Schaaf and Chambre (1956) subdivide the flow regimes of gas resulting from their experiments by utilizing the Knudsen Number to: free molecule (Kn > 10), transition (10 > Kn > 0.1), temperature jump (0.1 > Kn > 0.01), and continuum regimes (Kn < 0.01). This classification has been used later by many researchers (e.g. Springer, 1971; Tien and Cunnington, 1973; Madhusudana, 1996; Frohn and Anders, 2002). For high Knudsen number

in the free molecule regime where almost exclusively collisions between the gas molecules and the enclosure's walls are present, the gas is called in this state: ‘‘Knudsen gas’’ (Cercignani, 2000). Heat transfer in every regime has its individual rules. The ‘‘Knudsen effect’’ means that the gas is not any more a free gas (i.e. a continuum). The gas begins to enter a low density state and it is classified in one of the above mentioned regimes according to the Knudsen number. In the literature for rarefied gases there is also another expression called ‘‘non-continuum effect’’ (Baker, et al., 1996), undoubtedly it is the same as Knudsen effect. The Knudsen effect has been observed in porous materials. Increasing the Knudsen number of a filler gas in porous materials aiming to reach the Knudsen effect can be achieved through optimization of two parameters: gas pressure and pore size, as seen in eq. (15) . This will be presented in the following sections.

3.2.2 Knudsen Effect by Changing the Gas Pressure (Smoluchowski Effect)

The fundaments of kinetic theory of gases indicate heat conduction through a gas is independent of gas pressure. This flawed hypothesis was accepted till the polish scientist Smoluchowski (1910) obtained a different conclusion from his experiments. He measured the effective thermal conductivity of powders from several materials (quartz, sand, rise… and others) in gas at low pressure. He found a strong decrease in the effective thermal conductivities during evacuation of gas from the porous media. Since solid conduction and radiation are rather independent from the gas pressure, it was concluded that the decrease in effective thermal conductivity is due to reduction in the gas thermal conductivity at lower pressure. A similar effect has been observed by Wakao and Vortmeyer (1971); Caps, et al. (1997); Wu, et al. (1999).

This effect of low gas pressure is usually called Smoluchowski effect. It could be interpreted by the Knudsen theory for the gas, which filled the porous structure, as both the mean free path and the respective Knudsen number are increased by evacuation. This leads the gas to be rarefied and has free molecules regime conditions, and thus it has lower thermal conductivity when compared to its value in continuum regime (Low Kn-numbers).

By Plotting the effective thermal conductivity vs. the logarithmic gas pressure, Smoluchowski (1910) found an S-shape curve. In contrast, Aberdeen and Laby (1926) found a linear relation for their experiments with fine powder. Kannuluik and Martin (1933) confirmed the results found by Smoluchowski.

In order to present the S-curve of Smoluchowski effect the gas thermal conductivity for nitrogen at different gas pressures have been calculated for various pore sizes ranges from 500 nm till to 500 µm using the Kaganer’s model, see below eq. (27). The results are presented in Figure 3. As could be seen the Smoluchowski effect depends strongly also on the pore size. That implies decreasing the pore size (the characteristic length associated with the pores) shifts the S-curves to lower thermal conductivity values at higher pressures.

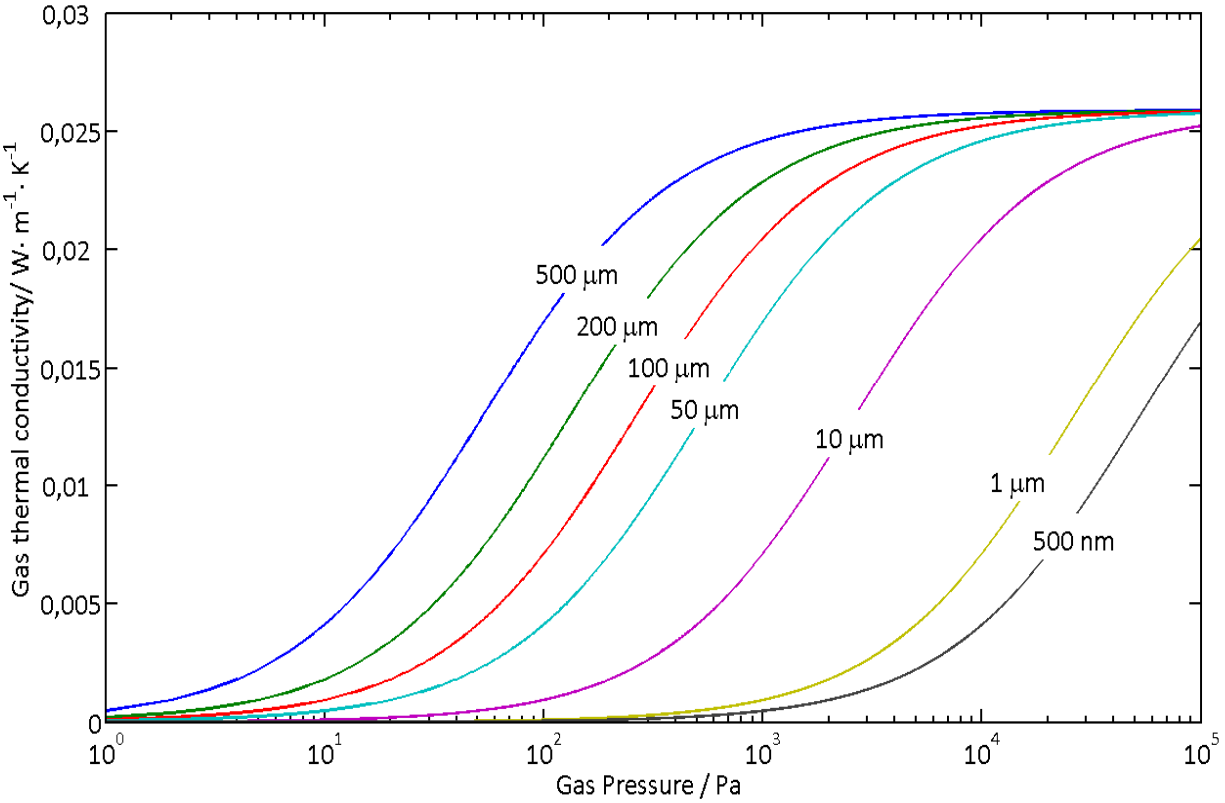

Figure 3: Relation between gas thermal conductivity in porous media and pressure of the filling gas for nitrogen at 25 °C (Smoluchowski's effect)

3.2.3 Knudsen Effect in Nano-Materials

In the 20th century a big challenge was to find materials with thermal conductivity lower than the bulk thermal conductivity of air. Mason (1933) applied aluminum foil layers for insulation by reducing radiation and also gas conduction by the narrow spaced air-foil cells. By this, he obtained the thermal conductivity of air for the whole arrangement. Russell (1933) discussed pore size effects on the thermal conductivity of refractories, and has interpreted the lowness of the thermal conductivity of refractories by the small pores eliminating the radiation. Russell did not mention the Knudsen effect in his study.

Kistler (1931) used his chemical engineering science to introduce a new material, now called aerogel, that is derived from a sol-gel process. Kistler and Caldwell (1934) found the thermal conductivity of aerogel is less than that of air at standard pressure and room temperature. This material features a structure of very small pores, sized in the nano range (1-100 nm) This size structure increases the Knudsen number to the region where the gas acts as free molecules, even at normal pressure. This decreases gas heat conduction and leads to lower effective thermal conductivity than thermal conductivity of air. Such materials are considered to be as super insulation. Further development was done to produce porous insulation materials based on Knudsen effect (e.g. Material WDS® produced by Poroxtherm©, Silcapor high® produced by Silca©, or Microtherm® produced by Microtherm nv© see the data sheets of these materials in Appendix A).

3.3 Models of Gas thermal Conductivity in Porous Media

The knowledge of gas thermal conductivity, one of the unique thermo physical properties, is essential for numerous industrial applications involving heat transfer, e.g. high temperature furnaces or heat reservoirs etc. Since the 18th century this property has been an active research topic. Often the research goal was to find and evolve experimental methods and facilities for accurately measuring the thermal conductivity of gas under widely varying conditions of temperature, pressure and gas type. In addition strong efforts have been devoted to develop and test theories and to create models aimed to estimate and explain the gas thermal conductivity.

There are many issues in making an estimation of gas thermal conductivity in porous media: How will the heat be transferred through gas in porous materials? Does the Knudsen effect appear in all porous materials? How is heat transferred in porous materials with a wide pore size distribution from macro to the nano scale range? With time many ideas and concepts have been developed by researchers to answer those questions. Some success has been reached to estimate the gas thermal conductivity in porous structures. Basically, the heat transfer from one side of a pore to the opposite side is governed by intermolecular collisions and collisions with the wall. The order of magnitude of the Knudsen number determines the prevailing kind of collisions.

The fundamental problem is the proper estimation and calculation of the gas thermal conductivity in porous media depending on their structure. After studying and analyzing studies available from literature, the models of gas thermal conductivity applied for non-flow porous media were sorted in this work to five different groups according to the principle of developing the model from the basic theories of gas heat transfer, see Table I.

Table I: Overview of models for gas thermal conductivity in porous media

Section	Group of the developed model
3.3.1	Bulk gas thermal conductivity model
3.3.2	Improved gas thermal conductivity model based on kinetic theory
3.3.3	Gas thermal conductivity temperature jump model
3.3.4	Gas thermal conductivity model based on low gas pressure effect
3.3.5	Gas thermal conductivity models based on Knudsen number regimes

3.3.1 Bulk Gas Thermal Conductivity Model

At the beginning of this study of heat transfer in porous media the major concern was the mathematical modeling of the heat flow through two-phase materials including respective contributions of solid and fluid phases where mostly the bulk (continuum) thermal conductivity has been taken for the filling gas (Gorring and Chruchill, 1961; Chaurasia, et al., 1978). This is proper for porous materials with big sized pores, hence, a Knudsen number is less than unity (Kaviany, 1995). This approach is also fine if the gas is a still (free) gas as

found in the cellular materials such as foams with large cell size (Doermann and Sacadura, 1996; Placido, et al., 2005; Knodapi, et al., 2006), or in granular and powder materials formed by big particles producing macro scale pores (Deissler and Eian, 1952; Pande, et al., 1984; Singh and Kasana, 2004).

In the kinetic theory the bulk gas thermal conductivity is proportional to viscosity (η) and specific heat at constant volume (C_V), (Loeb, 1934; Kennard, 1938):

$$\lambda_{bulk} = \varepsilon\, \eta\, C_V \tag{16}$$

where the proportionality constant ε is dependent on the mathematical analysis, as given by Eucken, see (Loeb, 1934; Kennard, 1938), as $^1/_4\,(9\gamma - 4)$. This relation is surely restricted to rarefied gases. The viscosity is proportional directly to the mean free path(Λ) as follows:

$$\eta = \frac{1}{3}\, \rho\, \bar{v}\, \Lambda \tag{17}$$

3.3.2 Improved Gas Thermal Conductivity Model Based on Kinetic Theory

After observing the Knudsen effect in porous media, many researchers tried to extend that model of bulk gas thermal conductivity to the large Knudsen number range. This is found for porous media with small size pores and also for low pressure by modifying the mean free path.

$$\lambda_{gas-p} = \frac{1}{3}\varepsilon\, \rho\, \bar{v}\, C_V\, \Lambda_{mod} \tag{18}$$

In the continuum regime the gas has a certain mean free path (Λ_o) which, however, is limited by the pore size diameter (d) in the free molecules regime with molecules moving just between the enclosure walls. The modified mean free path (Λ_{mod}) can be considered as a serial model of the two limiting regimes

$$\frac{1}{\Lambda_{mod}} = \frac{1}{\Lambda_o} + \frac{1}{d} \tag{19}$$

and subsequently the gas thermal conductivity:

$$\lambda_{gas-p} = \frac{\lambda_{bulk}}{1 + Kn} \tag{20}$$

This model has been used for evaluation of gas thermal conductivity by Kistler and Caldwell (1934) for aerogel, by Woodside and Messmer (1961) for rock and sand, by Verschoor, et al. (1952) for fibrous materials, and by Strong, et al. (1960) for vacuum thermal insulations.

The same model by eq. (20) was used by Tsotsas and Martin (1987) for evaluation of the gaseous heat transfer inside packed beds, but with a modified mean free path (Λ_o^*)

$$\Lambda_o^* = 2\frac{2-\alpha}{\alpha}\sqrt{\frac{2\pi RT}{M}}\frac{\lambda_{bulk}}{p\left(2C_P - \frac{R}{M}\right)} \tag{21}$$

Tseng, et al. (1997) used the model eq. (21) multiplied by the accommodation coefficient to estimate the change of gas thermal conductivity in foam at cryogenic temperatures.

Kistler (1935) used aerogel for insulation at low pressure gas atmospheres, and he considered the molecules moving in straight lines between the surfaces with only occasional impacts between them. Hence he modified the model eq. (16) by inserting the pressure parameter p:

$$\lambda_{gas-p} = \frac{\lambda_{bulk}\, d}{d + {\Lambda_o}/{p}} \tag{22}$$

Wolf and Strieder (1994) improved a model based on the kinetic theory for estimation of conductive heat transfer by a gas within a spherical pore:

$$\lambda_{gas-p} = \left(\frac{2}{dC}[\sigma_3(\sigma_1\sigma_3 - \sigma_2^2)^{-1} + (1-\alpha)\alpha^{-1}]\right)^{-1} \tag{23}$$

$$\sigma_{1,2,3} = f(Kn)$$

where (C) is a constant depending mainly on particle density and mean thermal speed. For testing the model they have taken thermal conductivity data of plastic foam at different pressure levels measured by Harper and Sahrigi (1964). Because of scarcity of data for the accommodation coefficient in insulation materials, they have varied the accommodation coefficient between 0 and 1 to fit the experimental data.

The mean free path obtained from the kinetic theory model was emerged for free gas. The first trial to modify the mean free path calculation by relating it to the surface area of a porous solid came from Kistler (1941) by deriving the characteristic length (L_{ch}) as the average distance a molecule moves between impacts with a solid cylinder.

$$L_{ch} = \frac{1}{S_s}(V_{por} - \frac{\pi^2}{16} b_{struc}) \tag{24}$$

where (b_{struc}) is a coefficient depended on structural elements. In eq. (22) the pore diameter (d) has been replaced by (L_{ch}). This method has been used inversely, i.e. the scope was to investigate the surface area of porous media by measuring their effective thermal conductivity. The same method, however with a different model, has been applied by Lee, et al. (2002) to determine the mesopore of aerogel by measuring their thermal conductivity. Zeng, et al. (1994) succeeded in modeling the mean free path of gas molecules distributed between a solid matrix made up of spherical particles. This was done by substituting the

modified mean free path in the gas thermal conductivity model from the kinetic theory, eq. (16), as:

$$\lambda_{gas-p} = \frac{(2.25 - 1.25\gamma)0.461\left({}^{p}/_{kT}\right)\left({}^{8\,kT}/_{\pi\,m_g}\right)^{1/2}}{0.25\,S_s\rho_{por}\psi^{-1} + \sqrt{2}\left({}^{p}/_{kT}\right)\pi d_m^2}\frac{C_V}{N_A} \tag{25}$$

This gas thermal conductivity model is also dependent on density (ρ_{por}) and surface area (S_s) of the porous structure. They have tested the model by structural investigations and measured the pressure dependence of the effective thermal conductivity of aerogel and then subtracted the solid and radiative conductivity contributions to obtain the gas thermal conductivity. Zhang, et al. (1999) tested this model in the same way by measuring the thermal conductivity of silica aerogel by the hot wire method with reduction of the gas pressure. The calculated results of model eq. (25) show good agreement regarding the pressure effect on gas thermal conductivity, however the calculated curve runs lower than the measured one by 10 to 30%. Swimm, et al. (2009) have evaluated recently Zeng's model eq. (25) to estimate the gas pressure effect on effective thermal conductivity of aerogel, the calculated results are lower than measured one up to 3 times in the pressure range 10^4 Pa till 100 bar.

3.3.3 Gas Thermal Conductivity Temperature Jump Model

The temperature jump theory by Smoluchowski (1911) is important for rarefied gases which has been applied by Kennard (1938) to gas thermal conductivity. He modeled the jump distance (g) by comparing the energies carried to and away from a plate by incident and reflected gas molecules streams respectively. He considered a low density gas in the gap (d) between two parallel plates with the jump distances at both plate (g1 and g2):

$$\lambda_{gas-gap} = \frac{\lambda_{bulk}\,d}{d + g_1 + g_2}$$
$$g_{1,2} = \frac{2 - \alpha_{1,2}}{\alpha_{1,2}}\frac{2}{\gamma + 1}\frac{\lambda_{bulk}}{\eta C_V}\,\Lambda \tag{26}$$

Corruccini (1959) applied the temperature jump equation to calculate the gaseous heat conduction in vacuum insulation for cryogenics devices (no porous media). Madhusudana (1996) used the jump temperature equation to evaluate the gas gap conductance between rough surfaces (semi-porous structure). Kaganer (1969) used the temperature jump equation, eq. (26), for evaluation of the heat conduction through gas in granular and fibrous insulation (porous structure) and formulated it by help of eq. (16) by assumption of identical accommodation coefficients for both surfaces, as follows:

$$\lambda_{gas-p} = \frac{\lambda_{bulk}}{1 + 2\,\beta\,Kn}$$
$$\beta = \frac{2 - \alpha}{\alpha}\frac{2\varepsilon}{\gamma + 1} = \frac{2 - \alpha}{\alpha}\frac{2\gamma}{\gamma + 1}\frac{1}{Pr} \tag{27}$$

This model became the most cited model in the literature to evaluate the gas thermal conductivity, e.g. in fibrous materials (Luu, et al., 1986a; Bondarenko, et al., 1989; Stark and Fricke, 1993; Daryabeigi, 1999; Daryabeigi, 2003), in powder and packed spheres (Ogniewicz and Yovanovich, 1977; Moore, et al., 1982), in aerogel (Lu, et al., 1992b), and in refractories and ceramics (Litovsky and Shapiro, 1992a; Litovsky, et al., 1996). Nevertheless, this model has been presented in different ways, concerning the quantity (2β) in the denominator (see Table II).

Table II : The Difference of Quantity (2β) as cited in the literature

Study	Change	Eq.
Fricke, et al., 1992; Lu, et al., 1995	Just β instead of 2β	(28)
Wakao and Kagnei, 1982	$2\beta = 2\frac{2-\alpha}{\alpha}$	(29)
Wawryk and Rafalowicz, 1988	$2\beta = \frac{19}{6}\frac{2-\alpha}{\alpha}$	(30)
Heinemann, et al., 1996	assumed to be constant 2β = 6	(31)

Kaganer's model by eq. (27) is indirectly related to the structure of the porous medium by means of the characteristic length which varies in respect to the kind of the insulation material:

$$\mathrm{Kn} = \frac{\Lambda}{\mathrm{L_{ch}}} \qquad \mathrm{L_{ch}} = \mathrm{f(porous\ structure)} \tag{32}$$

The temperature jump model simulates the gas thermal conductivity in porous media by replacing the gap width between parallel plates by this characteristic length.

Cunnington and Tien (1977) reported experiments with a microsphere insulation in presence of helium and nitrogen atmospheres. The scope was to test the model, eq. (27), by Kaganer for the gas thermal conductivity, and good agreement was obtained with the measured results.

All the above mentioned researchers applied the temperature jump model to estimate the gas thermal conductivity without limitation of the Knudsen number which was considered to be equal or greater than unity. This means there is no restriction for the model to a certain Kn number regime. A generalization of this model was made by Praslov (1961) for covering different gas regimes:

$$\lambda_{\mathrm{gas-p}} = \frac{\lambda_{\mathrm{bulk}}}{\chi + \varphi\ 2\ \beta\ \mathrm{Kn}} \tag{33}$$

Where χ and φ depend on the Knudsen number as follows in Table III:

Table III : Constants for Equation (33)

Kn Range	Constants
0.01 > Kn	$\chi = 1;\ \varphi = 0$
0.01 < Kn < 10	$\chi = 1;\ \varphi = 1$
Kn > 10	$\chi = 0;\ \varphi = 1$

This was used later by Sullins and Daryabeigi (2001), and also by Grujicic, et al. (2005).

3.3.4 Gas Thermal Conductivity Model Based on Low Gas Pressure Effect

As mentioned in section 3.2.2, the Smoluchowski effect describes the effect of decreasing the gas pressure on the gas thermal conductivity. Many researchers have measured the effective thermal conductivity with reduction of gas pressure and showed such changes of the S-curve with variations of pore size and pore size distributions respectively, e.g. for foams (Tao, et al., 1997), fibrous materials (Ziegenbein, 1983), powders (Swift, 1966; Singh, et al., 1985), and aerogel (Smith, et al., 1998).

Some gas thermal conductivity models have been developed in order to fit measured effective thermal conductivity (S-curve). Kistler and Caldwell (Kistler and Caldwell, 1934) evacuated the aerogel granules and subdivided the gas in this granular arrangement to two parts: gas inside the aerogel granules and gas between the various aerogel granules. The effective thermal conductivity was modeled by a serial set-up of all thermal resistances.

The most common model for temperature and pressure effects on the mean free path is given by:

$$\Lambda = \Lambda_o \frac{T}{T_o} \frac{p_o}{p} \tag{34}$$

with Λ_o, T_o, p_o for normal conditions.

By substituting eq. (34) in (27), generally the relation of gas thermal conductivity with the gas pressure can be represented as follows:

$$\lambda_{gas-p} = \frac{\lambda_{bulk}}{1 + {}^{C}/_{P}} \tag{35}$$

The variable (C) can be determined mathematically depending on the structure of the porous arrangement and on the thermal properties of the filling gas (e.g. specific heat, accommodation coefficient) (Wakao and Vortmeyer, 1971; Büttner, et al., 1988; Grochal, 1995; Lee and Cunnington, 2000). Pande, et al. (1994), Caps, et al. (1994) and Fricke et al. (Fricke and Caps, 1988; Caps and Fricke, 2000b) determined (C) from measured S-curves and called it $P_{0,5}$, i.e. the gas pressure required for a decrease of the effective thermal conductivity of porous arrangement by one half of that at normal pressure. In some cases an

extra constant has been added to the numerator to get a better agreement with experimental data.

Zeng et al (Zeng, et al., 1994) improved the last model, eq. (35), by considering pore size distribution effects:

$$\lambda_{gas-p} = \frac{\lambda_{bulk}}{1 + {C}/{d_{mp}\, p^{y}}} \tag{36}$$

where d_{mp} is the most probable pore size which is determined from the measured pore size distribution of the porous arrangement. C and y are constants determined from measured effective thermal conductivities.

3.3.5 Gas Thermal Conductivity Models Based on Knudsen Number Regime

The models above, except model eq. (33), do not take into account in which Knudsen number regime the gas is situated. They are trying to estimate the gas thermal conductivity in porous media without concerning the degree of rarefaction of the gas in the pores. Heat transfer in rarefied gases is of prime importance for many applications. Many experiments are found in literature considering heat conduction in micro scale channels (between parallel plates, coaxial-cylindrical and concentric-spherical surfaces) (Dybbs and Springer, 1965; McCoy and CHA, 1974; Harding and Window, 1981; Demirel and Saxena, 1996). Other studies established models for microscale gas heat conduction either by improving the mean free path for a certain Knudsen number regime (Stops, 1970; Reich, 1990), or by using Direct Simulation Monte Carlo (DSMC) method to extend the Smoluchowski model for covering wide Knudsen number ranges (Denpoh, 1998).

However, there are only two studies, according to this presented research, developed for gas heat conduction in a porous arrangement. (a) Wonchala and Wynnyckji (1984) developed a model based on the analogous diffusion model for complex pores considering the transition and Knudsen regimes. They subdivided the gas heat conduction to the macroscopic (bulk thermal conductivity, λ_{bulk}) and microscopic (Knudsen thermal conductivity, λ_{Kn}) ranges and formulated the respective model:

$$\lambda_{gas-p}^{-1} = \lambda_{bulk}^{-1} + \lambda_{Kn}^{-1}$$
$$\lambda_{Kn} = \frac{25}{18}\sqrt{\frac{8R}{\pi MT}}\left[\frac{2}{5}\frac{C_p}{\gamma R} + \frac{9}{10}\right] p \left(\frac{d}{2}\right) \tag{37}$$

However no further investigation on this model has been done with respect to its confirmation by experimental data. (b) The other one was from Zheng and Strieder (1994) who developed a model for a gas situated in the transition and Knudsen regimes inside fibrous media. This model is specified for fibrous arrangement containing many respective parameters like fiber orientation and it is not generally applicable for porous arrangements.

3.3.6 Inspection of Gas Thermal Conductivity Models

The current work has collected and presented several models to estimate the gas thermal conductivity for free gas and also for the various Knudsen number regimes based on different principles and theories. The development of those models aimed to include the critical factors or parameters like gas pressure, pore size distribution, accommodation coefficient, and temperature. Evaluating some of those models is restricted for a specific kind of porous material, which supplied the model with specific geometrical parameters. Therefore a quantitative comparison is not applicable for all models. Evaluation of some models was made in this work for the thermal conductivity of nitrogen in wide Knudsen-numbers range, from continuum regime down to free molecules regime. The results are presented in Figure 4. According to these evaluations, the right hand side plateau in the gas thermal conductivity curve describes the continuum regime of low Knudsen numbers where the gas is near to its bulk value as free gas. The different models show no difference in this regime. Increasing the Knudsen numbers reduces the gas thermal conductivity dramatically. The end of quasi plateau and beginning of the drop off regime (transition regime) varies according to the model. The model by Tsotsas and Martin eq. (21), the model by Kennard and Kaganer eq. (26)/ eq. (27), the modified model by Wawrky and Rafalowicz eq. (30) and the diffusion model by Wonchala and Wynnyckyj eq. (37), all have an identical trend, as seen in Figure 4 the results of these models are overlapped. By higher Knudsen number the difference between models gets smaller. The estimation of some models shows the disagreement in results particularly in the transition regime. This quantity estimation, however, is not enough to examine and choose the suitable model for calculating the gas thermal conductivity in porous media. So in this work a criterion is introduced to evaluate and compare the models of gas thermal conductivity in porous systems based on different critical factors and the applicability of each model for different porous media. All mentioned models are tabulated as a kind of survey (see Table IV).

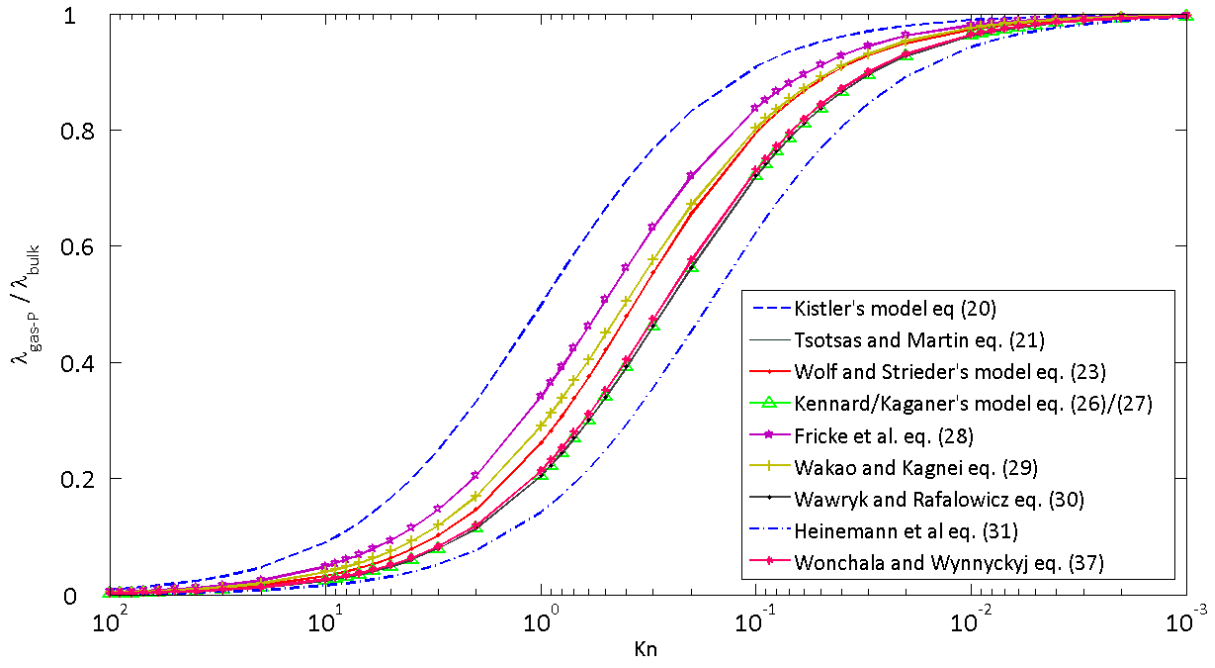

Figure 4: Comparison of different models for gas thermal conductivity in porous media calculated for nitrogen at 25 °C

Table IV: Survey of the models

Models group	Kn-effect	Appl. range	eq. Nr.	Reference	Applied for	Reflection of + AC	++ PSD	# T	## p
Bulk Gas thermal conductivity model		macro-scale Kn < 0.01	(16)	Placido, et al., 2005 Singh, 2004 Doermann and Sacadura, 1996 Pande, et al., 1984 Deissler and Eian, 1952	Foam granular powder			✓	
Improved gas thermal conductivity model based on kinetic theory	✓	micro and nano-scale	(20)	Woodside and Messmer, 1961 Woodside and Messmer, 1960 Strong, et al., 1960 Verschoor, et al., 1952a Kistler and Caldwell, 1934	fibrous materials, aerogel, sand.			✓	✓
			(21)	Tsotsas and Martin, 1987a	packed beds	✓		✓	✓
			(22)	Kistler, 1935a	aerogel			✓	✓
			(23)	Wolf and Strieder, 1994	foam	✓		✓	✓
			(25)	Zeng, et al., 1995a Zeng, et al., 1995c	aerogel	✓	✓	✓	✓
Gas thermal conductivity temperature jump model	✓	micro and nano-scale	(27)	Daryabeigi, 1999; Daryabeigi, 2003 Litovsky, et al., 1996 Stark and Fricke, 1993 Lu, et al., 1992a Litovsky and Shapiro, 1992a Bondarenko, et al., 1989 Wawryk and Rafaowicz, 1988 Kaganer, 1969; Luu, et al., 1986a Moore, et al., 1982 Wakao and Kagnei, 1982 Ogniewicz and Yovanovich, 1977 Cunnington and Tien, 1977	fibrous materials, powder, packed beds, aerogel, ceramic refractories.	✓		✓	✓
			(33)	Grujicic, et al., 2005 Sullins and Daryabeigi, 2001 Praslov, 1961					
Gas thermal conductivity model based on gas pressure effect	✓	micro und nano-scale	(35)	Lee and Cunnington, 2000 Caps and Fricke, 2000b Grochal, 1995 Büttner, et al., 1988 Pande, et al., 1984 Wakao and Vortmeyer, 1971	packed beds fibrous aerogel	✓		✓	✓
			(36)	Zeng, et al., 1994	aerogel	✓	✓	✓	✓

+ AC: Accommodation coefficient. **++** PSD: Pore size distribution. **#** T: Effect of Temperature **##** P: dependence on pressure

For each model the source is given, and also the kind of porous material which it has been applied to. The reflection parameters contain effects of four parameters: accommodation coefficient (AC), pore size distributions (PSD), Temperature (T) and pressure (p).

3.4 Accommodation Effect

The Impact of thermal accommodation between gas molecules and the solid surface starts to be evident when developing the heat transfer in rarefied gases where the collision rate between gas molecules and solid surface is much higher than the collisions rate between molecules. The thermal accommodation coefficient is defined as a measure of the average efficiency of the energy exchange per encounter of a gas molecule with a solid surface at the gas-solid interface (Goodman, 1968). The accommodation coefficient could be mathematically defined in terms of the energies of the various gases by the equation (Saxena and Joshi, 1989):

$$\alpha = \frac{E_r - E_i}{E_{su} - E_i} \tag{38}$$

Here, E_i represents the energy brought to the solid surface in unit time by incident gas stream; the total incident energy flux, E_r denotes the energy carried away by these molecules as they leave the surface after reflection; i.e. the total reflected energy flux, and E_{su} is the energy of the reflected stream which it would carry away if it acquired the same mean energy per molecule as does a stream issuing from a gas in thermal equilibrium at the wall temperature, T_s. Thus, $(E_r - E_i)$ represents the total energy flux through the surface of the solid and $(E_{su} - E_i)$ will be its value if the interaction between the gas and the solid atoms were ideal. Since the energy can be expressed by term of an effective temperature, Knudsen used the temperature in eq. (38) instead of energy (Knudsen, 1934). Baule (Baule, 1914) applied the classical theory and used a model in which the gas and surface atoms behave like elastic spheres and have a Boltzmann distribution of energies. He supposed each gas atom to make a single collision with a solid atom before rebounding, and applied the laws of conservation of energy and momentum to obtain the following expression for accommodation coefficient (Wachman, 1962):

$$\alpha = \frac{2\, m_g\, m_s}{\left(m_g + m_s\right)^2} \tag{39}$$

where m_g, m_s are the masses of gas and solid molecules/atoms. Some research has developed the model by Baule to match the experimental data either by introducing the effective solid mass (Saxena and Joshi, 1989) or by adding empirical constant to give accurate estimation of accommodation (Goodman, 1980). The version of Goodman for the formula of Baule is:

$$\alpha = \frac{2.4\,\mu}{(1+\mu)^2} \tag{40}$$

Results of calculated Accommodation coefficient for various inert gases with different solid surface according to the model by this eq. (39) are presented in Figure 5. Regarding to this model the accommodation coefficient is not a property of gas but it is dependent upon the

mass ratio gas/solid. helium has lighter gas molecules than others gases like argon, krypton and Xenon, and thus the molecules will come back to gas zone after collision with the solid surface faster than other gases, i.e. less accommodation time and hence lower accommodation coefficient.

Other researchers developed Baule's model and considered the particle vibration by introducing the Debye temperature (Saxena and Joshi, 1989). The last parameter characterizes the substance and reflects its structure stability, strength of the bonds, availability of structural defects (such as dislocations in crystalline structure of mineral grains, pores, and microcracks), and its density (Vladimirov, 1998).

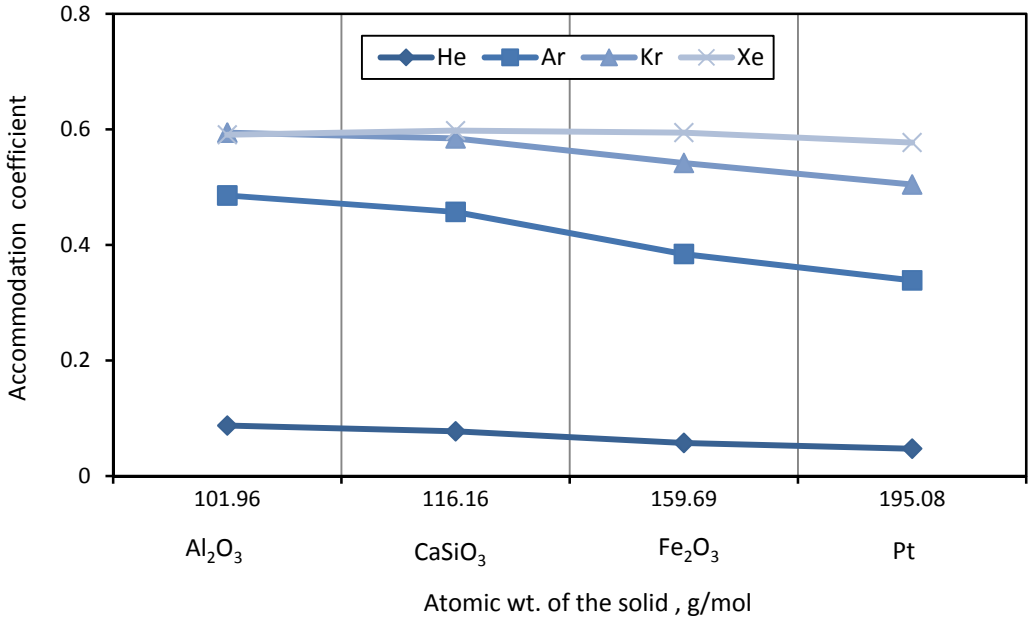

Figure 5: Accommodation coefficient for different gas-solid systems calculated from model by eq. (39)

Goodman and Wachman proposed a formula for estimating the accommodation coefficient based on Goodman's lattice theory and the three dimensions theory of scattering surface. The formula gives good agreement with the experimental data of accommodation coefficient (Goodman and Wachman, 1967). However, this formula includes two parameters, one specifies the kind of gas and other describes the solid surface. These parameters should be determined by previous measurements of accommodation coefficient minimally for one gas at defined temperature for the same solid surface. Different models were developed for estimation of accommodation coefficient, arisen from various theories and principles such as temperature jump theory and low pressure theory. However, most of the models are related to parameters or to another model with high uncertainty, Wachman recommended (Wachman, 1962) in his critical review of different theories and models to measure the accommodation coefficient.

3.4.1 Temperature Dependency of Accommodation Coefficient

Increasing the temperature increases the velocity of the molecules and thus decreases the accommodation time, consequently the accommodation coefficient is reduced. This conclusion was confirmed by many researchers, with exception for helium which was found

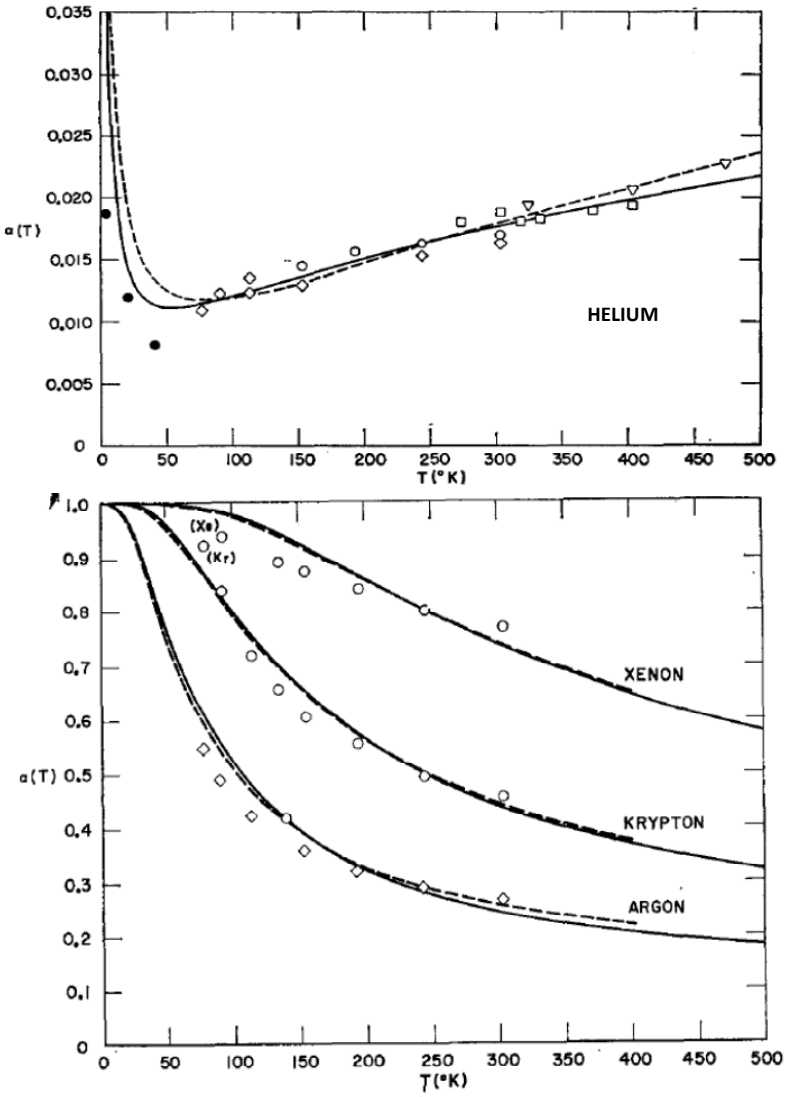

Figure 6: Change of accommodation coefficient with temperature for different gases with Tungsten (Goodman and Wachman, 1967)

to experience a small increase of accommodation coefficient with increasing temperature (see Figure 6). Whereas, Wachman found out that accommodation coefficient of helium to be constant (Wachman, 1962). The formula of Goodman and Wachman describes also the temperature dependency of accommodation coefficient and agrees well with the experimental data by different temperature (see Figure 6). As can be seen, for the same solid surface the decreasing rate of Accommodation coefficient depends on the kind of gas. These relations were mathematically described by Martin (Martin, 1980) as following:

$$\log\left(\frac{1}{\alpha}-1\right)=A-\frac{\frac{1000}{T}+B}{C} \tag{41}$$

Where *A, B, and C* are constants depending on the gas characteristics, gives the same trend as the formula of Goodman and Wachman, however it does not consider the kind of solid surface. The accommodation coefficient fluctuates between the zero and unity (Goodman and Wachman, 1974).

Historically, many facilities were built to measure the accommodation coefficient between a gas and metal surface, e.g. tungsten or Platinum. However, the tough conditions of the measurements and the difference of applied model to evaluate the accommodation coefficient produced disagreement in the experimental results (Saxena and Joshi, 1989). Recently a new experimental facility for measuring accommodation coefficient is developed based on hot plate method. However, it is also prepared just for metallic surfaces such as stainless steel and others (Rader, et al., 2004; Rader, et al., 2005). Actually, description of gas-solid collision and prediction of accommodation coefficient is not smooth, since there are many factors which have a large influence in determining the accommodation coefficient, such as: gas purity, the surface roughness, the cleanness grade of solid surface, the kind of gas and solid, the temperature of both gas and solid, and the operative pressure. Thereby the experimental results of accommodation coefficients are restricted to the gas-solid system where the experiments are performed. For porous insulation materials there are no measured experimental data, and the most of predictive models for accommodation coefficient do not reflect the case of solid surface for such porous media.

3.5 Effect of Changing the Filling Gas

Insulation materials are applied in different gas atmospheres, for example inert gases atmospheres in some industrial furnaces, air in residential applications, for space application, and also in food industries. Various gases have different bulk gas thermal conductivities. As mentioned in the beginning of this chapter, the bulk gas thermal conductivity depends mainly upon molecule diameter, specific heat capacities and molecular weight, see eqs. (12, 14, 16 and 17). These differ according to the kind of gas, see Tables in Appendix B. The effective thermal conductivity of each porous structure can be changed by changing the filling gas. The experimental data of effective thermal conductivity of different porous materials filled with various gases (such as, Freon-12, argon or nitrogen and others) have been taken from literature.

Some of these data are presented as ordinate against the bulk thermal conductivity of the filling gas as abscissa, as seen in Figure 7. The data for bulk gas thermal conductivity are either taken directly from reference when it is reported, or calculated at same temperature (Kleiber and Joh, 2006). Changing the filling gas with one that has higher thermal conductivity increases the effective thermal conductivity for any material. This relation could be mathematically described by the lines which are drawn in Figure 7. However the amount of the increase of the effective thermal conductivity is not a constant. This is obvious by comparing the different slopes of the lines through the data.

Each material measured at the same temperature by two different gases represents a study case, see Table V. For all study cases the change of effective thermal conductivity ($\Delta\lambda_{eff}$) due to change of the filling gas is compared with the difference between bulk thermal conductivity of the filling gases ($\Delta\lambda_{gas}$), see Figure 8. When the ratio $\Delta\lambda_{eff}/\Delta\lambda_{gas}$ (Slope of line in Figure 7) is equal to 100 %, that means the change of effective thermal conductivity is equal to the difference of gas thermal conductivities, as in cases 3 and 19. In many cases the

ratio is over 100 % which shows that by changing the filling gas a coupling effect can be emerge. That increases the effective thermal conductivity in some porous structures more than 400 % X $\Delta\lambda_{gas}$, as in cases (20-27). This effect is not specified by the kind of material as can be proved by considering the cases 14-16 for instance. The investigated material in these

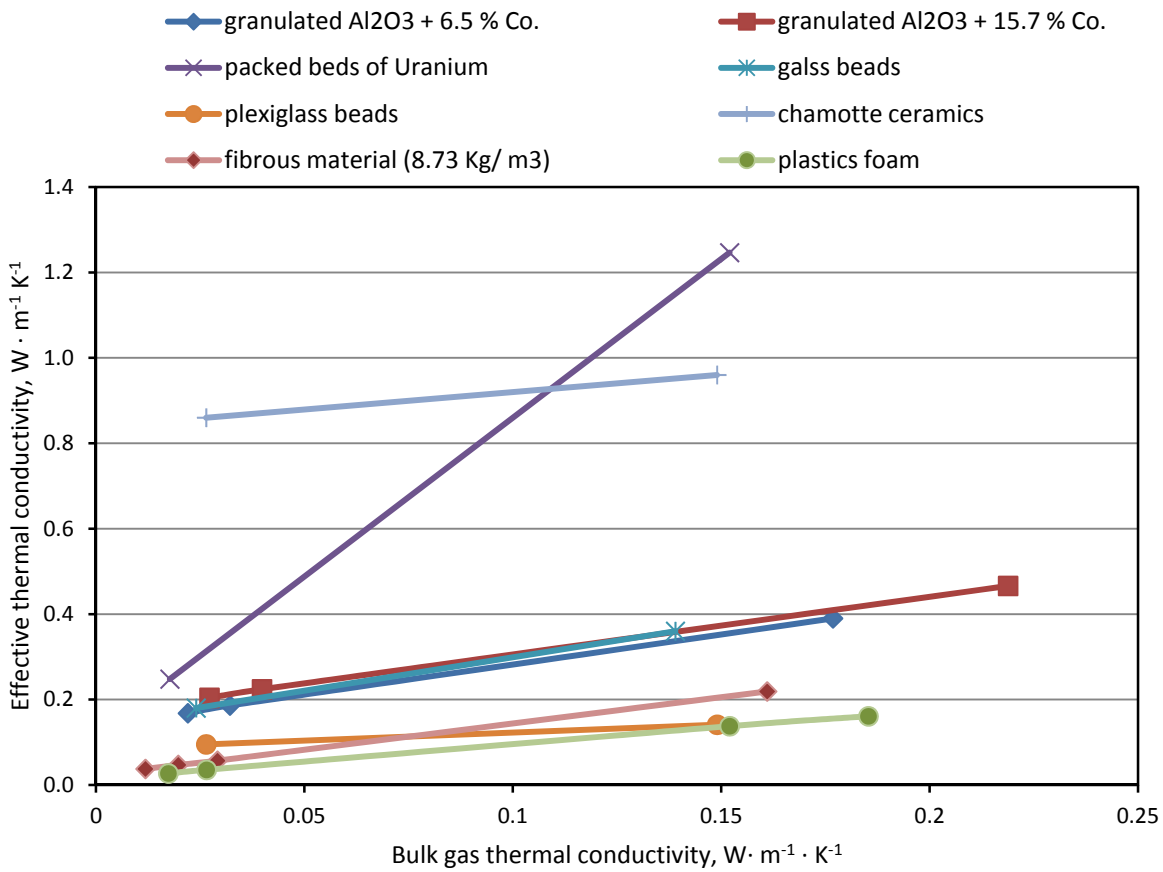

Figure 7: Effect of changing the filling gas on the effective thermal conductivity.
Points: measured Data, References are listed in Table V

cases is the same and at the same temperature. Only filling gases are different, and this gives, however, different ratios ($\Delta\lambda_{eff}$ /$\Delta\lambda_{gas}$). The same could be noticed also for cases (12-14) and for cases 23 and 24.

In a few cases (6, 8-13) the ratio ($\Delta\lambda_{eff}$ /$\Delta\lambda_{gas}$) is lower than 100 %. That means the evaluation based on bulk gas thermal conductivity overestimates the change of effective thermal conductivity by changing the filling gas. That could be an indication of Knudsen effect in such porous structures. There are in literature many studies and experiments about the change of effective thermal conductivity of porous arrangement through change of the filling gas: Woodside and Messmer investigated the thermal conductivity of different porous media from consolidated rocks and unconsolidated sands (Woodside and Messmer, 1961) by various gas atmospheres (Freon-12, argon, Air, helium and Hydrogen), they formulate equation of effective thermal conductivity as following:

$$\lambda_{eff} = W\,\lambda_{gas} + \lambda_{evac} \tag{42}$$

Where (W) is the slope of the line. However, they bounded this equation for low thermal conductivity gases (F-12, Ar and Air). As seen in Figure 7 and Figure 8 the slope differs from material to material, and also for the same material by different gases. Measuring the effective thermal conductivity gives y-values. The x-values are the gas thermal conductivity in porous structure, which is complicated to estimate as we saw in section (3.3). So it is still arguable how to estimate the slope in eq. (42) and which factors affect this slope.

Table V : List of the collected study cases from literature

Case no.	Material	T [K]	Exchange gas atmosphere		Reference
			from	to	
1	granulated Al_2O_3 + 6.5 % Co.	392.8	Ar	He	Madzhidov, et al., 1988
2	granulated Al_2O_3 + 15.7 % Co.	520.3	N_2	He	Madzhidov, et al., 1988
3	granulated Al_2O_3 + 25 % Co.	929.5	N_2	He	Madzhidov, et al., 1988
4	granulated Al_2O_3 + 25 % Co.	929.5	Ar	He	Madzhidov, et al., 1988
5	glass beads	300	Air	He	Luikov, et al., 1968
6	Plexiglas beads	300	Air	He	Luikov, et al., 1968
7	Perlite	77	He	H_2	Luikov, et al., 1968
8	chamotte ceramic*	300	Air	He	Luikov, et al., 1968
9	plastics foam	308	He	H_2	Harper and Sahrigi, 1964
10	plastics foam	308	N_2	He	Harper and Sahrigi, 1964
11	plastics foam	308	CO_2	He	Harper and Sahrigi, 1964
12	Aerogel, pore size 7 μm	300	Ar	He	Swimm, et al., 2009
13	Aerogel, pore size 0.6 μm	300	Ar	He	Swimm, et al., 2009
14	fibrous material (8.73 Kg/ m3)	338	Air	He	Pratt, 1969
15	fibrous material (8.73 Kg/ m3)	338	CO_2	Air	Pratt, 1969
16	fibrous material (8.73 Kg/ m3)	338	F-12**	CO_2	Pratt, 1969
17	fibrous material (24 Kg/ m3)	338	CO_2	He	Pratt, 1969
18	fibrous material (74 Kg/ m3)	338	F-12	He	Pratt, 1969
19	microsphere insulation	300	N_2	He	Cunnington and Tien, 1977
20	packed beds of Uranium	298	Ar	He	Swift, 1966
21	packed beds of Zirconium	298	N_2	He	Swift, 1966
22	Pericalse (MgO)	473	N_2	He	Fedina, et al., 1997
23	quartz sand, Porosity= 39%	300	F-12	Ar	Woodside and Messmer, 1961
24	quartz sand, Porosity= 39%	300	Ar	Air	Woodside and Messmer, 1961
25	quartz sand, Porosity= 36%	300	F-12	Ar	Woodside and Messmer, 1961
26	Berea Sandstone	300	Air	He	Woodside and Messmer, 1961
27	Teapot Sandstone	300	Ar	He	Woodside and Messmer, 1961

* Kind of ceramic with high percentage of silica and alumina

** F-12 is brand name for Dichlorodifluoromethane (CCl_2F_2)

Numerous works have sought a general mathematical model to estimate the effective thermal conductivity of porous media as a function of thermal conductivity of each phase (solid and gas):

$$\lambda_{\text{eff}} = f\left(\lambda_{gas}, \lambda_s, \psi\right) \tag{43}$$

$$\frac{\lambda_{\text{eff}}}{\lambda_{\text{s}}} = f\left(\frac{\lambda_{gas}}{\lambda_s}\right) \tag{44}$$

Big differences are in the literature about the function in eq. (43). Appendix D lists some of most famous models. Developing mathematical models of effective thermal conductivity does not always succeed estimating the filling gas effect. Some of researches (Luikov, et al., 1968; Luu, et al., 1986b) considered the convection effect as interpretation to the discrepancy between calculated and measured results, where (Gusarov and Kovalev, 2009) referred the discrepancy to the rigorous evaluation of Knudsen effect.

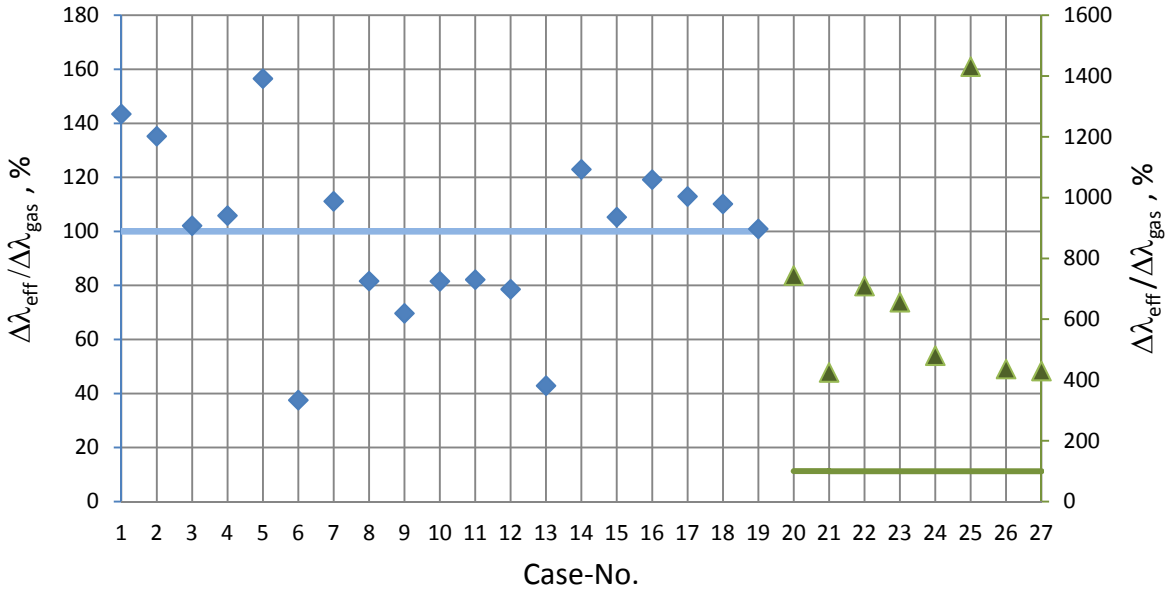

Figure 8 : Evaluation of all study cases by changing the filling gas
blue points referred to left y-axes, green points referred to right y-axes
lines presents the 100 % ratio

Others (Wakao and Vortmeyer, 1971) changed the accommodation coefficient to get good agreements with experimental results, and others (Harper and Sahrigi, 1964; Pratt, 1969) implemented an empirical factor in the model without physical interpretation to the value of this factor. So in literature, there is difficulty in estimating the change in effective thermal conductivity due to change of the filling gas.

3.6 Résumé of Literature Review

Chapter 3 presented a review of more than 100 studies reported in the literature. These were aimed to understand the behavior of filling gas in porous media and which factors affect this behavior. The following conclusions are based on the literature review:

- The Knudsen effect is an important effect which should be helpful in studying the heat transfer in porous media, in particular for micro and nano pore-sized materials and by porous media at low gas pressure

- The developments of models for estimating the gas thermal conductivity in porous media are based on different theories and principles. Disagreement by evaluation the different models are abundant for the following reasons:

    - The improvements of some of these models are done only to estimate the change of the gas thermal conductivity due to change of one of the main parameters like gas pressure (Smoluchowski effect) or pore size (Knudsen effect, e.g. the model for Aerogel by Kistler).
    - The modification of some models yields better agreement with the experimental results (e.g. the quantity 2β in the model by Kaganer).

  - Any generalization of any model should only happen after validation of the model by proofing it with various kinds of materials.
  - The description of the behavior of the rarefied gas, e.g. estimation of accommodation coefficient is complex.

- The geometrical characterization of porous structures through ‘‘mean pore size’’ is imprecise description when the pore size is a significant parameter in determining the rarefaction of the filling gas. The models, where the pore size distribution as parameter is considered, are rare, not mature and not valid to generalization.

- Accommodation effect, as reflected by accommodation coefficient is very important in heat transfer by gas in transition and free molecules regimes. However, it is difficult to determine because of:

  - The scarcity of measured data of accommodation coefficient for such in the literature
  - The developed experimental facility to measure the accommodation coefficient and the predictive models to estimate the accommodation coefficient are not for the solid surface of porous structure of insulation method.

- The estimation of change of effective thermal conductivity of porous media by changing the filling gas has difficulties for the following reasons:

  - Difficulty in estimating gas thermal conductivity in porous media
  - Scarcity of date for accommodation coefficient of the filling gas
  - The coupled effect in conduction between gas and solid phase
  - Temperature dependency of different parameters (gas and solid thermal conductivities, mean free path of gas, viscosity, and others)

Since the direct experimental determining the quantity of heat transfer by the filling gas in porous media is not possible. The estimation method is the only method. Therefore it is very important to choose or develop a proper model for all above mention critical parameters and to validate this model over various materials. This would be the main scope of this work.

PART II: EXPERIMENTAL INVESTIGATIONS

4 Structural Characterization of Materials

4.1 Structure-Controlled Properties

Characterization of the porous structure is necessary to measure the porosity and the pore size distribution. These are needed to evaluate and model the effective thermal conductivity of porous materials. Insulation materials which are based on consolidated particles structure have two different kinds of porous systems: closed and open pore system. Closed pore systems, e.g. like in foam, have very thin membranes and struts that form the cell boundaries in a soap-bubble like structure that enclose the foaming gas. Materials with such structure are described as cellular materials; see Figure 9 (a). The size of closed pores/cells varies in narrow range and described as *regular porous structure*. On the other hand, open pore systems consist of pores that allow the gas to flow through, like in ceramics, and it is called accessible pores; see Figure 9 (b). The complexity in such structure yields to great fluctuation in pore size. The *irregular porous structure* of these materials is depended mainly on the number of substance and preparation process of porous solid (Meyer, et al., 1994).

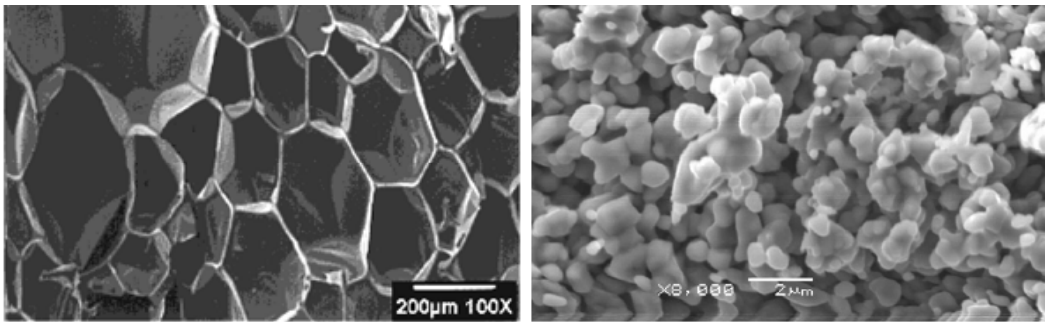

(a) (b)

Figure 9: Scanning electron microscope (SEM) images:
(a) Closed pore System: Polyurethane foam -magnification 100 X-(Newman and Forciniti, 2001
(b) Open Pore system: $CaTiO_3$ ceramics -magnification 1000 X-(Wang, et al., 2010)

The most used preparation methods of porous media with open porosity are (Meyer, et al., 1994):

- Aggregation or agglomeration and formation of networks. For example producing silica aerogel through gel sol process.
- Recrystallization (sintering process) like producing porous aluminum oxide ceramics.
- Subtraction and addition, as in porous glass fabrication.

The pores resulted in such irregular porous structure could be having various forms: (a) blind pores: pores with only one open side, (b) closed pores, which are difficult to be determined through usual characterization methods such as fluid intrusion method, and (c) through pores: pore like continuous canal. The shapes of blind and through pores normally look like ink-bottle-shape (d) or like cone shape (e), see Figure 10.

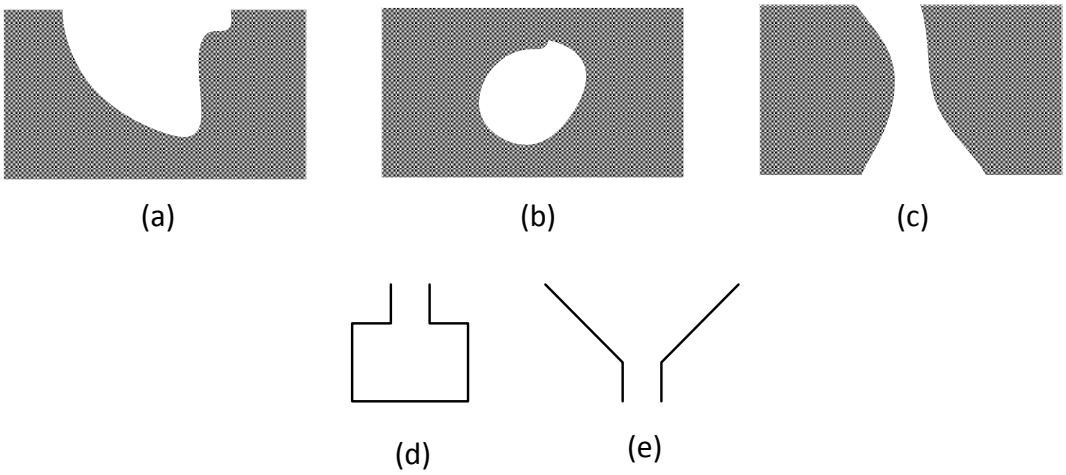

Figure 10: Kind of pores in irregular porous structure: (a) blind pore (b) closed pore (c) through pore (d) ink-bottle shape of blind pore (e) cone pore shape of through pore

Such porous structures are usually characterized through two major categories of parameters:

- **Global characterization parameters:** these give an overall description of the porous media. i.e. open or closed porosity, overall porosity, bulk density, mean pore size, median value of pore diameters and specific surface area.
- **Specific characterization parameters:** these characterize the porous structure in more detail and are usually given as distribution function, e.g. the pore volume distribution or pore size distribution, specific area distribution and pore shape distribution. The last describes the deviation in pore shape from the spherical one.

Measurements and evaluation methods of parameters that are important for further comparison will be discussed in the following two sections.

4.2 Density and Porosity:

Non-porous materials have defined solid density (ρ_s), also termed as true or real density (ASTM D5004, 2009), which represents the mass of the solid matrix divided by the occupied volume. Porous materials are characterized also by bulk density (ρ_{bulk}), which is defined as the mass of the particles divided by the volume they occupy including the space between the particles (ASTM D5004, 2009).

4.2.1 Measurement of Solid (True) Density:

Measurement of solid density is done through using the helium pycnometer. The principle of density measurement using a helium pycnometer is based on the determination of the volume occupied by a known weight of sample in a chamber of known volume using the gas displacement technique. A schematic of gas pycnometer is sketched in Figure 11. The sample of porous media is finely pounded to ensure having a sample free of closed-pores. The produced powder (1) with unknown volume is located in gas chamber (2) and then the gas chamber is closed through the sealed lid (3). The pressure is measured in the gas chamber (4) before the expansion of helium into the external isolated reference chamber (5) with known volume.

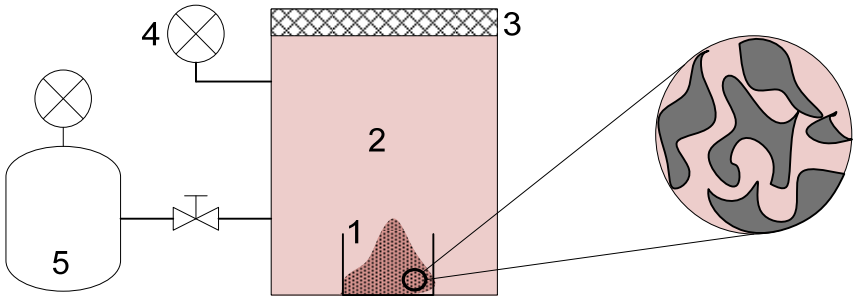

Figure 11: A schematic of gas Pycnometer, the light red color refers to helium

The pressure is measured in the reference chamber (5). The process is repeated without sample inside the gas chamber. The unknown volume of sample is evaluated from the resulted pressure change and by using the equilibrium law (Webb, 2001). This gas displacement technique gives an accurate evaluation of solid density because the helium gas molecules fill all gaps and pores in the sample, see Figure 11. The solid densities of all porous media selected for this study were measured using Accupyc 1330 from Micromeritics©[2] by department IKGB[3]. The results of the densities will be presented later in this part.

4.2.2 Measurement of Bulk Density:

Measurement of bulk density is done according to the Archimedes' principle. First the sample of porous material is weighed in air at room condition. The sample is then totally immersed in mercury vessel. The displaced volume of mercury is equal to the volume of the sample. The advantage of using mercury is that mercury has high surface tension and cannot enter the pores spontaneously. The experimental facility based on the Archimedes' principle was developed by Department IKGB, See Figure 12.

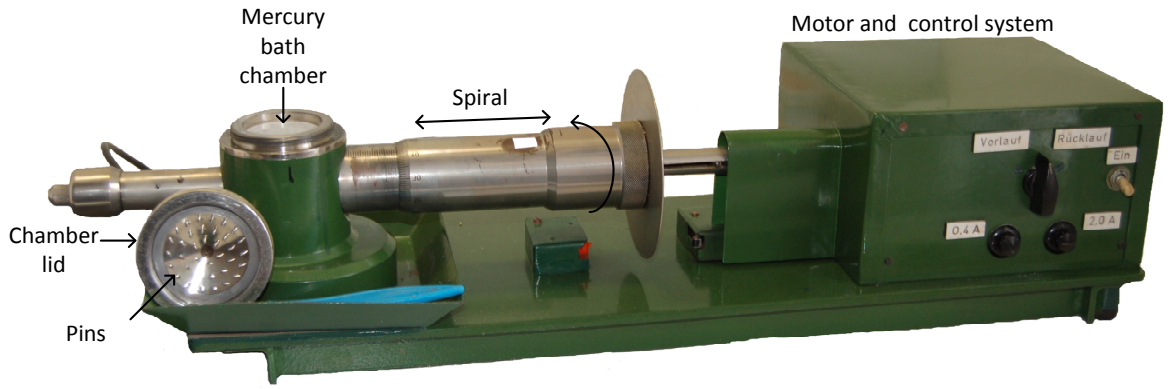

Figure 12: Experimental facility (volume-meter) for bulk density measurement

The sample is situated in mercury bath chamber. Chamber lid is supplied with pins to ensure that the sample will be totally immersed in the mercury bath. It is supplied with additional moveable spiral with a motor. Moving the spiral forward moves up the bottom of the mercury bath chamber. This minimizes the chamber volume continuously until the mercury

[2] www.micromeritics.com
[3] IKGB: department of Ceramic, Glass, and Construction Materials in TU Freiberg, Germany

flows through the cover. Once mercury flows, a sensor implanted in the cover will immediately stop the movement of the spiral. The volume of the displaced mercury is determined precisely by reading the volume scale on the spiral.

A different method offered from Micromeritics © to evaluate the bulk density used free-flowing dry powder as an alternative displaced medium for measuring the volume of porous media. However, the precision of this method is strongly dependent upon the diameter of powder.

4.2.3 Evaluation of Overall Porosity:

Porosity (ψ) is the ratio of the volumes of the pores to the total volume occupied by their envelope (ASTM D3766, 2008). Regarding to (DIN EN 993-1, 1995) porosity is calculated as following:

$$\psi = \frac{V_{pores}}{V_{total}}\ 100 = \left(1 - \frac{\rho_{bulk}}{\rho_s}\right)\ 100 \tag{45}$$

The experimental results of the solid and bulk density are used for determining the porosity of the investigated materials. Since the solid density is measured for the sample without closed pores, the evaluated porosity regarding to eq. (45) is the overall porosity.

4.3 Pore size distribution:

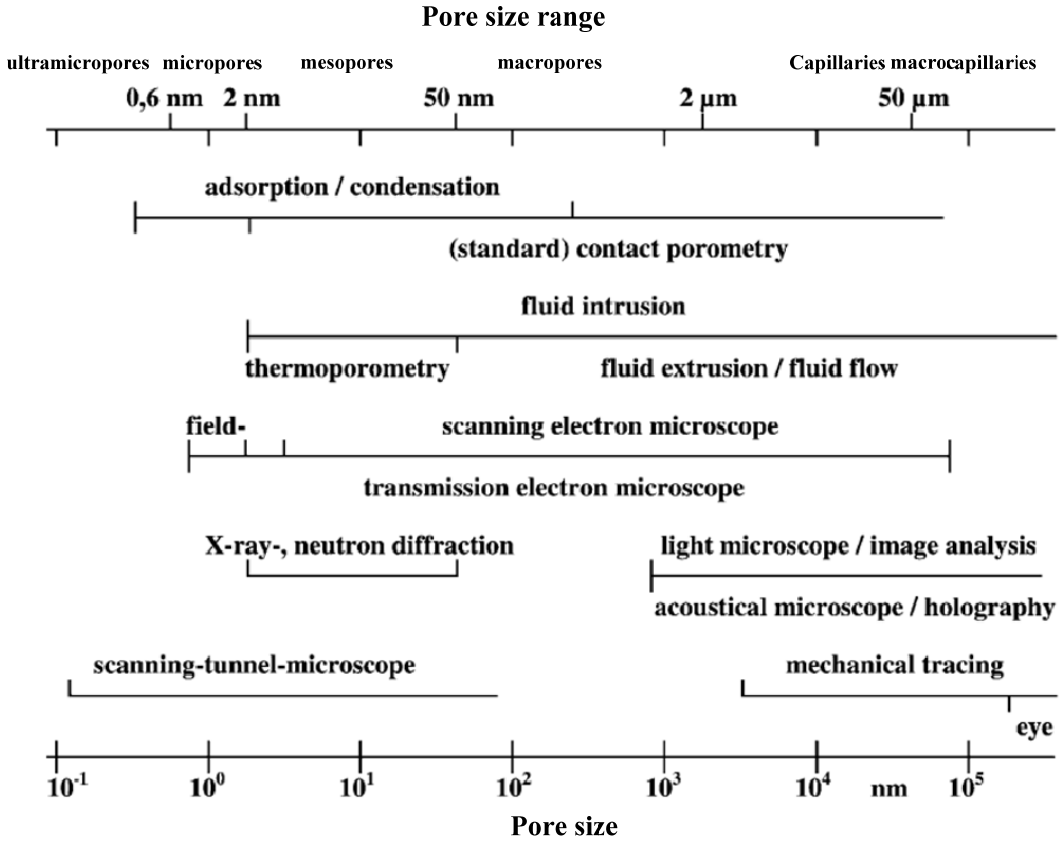

Figure 13: Overview of methods for determining the pore size distribution, (Dabrowski, et al., 2003)

Pore size distribution is a probability function that describes the relation between the quantities of pore sizes or pore size classes and the pore size. There are many methods with different principles to determine the pore size distribution. Each method is valid in a limited range of pore size. An overview of all methods is presented in Figure 13

The chosen method to determine the pore size distribution is the mercury porosimetry, which is based on fluid intrusion method. This method is applied in a wide range of pore size, see Figure 13, and it is recommended for the investigated materials in this work. In the following subsection more details and limitation of this method are discussed.

4.3.1 Mercury Intrusion Porosimetry (MIP):

Mercury intrusion porosimetry is based on the physical principle that a non-wetting fluid will not enter the pores under capillary attraction, but it will only intrude the pores or capillaries by applying an external pressure. A fluid is considered a non-wetting fluid when having a contact angel greater than 90°. Mercury has a contact angle (Θ) varying between 130-145°, which depends on the material of solid surface and temperature (Ellison, et al., 1967). The size of intruded pores is inversely proportional to the applied pressure, and this relation is described by Washburn equation (Abell, et al., 1999):

$$\mathrm{d} = \frac{-4\gamma_{\mathrm{ten}} \cos \Theta}{\mathrm{p}} \tag{46}$$

Where d is apparent diameter of pores, p is applied pressure, γ_{ten} is surface tension of mercury, and Θ is contact angel between mercury and the solid.

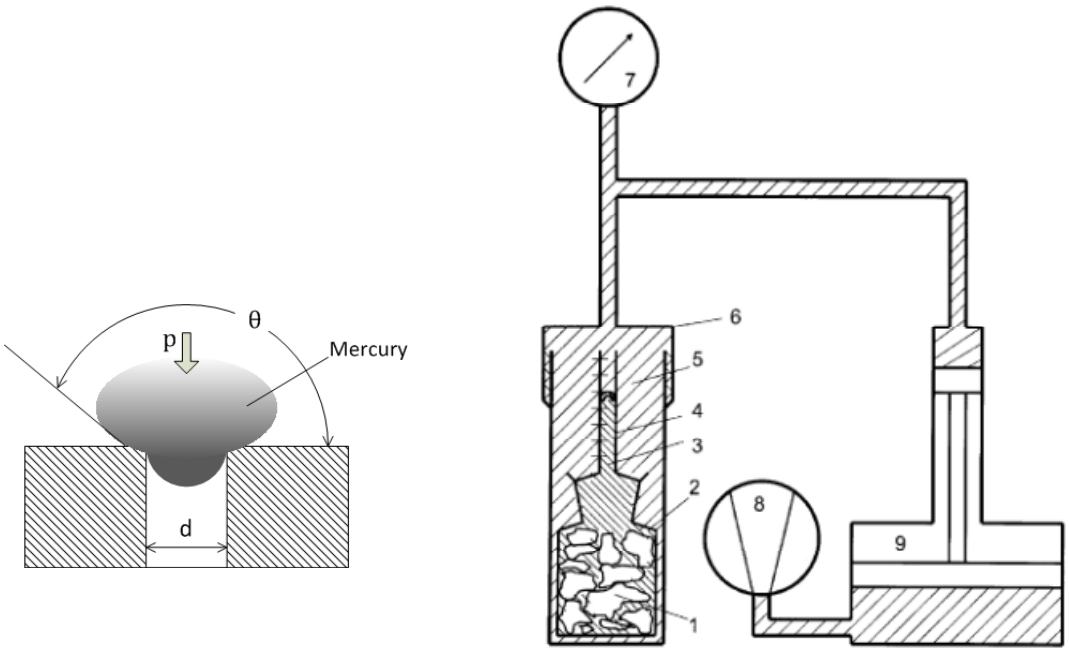

(a) (b)

Figure 14: (a) Mercury instruction to one cylindrical pore.
(b) Mercury intrusion porosimetry (Dabrowski, et al., 2003): 1 sample, 2 Sample vessel, 3 mercury, 4 graduated capillary, 5 hydraulic fluid, 6 autoclave, 7 pressure gauge, 8 pump, and 9 hydraulic pressure intensifier.

The Washburn's equation, eq. (46), is based on the cylindrical model of pore, see Figure 14 (a). Mercury intrusion porosimetry uses a hydraulic fluid, usually oil, to produce the high pressure of mercury which is required to intrude the very small pores, see Figure 14(b). The oil will be supplied to the porosimetry through hydraulic pump (8) and oil intensifier (9). The oil (5) goes through the graded capillary (4) and transmits the pressure to the mercury (3). The latter fills out the sample vessel (2) and depending on pressure, mercury intrudes some of the pores in the sample (1).

The MIP is widely used because it is fast to get information about the microstructure of different materials using this method. It has also no complexity in preparation of the sample. However this method has many limitations arisen from the physical principle of the intrusion method and the evaluations regarding the Washburn's equation. These limitations are:

- The volume of pores that are completely enclosed will not be determined. The volume of pores that have a shape like ink-bottle, see Figure 10, will be incorrectly measured. The measured size of such pores will be equal to a small constriction of the bottle. This effect is called ''ink-bottle-effect' (Rutledge, et al., 2009).
- Washburn's equation is developed for cylindrical shape of pores. Whereas real structures in some cases have a big deviation from cylindrical shape.

Therefore many researchers tried to evaluate the error in this method by comparing its experimental results of some materials with results evaluated by other structural analysis method like scanning electron microscopy (SEM). In many studies a deviation from SEM results was detected (Abell, et al., 1999; Diamond, 2000). Abell, et al., 1999 used the Wood's metal, low temperature casting metal with a melting point of approximately 70 °C, instead of mercury as intrusion fluid, this combined with SEM gives better evaluation of pores that have ink-bottle shape. Whereas Kaufmann, 2009 applied combined method of MIP and Wood intrusion porosimetry to evaluate the volume of ink-bottle shaped pores.

Recently a new method based on pressurization–depressurization cycling of mercury was developed by Zhou, et al., 2010, which gives better estimation of pore size distribution. Ye, 2003 discussed in his dissertation many structural analysis methods and mentioned that each method has its limitations. The classical MIP is already standardized in different countries (Robens, et al., 2002), so it has been chosen to evaluate the pore size distribution. The measurements were performed by using MIP produced from Thermo scientific[4], department IKGB, which works in pressure range from 0.016 to 400 MPa.

4.3.2 Evaluation Process and Presenting the Experimental Data:

The output data of MIP measurements are used to evaluate different parameters, to characterize the porous media i.e. pore size distribution, mean pore diameter, minimum and maximum pore size and specific surface area. The applied pressure increases continuously until the maximum limit of pressure range. The volume of intruded mercury is recorded at the different pressures. The pressure is also recorded. The recorded data could be presented as cumulative distribution function, which describes the probability distribution of pore size,

[4] http://www.thermoscientific.com/

see Figure 15. The curve in Figure 15 describes the relation between the intruded volume of mercury and the logarithmic scaled applied pressure.

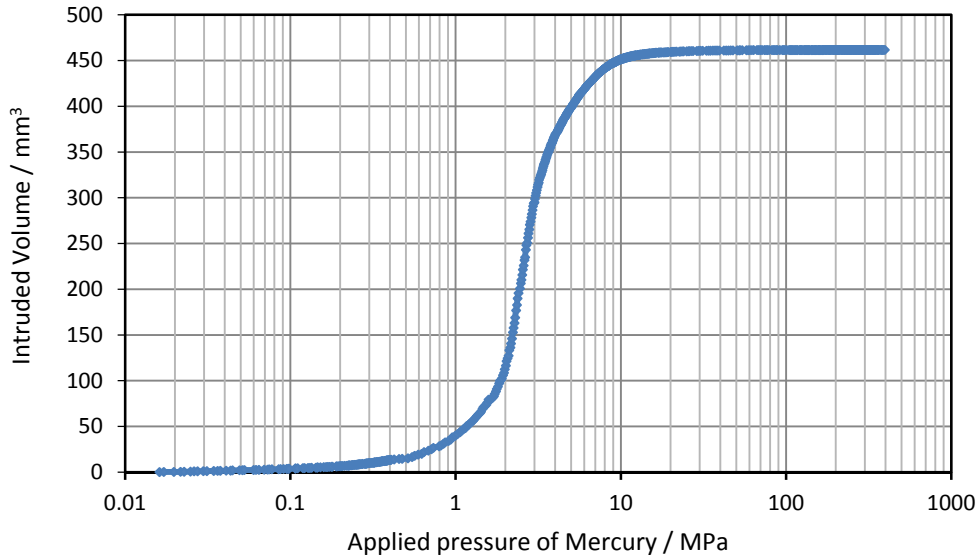

Figure 15: Measured data for one of the materials in this study; the output data of MIP as cumulative distribution function

However this curve is only an example taken for a material of the twelve materials which will be later presented. The trend of the curve could be totally different, as we will see later. The diameter of pores, also called pore size, will be evaluated through the Washburn's equation, eq. (46). The volume could be normalized to be unity by maximum intruded volume. Evaluating the intruded volume as percentage simplifies reading such diagrams. The results of these evaluations are presented in Figure 16 .

The detection of pore size begins with bigger ones, corresponding to applying low pressure of mercury. By increasing the pressure, smaller pores will be detected and so on until reaching the maximum pressure, which determines the smallest pore size that is intruded by mercury, see Figure 16. A defined pore size d_x on the curve in Figure 16 gives the volume fraction V_x of the sample which has pore sizes bigger than d_x. The residue of volume has pore sizes equal or smaller than d_x. The output data could be also presented as probability density function. This is helpful to determine the frequent pore size range. The density distribution function is determined by dividing the cumulative distribution function into many ranges (d_{x-1}-d_x) and calculating following ratio for each range:

$$f(\log(d_x)) = \frac{d(V)}{d\log(d)} = \frac{V_x - V_{x-1}}{\log(d_{x-1}) - \log(d_x)} \tag{47}$$

The density distribution function for the above material is calculated and presented in Figure 17. The absolute value of volume is taken to calculate the ratios in eq. (47). Specific volume (Volume / weight) could be used instead of volume.

The high frequent pore size range could be defined by the area under the density distribution curve, as it is equal to 90 % of the overall area, see Figure 17.

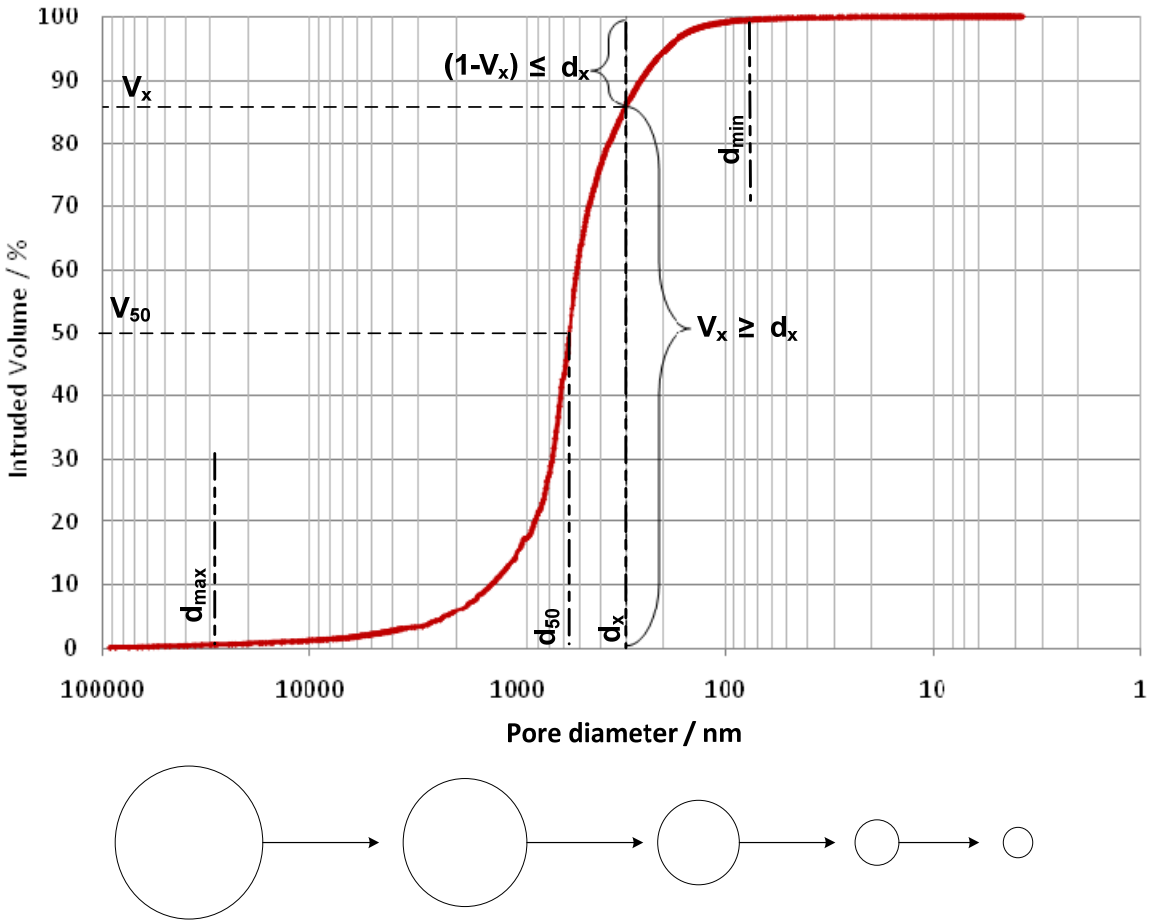

Figure 16: Evaluation of cumulative distribution function of pore size

Many parameters could be evaluated depending on the resulting data of pore size distribution:

- Median pore size (d_{50}): it is evaluated by determining the pore diameter as the intruded volume reaches 50 % of the total intruded volume, see Figure 16. In some porous media which has pore sizes distributed as normal distribution, the median pore size is the same as the mean pore size (d_{mean}). Whereas for other porous systems the mean pore size could be determined mathematically by evaluating the weighted mean value as following:

$$d_{mean} = \frac{\sum_{i=1}^{k} d_i V_i}{\sum_{i=1}^{k} V_i} \tag{48}$$

- Minimal and maximal pore size (d_{min}, d_{max}): these could be detected while increasing the pressure of mercury and the change of relative intruded volume is less than 0.5 %. The minimal and maximal pore size are sketched in Figure 16.

- Most frequent pore size (d_{freq}): corresponds to the maximum of density distribution function, as sketche Figure 17.

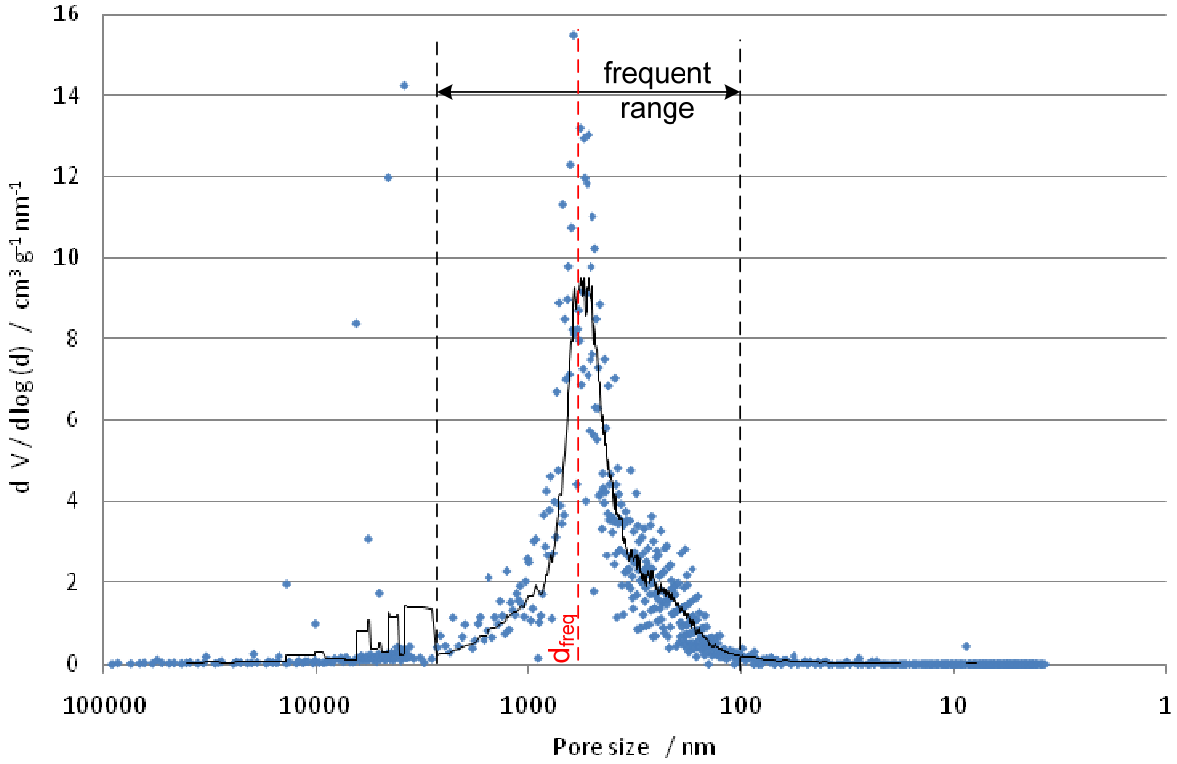

Figure 17: Evaluation of density distribution function of pore sizes

4.4 Summary of Chapter 4:

Understanding and characterization of the microstructure of porous insulation materials are very important in analyzing their thermal behavior. In this chapter the criteria for choosing the investigated materials are discussed. Studying and characterization of the porous structure were reviewed.

Additionally, the principles of chosen experimental facilities for investigation of the porous structure were explained. The limitations of each method were discussed. Evaluation processes are depicted for the different structural parameters: solid and bulk density, overall porosity, pore size distribution, median and mean pore size, minimal and maximal pore size, and most frequent pore size. The results of characterization procedures will be presented in a later chapter.

5 Effective Thermal Conductivity Measurements

5.1 Survey of Methods for Measuring the Thermal Conductivity of Insulation Materials:

Since the 19th century, evaluation and developing of methods for measuring the thermal conductivity of insulation material have been a topic for many studies. These methods are generally categorized into steady state methods and transient methods. Steady state methods are based on establishing a temperature gradient over the sample which is not changing with time. Transient methods depend mainly on transmitting energy to or from the sample and evaluating the time dependent temperature change during the heating up phase.

In the last two decades many researches and developments have been focused on transient methods. The common used techniques in this category are the transient hot wire, laser flash thermal diffusivity apparatus and transient-Plane-source method (hot disk method). These test methods have large advantage concerning time. They are quickly and need short time to deliver results about the thermal properties of material. However, some of these methods have their limitations, for example hot wire technique is not a suitable for measuring the thermal conductivity of anisotropic materials, such as exist in some fibrous material (Wulf, et al., 2007). Applying the laser flash method to porous media is faced with many difficulties, as found later in this study, see chapter 6. A recent intensive work with hot disk method to measure the effective thermal conductivity of ceramics foams shows many limitations of this method by applying it to porous media (Götze, et al., 2012). Thus, steady state methods are still the reference methods for measuring thermal conductivity of porous media.

Measuring thermal conductivity using steady state method is performed by applying a heat flux to a known geometrical configuration of the sample. There are three kinds of steady state configurations in regard to the geometry: plate, cylindrical and spherical , see Table VI.

In some specialized literature the axial heat flow apparatus is classified also as another kind of steady state method. However, it has the same principle as plate, which is considered as an axial heat flow apparatus. Therefore, only the plate configuration will be mentioned later on.

As seen in Table VI, all principles depend on generating a temperature gradient across the sample by using a heater and a cold sink. Thermal conductivity is evaluated by solving the Fourier differential equation of the suitable coordinates system by defined boundary conditions. The solutions are tabulated in last line of Table VI. The required parameters to evaluate thermal conductivity in the different geometrical configurations are easily understandable: heat flow, temperature difference, and characteristic dimensions. However, realization of these principles by building the necessary facilities involves numerous technical problems and challenges. Some of these technical challenges are: to guarantee that the actual amount of flowing heat flux through the sample is being accurately measured; the accuracy of temperature measurement and preparation of the sample. Each geometrical configuration has advantages and disadvantages. For examples, the spherical system has a big advantage because it has no edge losses.

Table VI: Geometrical configurations for the steady state measurements of thermal conductivity

Kinds of Steady state methods	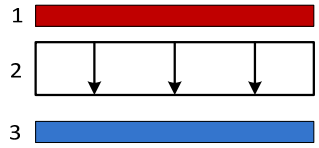 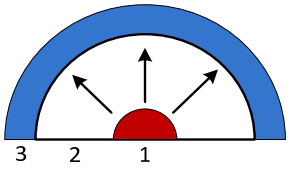 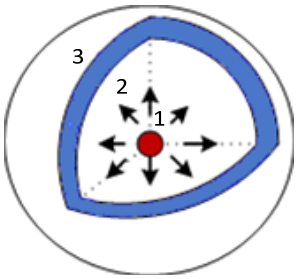 1: heater, 2: sample and 3: heat sink		
Geometry	Plate	Cylinder	Sphere
Dimensions	1D	2D	3D
Name of apparatus	Guarded hot plate apparatus (GHPA)	Radial heat flow apparatus (RHFA)	Spherical heat flow system (SHFS)
Evaluation thermal conductivity	$\lambda = \frac{\dot{Q}}{\Delta T\, A}\, S$	$\lambda = \frac{\dot{Q}}{2\pi\, \Delta T\, l} \ln \frac{r_a}{r_i}$	$\lambda = \frac{\dot{Q}}{2\pi\, \Delta T} \left(\frac{1}{d_i} - \frac{1}{d_a}\right)$

Thus, it is easier in terms of building regulation system and it provides better accuracy in evaluating thermal conductivity comparing guarded hot plate. The latter one needs many guarded heaters to overcome the heat losses. However, the spherical system comes with many disadvantages: like building a spherical heater, construction of spherical sample and determining the location of the temperature measurement.

Most of porous insulation materials are produced as plates. Thus, the guarded hot plate method is the most commonly used method for measuring thermal conductivity of such materials. It is considered as a reference method and it is standardized by many countries (DIN EN 12664, 2001 ; ASTM C177-10, 2010) as well as in international standards (ISO, 1991). However, guarded hot plate apparatus (GHPA) with possibility to change of gas atmosphere was not available in the Institute for Thermal Engineering, TU Freiberg, when this research has begun. However, the development of GHPA for investigating Knudsen effect will be described at the end of this dissertation. In the current research, the thermal conductivity of porous insulation materials will be mainly measured by using radial heat flow apparatus (RHFA), which also has its advantages. Details about using RHFA, criteria, limitations and evaluation procedure will be discussed in the next subsections of this chapter.

5.2 Radial Heat Flow Apparatus (RHFA)

5.2.1 Principle of Measurement

In literature, radial heat flow apparatus is used often in measuring thermal conductivity of nonconsolidated materials as packed beds (for example see le Donne, et al., 2000). However, it is used also for measuring porous insulation such as fibrous materials (Vishnevskii, et al., 1975) and ceramics (Godfrey, et al., 1965). A major use also of RHFA is to measure the thermal conductivity of pipe insulation materials (ASTM C335, 2003). The applied principle of RHFA is always the same regardless of the use. A sketch to explain the principle is drawn in

Figure 18. A concentrated heater (1) supplied with electrical power (P_e) produces heat flux that flows through a cylindrical formed sample (2). The sample is surrounded by insulation powder (3). The heat sink (4) is cooled through fluid (usually water). It is important to guide the direction of heat flux and to control the cold side of the sample and the boundaries to maintain a steady state. The temperatures (T_1, T_2) in the midplane are measured through thermocouples (5) positioned at (r_1, r_2) in the sample. The thermal conductivity of the sample is evaluated using the following equation (49):

$$\lambda = \frac{P_e}{l} \frac{\ln(\frac{r_2}{r_1})}{2\,\pi\,(T_1 - T_2)} \tag{49}$$

The above presented principle is the easiest arrangement for such apparatus. Moore discussed in more details further developments such as the installation of a muffled heater or an edge heater and their influence on measurement errors in RHFA (Moore, 1984). The developed radial heat flow Apparatus (RA1) by Institute for Thermal Engineering in TU Freiberg is based on the same above presented principle with a major difference. The heat flux in typical RHFA is evaluated by measuring the electrical power, while in RA1 a guarded water calorimeter system is installed instead of the heat sink to measure the heat flow in the metering range. More details will be described in the next subsections.

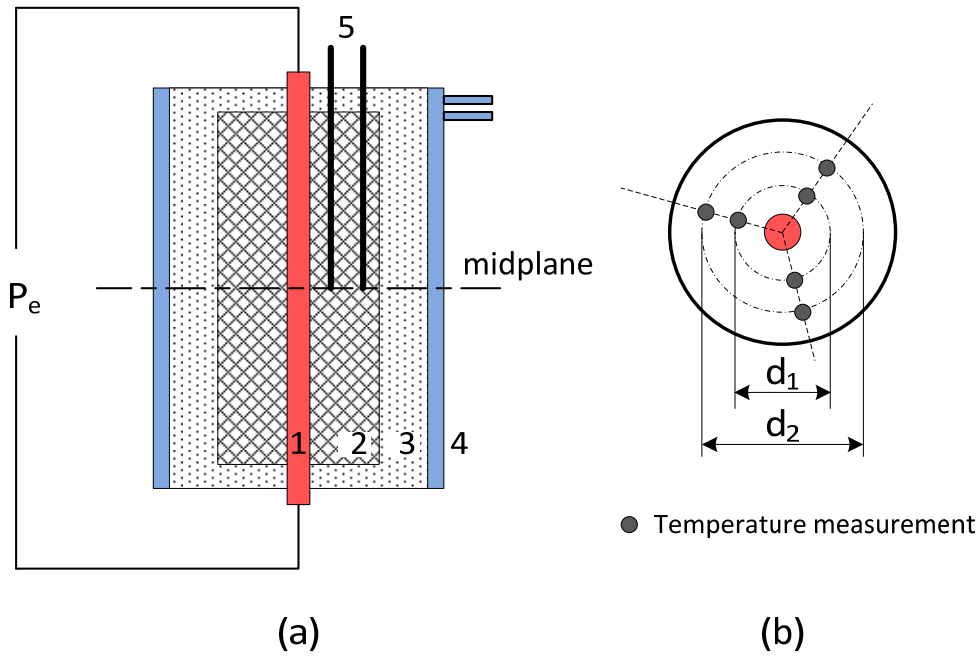

Figure 18: (a) General principle of RHFA; 1 heater, 2 sample, 3 insulation, 4 heat sink, and 5 Thermocouples. (b) Position of Thermocouples in the sample

5.2.2 Description of the Applied RHFA (RA1):

The design of RA1 was developed in the Institute for thermal engineering, TU Freiberg, in order to measure the thermal conductivity of different ceramics and insulation materials with cylindrical geometries in different gas atmospheres. A 3D graphic of RA1 is presented in Figure 19. The apparatus consists of main cylindrical enclosure (1) to form a gas chamber and also a furnace with the ability to open through top and bottom lids. The lid closes the gas chamber (1) using screws, and the seals (2) ensure better impermeability of the apparatus. The apparatus is supplied with a calorimeter system (4) consisting of three calorimeters with many inlets and outlets (8). The calorimeter system (4) is curled up on the outer surface of enclosure (1) and brazed to by using aluminum, to ensure better thermal contact. The calorimeter system is also isolated, but the insulation is not presented in Figure 19. More details about the calorimeter system (4) will be discussed later. The chamber (1) contains many openings: e.g. (3) for passing out the thermocouples, (5) for emptying the insulating powder, (7) and (9) as gas inlet and outlet. The sample and heating system are located in the core of the cylindrical enclosure. They are in the right part of the Figure 19.

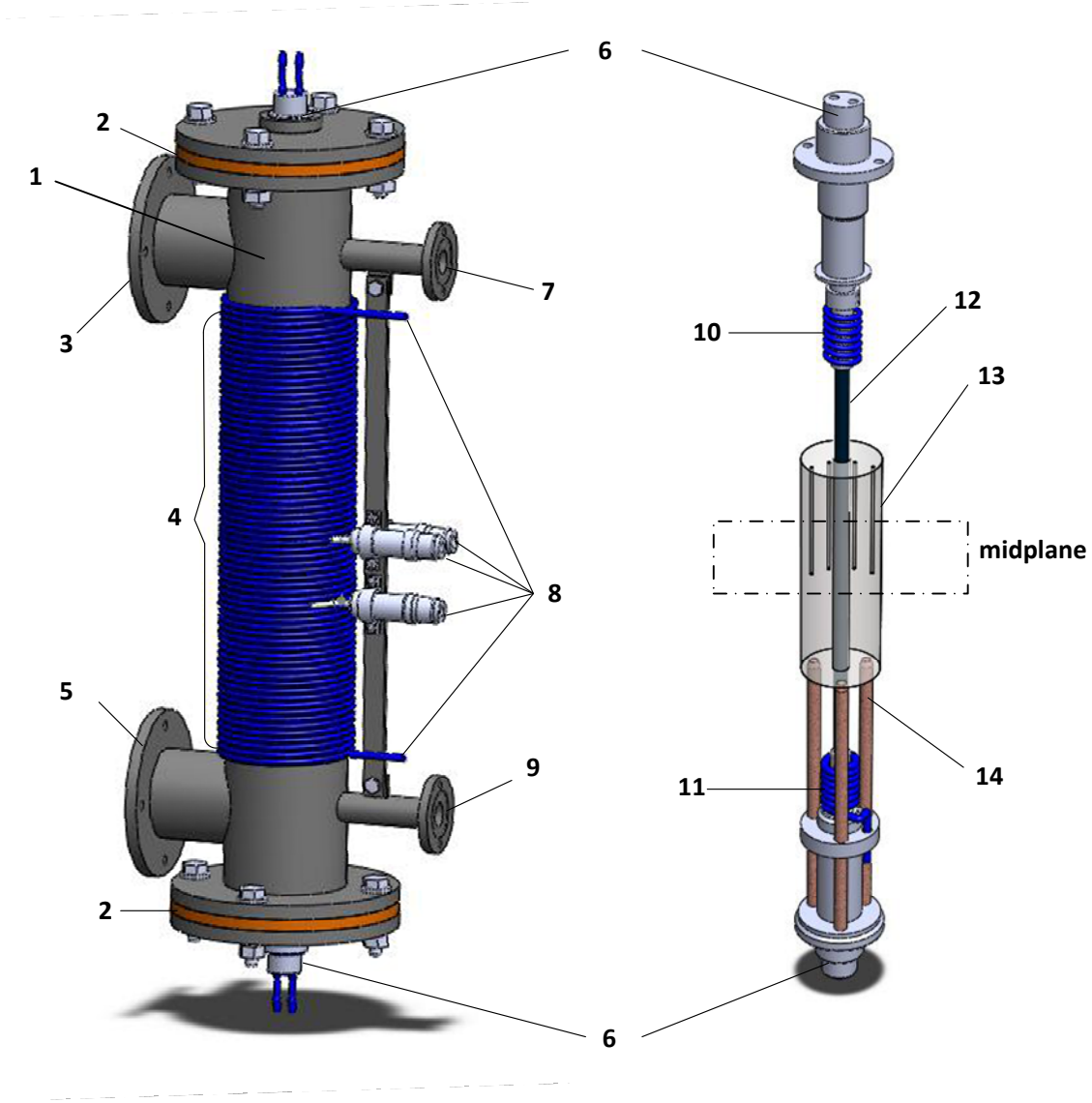

Figure 19: 3D graphic of the applied radial heat flow apparatus (RA1), developed by Institute for Thermal Engineering, TU Freiberg, the numbered parts are referred above in text (not to scale)

The space between the core and the enclosure is filled with corundum (a powder of aluminum oxide). In Figure 19, the graphite heating rod (12) constitutes the center of the apparatus. The rod (12) is electrically connected through the lids. The electrical connections (6) are isolated and cooled by water (10, 11). The sample (13) is located vertically in the middle of the apparatus; this is achieved through a ceramic sample holder (14).

A more detailed illustration of the RA1, such as Measuring and gas/water supplying cycles is presented in Figure 20.

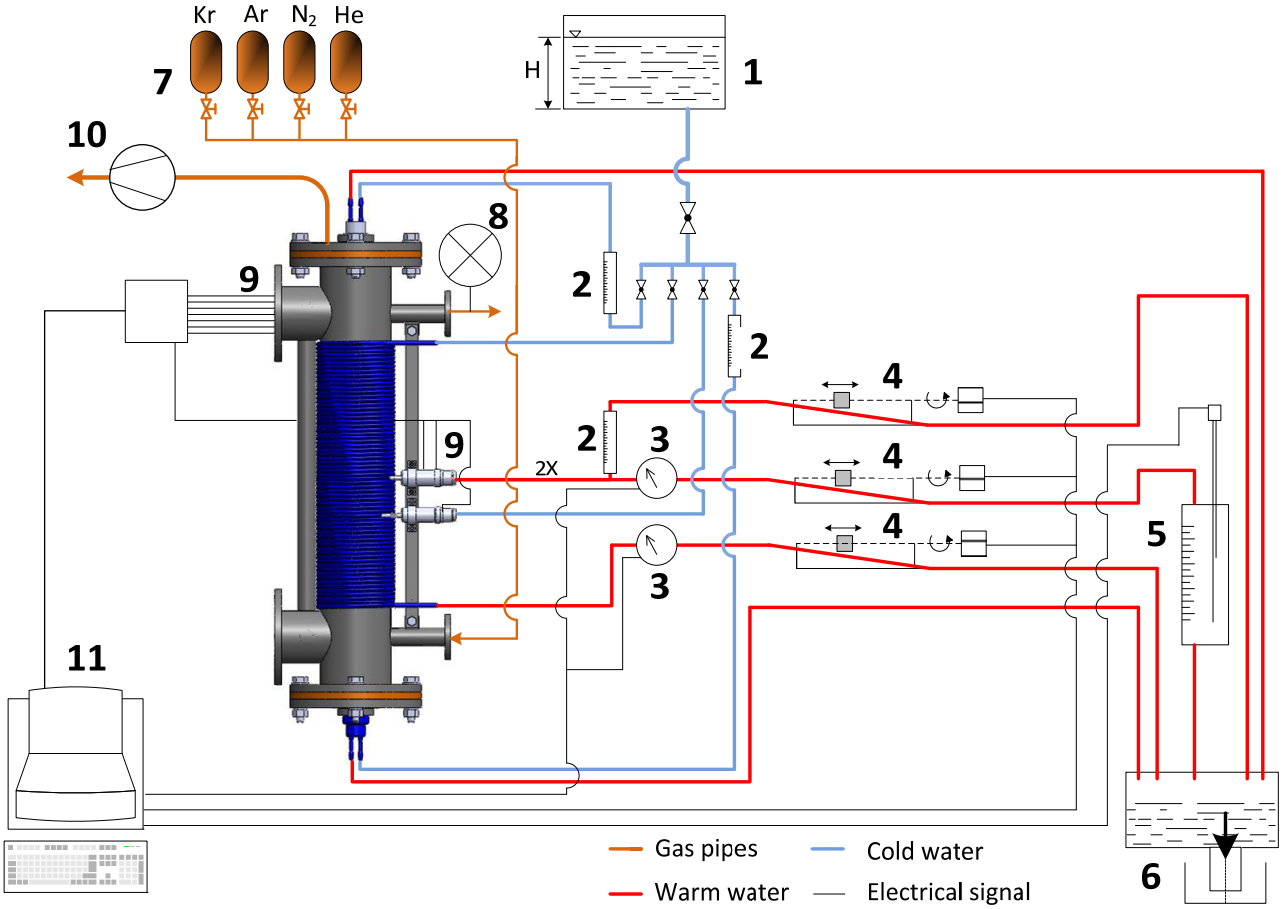

Figure 20: Measuring and supplying cycles of radial heat flow apparatus (RA1).
1 water tank, 2 water flowmeter, 3: water flowmeter with measuring signal, 4 regulator of water volume flow, 5 a gage for measuring the volume flow, 6 outflow, 7 gas supplying system, 8 manometer, 9 thermocouples, 10 vacuum pump, and 11 two computers.

The water tank (1) is always refilled to keep a defined height of water column (H), see Figure 20. This ensures the same water pressure in the cycles and avoids the fluctuation in the water network. A Flowmeter (2) measures the flow of the cooling water in the electrical connection of the heating rod. The flow is adjusted through a ball valve to provide the same flow in top and bottom coolants in order to keep symmetry of the temperature field in the chamber. The flow in three calorimeters is measured by using flowmeter (3) except for the upper one which is measured through (2). Control of water volume flow in the three calorimeters cycles is achieved through regulator (4). In the end (4) is a mechanism based on throttle principle. This works by moving a piston using a step motor controlled by computer (11). A gage (5) is installed on the metering calorimeter cycle for measuring the

volume flow. It consists of a vessel with an electrical sensor connected to computer (11) to measure the time that water needs to fill a defined volume. The gas is supplied through gas cylinders (7). The apparatus is evacuated with a vacuum pump (10), which is used mainly to change the gas atmosphere. A manometer (9) shows the momentum pressure inside the chamber during the measurements. The different temperatures are measured through many thermocouples (9) i.e. seven thermocouples inside the sample, four at the water inlet and outlet, and two thermal chains. Two computers (11) are connected to the entire system. One records the different data (temperatures, temperature differences, and volumes flows). The other is responsible for controlling. An overview of all specifications of RA1 is tabulated in Table VII.

Table VII: Specifications of RA1

Principle	Radial heat flow (Steady state)
Specimen geometry	Hollow Cylinder
Specimen length	180 mm
Specimen diameter	60 mm
Range of temperatures (hot side)	150 – 1450 °C
Gas pressure	Low vacuum- 1 bar
Gas atmospheres	Xe, Kr, Ar, N_2 or He
Uncertainty at 500 °C[5]	approx. 5%

5.2.3 Preparation of Samples for Thermal Conductivity Measurement:

Samples for thermal conductivity measurement are prepared from the 12 different porous insulating to be suitable for RA1. Three parts, each one is a Hollow cylinder (with 60mm, 12mm, and 60mm as the length and inner and outer diameters, respectively), are cut out from each material.

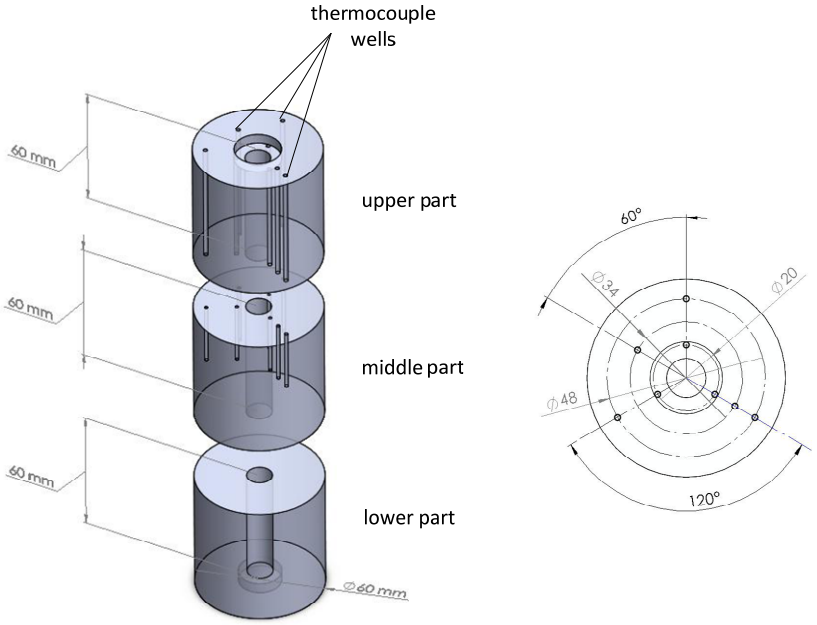

Figure 21: Geometry of the sample for RHFA and positions of thermocouple wells

[5] evaluated from different measurements performed by RA1. The calculation-algorithmus for uncertainity is presented in previous work (W. Fütterer, Diplom-Thesis, TU Bergakademie Freiberg, 2005)

Eight thermocouples wells are spread at three different diameters (20 mm, 34 mm and 48 mm) and along four different axes, as shown in Figure 21. The thermocouple wells with a radius of 1.5 mm are drilled in the upper and middle parts of the sample until the midplane as seen in Figure 21. Samples from some materials are tempered before performing the measurements. The data of the tempering process will be presented in the chapter 7.

5.3 Experimental Procedure:

The experimental procedure begins with the gas circulation process after installing the sample in RHFA and positioning all thermocouples. The gas circulation process is composed of three evacuation and filling operations. The apparatus is filled following each evacuation operation with the wanted gas atmosphere. This ensures that all pores are filled with the wanted gas. The measurements of thermal conductivity are performed over a range of temperatures. The upper limit of this range is defined by maximum heat resistance of each material. Several temperature levels (at least three) are taken between minimum and maximum temperatures to measure thermal conductivity. The intermediate levels are helpful to get good interpolation of thermal conductivity over the measurement temperature range. The heating rod produces the required thermal energy to reach the desired temperature levels. The thermal steady state of apparatus is reached by regulating electrical power supplied to the heating rod. At a defined temperature level the data needed to calculate thermal conductivity are recorded at three different volume flow rates of water in the metering calorimeter. The measurement is repeated three times at each volume flow. Hence, for each temperature level, the heat flow rate and thus thermal conductivity is evaluated nine times. Three parameters In RA1 should be determined in order to evaluate the thermal conductivity: exact positions of thermocouples, Temperatures and heat flow:

- Examination of radial positions of the thermocouples
- Measuring the temperatures in sample
- Measuring the heat flow through calorimeter system

5.3.1 Examination of Radial Positions of the Thermocouples

Examination of positions of the thermocouples is important because the radial temperature gradient is large and thus any small change in position will lead to a significant change in the measured temperature, as seen below in Figure 22 (b). The positions of thermocouples are usually defined and measured during the drilling process of wells when preparing the samples. Examination of these positions is performed by measuring the radial displacements between thermocouples using a caliper. Sometimes these displacements are measured in midplane. This is possible by slicing the sample along the midplane after finishing the thermal conductivity measurement.

5.3.2 Measuring the Temperatures in Sample

The temperature is measured using type K thermocouples calibrated in temperature range from 30 °C to 1050 °C. Temperature in the sample is measured at seven different positions spread in three cylindrical surfaces S1, S2 and S3, as shown in Figure 22(a). There are at least two thermocouples in each surface. The radial temperature differences are evaluated across the sample between the three isothermal surfaces (S1, S2 and S3). That enables us to

evaluate thermal conductivity in three layers: the inner layer (S1-S2), the outer layer (S2-S3) and the combined layer (S1-S3).

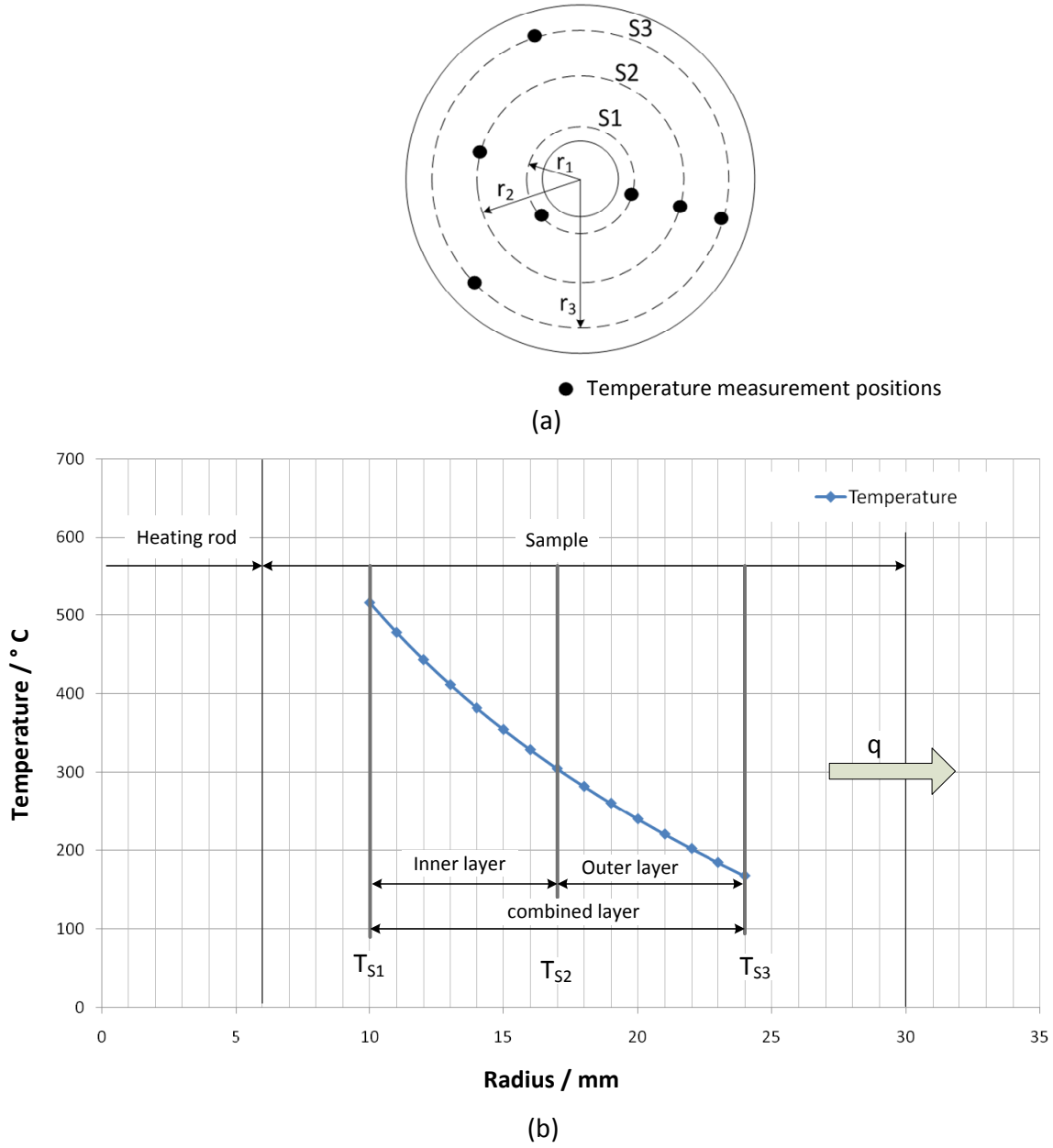

Figure 22: Cross sectional view of the sample with (a) positions of the thermocouples and (b) temperature gradient

5.3.3 Measuring the Heat Flow using Calorimeter System

Measuring the radial heat flow that passes through the sample using calorimeter system is based on first law of thermodynamic. The change of internal energy of the circulation fluid (water) is equal to the amount of heat that is fed into the system without heat losses. The heat flow is calculated as following:

$$\dot{Q} = \rho_w \dot{V} C_{p,w}(T_{W_{out}} - T_{W_{in}}) \quad (50)$$

The properties of water (density and heat capacity) are taken from data sheets of water at the mean temperature between inlet and outlet temperatures.

The calorimeter system in RA1 consists of three calorimeters: metering calorimeter (C_0), lower guarded calorimeter (C_1) and upper guarded calorimeter (C_2), see Figure 23. The guarded calorimeters are installed to avoid the axial heat flux and insure that temperature difference in the axial direction is equal to zero through plane 1 and plane 2 as sketched on Figure 23.

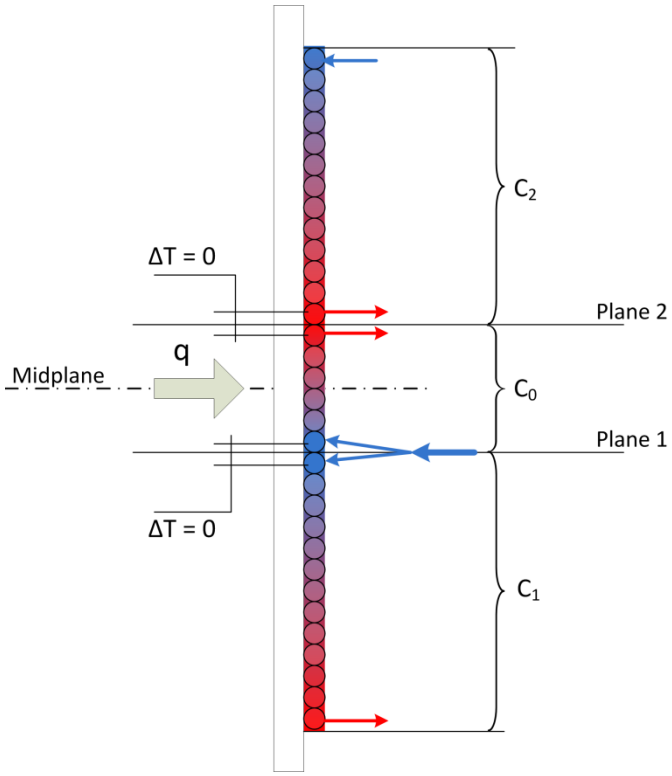

Figure 23: Guarded Water calorimeter system in RA1 (not to scale)

Water flow in the metering and lower guarded calorimeters with same inlet temperature and same volume flow rate let the temperature difference through plane 1 equal to zero. Whereas the volume flow rate in the upper guarded calorimeter should be much greater than in the metering calorimeter in order to reach zero temperature difference through plane 2. Fulfilling these two conditions is done through the regulation and controlling cycle as above mentioned, see Figure 20. In steady state, and with the two guarded calorimeters conditions satisfied, the following parameters are recorded for the evaluation of the heat flow: the temperature difference between inlet and outlet in the metering calorimeter through thermocouples chain and the volume flow through the gauge (5) in Figure 20.

5.3.4 Data Reduction:

Steady state measurements of the guarded hot plate and radial heat flow types regularly yield averaged thermal conductivity data which usually vary with the applied temperature

range. This requires the evaluation of the so called “true” effective thermal conductivity which typically follows eq. (51) for highly porously materials:

$$\lambda_{\text{eff, true}}(T) = a\sqrt{T} + \frac{b}{T} + c\,T^3 \tag{51}$$

This equation is based on a parallel heat flow model where the first term represents the contribution of gas conduction, the second one represents solid conduction in a well-ordered material, and the last one represents radiation heat transfer. It should note that eq. (51) do not consider the interaction between these contributions. The measured effective thermal conductivities are the integral mean values of the true ones

$$\bar{\lambda}_{\text{eff}} = \frac{1}{\Delta T}\int_{T_2}^{T_1} \lambda_{\text{eff, true}}(T)\,dT \tag{52}$$

where T_1, T_2 are the temperatures of hot and cold sides of the sample, respectively. Data reduction for an entire series of measurements at various temperatures enables least-square approximation of constants a, b, and c in eq. (51). This method is discussed in details in (Wulf, 2009), also a standard practice for application this procedure for calculating the thermal transmission properties is published from ASTM, see ASTM C1045-07 .

5.4 Improvements in Experimental Procedure and Evaluation Process in RA1

The experimental procedure in RA1 contains many parameters which should be optimized in order to reach better accuracy in the measurements of the different porous insulation materials. Many factors should be considered or calculated during the evaluation process of the data produced from the measurement by RA1. In the following subsections all these improvements in experimental procedure and evaluation process of RA1 will be presented.

5.4.1 Two-Layers Measurement System

In the past, temperature was measured between two surfaces, and evaluation process in RA1 was performed for one layer samples, which is mentioned above as ‘‘combined layer’’. In this work, the samples were prepared with two layers system. The advantage of such system is that it produces more data of thermal conductivity expanded over larger temperature range. That yields to a smaller residual error in evaluating the true thermal conductivity and better extrapolation over the temperature rang. This could be explained by taking an example for the evaluation of the true thermal conductivity of one of the investigated material in this work, see Figure 24. The material is measured in RA1 by nitrogen atmosphere in temperature range 300 °C – 650 °C for the hot side. The true thermal conductivity is evaluated using the equations (51, 52). It is evaluated once using one-layer system and then using two-layers system. The trends of the two curves of true thermal conductivity are different. The difference between them increases in high temperature range to reach 9 % at 650 °C. The one based on two-layers system (red curve) reflects the usual trend of such material, whereas the other (black curve) show a minimum in range between 250 °C till 300 °C, which is not typical for such material. However, the measurements are evaluated with considering the same heat flow, which is measured in the metering calorimeter. Actually, the axial heat losses should be considered to get better comparison between the two systems. The method of two layers system is used in this work

to evaluate the measurements of thermal conductivity and also to evaluate the gas atmosphere effect upon thermal conductivity.

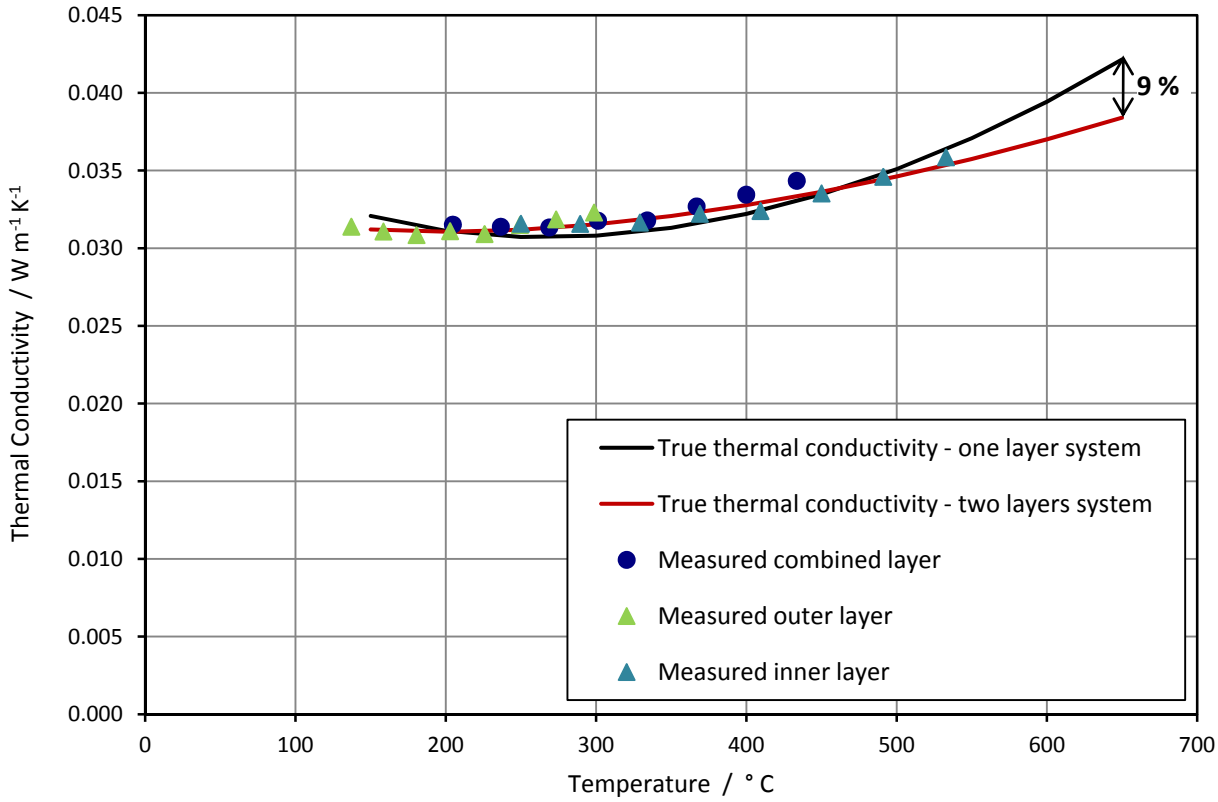

Figure 24: Comparison between one layer and two layers systems evaluation

5.4.2 Optimization of the Volume Flow Rate in the Calorimeter System

Measurement of the thermal conductivity at same temperature for the hot side is repeated for three different volume flow rates through the metering calorimeter, as above mentioned. These three volume flow rates are as follows: the first one is taken to be the maximum volume flow with no throttle in the flow system, and the other two were reduced by factors 0.9, 0.85 respectively. These factors were chosen based on a former optimization for RA1 to ensure good accuracy in measuring the heat flux. There is a dependency between the volume flow rate and the temperature difference between inlet and outlet. The latter is measured by thermocouples chain. Reducing the volume flow rate will increase the temperature difference and thus increase the measured output electrical voltage. The heat flux evaluated physically from the calorimeter should not be changed. This is valid as long as the measured thermal conductivity is greater than 0.1 $Wm^{-1} K^{-1}$. An example for such materials is presented in Figure 25 (a). The heat flow rate is evaluated by three different volume flow rates for a material which has thermal conductivity of 0.46 $Wm^{-1} K^{-1}$ at 702.3 °C. The results show no dependency for such material upon the volume flow rate. However, measurements in low temperature range (smaller than 300 °C) or measuring the thermal conductivity of materials with low thermal conductivity such as super insulation give different measurements for heat flow rates by changing the volume flow rate, as seen in Figure 25 (b). Reducing the volume flow from 9.57 to 4.31 l/h leads to a reduction in the

evaluated thermal conductivities from 0.069 to 0.063 $Wm^{-1} K^{-1}$, a difference of about 8.6 %. The change of heat flow rate is due to the error of the thermocouples chain which becomes noticeable when the output voltage is low (large volume flow rate). So that it is better to choose a low volume flow rate and thus a high output voltage of the metering thermocouples chain. However, this also has limitations because a very low flow produces two problems: first, bubble building in calorimeter system, which leads to local overheating and flow resistance, and second, increasing the error in flowmeter. Thus, it is important to optimize the volume flow rate between these limits. Many experiments were done to optimize the volume flow in low temperature range as well for measurements of low thermal conductivity materials. The criterion of choosing the volume flow rate is the reproducibility of the measurement at this rate.

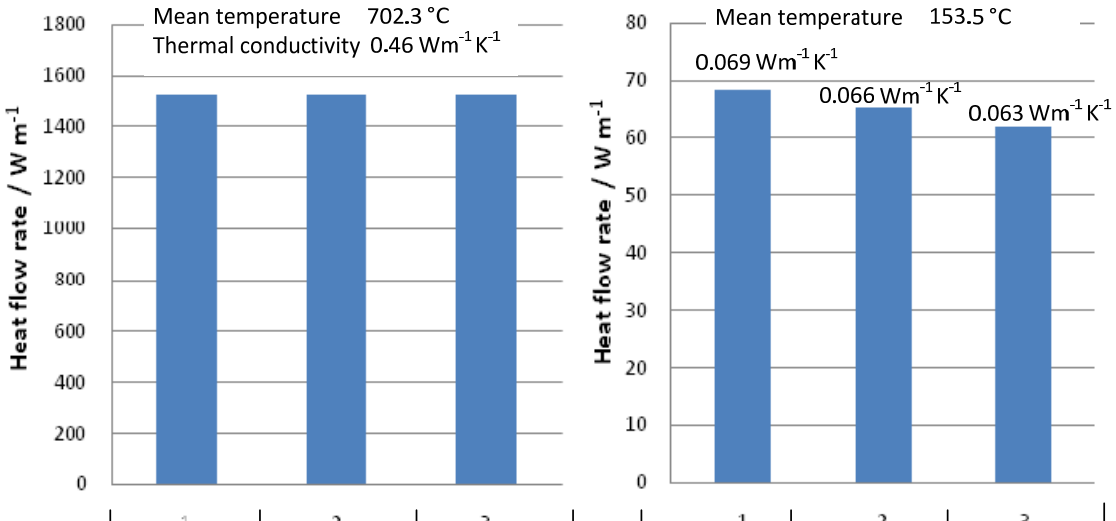

	1	2	3
Volume flow (l/h)	13.34	12.23	11.52
Output voltage (µV)	1121.87	1219.87	1301.87

(a)

1	2	3
9.57	6.20	4.31
70.17	103.13	140.80

(b)

Figure 25: Evaluation of heat flow rate for two different materials (a) and (b)

5.4.3 Correcting the Evaluation of the Heat Flux in Calorimeter System

Effect of surrounding environments on the calorimeter system:

The heat flux used for thermal conductivity evaluation is corrected by excluding the heat gain from the surrounding environments. The calorimeter system is isolated by fibrous insulation material with 18 mm thickness and then by thin aluminum sheet with 4 mm thickness, as seen in Figure 26. This Insulation is used to prevent the influence of the surrounding environment on the calorimeter system. However, the water that circulates in the calorimeter system is fresh water, which is supplied directly from the water network. It is usually much colder (T_w = 5 to 8 °C) than the lab room temperature (T_R= 20 to 22 °C). This increases the heat transfer rate into the calorimeter system. The calorimeter system is

modeled using finite elements method (FEM) to calculate the heat gain from the surrounding environment. The model is based on the heat transfer in a cylindrical wall, which consists of multi layer (fibrous material and aluminum sheets), see Figure 26.

The aim of this model is to estimate the effect of the surrounding environments on the measurements of thermal conductivity. The model is very simple and will not be presented in this work.

The heat gain is calculated as a function of the temperature of the inlet water. The heat gain varies from 0.05 % to 12 % of the heat flow rate evaluated from the metering calorimeter. This ratio varies according to three parameters: thermal conductivity of the sample, the temperature of the inlet water and the room temperature. As the investigated material has relative small thermal conductivity increases the effect of the surrounding environment. The heat flow rate measured by the calorimeter system is corrected regards the heat gain from the surrounding environments in aiming to perform accurate measurements of low thermal conductivity materials by RHFA.

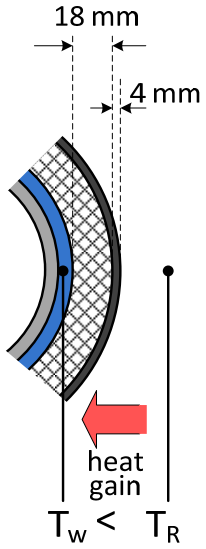

Figure 26: Sketch shows the insulation of the calorimeter system

Axial error in guarded calorimeter system:

The upper and lower calorimeters have different volume flows and different temperature gradient. This implies that transfer different heat flows. This leads to different heat losses in the axial direction. This error is difficult to calculate, because the temperature field should be modeled for each measurement at the different temperature. However, this error should be considered by comparing the results of thermal conductivity measured in RHFA with others measured using different facility.

5.4.4 Optimization of the Axial Symmetry of RA1:

Approaching an axial symmetry for RA1 is combined with many technical difficulties. For example, the sample holder is placed on the lower side of the sample whereas the upper

side contains the thermocouples connections. However, many actions are taken to improve the axial symmetry:

Increasing the dumping highness of the insulating powder:

After installing the sample in RA1, the remaining space is usually filled with two kinds of insulations. The first is corundum powder which is filled up to height (H_0). The other is fibrous material which is congested for height of (h_0), see Figure 27.

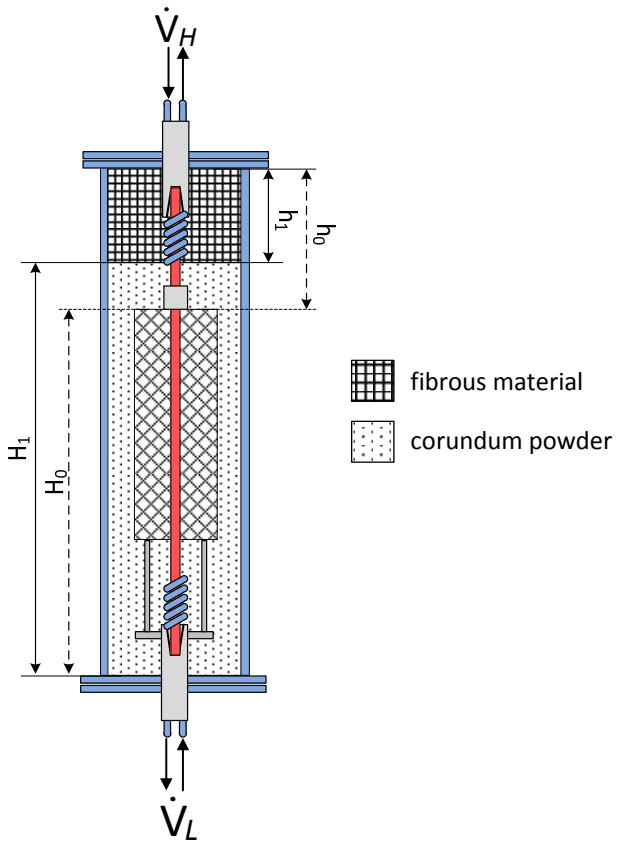

Figure 27: Arrangement of insulations in RA1, dashed line: former, continues lines: new

The fibrous material is used because the upper space contains many connections and could be only filled with flexible material. The chosen fibrous material has thermal conductivity of 0.1 $Wm^{-1} K^{-1}$ at 300 °C, whereas corundum has at the same temperature thermal conductivity of 0.42 $Wm^{-1} K^{-1}$. The aforementioned arrangement promotes different edge conditions of sample in axial direction. In this work, the filling height of corundum is increased from (H_0) to (H_1) and thus the filling height of fibrous material is reduced from (h_0) to (h_1) as seen in Figure 27.

The new filling height H_1 is chosen carefully so that the connections are not affected. Two tests are performed with the same sample material in two different filling height of the powder, i.e. the former one (H_0) and the new one (H_1), see Figure 28. The results show that the measurement with the new edge condition is lower than with the former ones. The difference between the results is around 2.5 % at 150 °C and decreases to reach 1.4 % at 700 °C. This indicates that the axial asymmetry in the RA1 has a roll in the evaluation of the thermal conductivity even when using a guarded calorimeter system.

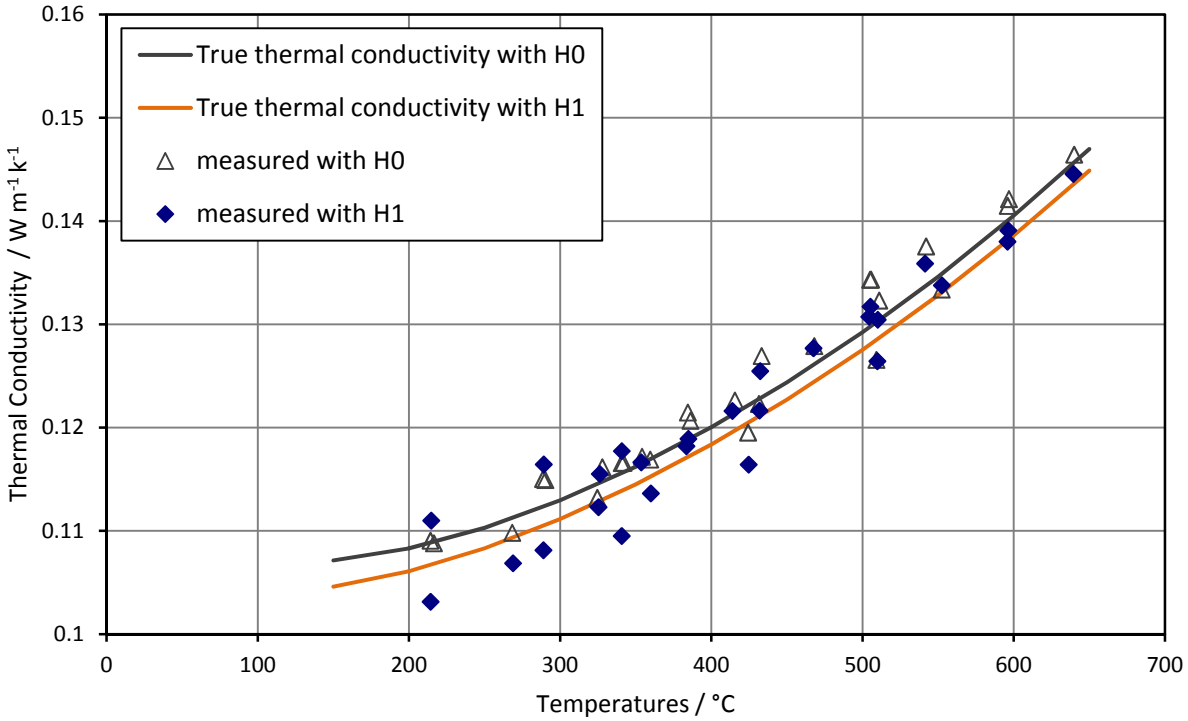

Figure 28: Effect of the new edge conditions on the thermal conductivity evaluations

Optimization of volume flow for the cooling of electrical connections:

Cooling of the electrical connections has an influence on the temperature field in RA1. The electrical power needed for the heating rod is low when experimenting on materials with low thermal conductivity. The large volume flows for cooling of the electrical connections, see ($\dot{V}_L$, $\dot{V}_H$) in Figure 27, cause strong changes in the temperature field and in the calorimeter system, and produce different edge conditions for the sample.

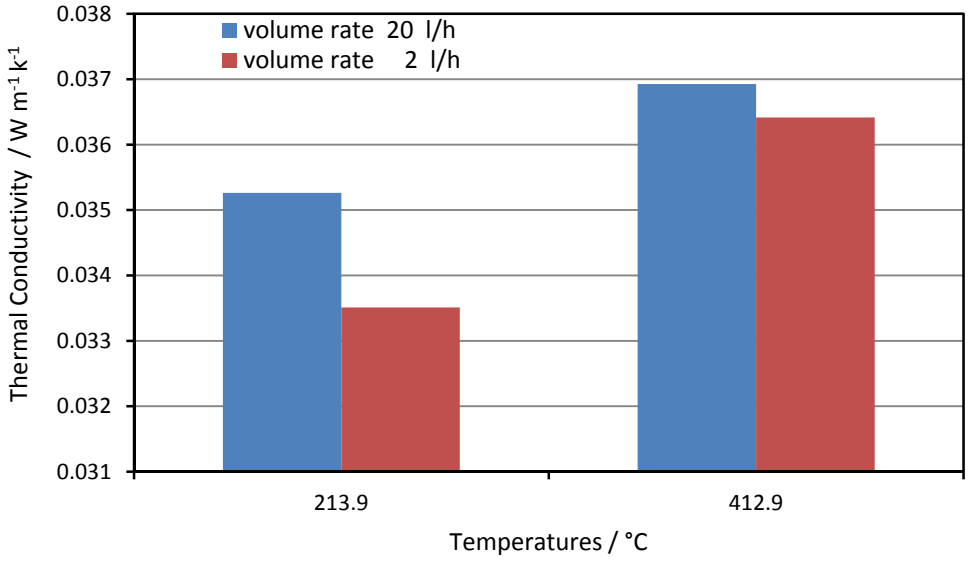

Figure 29: Change of thermal conductivity evaluation according to the different cooling rates of electrical connection of the heating rod

Many tests were performed to show the influence of cooling the electrical connections on the evaluation of thermal conductivity. Two measurements will be presented in this work. These two measurements were performed with the same sample and the same setup. The only changed parameter was the volume flow in the cooling of the electrical connections. As seen in Figure 29. the volume flow is reduced from 20 l/h to 2 l/h. This leads to 5 % decrease in the thermal conductivity. The lowest volume flow rate in the cooling of electrical connections leads to a smaller temperature difference in the heating rod in the axial direction. i.e. the temperature field has better homogonous distribution in axial direction.

5.4.5 Validation of the Thermal Conductivity Measurements in RA1

Validation of thermal conductivity measurements in RA1 is performed by direct comparison between the experimental results of the material in nitrogen atmosphere and results measured by another facility such as hot plate apparatus in air atmosphere. Another comparison is also performed with the data taken from the producer. The measurement in RA1 was repeated since the experimental results show big deviation.

5.5 Summary of Chapter 5

This chapter describes the radial heat flow apparatus and technique improvements used to measure the thermal conductivity of porous materials selected for this study in various gas atmospheres. Understanding the method and the impact of the surrounding condition are needed in order to measure the effective thermal conductivity of porous materials by exchanging the gas atmosphere. This requisitions many changes and improvements in preparation of sample, in the radial heat flow apparatus as well as in evaluation process. In this chapter these improvements are reviewed. The results of the changes are presented and discussed.

6 Thermal diffusivity measurements by Laser Flash Method

6.1 Motivation for Thermal Diffusivity Measurement

In Chapter 5 the radial heat flowmeter method (RHFM) was presented as a means to evaluate the impact of changing the types of gas on the thermal conductivity of porous media. This chapter discusses the laser flash method (LFM), which yield thermal diffusivity, as an indirect means to evaluate the thermal conductivity. This is possible by measuring the thermal diffusivity, density and the specific heat capacity. The overall uncertainty of thermal conductivity estimated according to this indirect method is within the accepted range of 10 %, whereas thermal diffusivity measurement has an uncertainty of 7 % (Hohenauer and Lager, 2010). The scope of this work is to analyze the influence of changing the gas atmosphere upon the thermal conductivity.

However, changing the gas atmosphere will be noticeable in thermal diffusivity measurement. Since the gas-to-solid ratios of density and specific heat capacity are very small, no apparent difference in density and heat capacity measurement will be detected when exchanging the gas atmosphere. Another motivation point to thermal diffusivity measurement is the ability of the applied Laser flash apparatus to perform measurements under vacuum. This is not possible with the previously mentioned radial heat flowmeter apparatus, which works only under normal pressure. In this chapter, the principle of laser flash method and the problems and challenges by measuring porous media will be presented in details.

6.2 Laser Flash Method

6.2.1 Principle of Laser Flash Method

The **L**aser **F**lash **M**ethod (LFM) is a rapid transient method for measuring thermal diffusivity of metals and metallic alloys that was developed in 1961 by Parker, Jenkins, Butler and Abbott (Parker, et al., 1961). Currently, this is widely used to determining the thermal diffusivity of variety of materials including porous media like ceramics (Hahn, et al., 1997) or metal foam (Coquard, et al., 2009). The simplicity of measuring and handling of the apparatus, in addition to the ability to obtain results quickly, make this method very attractive. Furthermore, when using this method, it is possible to obtain data at various temperatures.

Figure 30 presents the principles of the LFM. A laser beam of short duration and high intensity is applied to the front face of a coplanar specimen disk of thickness (h). The sample receives and absorbs a defined amount of energy that passes through it in the form of heat and causes a rise in temperature on the rear face of the sample T(x, t). This rise is detected and registered by an infra-red detector, which delivers a response to describe particularly the change of temperature change of the back face of the specimen. The temperature field of the sample is described by the Fourier differential equation for one dimension (x) without any intrinsic heat source as follows:

$$\frac{\partial T}{\partial t} = a\,\frac{\partial^2 T}{\partial x^2} \tag{53}$$

where T, t, a are the Temperature, time and thermal diffusivity, respectively.

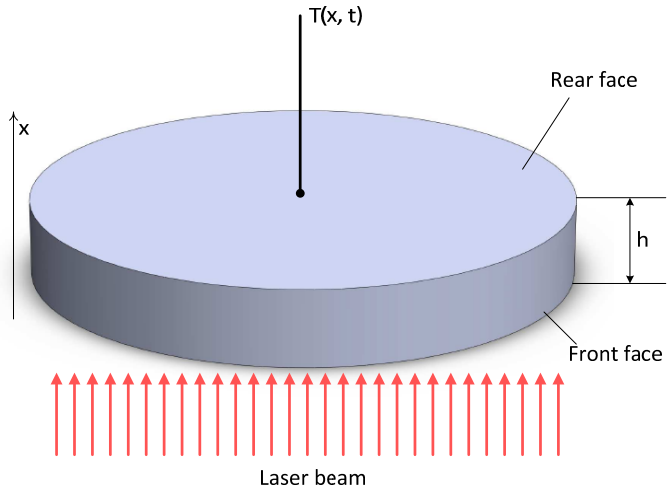

Figure 30: Principle of laser flash method

The general solution of this differential equation is formulated as followed:

$$T(x,t) = e^{-act} \cdot \left[A\,\cos(\sqrt{c}\,x) + B\,\sin(\sqrt{c}\,x)\right] \tag{54}$$

Where A, B, C are unknown variable, which could be defined through fitting the general solution to a defined boundaries. Assuming adiabatic boundaries with no heat flux at surfaces and a coplanar specimen leads to the following specific solution (see Parker, et al., 1961):

$$T(x,t) = \frac{1}{h}\int_0^h T(x,0)\,dx + \\ + \frac{2}{h}\sum_{i=1}^{\infty}\cos\left(\frac{i\,\pi\,x}{h}\right)\cdot e^{\frac{-i^2\cdot\pi^2\cdot a\,t}{h^2}}\int_0^h T(x,0)\,\cos\left(\frac{i\,\pi\,x}{h}\right)dx \tag{55}$$

Assuming the energy of laser beam to be instantaneously and uniformly absorbed, and given an infinitesimal impact duration, the temperature distribution of the rear face for opaque materials is formulated as followed (see Taylor and Maglic, 1984):

$$\Delta T(x=h,t) = \Delta T_\infty \cdot \left[1 + 2\sum_{i=1}^{\infty}(-1)^i \cdot e^{\frac{-i^2\cdot\pi^2\cdot a\,t}{h^2}}\right] \tag{56}$$

where ΔT_∞ is the maximum temperature rise of the rear face. Thermal Diffusivity could be evaluated by simplifying the solution in equation (56). This is reached by using the first limit (i=1) and applying the half time value ($t_{1/2}$) of the temperature rise of the rear face. The result is formulated as follows:

$$a(T) \cong \frac{\ln(1/4)}{\pi^2}\,\frac{h^2(T)}{t_{1/2}(T)} \tag{57}$$

The half time value ($t_{1/2}$) of the temperature rise is described as the elapsed time required for the rear face to reach half of its maximum temperature value (see Figure 31). The thickness of the sample (h) is a constant geometric parameter; however, it is also a function of temperature because of the thermal expansion.

Understanding the mathematical analysis of this method is the basis for precise evaluation of thermal diffusivity of materials. The advantage of LFM is that no need to measure or estimate the incoming energy on the front face. Detecting the temperature rise of the rear face over time and the measured thickness of sample are enough to compute the thermal diffusivity of the material (see eq. 57). However, estimating the half time value ($t_{1/2}$) of temperature rise requires a fine fitting of the curve of temperature rise. The latter is resulted from the experimental data that are detected by the infra-red detector. The task of fitting the temperature rise curve is faced with many difficulties and it counts as the most important step in the evaluation process of LFM. These difficulties emerge from the deviation between the actual experimental conditions and the assumed boundary conditions in the mathematical analysis. For example the above-mentioned solution for temperature distribution, presented by eq. (57), is based on adiabatic boundary conditions, whereas the experimental data show a noticeable heat loss effect (see Figure 31). These errors affect the evaluation of thermal diffusivity. Many researchers developed different models to estimate these errors and approach a better fitting of temperature rise curve (Vozár and Hohenauer, 2003). A short survey of these models will be presented in the following section.

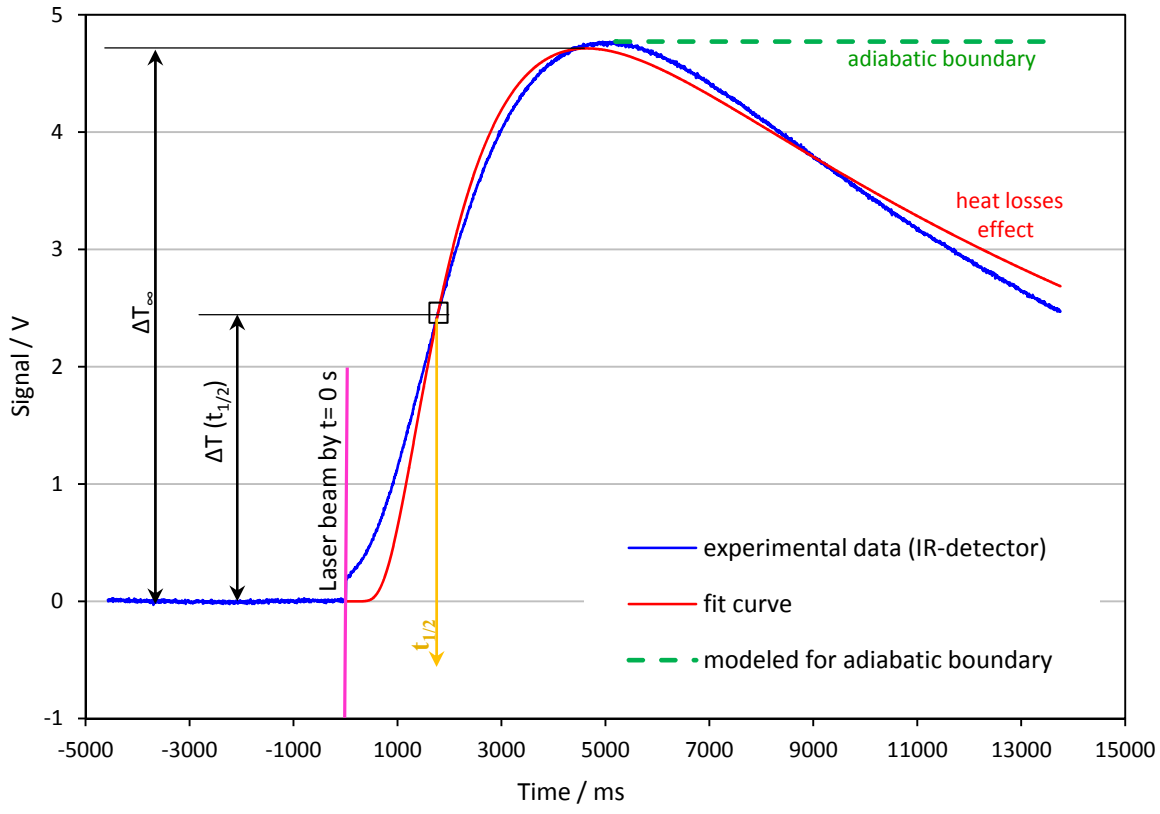

Figure 31: Difference between the experimental and theoretical temperature rise curves (Sample: porous insulation material; Temperature: 100 °C)

6.2.2 Evaluation of thermal diffusivity based on different LFM-models

The experimental data for temperature rise curve show apparent deviation to the estimated theoretical ideal trend resulted from adiabatic model (see above Figure 31). This is due to the difference between the assumed ideal boundary conditions and the actual experimental conditions. Many models are developed to correct the adiabatic model and to overcome effects caused mainly by heat losses:

- Adiabatic model (Parker, et al., 1961): the temperature distribution of rear face and the thermal diffusivity model introduced above by equations (56) and (57) are based on adiabatic boundary. The results of thermal diffusivity based on this model have big deviation from actual ones. However, the adiabatic model is the basis for all following models, which integrate different correction factors to estimate the heat losses.

- Cowan model (Cowan, 1963): Cowan corrected the adiabatic models from Parker by estimating the radiation heat losses. This is done by evaluating the temperature rise according to equation (56) at time (5 $t_{1/2}$) or (10 $t_{1/2}$) and then comparing this value to that evaluated at time ($t_{1/2}$) to estimate the radiation heat losses parameter, thus correcting the value of thermal diffusivity. This model produces two results for thermal diffusivity at each temperature depending on the referenced time, i.e. (5 $t_{1/2}$) or (10 $t_{1/2}$).

- Cape-Lehman model (Cape and Lehman, 1963): their solution involves two losses parameters to estimate the radial and facial heat losses. They found these parameters by computing the temperature rise at different time ratios (t/ $t_{1/2}$). They found increasing the radiation heat losses caused the leading constant in eq. (57) ($\frac{\ln(1/4)}{\pi^2}$ = 1.38) become smaller.

- Radiation model (Mehling, et al., 1998): mainly applied for materials with semi transparent properties. This model yields in fitting the curve, which has an immediate temperature rise when a laser beam reaches the front face of the sample. It is also useable in high temperature range as some materials become transparent for laser beam.

A comparison of the models and their produced trends of temperature rise curve are presented in Figure 32. As expected, the adiabatic model is not suitable to estimate the temperature rise curve. Cowan model and Cape-Lehman model produce the same fit curve because they have almost the same method in evaluating the heat losses, whereas the radiation model overestimates the transparency of the sample. This yields a trend in the beginning different than experimental data (see section view in Figure 32). A recent improved model for LFM shows that the Cape-Lehman model agrees with the improved model as well as with the exact solution of the differential equation for temperature field (Blumm and Opfermann, 2002).

Even a small deviation in fitting the temperature rise curve leads to a noticeable difference in the evaluated thermal diffusivity values as seen in Table VIII. i.e. choosing the right model is very important to evaluate the thermal diffusivity.

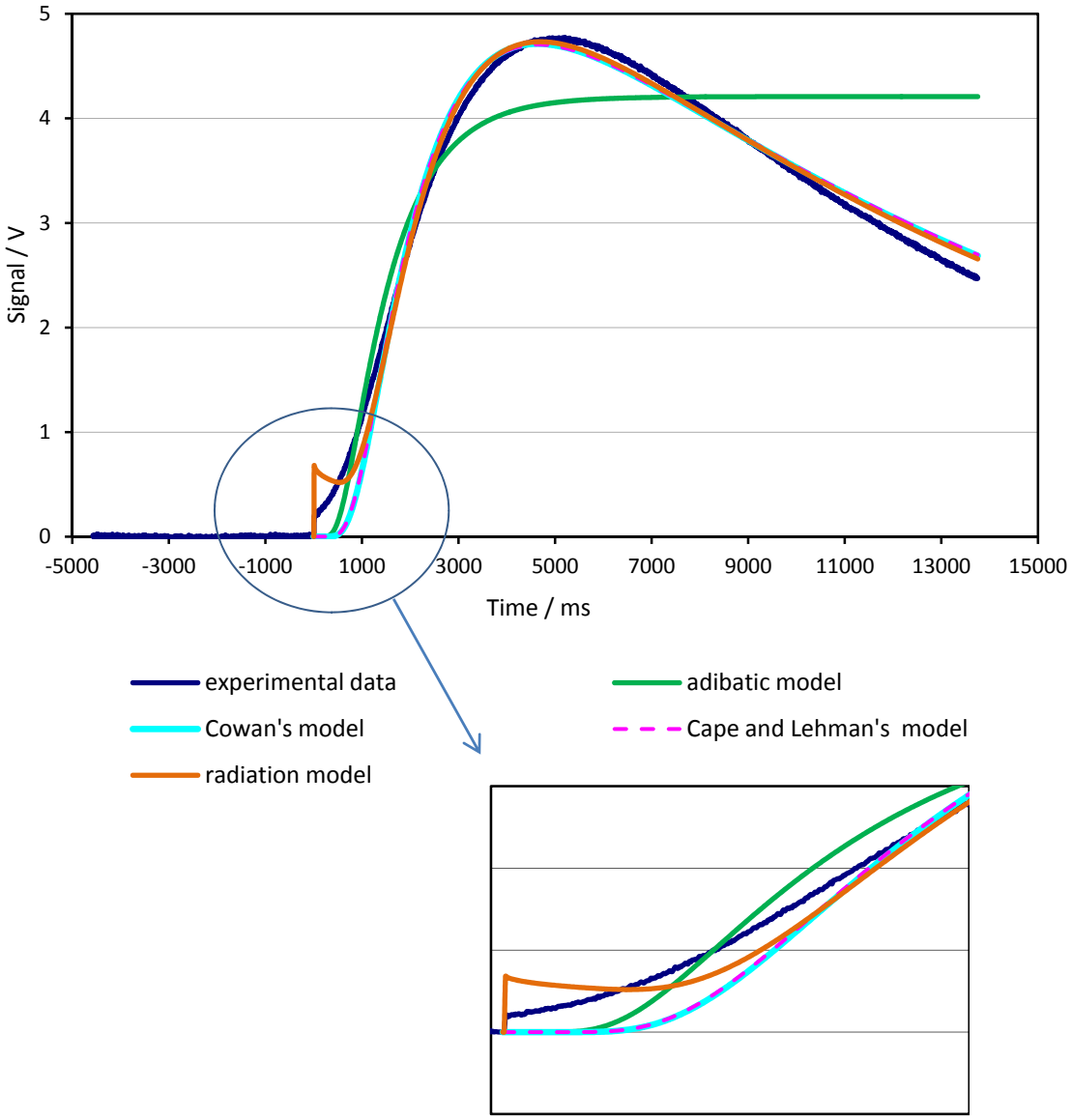

Figure 32: Comparison of models of laser flash method with experimental data of temperature rise curve (Sample: porous media, temperature 100 °C)

Table VIII: Evaluation of thermal diffusivity using the different models (Data from Figure 32)

Model	**Thermal diffusivity at 100 °C $mm^2 S^{-1}$**	**Ratio to Cowan's model %**
Adiabatic model	1.056	156
Cowan model	0.677	100
Cape-Lehman model	0.695	103
radiation model	0.563	83

In this work the Cowan's model was the most used model for the evaluation of thermal diffusivity. However, some materials show transparency at high temperatures, so evaluation of their thermal diffusivity was done based on the radiation model. There is an error in LFM caused by finite pulse effect. The above mentioned models could be also corrected to eliminate the finite pulse effect. However, this is not relevant for the measured insulation materials because the detection time is obviously bigger than the pulse duration of laser beam. Other errors occur in the measurements of thermal diffusivity using LFM like non-uniform heating or the transparency of the samples will be discussed later in this chapter.

6.2.3 Description of applied laser flash apparatus

In this work, the laser flash apparatus LFA 427 apparatus from NETZSCH®[6] was used for thermal diffusivity measurements of different porous insulating materials. A 3d-graphic of the applied apparatus is presented in Figure 33. This apparatus is supplied with laser system (1), which delivers a high intensity of laser beam (2) (Laser Voltage 320 V; pulse width duration 0.8 ms). The sample chamber is a cylindrical furnace (3) with a graphite- heater (4) to heats up the sample to 2000 °C. The furnace is cooled through water cooling system (5) that is embedded in the wall of the furnace, see Figure 33. This allows to measure temperature- dependent thermal diffusivity of different materials. The chamber is sealed (6) and connected from the down side to the vacuum system (7) which consists of two levels vacuum pumps (pre-pump to reach medium vacuum and turbo molecular pump to reach high vacuum). This enables measurements under different rare gas atmospheres as well as in high vacuum to 10^{-5} mbar.

The sample (8) is axially and radial centered in the furnace through sample holder (9) to insure a steady state and good thermal balance of the sample. The Sample holder (9) is a cylindrical pipe that contacts the sample at three points only, and the sample is covered with the sample-cup (10), see the right sketch in Figure 33. The aim of that is to avoid any heat losses through direct conduction to the sample holder. Thermocouple (11) is connected in the sample holder and measures the sample temperature. The laser beam (2) is focused through lens (12) then passes through the sample holder to hit the front side of sample (8). The Temperature rise of the rear side of the sample is detected through IR-detector (13), which its signal goes through an amplifier to the control and measurement system. Evaluation Software NETZSCH Proteus® developed by the company NETZSCH® and installed on computer performs fast and easy evaluating process using the above-mentioned different models. An overview of all specifications of the applied LFA is tabulated in Table IX.

Table IX: Specifications of LFA 427

Principle	Laser Flash method (transient method)
Specimen geometry	Disk-shaped
Specimen thickness	0.1 … 6 mm
Specimen diameter	6 … 12.7 mm
Range of temperatures	Room temperature – 2000 °C
Gas pressure	10^{-8}- 1 bar
Gas atmospheres	Ar, N_2 or He
Uncertainty [7]	approx. 7 %

[6] www.netzsch-thermal-analysis.com
[7] Hohenauer and Lager, 2010

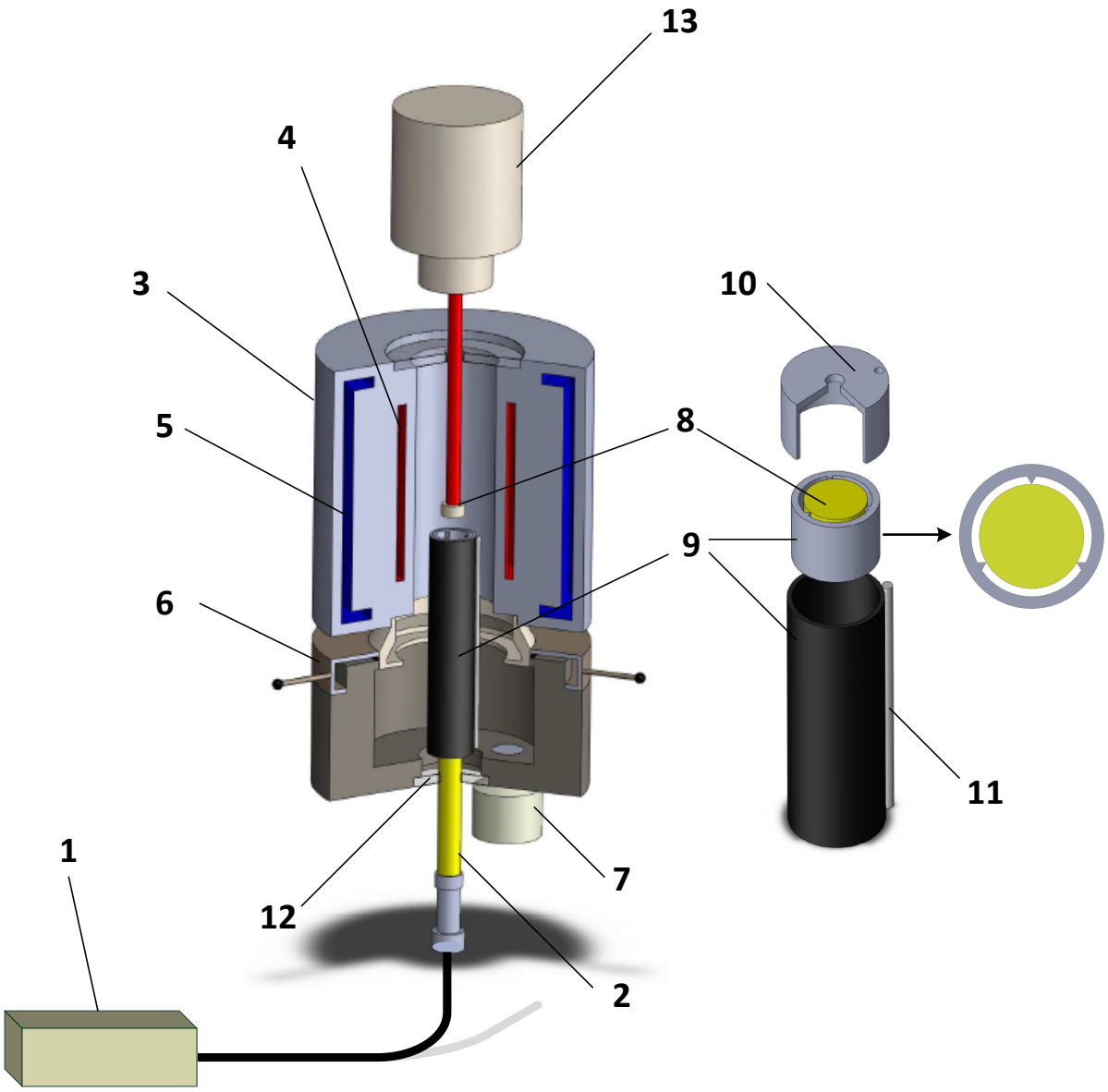

Figure 33: 3D-graphics of the applied Laser flash apparatus LFA 427 NETZSCH®

6.3 Performance of Experiments using LFM

The overall performed experiments in this work using LFM are classified in two categories: first one contains many experiments that were done on one material with different surface coatings in order to find the appropriate coating material. The second category is the experiments that were performed on chosen porous insulation materials in different gas atmospheres as well as in vacuum to measure the influence of exchanging the gas atmosphere upon the thermal diffusivity of the porous materials.

6.3.1 Application of Laser Flash Method to Porous Media

The samples, which are prepared for LFM measurements, have to be from fully dense, homogeneous and isotropic solid materials that are opaque to the applied energy pulse

(ASTM E 1461, 2007). They should also have an even surface. Porous materials are neither opaque, nor made of dense material, nor do they have an even surface:

- The transparency of the materials: A part of the laser beam will pass through the sample, i.e. a part of the incoming energy through laser beam will not be absorbed. That leads to difficulty in fitting the temperature rise curve and errors in evaluation of thermal diffusivity.
- High porous media: the heat transfer will be in two phases, which results an inhomogeneous temperature distribution in the sample.
- The unevenness of the surface: the incoming energy will non-uniformly pass through the sample, that means heat conduction in more than one direction heat conduction and leads to heat losses to the sample holder.

According to American and German standards (ASTM E 1461, 2007 ; DIN EN 821-2, 1997) of LFM: Deposition of opaque materials like metals (silver, gold copper, etc.) followed by a thin film of high emissivity coating like graphite on both faces of the sample should enhance the performance of the measurement. Unfortunately, *these standards do not contain any guidance about coatings, coating thickness, or coating procedure*. The next section deals with the task of changing the properties of the porous materials to fit the requirements of the LFM test method. LFM has so many advantages over other methods. Therefore, it is of interest to find a way to apply it to porous materials as well.

6.3.2 Experiments for Finding the Appropriate Surface Coating

The aim of these experiments was to find a way of applying the LFM to porous insulating material by coating the samples with a layer of different materials to make them less transparent and to make their surface even. It was also part of the experiments to find out how the different surface coatings affect the measurements and which coating material is best suited for determining the thermal diffusivity of the base material.

Base Material

To determine how the different coating materials affect the measurement of the thermal diffusivity of the base material, nineteen samples from the same base material were tested. One without any surface coating, the remaining eighteen were coated either with metallic or non- metallic materials.

The base material used in these experiments was made of calcium silicate with a density of 260 kg m^{-3} and a porosity of 93 %. It is a grey colored material, which is highly resilient and light. It is mainly used in insulation or in processes during which there are high temperatures up to 1100 °C. Its chemical composition is shown in Table X below. Porous media based on calcium silicate are fragile. So producing of samples with the required dimensions was accompanied with many problems. For the experiments, circular discs with a diameter of 12.6 mm and a thickness ranging from 2 to 5 mm were used. Before the experiment the material was tempered at 800 °C to prevent reactions or changes in structure during the measurements.

Table X: Composition of the base material

Composition	SiO_2	CaO	MgO	Al_2O_3	Fe_2O_3	Na_2O	K_2O	remnant
%	47	45	0.6	0.3	0.3	0.1	0.1	< 6

Surface coating

Pre-experiments with porous samples of such insulation materials without any surface coating have shown, that the base material is too transparent which leads to false results as of the results as the laser flash partly penetrates through the sample and thus heats the rear face immediately. This is seen clearly in Figure 34 (a). A jump of the temperature at t=0 s is clearly visible, which implies that part of the laser shot directly went through the sample and therefore heated the rear face immediately. It can also be seen that the detectors' curve could not be fitted perfectly with the fitting curve. This means that the data obtained is not usable. The surface coating is applied to improve the measurements, which could be noticed as good fitting of the signal as seen in Figure 34 (b) for the same sample measured in (a), however coated with graphite spray. Therefore the coating has to fulfill all requirements of the LFM. It should be opaque to avoid the laser flash penetrating directly through the sample, and homogeneous to insure uniform reception of the energy of the laser flash. Furthermore, the coating film has to adhere on the sample surface throughout the whole measurement otherwise there will be too much of a thermal contact resistance. It should not react with the base material even at high temperatures,. The coating material should not diffuse into the sample, which would influence the heat transfer process through the porous structure. When using a coating material of reflective metals, the sample has to be additionally coated/sprayed with e.g. a graphite film, because the surface of the samples shouldn't reflect the laser energy so that it can be absorbed. Also, to be able to disregard the coating material's thermal diffusivity, it has to be far higher than the base materials. In these experiments, coating materials were divided into two groups: metals and non metals.

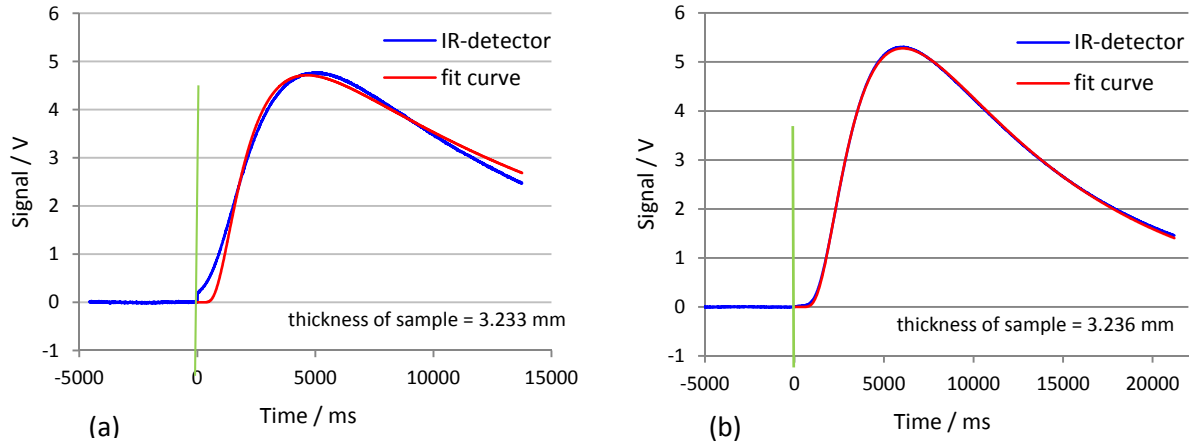

Figure 34: Temperature rise curve and fit curve at 100 °C for
(a) uncoated sample (only the base porous material)
(b) coated sample (base porous material coated with graphite spray)

According to German standard DIN EN 821-2 platinum, nickel, copper, gold or colloidal graphite are all suitable materials for the surface coating. They have a high thermal diffusivity, so that they transfer the applied energy straight to the sample. Nickel was excluded from this experiment because after evacuating the oven, there might be some oxygen left that would react with non-noble metals such as nickel at such high temperatures. The materials that were used as a surface coating are listed in Table XI. Thermal diffusivity of the coating materials is much higher than the measured one of the insulating porous materials, which ranges between 0.2 $mm^2 s^{-1}$ and 0.7 $mm^2 s^{-1}$. Thus, the coating material

plays a roll of high conductor to deliver the incoming pulse energy to the porous structure. In the following section it will be explained how the samples were prepared with each coating material.

Table XI: Materials of the coating surface

	Material	Thermal diffusivity [8] $mm^2\ s^{-1}$	
Metals	aluminum	104.43	@ 0 °C
	copper	117.47	
	Gold	128.72	
	silver	172.72	
Non-metals	graphite	39.01	@ 400 °C
	silicon carbide (SiC)	6.91	

Sample preparation

The Laser flash method demands certain properties which the samples have to possess. The raw material has to be as homogeneous as possible; furthermore the pore size should be smaller than 100 µm (ASTM E 1461, 2007). Also the thickness of the sample should be chosen to resemble that of the sampled material. The samples surface should be small enough to minimize heat loss over it, on the other hand though it has to be large enough so that $t_{0,5}$ is high compared to the pulse width and lies between 0.025 and 0.2 s.

The samples surface should furthermore be parallel within 0.5 % of the samples thickness. Transparent materials have to be coated to insure full absorption of the laser shot by the sample.

The samples were prepared according to ASTM E 1461, 2007. For these experiments the sample preparation is very important, because it plays big role in performance of the measurements. The base material was cut into circular discs with different thicknesses ranging from 2 to 5 mm. The samples were prepared with flat and parallel surfaces within 0.5 % of their thickness.

Then the discs, except for the one which was tested without any coating, were covered with the different coating materials. Eight samples were coated with a non-metallic material. Four samples of different thickness were sprayed with graphite. Figure 35 shows a scanning electron microscopy micrograph of a sample sprayed with graphite. The border between the base material and the coating can clearly be seen, this proves that no graphite particles penetrate the surface. It is also obvious that the coating material is less porous then the base material.

[8] Evaluated from available data for thermal conductivity, density and specific heat capacity of each material at defined temperature referred to VDI-heat atlas (Neubronner and Boeck, 2010)

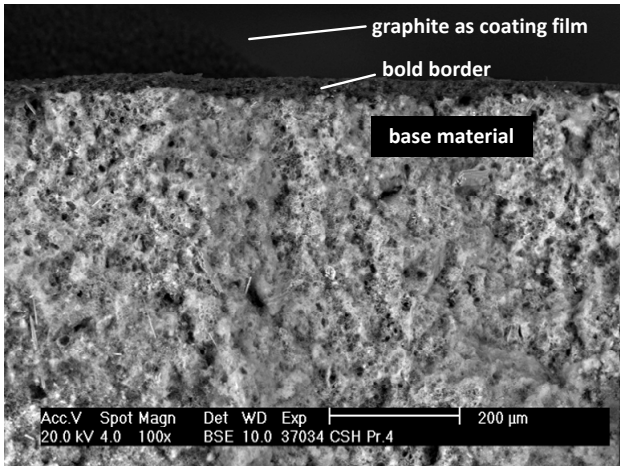

Figure 35: SEM- micrograph of sample coated with graphite

Two samples were also coated with graphite slurry by immersing the sample inside the graphite slurry. Since the base material is a porous media, the capillary suction attracts the graphite particles to be deposited gradually on the surface of sample. Then a drying process followed. Furthermore, there were two samples in this experiment that were coated with SiC-paste with different layer thickness. Both samples were coated with a thick layer through filling out the surface of sample with the SiC-paste by using a brush and scraper. Then one of them was sanded down until there was only a thin layer left.

Table XII: An overview of prepared samples

group	Coating material	Coating method	Sample No.
without coating	-	-	1
non-metal coating materials	Graphite	Spraying	2
		Spraying	3
		Spraying	4
		Spraying	5
		Immersing in slurry	6
		Immersing in slurry	7
	SiC-Paste	Brushing	8
		Brushing + sanded	9
	SiC-Paste + Graphite	Brushing + Spraying	10
metal coating materials	Gold	Sputtering	11
	Aluminum	Vaporization	12
		pressed between AL-foils	13
		AL-foils adhered by thermal grease	14
	Copper	Vaporized in Vacuum deposition	15
		Vaporized in Vacuum deposition	16
		wire flame spraying	17
	Silver	conductive varnish	18
		Vaporized in Vacuum deposition	19

The other group of samples was coated with metallic materials. A gold layer was sputtered on the surface of one sample. Three samples were covered with Aluminum. The first sample was prepared by vapor deposition of Aluminum. On both other samples Aluminum was applied in the form of a foil. On one of later two samples thermal grease was added. To get a copper layer, two samples were coated by vapor deposition and one other by wire flame spraying. Silver was applied both as a vacuum deposition and as a conductive varnish. All prepared samples are tabulated above in Table XII. Some photos of the prepared samples could be seen in Figure 36.

Figure 36: Photos of some prepared samples

Experimental procedure

All together, one uncoated sample and eighteen coated samples with six different coating materials were tested under the following conditions:

The laser was shot to the sample six times at each temperature, with temperatures ranging from room temperature to a maximum of 900 °C, which was only reached in few tests due to complications that will be explained in the following section. Most of the detector curves only provide good results up to a temperature of 200 °C.

Many problems and complications have been faced while performing of these experiments with non-metallic coating as well as with metallic coating. These are introduced through three effects and summarized as following:

- **Non-steak effect of surface coating**: The coating in some prepared samples becomes loose during the experiments. There is a difference in the thermal expansion between the base material and the material of the surface coating. This leads to the separation of surface coating in the measurement performed in high temperatures**.** The resulted temperature rise curve could not be fitted and the measurements are

interrupted, for example see Figure 37 (a). This effect was noticed in two samples; one thin sample (thickness of 1.85 mm) that was coated with graphite coating and another one that was pressed with Al-foils.

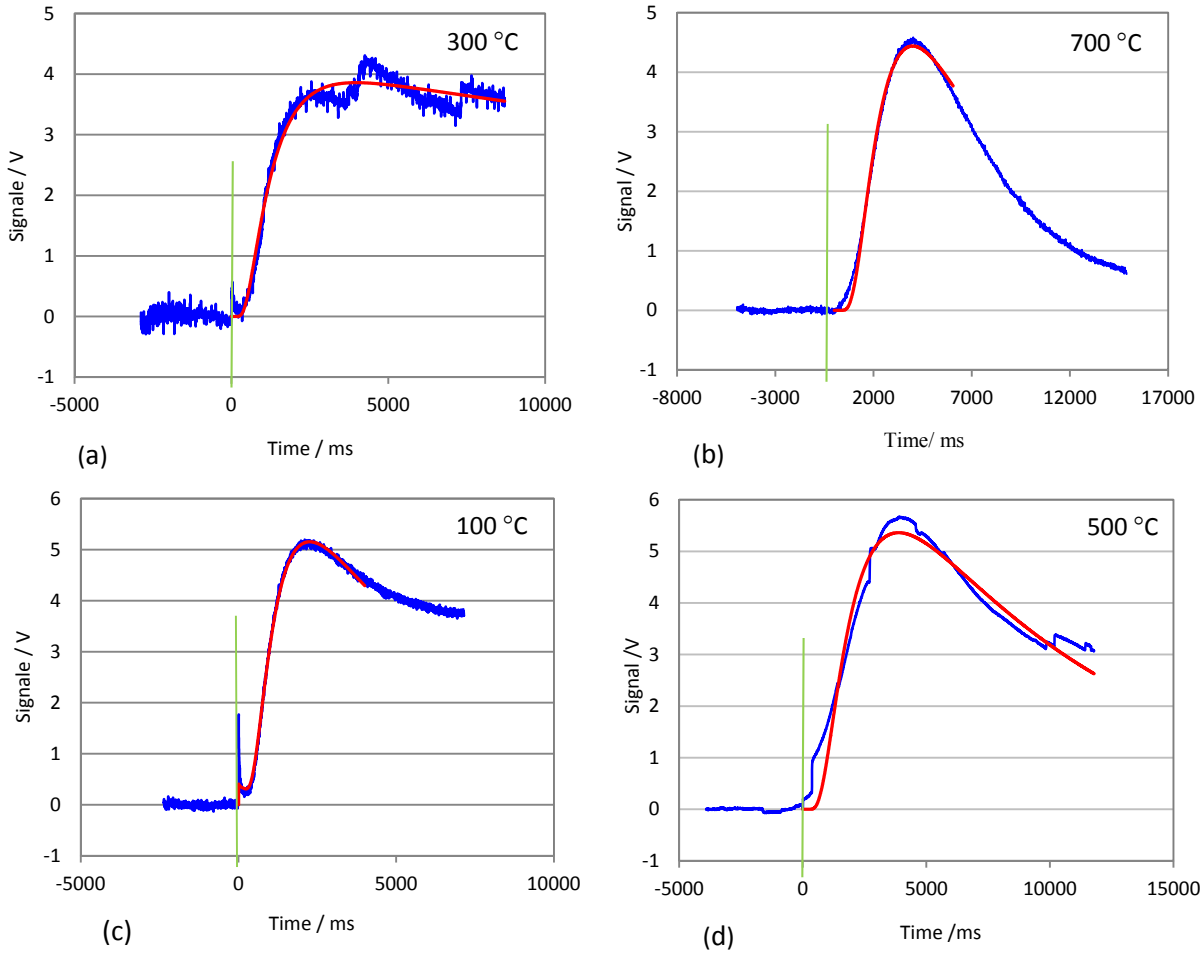

Figure 37: Temperature rise curves for sample coated with
(a) aluminum foils with gaphite: sample No. 13 (b) SiC-Paste sample No. 9
(c) aluminum foils with gaphite: sample No. 13 (d) gold sample No. 11
Blue: IR-detector curve; Red: fit curve ; Green: laser shot at t=0

- **Unexpected trend of IR-signal**: The IR-signal that represents the temperature rise of some samples has unexpected trend. At high temperature the curve of temperature rise reaches the maximum and then shows a rapid downward trend, which is interpreted as cooling effect. The signal has also noise disturbance. This is clearly seen in Figure 37 (b). Another unexpected trend of IR-Signal was noticed for the sample which was coated through gold sputtering. At high temperature the signal has great noise effect, as seen in Figure 37(d).

- **Transparency effect**: An immediate increasing in the recorded curve of temperature rise was noticed even in low temperatures range which points out to a transparency effect, as seen in Figure 37 (c) e.g. for the sample which was pressed with Al-foils at

100 °C. i. e. in spite of coating of the surfaces, the temperature rise curve of some samples shows a transparency effect. The resulted fitted curve using the radiation model could not estimate this effect; as seen Figure 37 (c). Some samples were opaque in low temperatures rang. However, they become transparent at higher temperatures. The evaluation of thermal diffusivity for these samples was done only for the lower temperatures range. This will be seen in the following results section.

Inspection of thermal diffusivity results

For the evaluation of the resulting data theoretical models were used. Mostly the evaluation was done based on the Cowan model. The radiation model was also applied for some samples that showed transparency. As above mentioned by many samples, due to some complications the temperature rise curves only provide usable data up to a temperature of 200 °C.

The thickness of coating layer ranges between 50 nm by vacuum vaporization to 100 µm by filling out the surfaces of sample with SiC-paste. Since also all coating materials have high thermal diffusivity compared to the base material, the coated layer will be neglected in the evaluation process (Maillet, et al., 2000).

In order to find the appropriate coating which produces a reliable experimental data a comparison will be done between the measured thermal diffusivity data of the different samples and reference data for thermal diffusivity of the base material. Reference data for the thermal diffusivity are evaluated using the following known equation:

$$a(T)_{ref} = \frac{\lambda(T)}{\rho\, Cp(T)} \tag{58}$$

where $\lambda(T)$ is thermal conductivity of the base material measured by radial heat flowmeter in argon atmosphere (the same gas atmosphere in LFA) in temperature range 300-600 °C. (ρ) is the density of the porous material determined from the structure analysis of the base material. $Cp(T)$ is the heat capacity of the base material measured up to 900 °C using Differential Scanning Calorimeter (DSC).

The thermal diffusivity results of the nineteen samples and the reference data will be presented now. Because of the big number of data, it is better to show the results separately in two diagrams according to the coating material: non-metallic and metallic ones.

The results with non-metallic coating materials as well as with metallic materials lay in a wide range, see Figure 38 and Figure 39. It can for example be seen that the curve of the uncoated sample (sample No. 1) lies above the rest. This is due to the predicted transparency, which can also be seen in the shot-curve, see Figure 34 (a). The curve of the sample coated with a thick layer of SiC-paste, on the other hand, lies far below the others, see Figure 38. Both preparation methods are consequently not suitable.

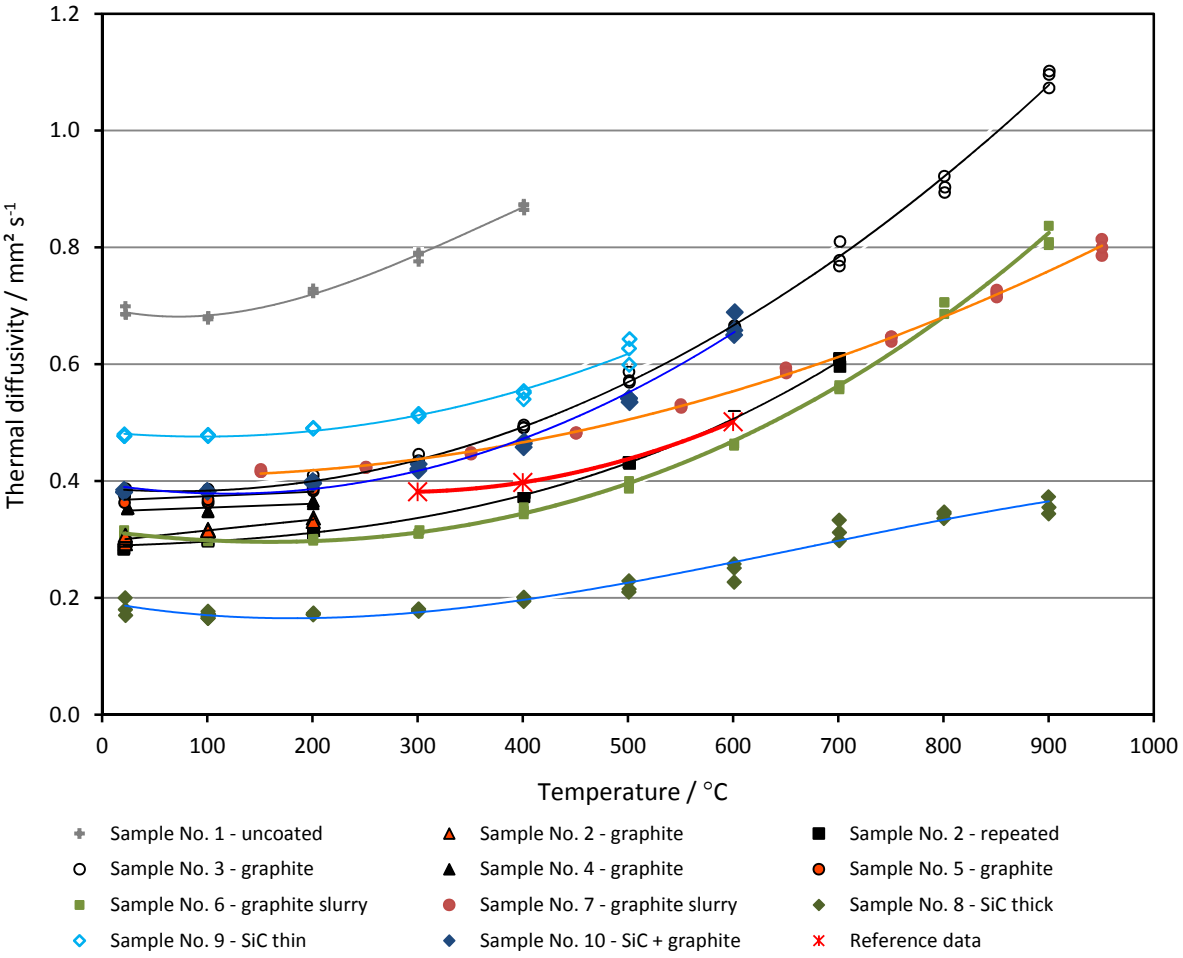

Figure 38: Results of thermal diffusivity of samples coated with non-metallic materials

As seen in both diagrams, Figure 38 and Figure 39, the values of thermal diffusivity clearly vary strongly with the different coating layers. However, they differ also for the same coating material according to the preparation method. For example, taking graphite as the coating material, the sprayed one (sample No. 3) lies more than 25 % higher than the one immersed in graphite slurry (sample No. 6). In both diagrams, the red curve symbolizes the reference curve. It can be clearly seen that the thermal diffusivity increases with the temperature. At higher temperatures the curves' gradients start to differ from each other. Some curves keep on rising, e.g. the curve of sample No. 15. Others stay at a constant level like the curve of sample No. 18. The curve of sample No. 13 shows some anomalies, which are due to the fact that this sample was coated with aluminum foils that came loose during the experiment. This shows that the preparation methods of the samples with different coating materials have a big influence on the results especially at higher temperatures.

Looking at the reference curve in both diagrams it can be noticed that the values next to it among non-metallic coated samples are those with graphite-spray (Sample No. 9 is excluded). Graphite was also the best non-metallic coating material as it was easiest to apply and it showed the best shot curves at low temperatures. Whereas compared to samples with metallic coating at higher temperatures the reference curve coincides with the values of the sample covered with copper through wire flame spraying (sample No. 17), As seen in Figure 39.

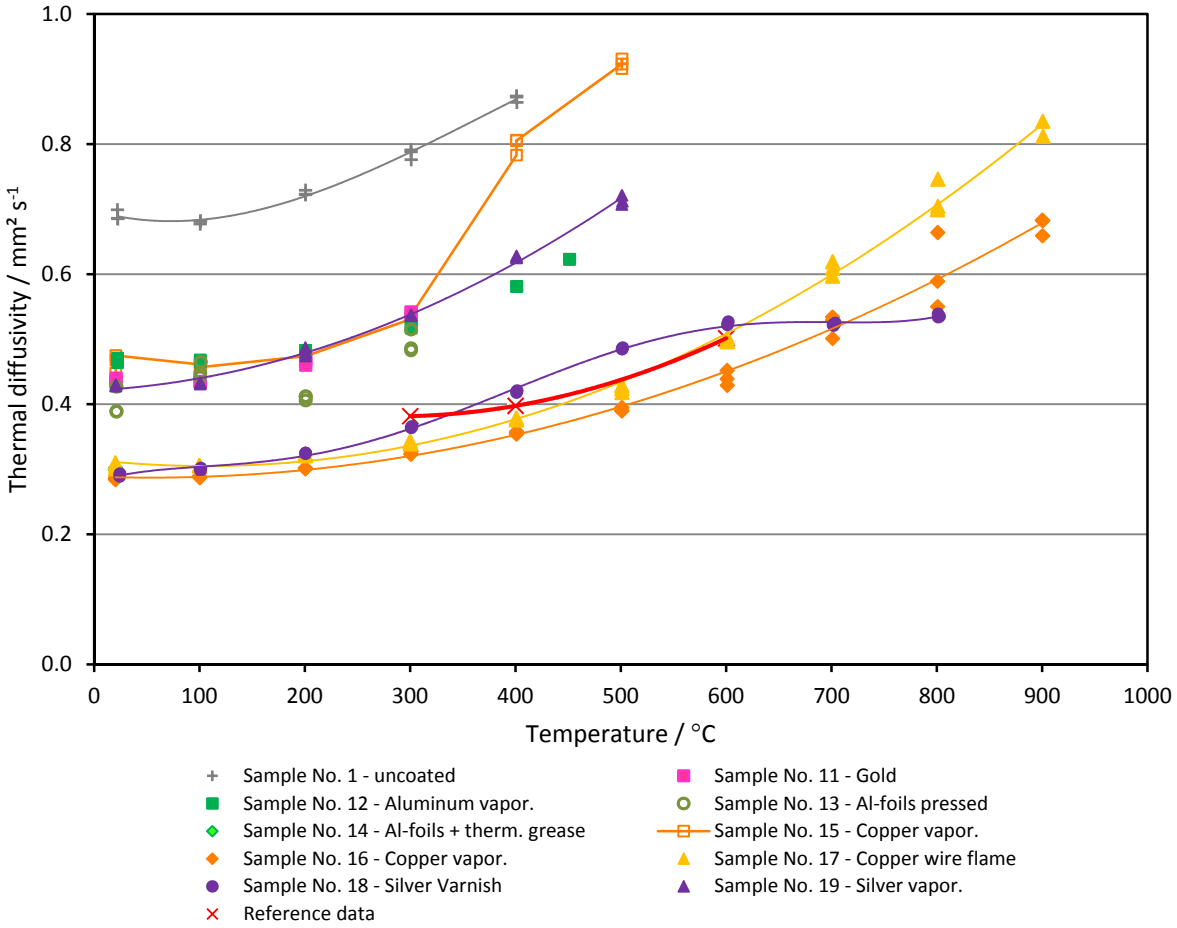

Figure 39: Results of thermal diffusivity of samples coated with metal materials

Discussion

The curves of the samples coated with SiC-paste (samples No. 8 and 9) lie far away from the reference curve. This can be explained with the fact that the thick layer of SiC-paste forms a passive protective SiO_2 layer, which has a low thermal conductivity and therefore influences the measurement as an insulation layer instead of a good conductive layer. The sample coated with a thin layer of SiC shows high transparency. The use of SiC-paste as a surface coating for this kind of measurement can thus be excluded. If, however, the SiC-paste is additionally covered with a graphite layer, then it doesn't have any influence on the measured thermal diffusivity. As seen in sample No 10, Figure 38. In a recent study (Hohenauer and Lager, 2010) about measuring metallic foams using LFA, influence of SiC-coating upon the results of thermal diffusivity has been noticed.

Graphite as coating material gives a very good trend of temperature rise curves at low temperatures. However, samples become transparent at high temperatures. The coating method through graphite spray is better than immersing in graphite slurry, because with the later one it is not possible to control the amount of the coating graphite. Two samples (sample No. 6 and No. 7) coated with this method show, hence, different values of thermal diffusivity and different dependency on temperature.

All metallic coating materials show a bad trend of the shot curves mainly at high temperatures and they show also high transparency. The aluminum coated sample provided no usable data, and in the case of Al-foils with thermal grease the experiments could not be

completed even at low temperature due to instability. Thus, the use of Al-foil is entirely unsuitable for this method as there is not enough contact with the base material and this increases the contact resistance.

In most cases of metallic coating materials at the high temperature range the coating materials became loose during the measurement, or the color of the coating material is changed. This change in the coating materials has a big influence on the results at high temperature, which could be seen clearly by noticing the trend of curves of thermal diffusivity at temperatures higher than 200 °C. This is due to the difference of thermal expansion between the base materials (ceramics with low thermal expansion) and the coating material (metal with higher thermal expansion).

In some cases, as in the sample coated with gold (sample No. 11), the color did not change and the coating material attached firmly to the base material. However, a very strange shot curve was detected at higher temperature. The change was then noticed by making a micrograph of the surfaces: surface of front side of the sample (incoming laser shot side), and the rear side (IR-detector reading side), both of them sputtered with gold. The results are shown in Figure 40. The micrograph of the front side shows that the gold somehow is molten and then frozen to form spherical shapes, see Figure 40 (b). This can be explained through local heating by the incoming laser energy at the front side in spite of choosing the minimum limit of the laser beam energy necessary to apply the LFA method.

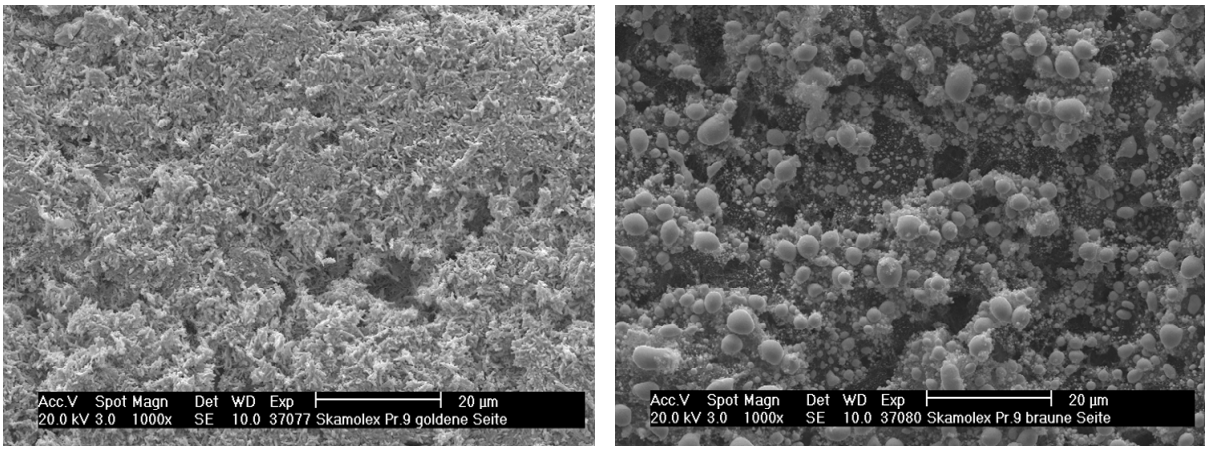

(a) (b)

Figure 40: Micrograph of surface of the sample coated with gold (sample No. 11)
(a) rear side; IR-detector side (b) front side; incoming laser shot side

Conclusion

In these experiments which are designed to find the appropriate coating, six different coating materials applied by ten different coating methods were tested. In conclusion, it can be said that the application of a surface coating on the base sample material only improves the measurements of the thermal diffusivity in a limited way. Also there are some difficulties applying the LFM to porous media. ***A graphite spray can be used as a coating material for estimation of the thermal diffusivity of such porous materials in low temperature range*****,** however, many samples should be measured to find out the fluctuation of the results.

According to the results driven from these experiments ***the wire flame spraying is a recommended method to coat such a porous material and to give a stable coating layer even for high temperatures*.**

An alternative experimental approach to measure porous insulating materials is to build the base material in a three layers sandwich system. The base material is situated between two thick layers with known thermal diffusivity. The thermal diffusivity of the base material is then evaluated through iterative evaluation (Wei, et al., 2006). However, this method requires considerable calculation effort and contains a big influence of thermal contact resistance between the respective layers.

Wire flame spraying was very expensive due to necessary technical effort. **Therefore, *for further experiments the graphite spray was chosen as the surface coating method*** for the investigated porous materials. However, for some materials that have big pores, a thin SiC-layer was spread under the graphite spraying to produce an even surface as possible.

6.3.3 Experiments in LFA by Exchanging the Gas Atmospheres

The furnace in the applied LFA (LFA 427) serves as a gas chamber. That allows performing measurements under different rare gases atmospheres as well as in vacuum. Two parameters in these experiments were investigated before performing the experiments on the selected porous materials for this work. One is connected to the apparatus: the gas flow in the furnace. The second is related to the sample: the thickness of the porous insulation sample.

- **The gas flow in the LFA**

The included heater in the applied LFA consists of graphite. Owing to that reason the measurements are usually performed under dynamic gas flow to avoid any oxidation gas through leaks. The gas inlet is located inside the sample holder and the gas flows directly through the sample holder and then through the sample to the furnace chamber.

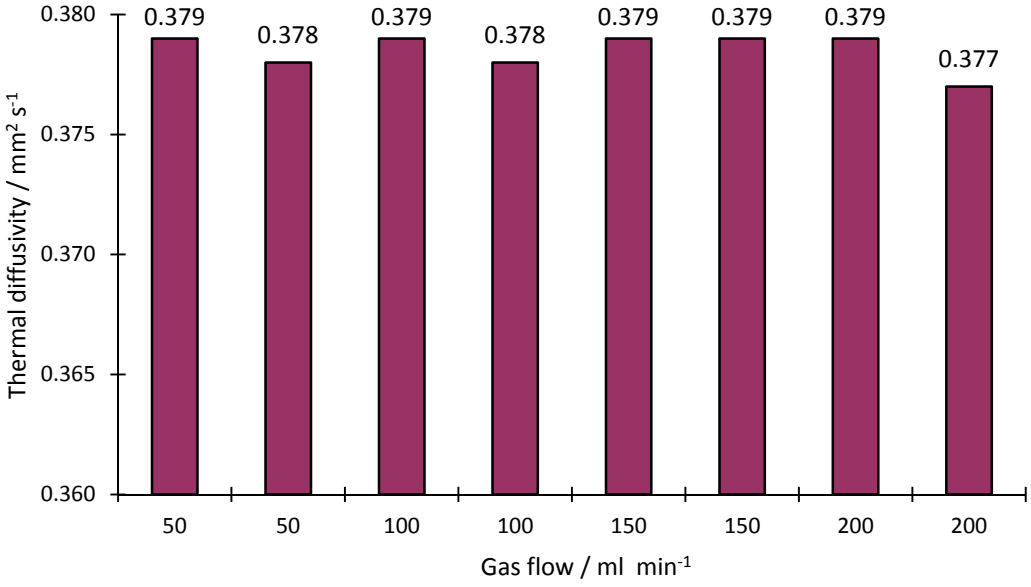

Figure 41: Thermal diffusivity for one sample of calcium silicate for different gas flows in the furnace at 100 °C

Since all others measurements of thermal conductivity are done under static gas atmosphere not dynamic one, the effect of this gas flow upon the results of thermal diffusivity should be investigated. The experiments were performed for one of the investigated porous materials with porosity of 93.4 % at a constant temperature 100 °C. The gas flow was varied from 50 ml/min to 200 ml/min. In each gas flow two measurements of thermal diffusivity are done. The results of thermal diffusivity are presented in Figure 41. It is obvious that there is no effect of gas flows upon the results of thermal diffusivity. The chosen gas flow for further experiments was 100 ml/min.

- **The thickness of the sample of porous material**

The thickness of the sample is the only dimension that is included in the evaluation in LFM, and thus the thickness should be carefully chosen. The dimensions of the sample for LFA are small comparing to the dimensions of practical plates made of such porous insulation materials. However, the thickness should be large enough to represent the whole porous structure of the material and to ensure that the sample is not transparent to the laser flashes. On the other hand increasing the thickness promotes two effects that lead to errors in the measurement. The first effect is the increase of heat losses through the side surfaces and through the internal radiation. The second one is extending the time of the measurement, which causes difficulties in fitting the temperature rise curve. The latter effect could be overcome by adjusting the time range that is considered for evaluating the fit curve. i.e. the fitting curve was generated only for a short time after reaching the maximum, see Figure 42. This leads to better fitting of the measured temperatures rise.

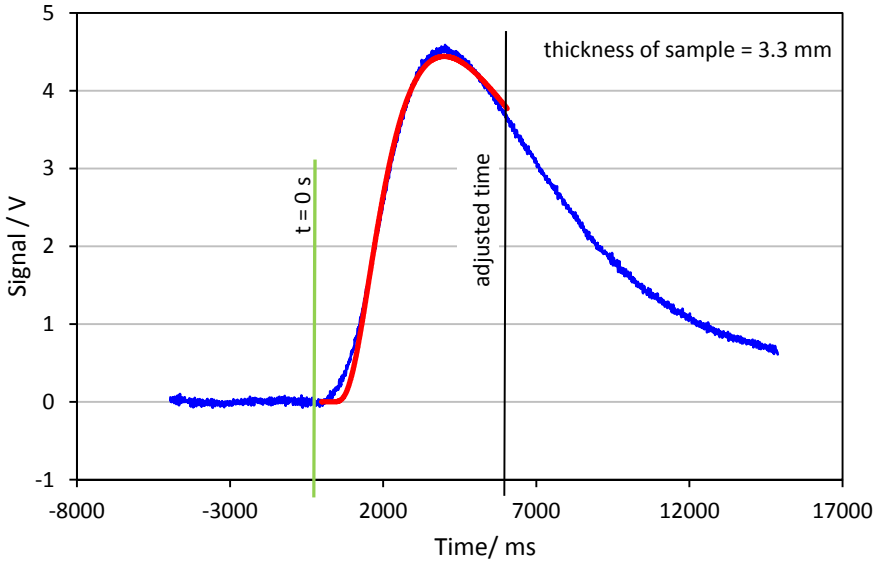

Figure 42: Adjusting the time range for sample coated with graphite at 700 °C

In order to investigate the effect of sample thickness on the detected value of thermal diffusivity, four samples from the same material were tested, with thicknesses ranging between 1.8 mm and 5 mm. These samples are also listed above in the previous subsection, check Table XII. They were sprayed with graphite and then measured up to a temperature of 200 °C. The results of thermal diffusivity are presented in Figure 43.

It can be seen in Figure 43 that there is no dependency between the thickness of the sample and the measured thermal diffusivity for thicknesses bigger than 3 mm because the value of thermal diffusivity for the 5 mm sample lies between those for the 3 and 4 mm samples. The

fluctuation of the thermal diffusivity is around ± 5 %, which is usual for such porous media. Thus, the subsequently prepared samples, for investigation of the effect of gas exchange, should have a thickness bigger than 3 mm.

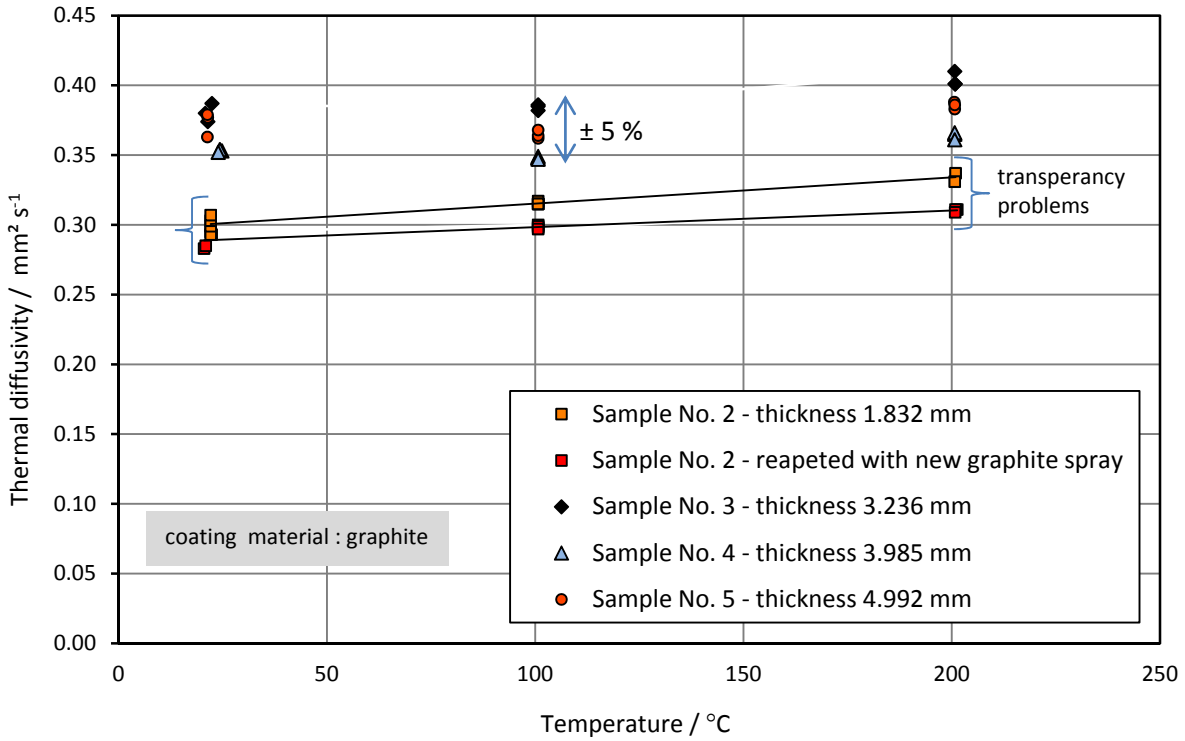

Figure 43: Evaluation of thermal diffusivity for samples with different thickness

Effect of exchanging the gas atmosphere on thermal diffusivity

Measurements of thermal diffusivity in LFA for porous materials were performed in different gas atmospheres. The aim of these experiments was to investigate the influence of exchanging the gas in the porous materials on their thermal diffusivity and to compare this effect to that found by measuring their thermal conductivity in RHFA.

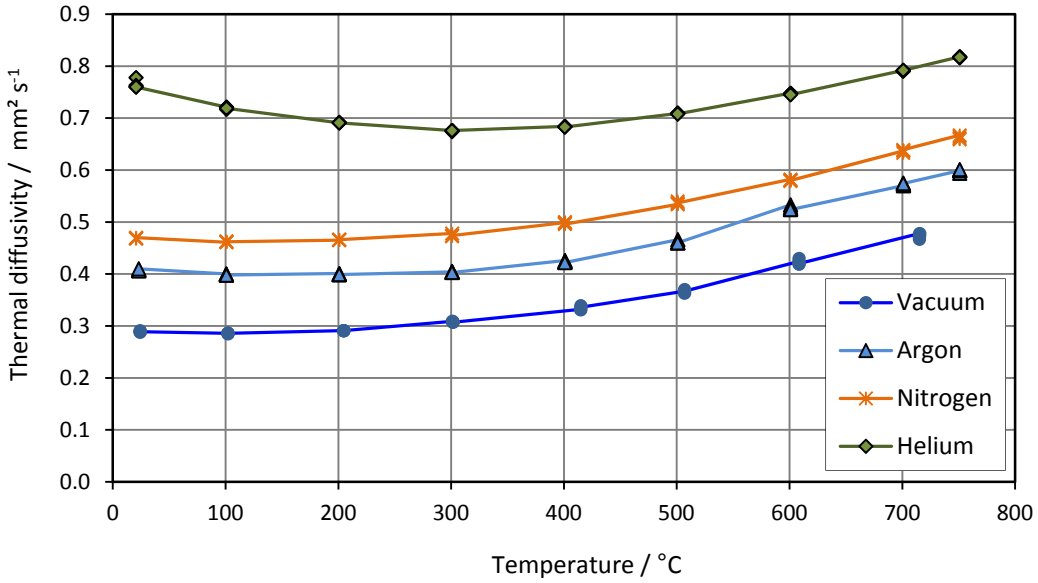

Figure 44: Thermal diffusivity of one of the investigated porous material in various gas atmospheres

An example of these measurements for one of the investigated materials within the present work is shown in this section, see Figure 44. All other results will be presented and discussed in detail in the next chapter 'results'. As expected, exchanging the gas in the pores leads to a change in the evaluated thermal diffusivity, as seen in Figure 44. The change of thermal diffusivity through exchanging the type of gas inside is directly related to the thermal conductivity of the filling gas. Thus, measuring in vacuum gives the lowest results of thermal diffusivity. The results of thermal diffusivity with argon, which has lower thermal conductivity than nitrogen, are lower than ones with nitrogen or helium. As previously mentioned, more discussion about this effect and its coupling with temperature for different porous materials will be explained in the next part.

6.4 Summary of Chapter 6

In the present work, the Laser flash method was used as a second method to investigate the influence of exchanging the gas atmosphere upon the thermal diffusivity of the analyzed porous materials. For this purpose, the Laser flash method should be carefully analyzed to be successfully applied to porous material.

In the present chapter the principles of laser flash method were introduced. The different models of the evaluation process for this method were presented and compared. The applied laser flash apparatus was described in detail.

However, applying this method to porous materials is faced with many problems and difficulties. It takes a huge effort to overcome these difficulties. The coating of the surfaces of the samples improves the measurements. However, many experiments were needed to find the appropriate surface coating and coating method that provide good and acceptable results comparing to reference data. Graphite spraying method outstands as an effective coating method.

Further results of thermal diffusivity measurements for the different porous materials will be presented in the next chapter of the present work.

7 Experimental Results and Analysis

7.1 Criteria for Selecting Porous Materials for This Experimental Study

Available porous materials possess many different chemical compositions, mechanical structures, thermal properties, shape of solid particles and hence a wide variety of applications. The porous materials for this experimental study were selected using the factors listed in Table XIII and Table XIV.

The chapters 2 and 3 contained discussions of two categories that affect the heat transfer mechanisms. The first category was structural characteristics that reflect the features of the

Table XIII: Factors that affect heat transfer in porous media

Category	Factor	Affected parameter
I. Structural characteristics	Density/Porosity	Heat conduction by solid phase and Radiation
	Specific surface area	Interface heat transfer between solid and gas phase
	Pore size distribution	Heat conduction by the filling gas (Knudsen effect)
	Contact between solid practical (nonconsolidated solid particles)	Thermal Contact resistance
	Chemical composition of solid materials	Heat conduction by solid phase and accommodation coefficient
	Pore shape / Particle shape	Radiation and heat conduction by solid phase
	Continuity in solid phase	Overall heat flux
	Solid surface treatment	Accommodation coefficient
	Thickness effect	Radiation
II. Internal and surrounding conditions	Temperature	Radiation and thermal properties of two phases (solid and gas)
	Gas pressure	Gas thermal conductivity (Smoluchowski effect)
	Kind of the filling Gas	Accommodation coefficient, Knudsen effect, gas thermal conductivity
	Humidity	additional heat flux
	Loading pressure	Solid thermal conductivity
	Open or closed top	heat transfer by convection

solid phase. The second category is the internal and surrounding conditions which relate directly or indirectly to the gas phase.

Table XIII lists the factors in both categories along with the parameters that are affected by increasing or decreasing each factor. The two categories have a main difference: varying the internal and surrounding conditions is easier than changing the structural characteristics.

The structural characteristics for a given porous material are dictated by the production process. In contrast, the internal and surrounding conditions are controlled by the application (or use). The latter is the case for this experimental study. The aim of this study was to investigate the Knudsen and gas atmosphere (and temperature) on the effective thermal conductivity of the selected porous material. The restrictive conditions are given in Table XIV. According to these restrictions, and with appreciated help of experts in insulating materials[9], twelve different materials from different manufactures were chosen to be investigated in this work.

Table XIV: Criteria of selecting the porous insulating materials

Factor	**restriction**
Connection between Particles	consolidated
Upper limit of effective thermal conductivity	insulation materials; $\lambda_{eff} < 0.5\ W\ m^{-1}\ K^{-1}$
Porosity	70 – 95 %
Structure of pores	open pores system
Chemical composition	no restrictions
Pore size distribution	macro to nano ranges
Specific surface area	no restrictions
Solid surface treatment	no treatment
Pore shape / Particle shape	no restrictions

7.2 Results of the Experimental Work

The results of the whole experimental work for all different materials will be presented in the present chapter. These results are described the porous structure and thermal properties (effective thermal conductivity and effective thermal diffusivity) of the investigated materials. Evaluation of these results also will be introduced here. This gives a complete perspective about the results of each material, and makes the comparison of the results and the different factors easier to understand.

[9] Dr.-Ing. Rhena Wulf and Mr. Gerald Barth, Institute of Thermal Engineering, TU Freiberg

7.3 The Investigated Materials

The investigated materials in this study, as mentioned in first section in this chapter, are porous insulating materials, which are commonly used for high-temperature insulation up to 1000 °C. These materials are ordered from different manufacturers in Germany. The selected materials have different composition, which is assumed to have a small influence on our investigation of effective thermal conductivity when exposed to various gas atmospheres. All these materials and their chemical composition are listed in Table XV. This information was taken from the data sheets of each material provided by the producer. For this reason the chemical composition for some materials is given as a range.

Table XV: Chemical Composition of the investigated porous materials

Material No.		Composition (%)						
		AL_2O_3	SiO_2	CaO	SiC	$ZrSiO_4$	Fe_2O_3	others
(a)	PM1	63	33				0.8	Remnant < 6 %
	PM2	35	58				1.7	
	PM3	50	49					
(b)	PM4		44-45	44-45			0.1	
	PM5		44-45	45-46			0.1	
	PM6		47	45			0.3	
	PM7		45-47	36-38			0.2	
	PM8		50-90	1-25	5-50			
(c)	PM9		80		15		5	
	PM10		50			45	5	
	PM11		69		30			
	PM12		80		15		5	

All the investigated materials contain silica in their chemical composition. That is usual for such high temperature insulating materials. By noticing the others compounds in the chemical composition, the investigated materials could be classified into three categories:

(a) Materials with Aluminum Oxide as the second largest portion in the composition (PM1-PM3)
(b) Materials based on Calcium Silicate (PM4-PM7)
(c) Materials containing Silicon Carbide or Zirconium Silicate (PM8-PM12)

The porous material (PM8) could be classified to either one of the last two categories. However, a further investigation in this study will show that it has a behavior similar to the materials in last group (c). There is a constituent in the chemical composition that is unknown due to confidentiality issues of each manufacture. This is usually a kind of binding material. Past experience (Wulf, 2009) with materials of group (b) based on calcium silicate shows that such materials undergo changes in mechanical and thermal properties after first tempering. That is why these materials should be specially tempered before performing the measurements. The chemical composition of the materials, i.e. the composition of the solid matrix, determines the thermal conductivity of the solid matrix and thus the effective thermal conductivity of the material. The following sections will show that there is also dependency between the composition of the materials and the kind of the porous structure.

7.4 Structure Controls Properties

The bulk densities of all material were also measured. The materials have a wide range of bulk densities ($215\ kg\ m^{-3} < \rho < 1000\ kg\ m^{-3}$), as seen in Table XVI. The porosity of the materials has also been investigated. Two classes of porosity are found with group (a) ranging from 68 % to 88 % and the other two groups (b and c) with higher porosities from 90 % to 94 %. Several samples from each material were prepared that are suitable for mercury intrusion porosimetry for determination of the **P**ore-**S**ize **D**istribution (PSD). The utilized porosimetry enables detection of pore sizes scaled from micro- (200 µm) down to the nano-range (6 nm) by applying the intrusion pressure in two stages. Table XVI includes significant data for the description of the pore size distribution, i.e. the near maximum diameter d10, the mean diameter d50, and the near minimum diameter d90 (with the indices 10, 50, 90 referring to the percentage of the intruded volume). Additionally the most frequent diameter $d_{freq.}$ for all materials is evaluated and listed also in Table XVI.

Table XVI: Listing of structural properties of the investigated materials

Material No.	Group No.	Bulk density kg m^{-3}	Porosity %	d_{10} nm	d_{50} nm	d_{90} nm	$d_{freq.}$ nm
PM1	a1 (a)	1000	67.4	34277	6389	784	6065
PM2	a2	639	75.7	50000	16000	700	81185
PM3	a3	250	87.4	50500	13000	7000	10255
PM4	b1 (b)	215	90.4	771	292	200	564
PM5	b2	275	90.8	300	250	90	554
PM6	b3	260	93.1	222	182	19	389
PM7	b4	217	93.4	56900	180	15	465
PM8	c1 (c)	272	92.3	16800	1000	12	23.6
PM9	c2	225	92.2	67530	867	17	14.8
PM10	c3	370	90.0	36676	490	15	15.2
PM11	c4	305	91.3	17600	350	7	13.8
PM12	c5	235	93.5	4000	200	7	13.7

The pore-size distribution of a material can be mathematically described as a normal distribution. The pore-size results are obtained from the cumulative distribution function (CDF) varying from 0 % to 100 % which gives a better overview of the measured materials, see Figure 45. For example, a CDF value of 0.3 at a pore size of 10 µm means that 30 % of the pores scale larger than 10 µm and 70 % are smaller. The results of pore-size distributions for the twelve investigated materials are presented in Figure 45, which can be classified into three groups:

- Group (a) includes three materials, which are located in the macro-range and they are characterized by narrow pore-size distributions ranging roughly from 1 µm to 100 µm. The shape of the CDF curves follows the normal distribution. One of them, (a1), is extending somewhat into the nano-range direction, i.e., this material has a larger portion of small pores than the other two (a2 and a3)

- Group (b) represents four materials distributed at the micro-scale and also having narrow pore-size distributions from 20 nm to 2000 nm. The shapes of these *CDF*s

correspond also to the normal distribution except (b4) with a small portion of pores in the macro-range, i.e., it has a wide distribution from the macro- to the nano-range. Otherwise, it has a narrow distribution in each of the two ranges, namely, the macro- and nano-ranges

- Group (c) covers five materials with wide pore-size distributions ranging from the macro- down to the nano-range. The curves extend more to the right (nano-scale) than the materials in group (b) which means that a larger portion of pores are located in the nano-range. The shape of *CDF* for this group is described mathematically as a beta distribution.

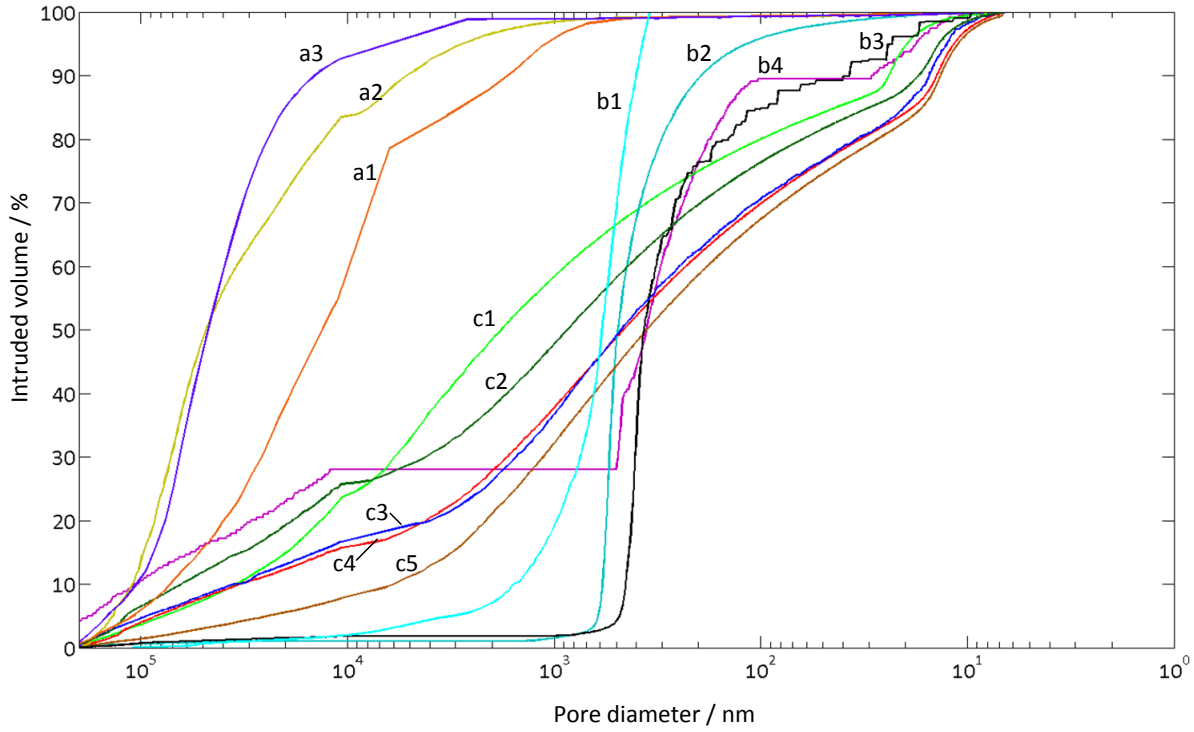

Figure 45 : Pore size distribution of all materials

It is obvious from the schematic presentation of pore size distribution of all materials that the mean diameter cannot be considered as a single characteristic parameter for identifying the porous structure. For example the materials (b3), (b4) and (c5) have almost the same mean diameter d_{50} (180 nm, 182 nm and 200 nm, respectively), however, they have totally different pore size distributions. Since the pore size distribution will be considered as structure control property, the resulted data should be reliable. It is therefore required to conduct further investigation about the following two effects: tempering effect and the structure effect.

7.4.1 Tempering Effect

Materials based on calcium silicate have thermal behavior in as-received state different than that one after exposure to elevated temperatures. The tempering effect (12 hours at 850 °C) leads to changes of geometry and also to mass losses up to 15 % in some materials. That was concluded in a previous experimental work on such materials (Wulf, 2009).

In the present work the tempering effect was also experimentally investigated in regards with the pore size distribution. The results of pore-size distribution of the new samples for each material before and after tempering are presented in Figure 46.

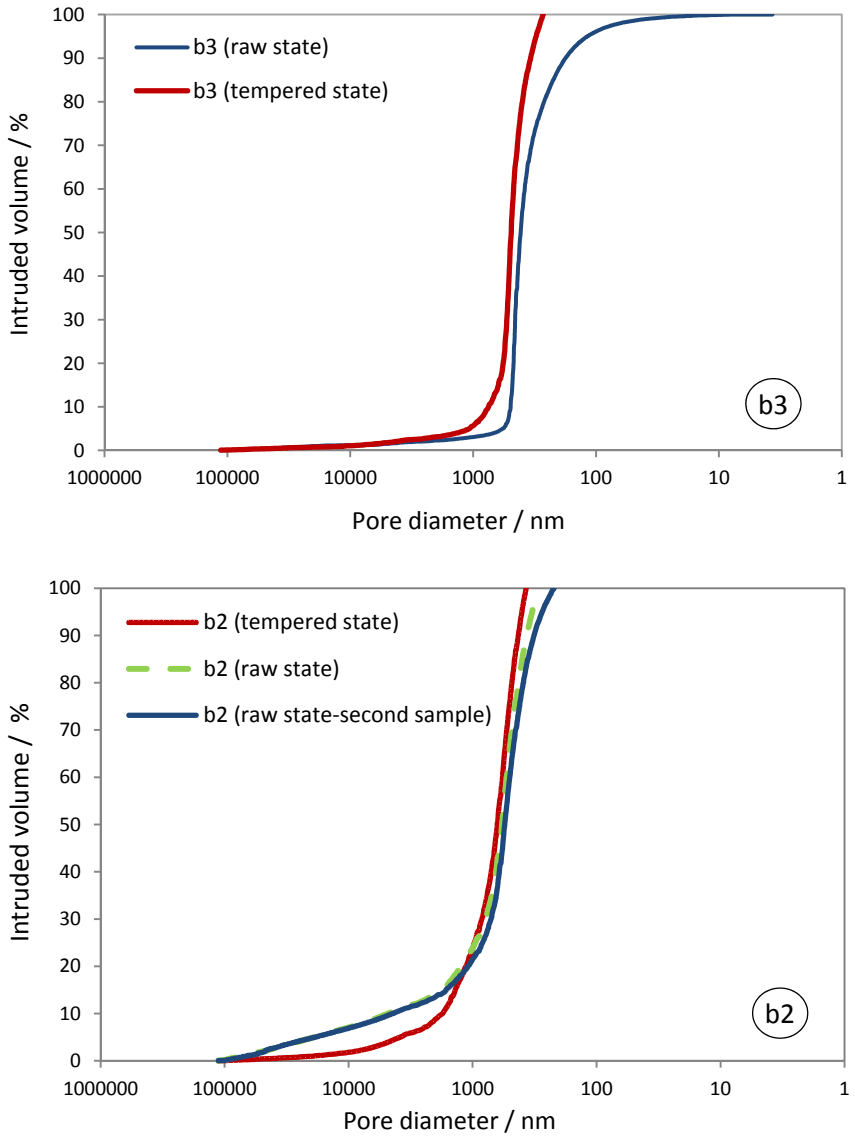

Figure 46: Tempering effect on pore size distribution of materials based on calcium silicate

The results of material (b3) show small difference in PSD after the tempering, see Figure 46 (b3). The difference is a kind of sliding of PSD curve to left side, which indicates an increase in the number of pores with bigger size. This result could be interpreted, that some fibers, which are used usually as binder through the production process, are burnt out. That leaves relatively big hollow spaces, which are recognized as new pores in PSD-curve. However, the results of PSD for material (b2) contradict with the above effect, Figure 46 (b2). They show a decrease in numbers of big pores. These results were unexpected. Measurement of PSD with new sample from same material (b2) leads to the same trend of the curve. This reverse effect is due to the shrinkages that the material is exposed to. As a conclusion *the tempering effect has no big influence on pore size distribution of materials based on calcium silicate.*

7.4.2 Microstructure Effect

The samples are made into fragments with volume of 1 cm^3, which are used for measuring the pore size distribution in the porosimetry. They are small comparing to the samples that were used for radial heat flowmeter. That leads to the question whether the results of PSD are reliable and representative for the whole porous structure. To answer this question samples of same material are taken from different positions. Measurements of PSD for these samples for three different materials are performed and the results are presented in Figure 47.

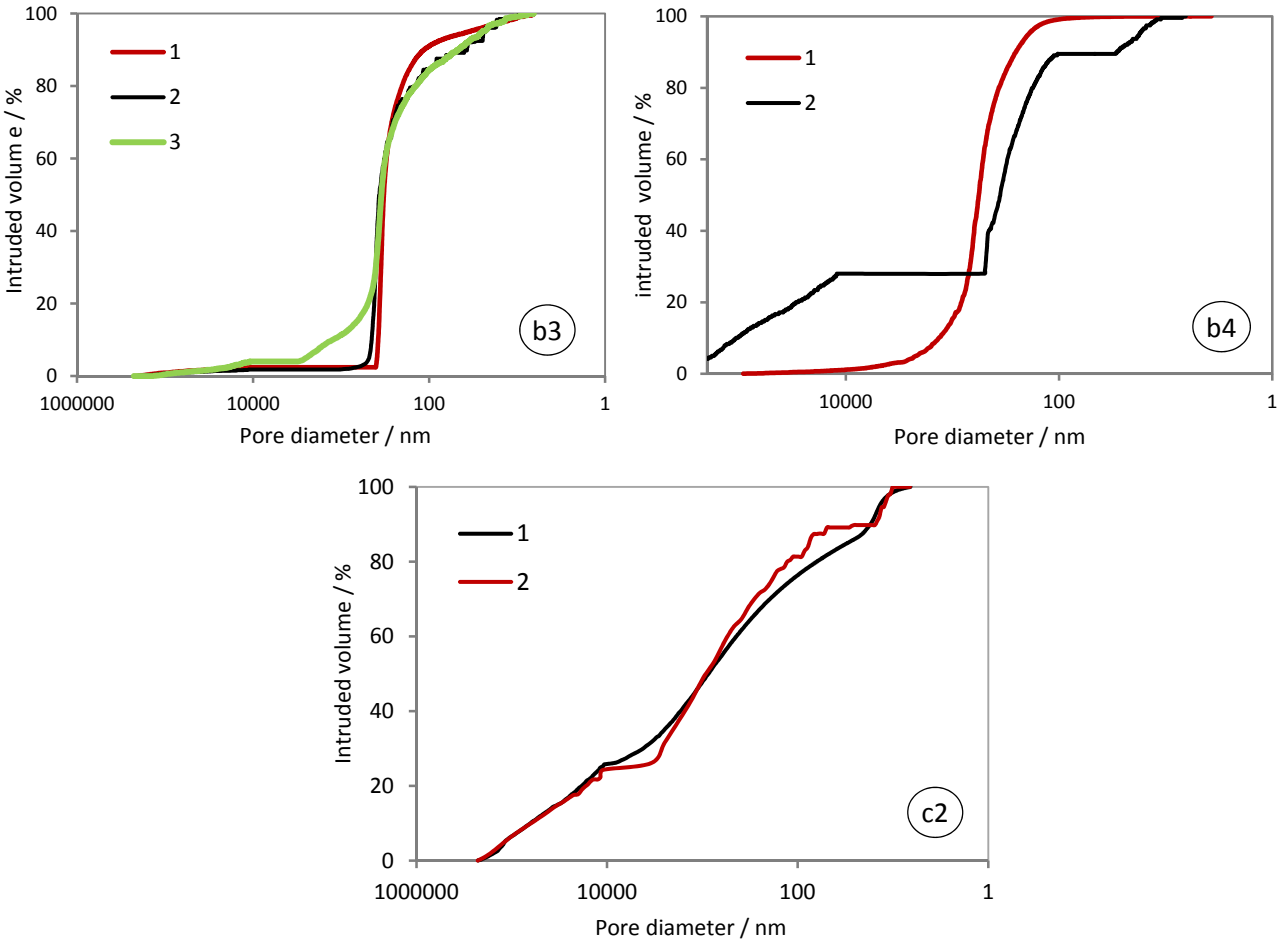

Figure 47: Comparison of pore size distribution of different samples from the same material

As seen above, there is a difference between PSD of the samples from the same material. The difference is very small for the material b3 considering results of samples (1) and (2). The results of samples of material c2 show also small difference. The difference becomes more pronounced for the material b4. The same is found by the sample 3 in material b3.

The difference between the results could be interpreted as inhomogeneous effect. The microstructure of the solid matrix and the morphology of the material affect the results of PSD. Microstructure of two materials (one from (b) group and one from (c) group) are compared through photos of SEM, see Figure 48.

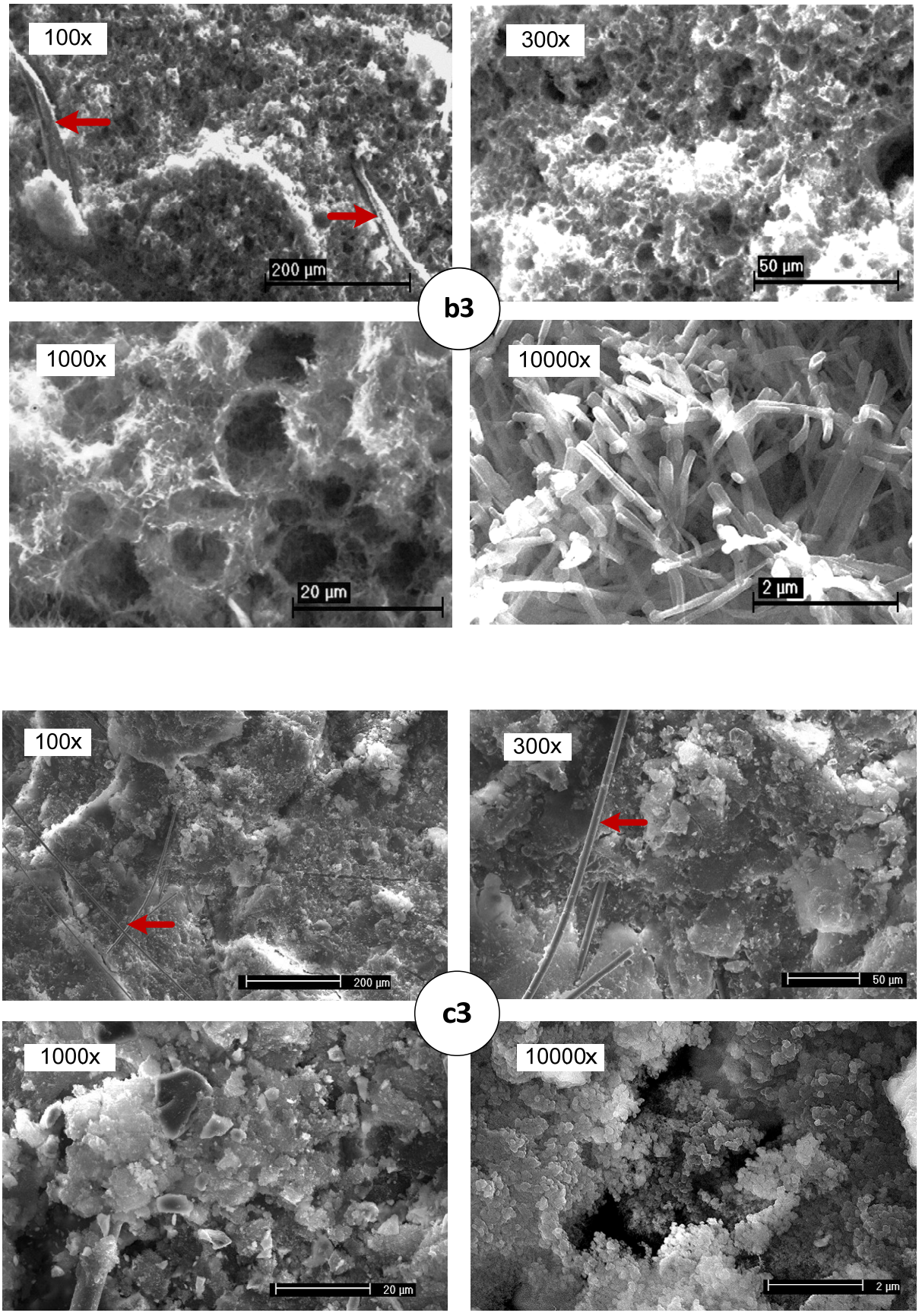

Figure 48: SEM-Images of materials (b3) and (c3) with different magnification varies from 100 to 10000 times

The bounded fibers in both materials (b3) and (c3) give the microstructure an inhomogeneous effect when measuring the PSD as seen in Figure 48, where the fibers are denoted with red arrows. The pore geometry is an important factor when evaluating the PSD. By scanning the material (b3), the constructed images show that pores are formed like spheres, which are recognized in images with magnification of 300 times and 1000 times. However, increasing the magnification to 10000 times, changes that perception and show even the pore walls contain fibers and include in their structure also small pores, see the right below image for material (b3) in Figure 48. On the other hand, by looking at the image of the material (c3) the porous structure is not recognized even in the image with magnification of 1000 times. The porous structure is only recognized at high magnification with 10000 times. The pore geometry is a kind of hollow spaces and the pore walls consists of many connected small balls.

Comparison both materials, a big discrepancy is found in microstructure of solid matrix. Thus, variability in the results for pore size distribution of the same material could be interpreted by evaluating the microstructure of solid matrix. For example, the microstructure of material b2 shows pore walls based on fibers, which gives an elastic effect while applying the pressure of intruded mercury. This explains the fluctuation for PSD curve of b3 in Figure 45. That leads to the conclusion that there is *a direct dependency between the microstructure and the reliability and reproducibility of results of Pore Size Distribution*.

7.5 Effective Thermal Conductivity Measurements

7.5.1 Overview of experiments

The thermal-conductivity measurements have been carried out using the radial heat flowmeter (RHFA) under various gas atmospheres, namely, krypton, argon, nitrogen, and helium. An overview of all experiments that were performed on the investigated materials is presented in Table XVII.

Table XVII: Overview of performed experiments by RHFA

Group	Material No.	The filling gas*			
		Kr	Ar	N2	He
a	a1	x	x	x	x
	a2	–	–	x	x
	a3	x	x	x	x
b	b1	x	x	x	x
	b2	–	–	x	x
	b3	–	x	x	x
	b4	x	x	x	x
c	c1	–	–	x	x
	c2	x	–	x	x
	c3	x	x	x	x
	c4	–	x	x	x
	c5	x	x	x	x

* x performed test, – no test

The aim of these experiments is to investigate the effect of changing the filling gas upon the thermal properties of porous media and the total thermal conductivity. The bulk thermal conductivity of helium is approximately 585 % bigger than that of nitrogen, whereas the thermal conductivity of nitrogen is 145 % bigger than that of argon and 270 % that of krypton, see properties of gases in Appendix B. Thus, all materials are tested mainly in nitrogen and helium atmospheres. Fewer materials from each group are tested also in argon and krypton, see Table XVII, due to the costs of these gases.

The measurements in radial heat flowmeter are performed in a furnace temperature in the range from 300 °C to 900 °C. The lower temperature of 300 °C is limited to the sensibility of the calorimeter system. Whereas the upper temperature of the experiment inside the hollow cylindrical samples is limited to the maximum allowed temperature for the respective material. The materials of group (b), which have composition based on calcium silicate, are tempered at 850 °C for 8 h before performing the experiments. For most of the materials only one test on each material is done per each respective filling gas. However, in some cases the experiments were repeated to verify the effect that is detected through the experimental results.

7.5.2 Effective thermal conductivity results

The effective thermal conductivity results are evaluated from the measured data of temperatures and heat flux, which are recorded from RHFA. The measurements are performed employing the improvements in experimental and evaluation procedure that were previously introduced in see chapter 5. Thus the presented final results of effective thermal conductivity include the corrections, e.g. heat gain from environments. Results of effective thermal conductivity measurements for all materials are given in Appendix C. In this Chapter, results are presented for one material from each materials-group. Figure 49, Figure 50 and Figure 51 show results for three porous materials (a1, b1, c5), respectively, measured in four different gas atmospheres, namely: krypton, argon, nitrogen and helium.

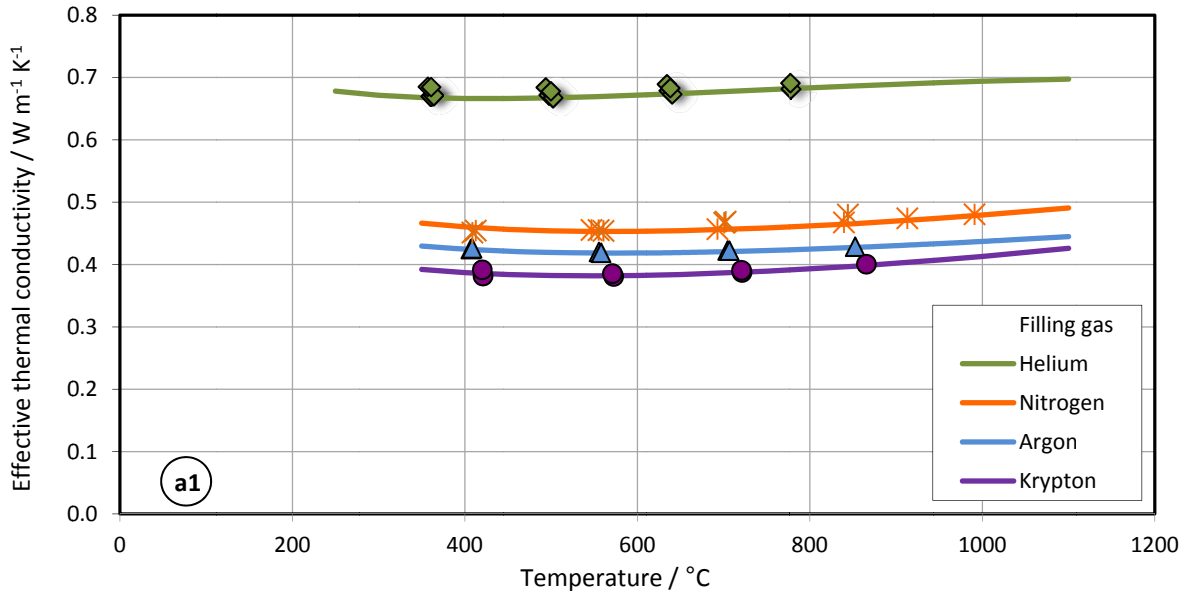

Figure 49: Effective thermal conductivity of material a1 in various gas atmospheres
points: measured, lines: true effective thermal conductivity

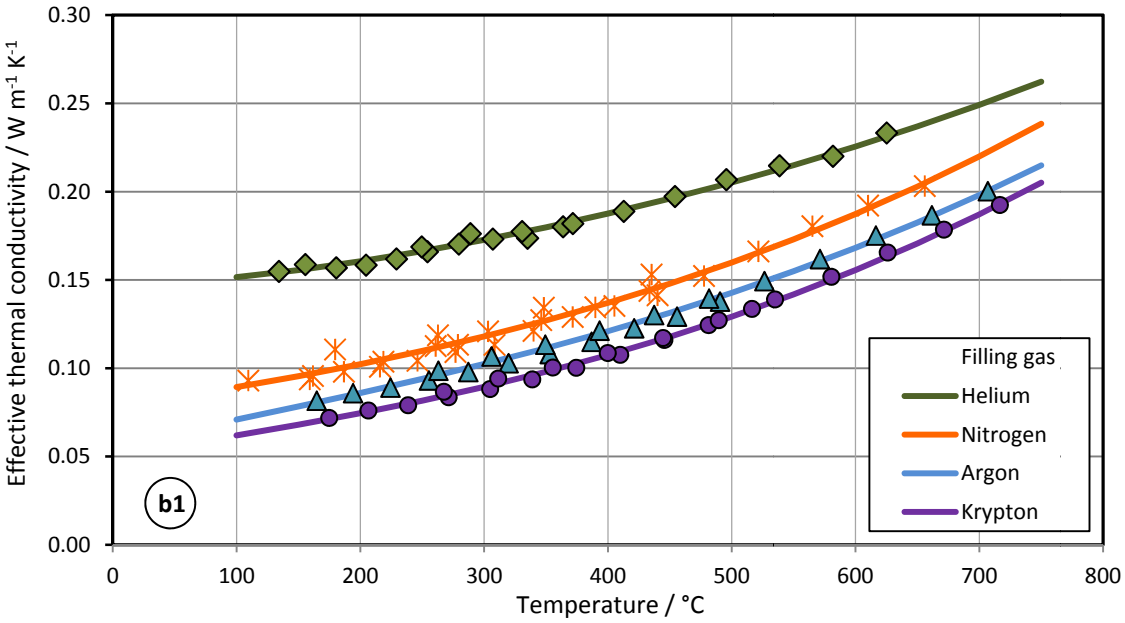

Figure 50: Effective thermal conductivity of material b1 in various gas atmospheres
points: measured, lines: true effective thermal conductivity

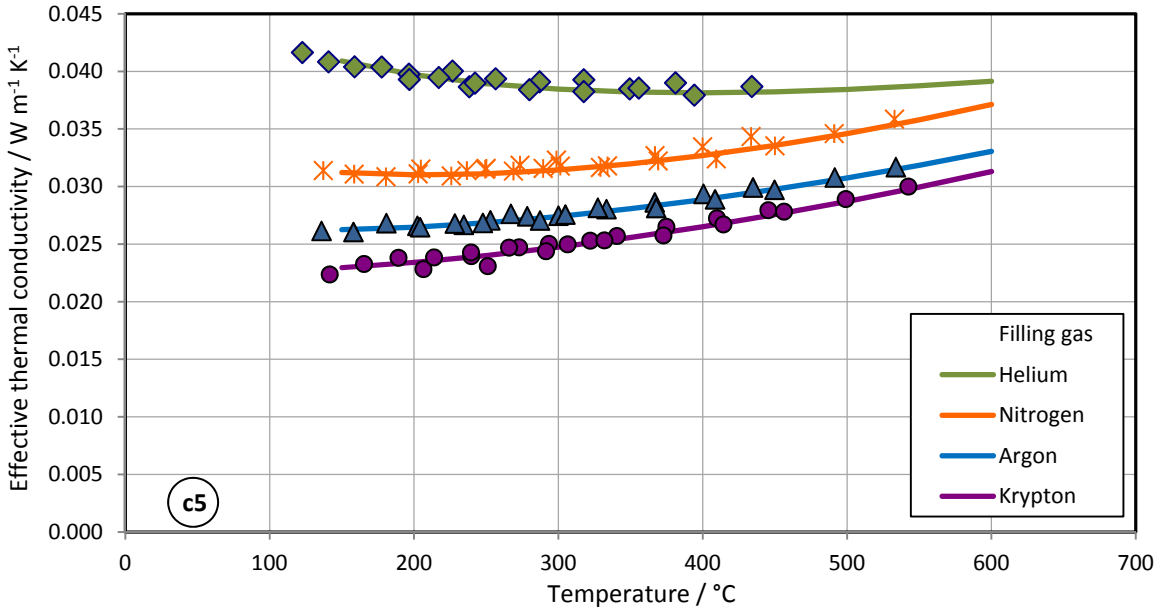

Figure 51: Effective thermal conductivity of material c5 in various gas atmospheres
points: measured, lines: true effective thermal conductivity

The results of effective thermal conductivities of each material that are measured using the RHFA are represented with points in Figure 49, Figure 50 and Figure 51. The true effective thermal conductivities have been evaluated for each material with the respective filling gas using the previously introduced function, see chapter 5- eq. (51):

$$\lambda_{\text{eff, true}}(T) = a\sqrt{T} + \frac{b}{T} + c\,T^3 \tag{59}$$

where T is the temperature and given in Kelvin. The curves resulting from this function are presented in these figures as lines to show the various dependencies of true effective thermal conductivity upon the temperature with respect to the various filling gases. As expected, effective thermal conductivity increases in the order: Kr – Ar – N_2 – He, which is the same order of increasing gas thermal conductivity. Furthermore:

- The largest effective thermal conductivities are obtained for a1 (nearly 0.7 W m^{-1} K^{-1} at 200 °C in helium), and only minor temperature effects are found, see Figure 49. The trend for all 4 gases seems to be the same, and the respective curves are more or less in parallel.
- Effective thermal conductivity of b1 is much lower than a1 (0.15 W m^{-1} K^{-1} at 200 °C in helium), and it exhibits an increased temperature effect showing a progressive gradient, see Figure 50.
- Finally, sample c5 shows lower results of effective thermal conductivity than a1 and b1 (only 0.04 W m^{-1} K^{-1} at 200 °C in helium), see Figure 51. A new and surprising effect is found in measurement in helium atmosphere comparing with other gases in the temperature range below about 350 °C where the effective thermal conductivity shows a tendency to decrease with increasing temperature. The general trend is characterized by curves that are getting closer to each other for increasing temperatures, i.e. the effect of changing the filling gas becomes less pronounced.

These observations will be discussed in details in the following chapter.

7.5.3 Validation of thermal conductivity Results measured by RHFA

Samples with plate geometry (300 mm X 300 mm X 20 mm) of some materials (two of each materials-group) are prepared to perform thermal conductivity measurements using **P**anel **T**est **F**acility (PTF) followed ASTM C201-93, in air atmosphere. Thermal conductivity of air (0.0264 W m^{-1} K^{-1} @25 °C) is near to that of nitrogen (N2) (0.0254 W m^{-1} K^{-1} @25 °C), for more data see Appendix B. That allows to validate the effective thermal conductivity results evaluated from RHFA in nitrogen atmosphere by a direct comparison with that measured in hot plate apparatus (PTF) along the respective temperature range. Figure 52, Figure 53, and Figure 54 show the compassion between the true effective thermal conductivity evaluated from RHFA measurements and the measured effective thermal conductivity in PTF.

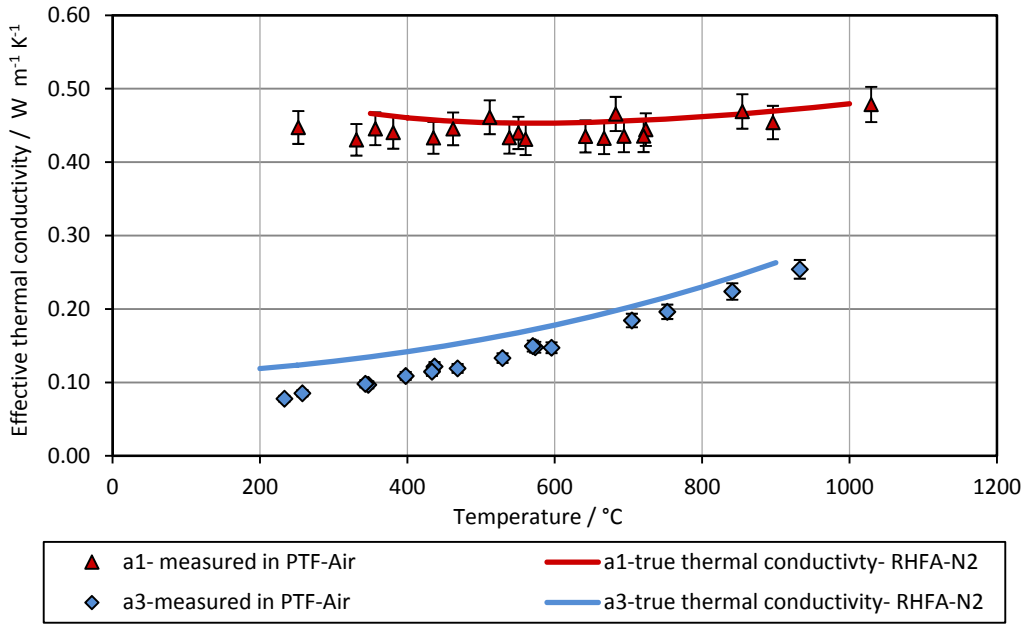

Figure 52: Comparison between the effective thermal conductivity results measured by RHFA and PTF for materials a1 and a3

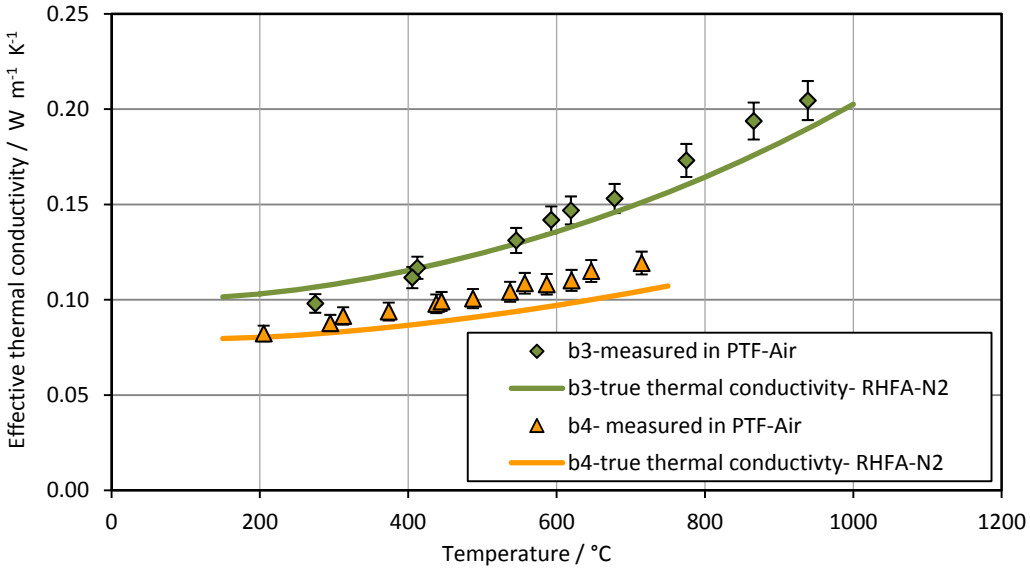

Figure 53: Comparison between the effective thermal conductivity results measured by RHFA and PTF for materials b3 and b4

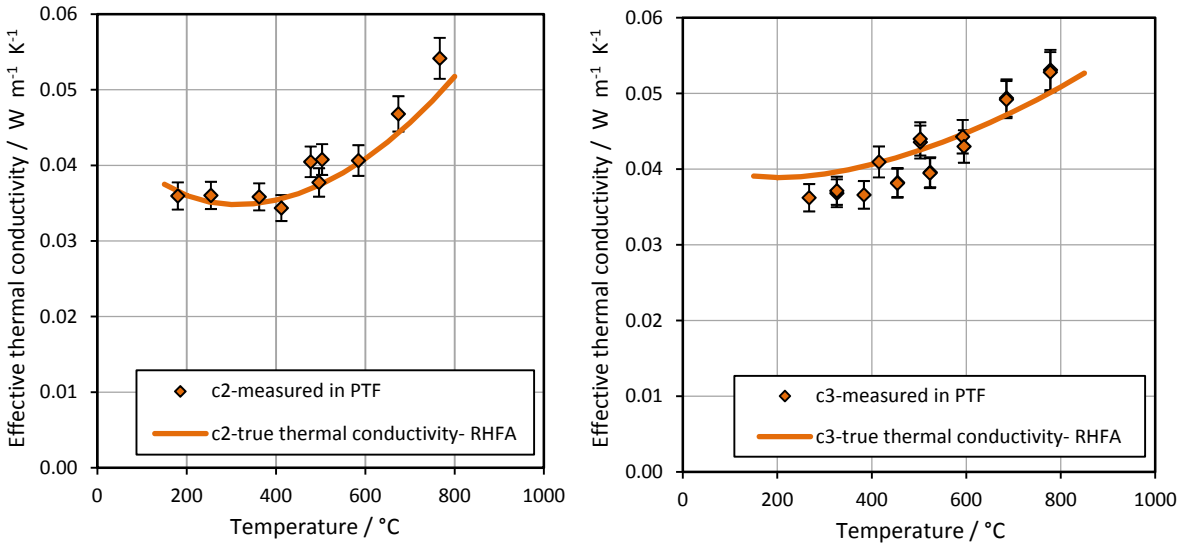

Figure 54: Comparison between the effective thermal conductivity results measured by RHFA and PTF for materials c2 and c3

As can be seen above, a very good agreement is observed between effective thermal conductivity results that measured in PTF with 5 % of uncertainty and those measured in RHFA for all materials except two materials a3 and b4. The results of the latter materials show deviations up to 30 % in thermal conductivity results for material a3 in temperature range under 400 °C. This could be interpreted due to two reasons. The first one is the difference in density between the samples. The samples for PTF are prepared with best possible to have identical bulk density with samples of RHFA with an oscillation of ± 2 %. However, material a3 has fibrous structure and owns bulk density in plate geometry 15 % lower than one of cylindrical geometry. The higher bulk density for sample of a3 explains the different slope of effective thermal conductivity in RHFA compared to PTF, as seen for material a3 in Figure 52. It has a higher value in lower temperature range and a flatter trend in higher temperatures than that of PTF. On the other hand, material b4 has bulk density in plate geometry 9.5 % higher than that of cylindrical one, which leads to an opposite effect comparing to the results of material a3, see Figure 53. The second reason is the anisotropy in porous structure. The measurements in RHFA are performed in a different direction comparing to that of PTF. That is restricted by the preparation method of cylindrical samples. As a conclusion of these comparisons, the measurements in PTF confirm generally the results of effective thermal conductivity in nitrogen atmosphere taken from RHFA and the different trends of dependency of effective thermal conductivity upon the temperature.

7.6 Effective Thermal Diffusivity Measurements

7.6.1 Overview of experiments in LFA

As mentioned in a previous chapter, application of laser flash method to porous media is accompanied with many difficulties. Using the surface coating for the samples improves performance of the measurements. However, it was not possible to apply LFM to all investigated materials within this work. An overview of successfully performed experiments is presented in Table XVIII. Many other experiments, which produced unexpected temperature rise curves, will be excluded in this work. This is due to the big error in fitting these curves and the resulted values of thermal diffusivity have fluctuation up to ±20 %. Thus the effect of filling gas upon thermal diffusivity could not be evaluated; an example of these faulty results is presented in Figure 55. The results of thermal diffusivity of material c5 in vacuum fluctuate above 500 °C and overlap the values of thermal diffusivity for the same material in argon, as seen in Figure 55. Such experiments give unreliable data. On the other hand, it was possible to perform valid measurements on four materials in the LFA. The results obtained in three different filling gases, as well as in vacuum are reliable and have good reproducibility.

Table XVIII: Overview of performed experiments by LFA

Group	Material No.	Filling gas			
		Vacuum 1.3×10^{-7} bar	Ar 1 bar	N_2 1 bar	He 1 bar
a	a1	X	X	X	X
b	b3	X	X	X	X
	b4	X	X	X	X
c	c2	X	X	X	X

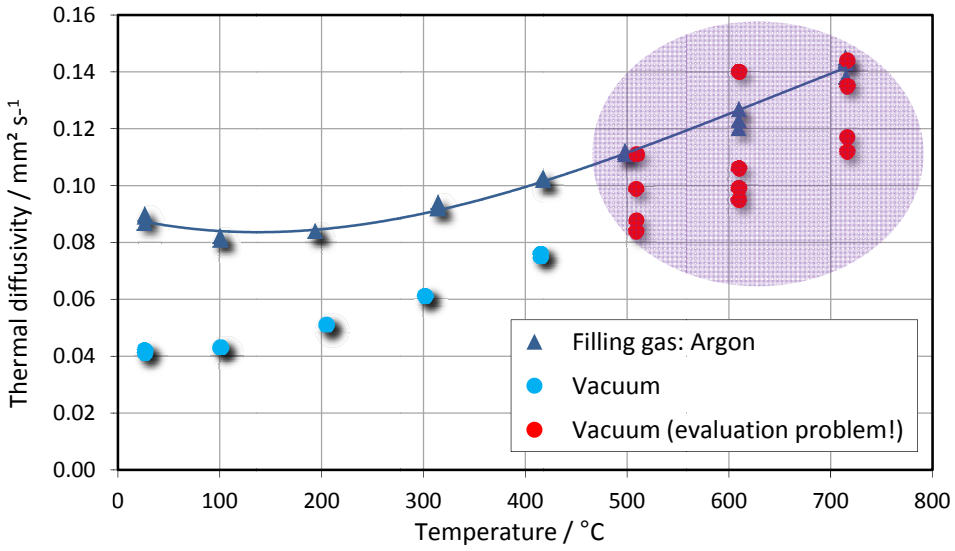

Figure 55: Faulty test results of thermal diffusivity of material c5

7.6.2 Effective Thermal Diffusivity Results

The thermal diffusivity was measured on four porous materials in three different gas atmospheres (argon, nitrogen and helium) at normal pressure 1 bar over the measured temperature range from 25 °C to 800 °C. The furnace chamber is evacuated through two supplied pumps and reaches the end pressure of 2×10^{-7} bar at 35 °C for argon. The final pressure is decreased a little with raising the temperature of the sample through the better outgasing of sample and the furnace chamber. The final pressure reaches a value of 1.4×10^{-7} bar at 750 °C. Thermal diffusivity is evaluated from the measured temperature rise curves using the Cowan-model. The results of thermal diffusivity of the chosen four materials are presented in Figures 56, 57, 58 and 59.

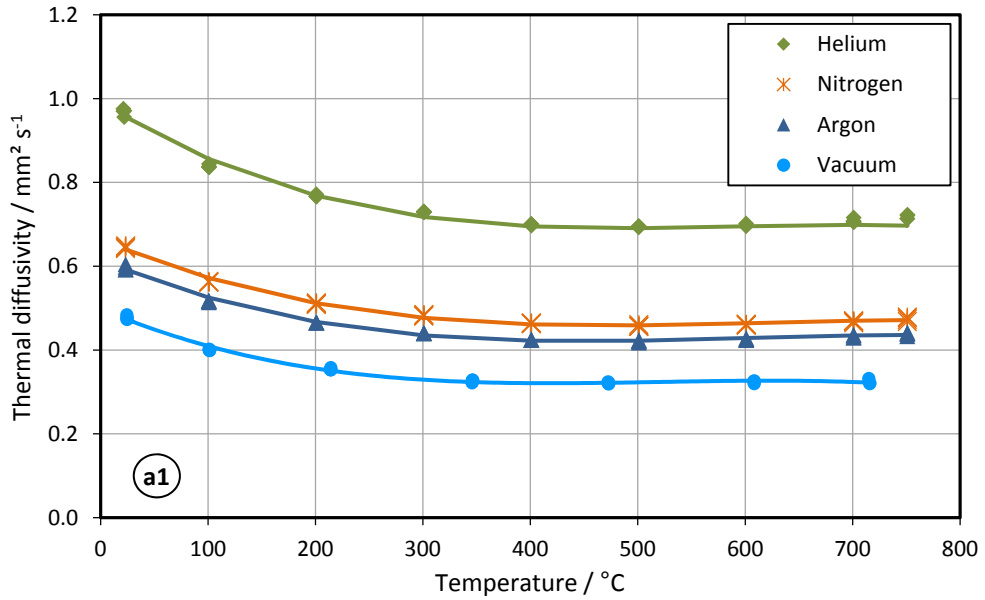

Figure 56: Effective thermal diffusivity of material a1 in various gas atmospheres
points: measured, lines: interpolation curves

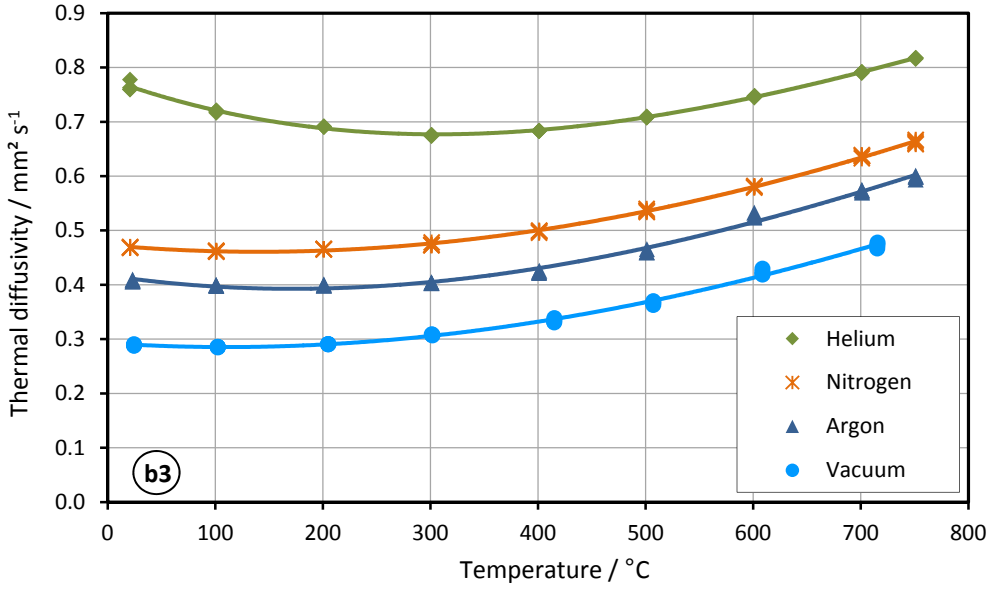

Figure 57: Effective thermal diffusivity of material b3 in various gas atmospheres
points: measured, lines: interpolation curves

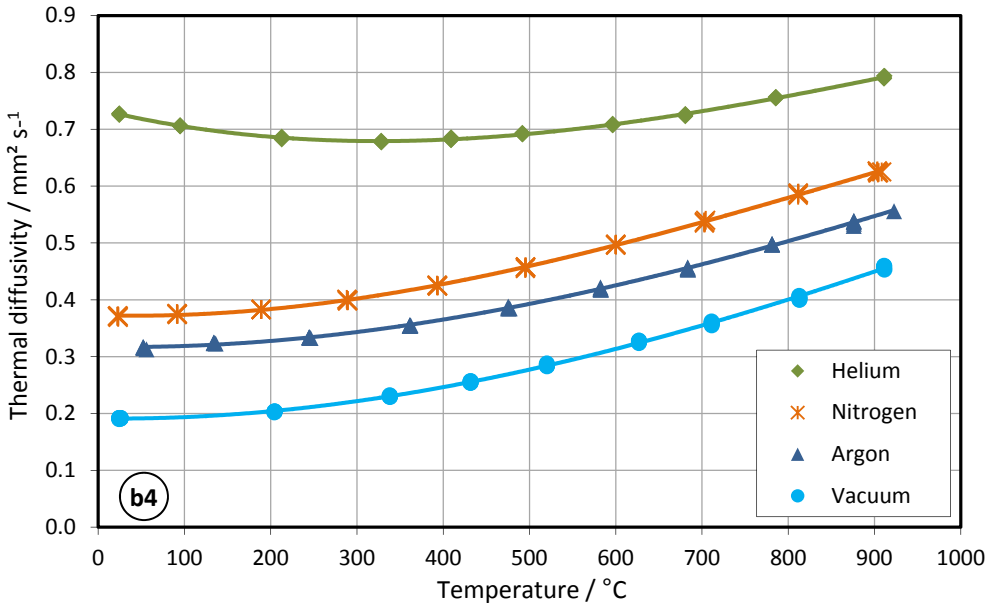

Figure 58: Effective thermal diffusivity of material b4 in various gas atmospheres
points: measured, lines: interpolation curves

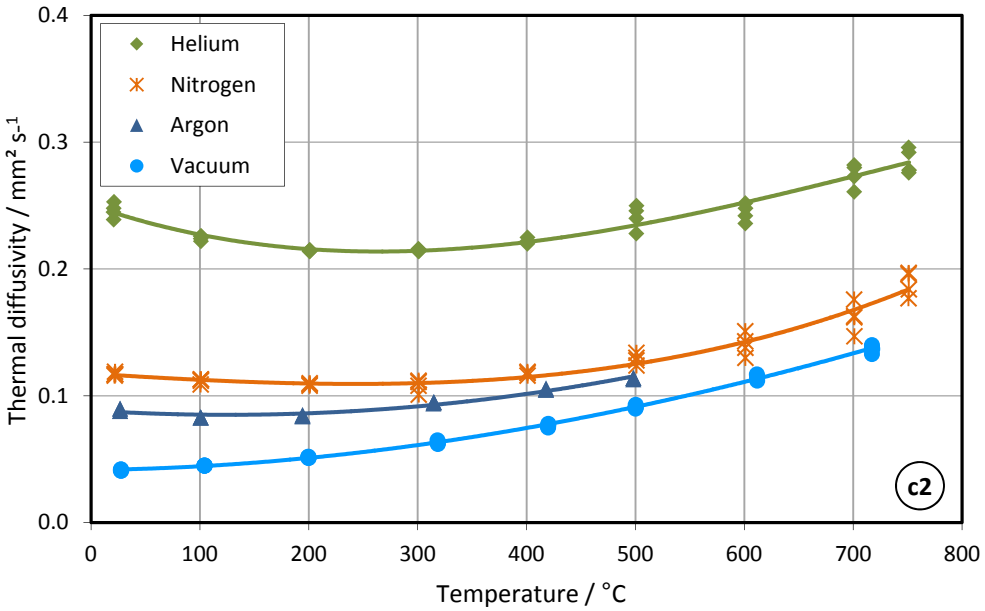

Figure 59: Effective thermal diffusivity of material c2 in various gas atmospheres
points: measured, lines: interpolation curves

The measured data are represented by points in the four figures. Interpolation of these data is achieved in order to find out the dependency of evaluated effective thermal diffusivity upon the temperature. The chosen polynomial curve is a function of the third order as following:

$$\alpha_{eff}(T) = a\,T^3 + b\,T^2 + c \tag{60}$$

where T the temperature given in Kelvin; a, b and c are constants of the polynomial curve. The resulting curves are represented as lines in last four Figures.

As expected, effective thermal diffusivity increases in the order: Vacuum- Ar – N_2 – He, the same order of increasing the gas thermal conductivity. It is the same noticed effect in effective thermal conductivity results. Furthermore:

- The largest values of effective thermal diffusivity are found to be for material a1 and then followed by both materials b3 and b4, and the lowest ones are for material c2. For example the effective Thermal diffusivity of material a1 200 °C in nitrogen is 0.531 $mm^2 s^{-1}$, whereas the material b3 has 0.465 $mm^2 s^{-1}$, b4 has 0.39 $mm^2 s^{-1}$, and c2 has only 0.11 $mm^2 s^{-1}$ as values for effective thermal diffusivity at 200 °C in nitrogen. The curves of effective thermal diffusivity for materials a1 with various filling gases have the same trends; i.e. it decreased from room temperature till around temperature of 300 °C and then become approximately straight lines, see Figure 56.
- The curves of effective thermal diffusivity for materials b3, b4 and c2 have the same trends with increasing the temperature. For Samples with helium as filling gas, thermal diffusivity decreased from room temperature to reach the minimum at a defined temperature and then increased with increasing the temperature of the sample, as an example see Figure 57, whereas for the samples with nitrogen, argon and vacuum the curves begin from room temperature with very low rise gradient and then raise from a defined temperature, which differs depending on the material and the filling gas, with increasing the temperature of sample.
- The results of effective thermal diffusivity for material c2 are accompanied with fluctuation starting at the temperature of 500 °C. The experiment with argon is also interrupted because of the resulting inconsistent temperature rise curves.

Interpretation of these observations will be discussed in detail in next chapter.

PART III: ANALYSIS AND MODELING

8 Discussion and Interpretation of Experimental Results

8.1 General

Experimental results for structure properties, thermal conductivity and thermal diffusivity were presented in the previous chapter. All investigated materials are classified as high porosity insulation materials. However, the experimental results and the behavior by exchanging the filling gas differ from one material to another. In this chapter, various physical effects will be discussed in order to interpret the results.

8.2 Knudsen Effect

8.2.1 Investigation of Knudsen Effect

The porous structure of material determined the rarefaction of the filling gas. Knudsen number, the ratio of mean free path to pore diameter, is a parameter that subdivides the flow regimes of gas into: continuous regime (Kn < 0.01), temperature jump regime (0.01< Kn < 0.1), transition regime (0.1 < Kn < 10) and free molecule regime (Kn > 10). The limitations of Knudsen regimes are evaluated based on the mean free path (68 nm) of nitrogen at 25 °C. Applying these limitations to the investigated materials shows the percentages of volumes of pores that are contained within the different kinds of flow regime, see Figure 60.

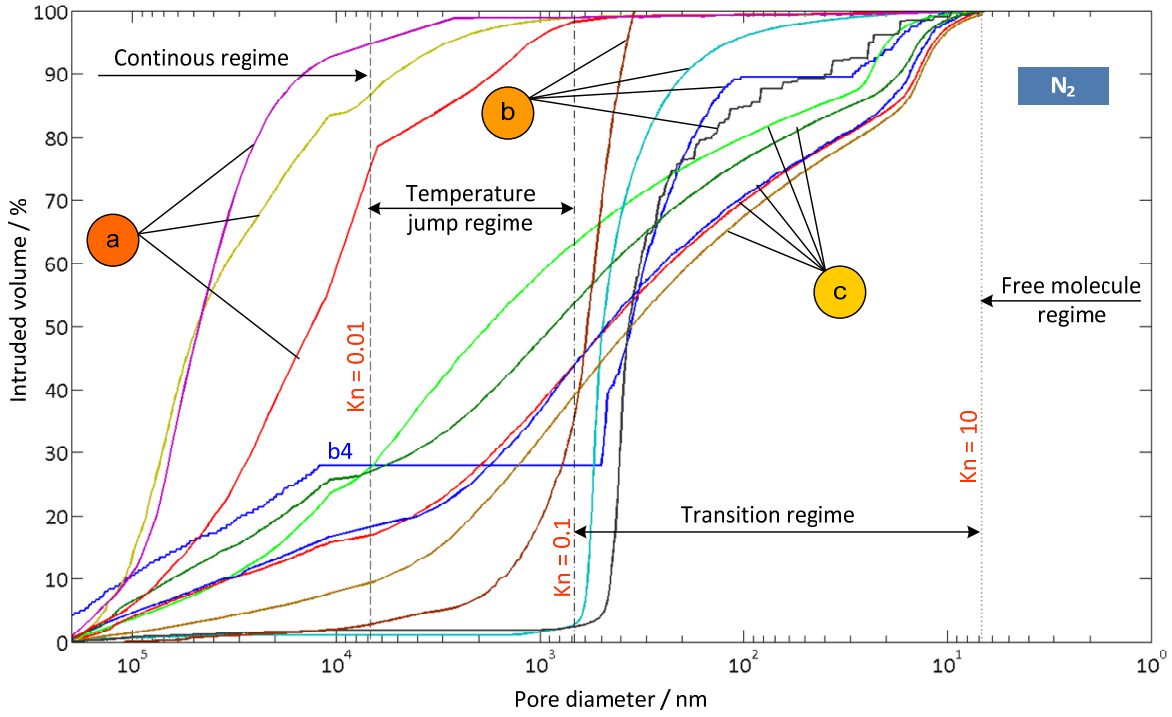

Figure 60: Knudsen regimes of the filling gas (N_2) of the investigated materials at a temperature of 25 °C

The results show that:

- Group (a): from 80 % to 90 % of pores from materials of this group are bigger than Kn of 0.01, which is enough to let the N2 filling gas behave as if it is a continuous gas regime. Less than 10 % to 20% of the pore volume is in the Temperature jump region.

- Group (b): from 65 % to 90 % of the pore volumes for these materials are characterized with Kn < 0.1. Thus a majority of the filling gas is situated in the transition regime. Only one material b4 has about 30 % of the pore volumes in the continuous regime.

- Group (c): The materials in this group have such a wide pore size distribution, that the filling gas varies from the continuous regime through the Temperature jump regime to the transition regime.

The results confirm that materials of groups (b and c) have small pores, which is enough to indicate a Knudsen effect in these two groups.

8.2.2 Knudsen and Non-Knudsen Materials

All researchers consider Knudsen number as a parameter to identify the rarefaction of gases. However, it is mainly suitable for one dimension disperse systems, such as the gas between two parallel plates. Thus it is difficult to intercompare the investigated porous materials, which are actually poly-disperse systems, as seen in the previous section. In this work a *new parameter is considered to investigate the Knudsen effect upon thermal conductivity of porous insulation materials*. This Parameter is the ratio of effective thermal conductivity (λ_{eff}) to the bulk thermal conductivity of the filling gas $\lambda_{\mathrm{bulk(gas)}}$, this parameter will be called Knudsen-ratio, and it is expressed as following:

$$\chi_{\mathrm{Kn}} = \frac{\lambda_{\mathrm{eff}}}{\lambda_{\mathrm{bulk(gas)}}} \tag{61}$$

When this ratio $\chi_{Kn} > 1$ the Knudsen effect is insignificant and the materials will be called non-Knudsen materials. When the Knudsen ratio $\chi_{Kn} < 1$, Knudsen effect will be significant and the materials will be called Knudsen materials.

The investigated materials in this work have been classified into two groups by comparing their effective thermal conductivity with the bulk thermal conductivity of nitrogen at 500 °C, as seen in Figure 61. Group I is the non-Knudsen materials, which are represented by groups (a) and (b). Group II is the *Knudsen materials*, which correspond to group (c), see Figure 61, with larger portions of pores sized in the nano-range. The measured values of effective thermal conductivity for the different materials are taken at furnace temperature of 500 °C. That leads to different mean temperature of sample with respect to the thermal conductivity of the material. The values of mean temperature are presented in x-axis in Figure 61.

The temperature of 500 °C is chosen as critical temperature, which is almost the middle value in the measured temperature range in thermal conductivity measurements by RHFA.

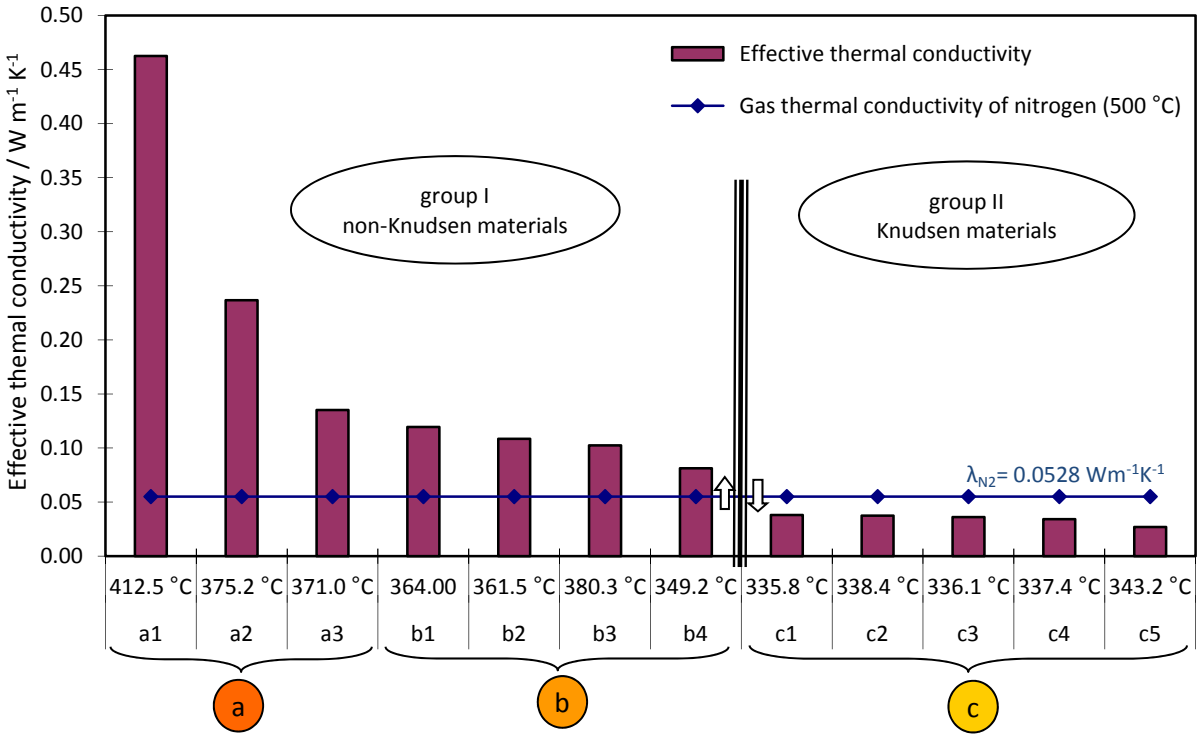

Figure 61: Effective thermal conductivity of 12 different materials measured in nitrogen atmosphere at a constant furnace temperature of 500 °C

Evaluation of Knudsen ratio for the investigated materials shows that the Knudsen ratio of group (a) and group (b) is relatively much higher than the unity; however, for group (b) it is closer to the unity. The last group could be called *near Knudsen- material*. Whereas for group (c) the Knudsen ratio is smaller than one, as seen in Table XIX.

Table XIX: The Knudsen ratio of the investigated materials

Group	a			b				c				
Material No.	a1	a2	a3	b1	b2	b3	b4	c1	c2	c3	c4	c5
$\chi_{Kn}(N_2)$ @ 500 °C	8.39	4.30	2.45	2.17	1.97	1.86	1.48	0.69	0.68	0.66	0.62	0.49

The Knudsen ratio is an important parameter that should be considered when predicting the change of effective thermal conductivity by exchanging the filling gas.

8.3 Effect of Exchanging the Filling Gas

8.3.1 The Change in Effective Thermal Conductivity

Exchanging the filling gas for example from nitrogen to helium, i.e. to a higher gas thermal conductivity, results in an increase in the effective thermal conductivity of materials. This is basically well known. However, the absolute and relative amounts of the increase depend on the kind of material and its pore structure as will be shown later in this work.

Figure 62 presents the results of thermal-conductivity measurements of two materials (a3) and (b1) plotted versus the mean test temperature of the samples. The two materials have approximately the same effective thermal conductivity when both of them are filled with nitrogen. However, totally different values of effective thermal conductivity are measured

after exchanging the nitrogen by helium. As shown in Figure 62, the increase of the thermal conductivity for the sample (a3) at a temperature of 400 °C is about $\Delta\lambda_{eff}$ = 0.21 W m^{-1} K^{-1} corresponding to increasing ratio of 250 %, whereas for the sample (b1) at the same temperature gives about $\Delta\lambda_{eff}$ = 0.05 m^{-1} K^{-1} corresponding to increasing ratio of 136 %. The difference between the bulk thermal conductivity of helium and that of nitrogen at the same temperature equals to λ_{bulk}(He) - λ_{bulk} (N_2) = 0.222 W m^{-1} K^{-1}, see Appendix B. This value is almost the same as $\Delta\lambda_{eff}$ for material a3. That is due to the difference in porous structure of both materials; pores of material a3 are almost sized in continuum regime whereas pores of material b1 are almost sized in transition regime, see Figure 60. It is obvious that the change of effective thermal conductivity mainly depends on the porous structure of the material. This is confirmed by presenting the evaluated data of effective true thermal conductivity at 400 °C over the bulk thermal conductivity of the filling gas, as seen in Figure 63. The bulk thermal conductivity of filling gas is considered Figure 63 as the reference value (the values of x-data). This value does not reflect the actual thermal conductivity of the gas filled in the porous material.

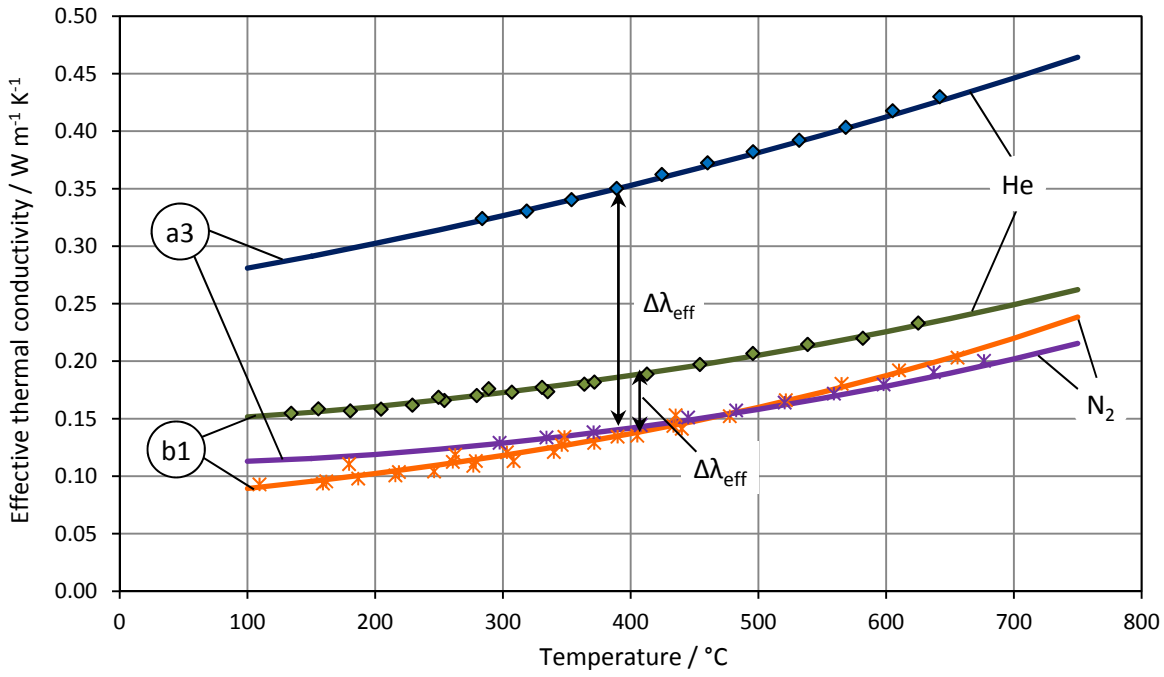

Figure 62: Measured effective thermal conductivity of samples from two different materials in nitrogen and helium

The filling gas contributing to heat transfer mechanisms through some porous materials, as example for group (c), has lower thermal conductivity than the bulk one with regards to the Knudsen effect, and thus this group has a Knudsen ratio lower than one, see Table XIX. The changes in effective thermal conductivity by exchanging the filling gas are presented as curves with various slopes, as seen in Figure 63. Since the number of experimental results is large, the comparison between the results of the different materials will be presented only at one mean test temperature, namely at 400 °C. Later on the effect of the temperature on the results will be discussed.

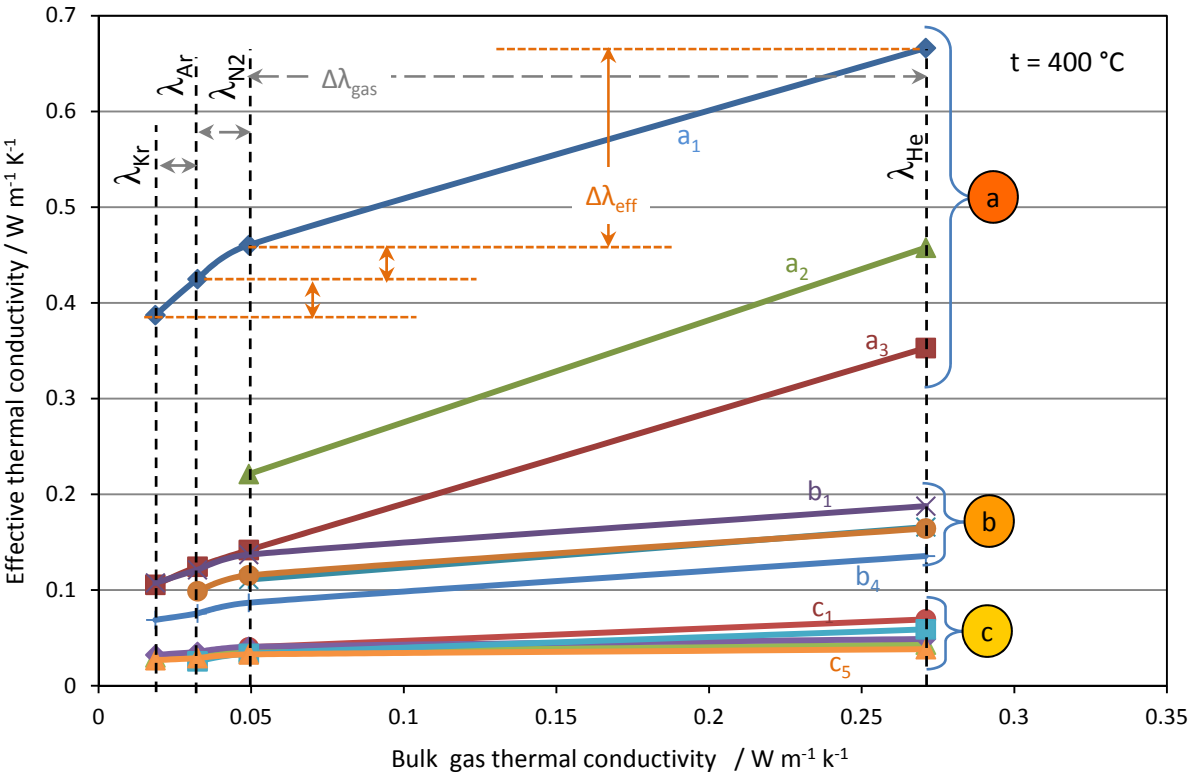

Figure 63: Change in effective thermal conductivity by exchanging the filling gas at temperature 400 °C

The change of λ_{eff} for materials of group (a) is presented with approximately parallel curves, which has larger slopes compared with materials of groups (b) and (c). The large slope $\Delta\lambda_{eff}/\Delta\lambda_{gas}$ indicates that exchanging the filling gas in these materials lead to noticeable absolute increase in effective thermal conductivity. The slope of curves becomes lower in materials of group (b); however the curves remain parallel. Materials of group (c) have the smallest slopes, which indicate that the absolute change in effective thermal conductivity is small compared to the other two groups. That is due to the fact that materials of group (c) have effective thermal conductivity much smaller than the materials of groups (a) and (b). The results show also that the slope is larger for the gases with lower thermal conductivity, for example by exchanging the Kr by Ar in material a1 the slope amounts 70 degree, whereas by exchanging the N_2 by He the slope amounts only about 43 degree. This signifies that these curves, which describe the experimental results of effective thermal conductivity of materials measured in four various gas atmospheres, are not straight lines. That contradicts with the relation suggested by Woodside and Messmer, 1961. They described the relation between the effective thermal conductivity and thermal conductivity of filling gas by linear relation as following, for more details see chapter 3- page 29:

$$\lambda_{eff} = W\,\lambda_{gas} + \lambda_{evac} \tag{62}$$

As seen in Figure 63, the relation is more complex and could not be described simply by a straight line. The conclusion by Woodside and Messmer, 1961 could be justified by the fact that they investigated materials with much lower porosity (20 - 39 %) than the investigated materials within the present work. Another reason behind these results could be the status of experimental facility at that time.

However, a recent experimental study was performed on Sander sandstone with different filling gases: Freon-12, Ar, N_2, mixture N_2/He, He and H_2 (Abid, 2011). The Sandstone has also a porosity of 19 % and it has a higher effective thermal conductivity than that of all investigated materials within the present work. This study confirms the trend of curves resulted in this work. As shown in Figure 64, the curve is not a straight line. Additionally, the Abid study shows also large values of slope at the low bulk gas thermal conductivity. For Example the calculated slope from the interloped curve $\Delta\lambda eff/\Delta\lambda gas$ has values of 6.7 at 0.02 W m^{-1} K^{-1} of λgas, whereas only 0.84 at 0.16 W m^{-1} K^{-1} of λgas .

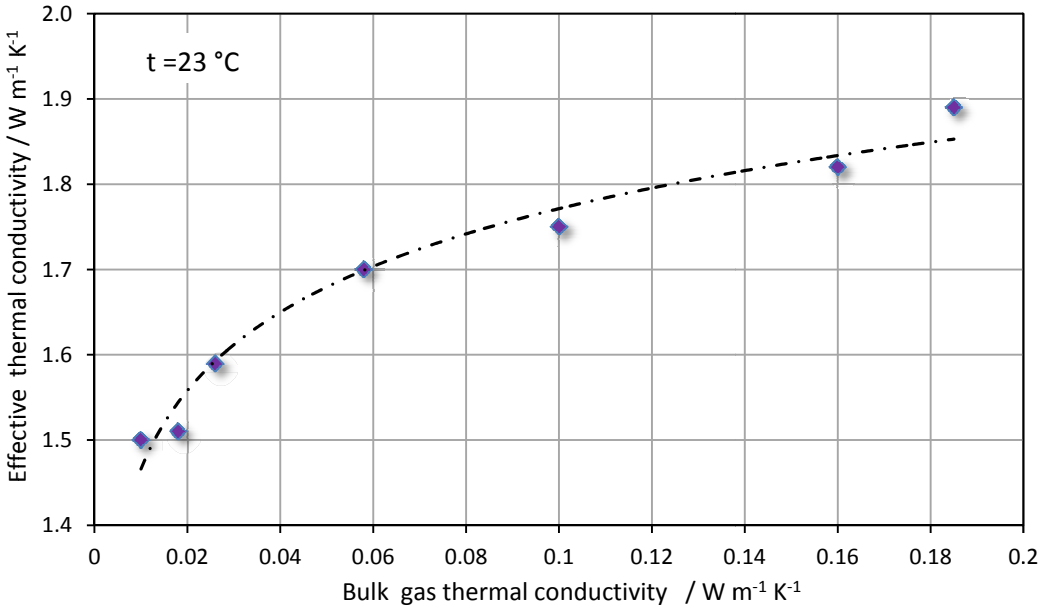

Figure 64: Change in effective thermal conductivity of Sander sandstone by exchanging the filling gas points: measured, line: interpolated (Abid, 2011)

The trend of curves introduced in this work could be physically interpreted by extrapolating the curve to zero gas thermal conductivity. An accurately predicted residual thermal conductivity is that of the solid matrix plus radiation, since the pores are not filled with any medium. Filling the pores with a gas of low thermal conductivity, such as krypton, provides molecules that work as energy carriers and help to transfer heat between the walls of the pores. Obviously, this results in an increase in the effective thermal conductivity. Exchanging the filling gas with one that has higher thermal conductivity increases the effective thermal conductivity. This effect becomes smaller as we keep exchanging of filling gas. Eventually, the effective thermal conductivity reaches a kind of saturation for a certain value of gas thermal conductivity. This depends mainly on the ratio of gas thermal conductivity to thermal conductivity of solid matrix and its porosity. In the following chapter, this effect will become obvious when evaluating the models of effective thermal conductivity. It is also important to keep in mind that the reference data (x-values) for the above described curves, also for one from literature (Abid, 2011), are the bulk thermal conductivity of the filling gas.

Considering the pore size of materials with respect to the Knudsen effect, the gas thermal conductivity becomes smaller. Evaluation of the gas thermal conductivity could be done through the Kaganer-model using the middle pore size of the investigated material, for more details about the model, see eq. (27) in chapter3. Gas thermal conductivity has been

evaluated with regards to Kaganer-model for three materials of group (c): c2, c3 and c5, which have been measured for more than two gases.

The evaluated gas thermal conductivity using the Kaganer-model will be called derived gas thermal conductivity in the pore. The results of effective thermal conductivity are presented versus, however, the derived gas thermal conductivity in the pore at temperature 400 °C, see Figure 65.

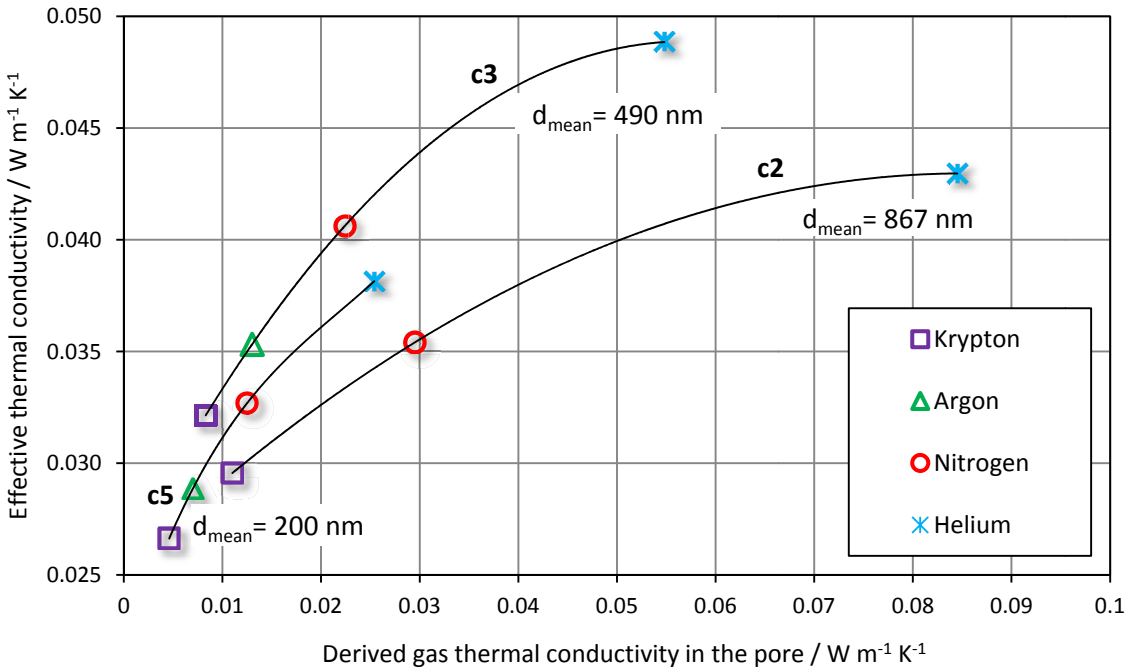

Figure 65: Change in effective thermal conductivity with exchange the filling gas regards Knudsen effect at temperature 400 °C
points: measured, lines: polynomial curve of third degree

As can be seen, there is a change in the mathematical description of the relation between the effective thermal conductivity of the material and the thermal conductivity of the filling gas. This is obvious by comparing it to the presented results versus the bulk gas thermal conductivity; compare Figure 63 with Figure 65. Here also this relation could not be described as straight lines. In this presentation, polynomial curves of third degree are used to explain the relation between the effective thermal conductivity and the thermal conductivity of filling gas. Figure 65 shows that filling material c2 with nitrogen results in a derived gas thermal conductivity using the Kanager-model of 0.0295 W $m^{-1}K^{-1}$. In contrast, filling material c3 with nitrogen results in a derived gas thermal conductivity using the Kanager model of only 0.0224 W $m^{-1}K^{-1}$, and doing the same for material c5 yields a derived gas thermal conductivity of only 0.0125 W $m^{-1}K^{-1}$. At 400 °C the bulk gas thermal conductivity is near 0.048 W $m^{-1}K^{-1}$.

This implies that Knudsen effect (caused by the pore size) has a big influence on the value of the derived gas thermal conductivity. The effective thermal conductivity of material c3 is higher than that of materials c2 and c5 because it has different composition, see Table XV in chapter 7. The materials c2 and c5 have almost the same composition; however the results of effective thermal conductivity of material c5 are lower than that of material c2 when filled

with same gas because of the difference in pore size distribution. Material c5 has more pores sized in nano range than material c2, Figure 45 in chapter 7.

8.3.2 The Change in Effective Thermal Diffusivity

The results of effective thermal diffusivity of four materials (a1, b3, b4 and c2) measured by LFA in vacuum as well as in three different gas atmospheres (Ar, N_2 and He) are presented in Figure 66. These results are presented versus bulk thermal conductivity of the filling gas. However, in vacuum the thermal conductivity of residual argon in furnace chamber at pressure 1.3 X 10^{-7} bar is around 2.7 X 10^{-9} W m^{-1} K^{-1}. This value is very small compared to thermal conductivity of other gases. Thus the effective thermal diffusivity in vacuum presented on the y-axis corresponds to the zero value of gas thermal conductivity.

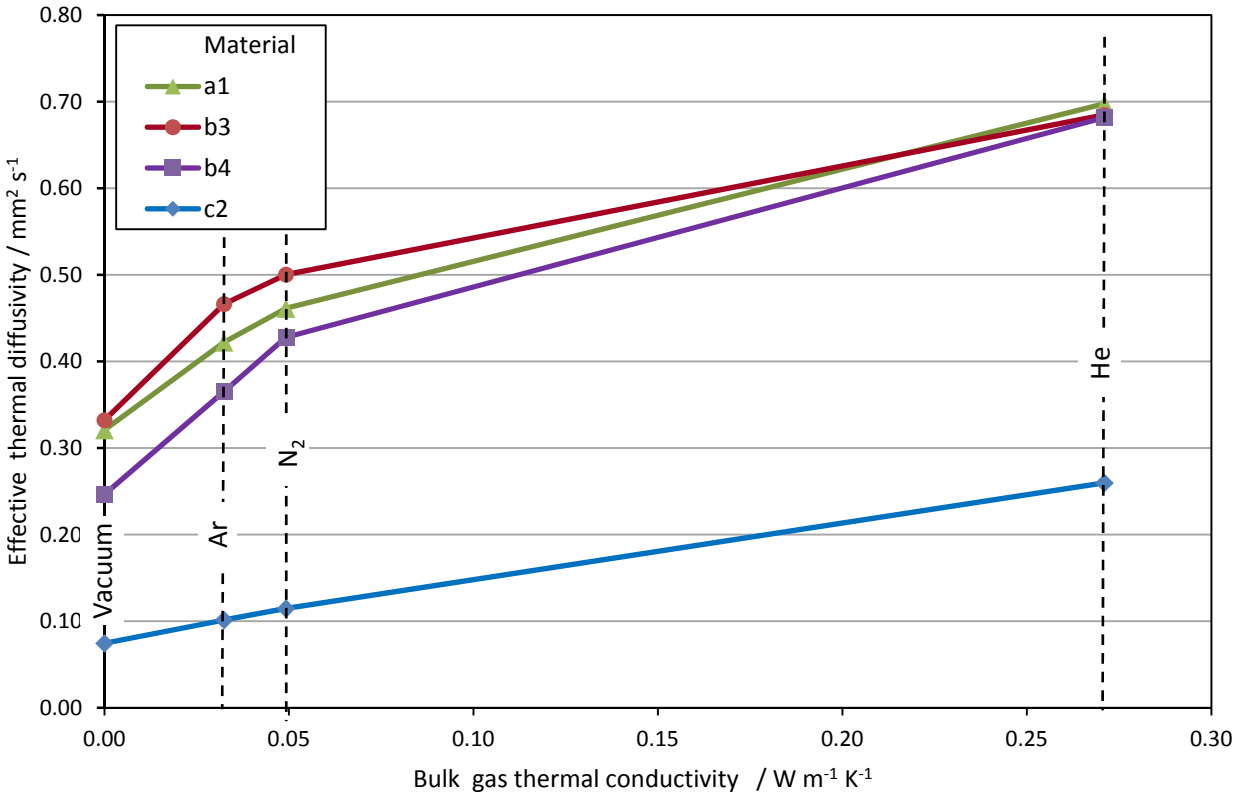

Figure 66: Change in effective thermal diffusivity by exchanging the filling gas at temperature of 400 °C

The results of effective thermal diffusivity show the same trend as the results of effective thermal conductivity. However, the difference between effective thermal diffusivity of material a1 and materials b3 and b4 is very small, whereas the difference in effective thermal conductivities between these materials is much bigger. This is due to the difference of bulk densities. The bulk density of material a1 is four times bigger than that of material b3 or b4. Basically, effective thermal diffusivity of each material is increased by exchanging the filling gas with a gas that has higher thermal conductivity. The results of effective thermal diffusivity show also that the effect of exchanging the filling gas is higher when the two filling gases have low gas thermal conductivity, for example exchanging vacuum by argon as a filling gas. The effect becomes smaller when exchanging the filling gas with a gas that relatively higher thermal conductivity like helium. These observations of the results indicate a saturation effect, which is also observed in thermal conductivity measurements. Results of effective thermal diffusivity of material c2 do not show this effect. However, by considering

the Knudsen effect in the material c2, the slope of curve would be different as found by the results of thermal conductivity. Thus, it makes no sense to present the results again here.

8.4 Coupling Effect of Knudsen Conduction/Radiation

8.4.1 Knudsen Conduction

Measurement results of the effective thermal conductivity are analyzed using pore size distribution and the filling gas as main parameters. The effects of these parameters are interpreted with no regard to the temperature. The difference in behavior of the investigated materials over the temperature in various gas atmospheres could be explained by the coupling of these effects.

As is known, bulk thermal conductivities of all applied gases increase by raising the temperature at about the same rate, see Appendix B. That implies that exchanging the filling gas in the investigated porous materials should not change the dependency of effective thermal conductivity upon the temperature. However, the observations of the experimental results of thermal conductivity show that this is valid only for group (a) materials, but the Group (b) and (c) materials show the rate of increase of effective thermal conductivity with temperature becomes smaller as the thermal conductivity of the filling gas increases (Kr-Ar-N2-He). This has also been confirmed by the thermal diffusivity experimental results. The dependency of bulk gas thermal conductivity on temperature is valid only in the continuum regime. In this region the bulk gas thermal conductivity is proportional to the square root of the temperature. With increasing the Kn-number, the slope begins slightly to decrease. Finally, in the free molecule regime (Knudsen gas), the gas thermal conductivity becomes inversely proportional to the root of the temperature (Wonchala and Wynnyckyj, 1984) , as seen also in Figure 67.

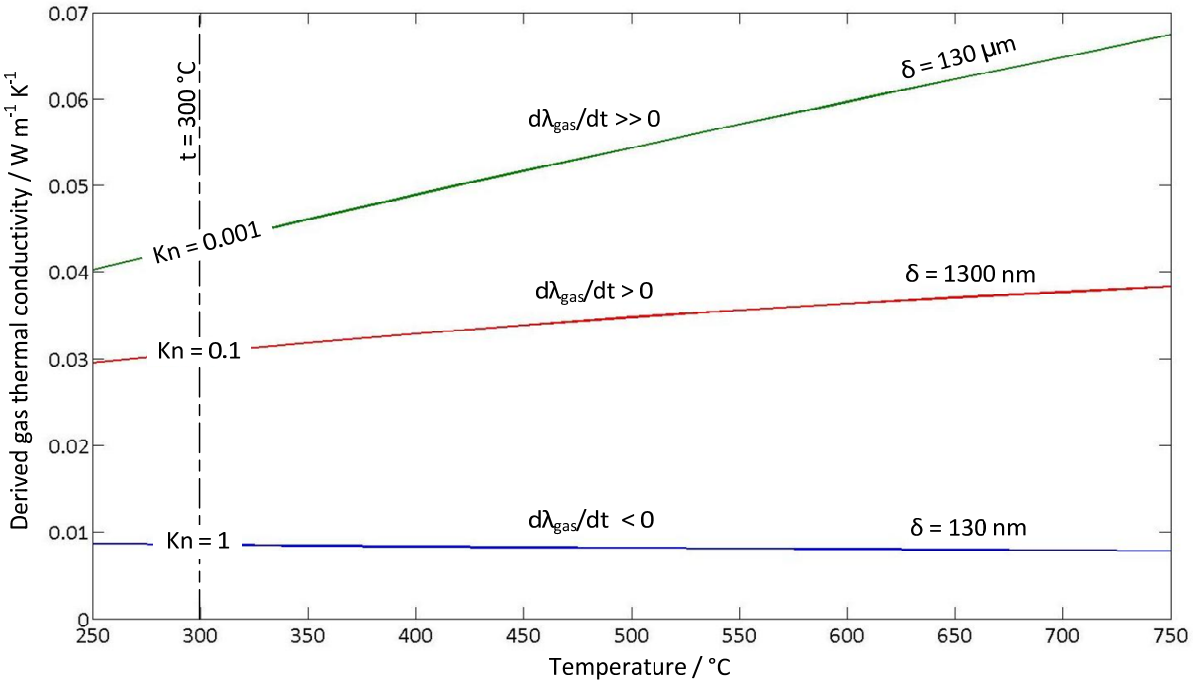

Figure 67: Effect of changing temperature on derived gas thermal conductivity of N_2 with increasing the Kn-number evaluated with regards to Kaganer- model

The gas thermal conductivity of nitrogen is evaluated with regards to the Kaganer-model eq. (27) for one pore arrangement including the Martin equation for accommodation coefficient eq. (42) with three different diameters (δ): 130000 nm, 1300 nm and 130 nm. These diameters correspond to the Kn-numbers at 300 °C of 0.001, 0.1 and 1, respectively. The temperature 300 °C is chosen as minimum limit to show the effect of temperature on the derived gas thermal conductivity in the pore. The inverse of the dependency of derived gas thermal conductivity upon the temperature could be explained through the Knudsen effect. The mean free path is increased with raising the temperature. This leads to an increase in the Knudsen number and to a decrease in the gas thermal conductivity. This is not relevant as long as the gas is in the continuum regime, where the heat conduction in gas is dominated by continuum one ($d\lambda_{gas}/dt >> 0$). However, the heat conduction through the gas in the transition regime is coupled of the continuum and Knudsen conductions. Thus, the temperature dependence of derived gas thermal conductivity in this regime is dependent mainly upon the Knudsen number. Increasing the Knudsen number causes the Knudsen conduction to dominate and to decrease the gas thermal conductivity ($d\lambda_{gas}/dt < 0$).

8.4.2 Radiation effect

The phenomena of changing the thermal conductivity dependence on temperature leads to question: since the porous structure of the material stays the same when exchanging the filling gas, in which material and for which gas should the phenomena of the Knudsen conduction be considered? To answer this question, the various conduction and radiation contributions of the evaluated effective thermal conductivities were studied. The function of true thermal conductivity, introduced by eq. (59), was applied with the parameters (a, b, and c) which are obtained from the least-square approximations. The analysis was done for three materials (a1, b1 and c5), i.e. one material from each group. The results are shown in Figure 68 for 250 °C and 600 °C, as minimum and maximal limits in the measured temperature range, and for all three materials filled with the four gases:

- Solid conduction is represented by the term (b/T) and it is regularly found to decrease with the temperature for a given sample/gas combination, see the red columns. This behavior is typical for well-ordered materials with crystal structures.
- It is extremely difficult to separate the contributions of gas and solid exactly. The coupled effects of gas/solid conduction are obtained from the sum of both ($a\sqrt{T} + b/T$), represented by the "red + blue" columns. This contribution decreases with the bulk gas thermal conductivity in the order He – N_2 – Ar – Kr for a given material/temperature combination. This shows the important effect of the filling gas
- Material a1, as known is a high density material characterized by low porosity (68 % versus 90 % and 94 % for the other materials) with big pores mainly in the macro range. The measured λ_{eff} is governed by the combined effects of solid and gas conduction whereas radiation does not play any significant role (cT^3, the green columns). This is clearly seen in Figure 68.
- For material b1, the combined solid/gas conduction increases slightly with temperature, Figure 68. One must not overestimate the individual contributions of solid and gas. However, it makes sense that $a\sqrt{T}$, standing for the gas contribution, increases from 250 °C to 600 °C, while b/T, for the solid, decreases.

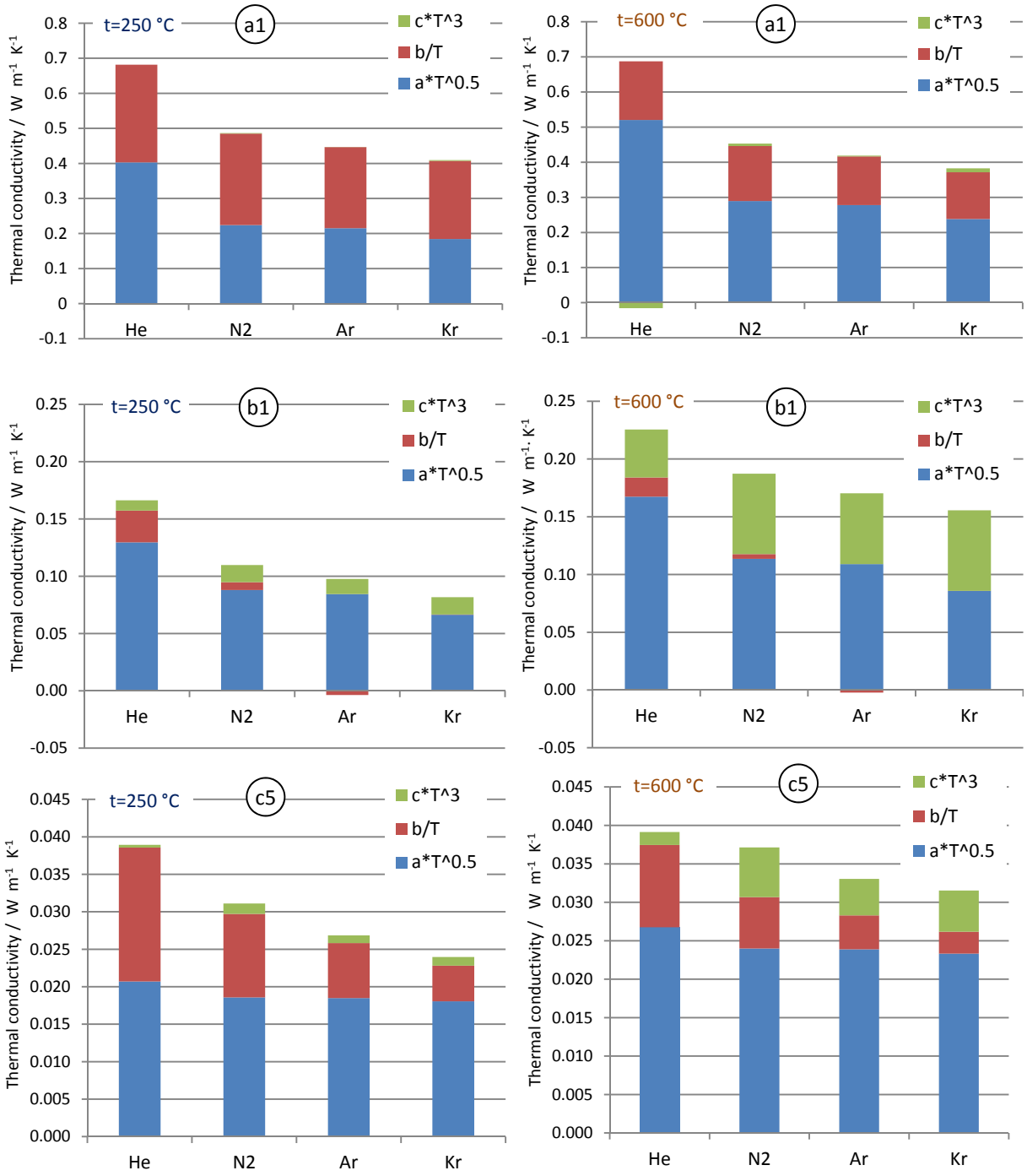

Figure 68: Estimated contributions for gas, solid and radiation using eq. (59) for the materials a1, b1, and c5

Radiation becomes more significant for material b1 versus a1, see Figure 68. The results of material b1 show increasing radiation contributions in the order He- N_2- Ar- Kr. It is more visible at 600 °C, although being valid for both temperatures. This is a surprising observation as nothing has changed but the gas and λ_{eff}.

- For material c5, as previous mentioned there is a new and surprising effect found in the temperature range below about 350°C where the effective thermal conductivity

shows a tendency to decrease with increasing temperature, see Figure 51 in chapter 7. This is mainly true for helium filled pores, but a certain trend is also visible for the other gases which are now assumed to approach the Knudsen range. In such cases, the temperature effect on the gas thermal conductivity exhibits an opposite behavior than in the continuum range ($1/\sqrt{T}$ instead of $\sqrt{T}$) as shown in Figure 67. This diagram in Figure 68 shows $a\sqrt{T}$ columns which are almost independent of the filling gas. As already mentioned, the individual gas contribution should not be overvalued. However, its dependence on the kind of gas is going to vanish, which is a clear sign for the approach of the Knudsen range. Furthermore, the radiation effect on λ_{eff} for material c5 is lower than for b1, due to the extremely small pores, and it is affected by the filling gas in a similar way.

There are two effects which have to be considered for the observed phenomenon:

- The Knudsen effect transition from the continuum to Knudsen range with respect to the temperature ($\sqrt{T}$ to $1/\sqrt{T}$). There are clear indications for the beginning of this transition in case of sample b1 and c5. To prove this effect, the mean free path and Knudsen numbers corresponding to the pore size of the materials were evaluated. Two criteria for the limitations were considered: the first is Kn > 1, where the Knudsen conduction begins, see Figure 67, and the second is Kn > 10 where the Knudsen regime begins. Table XX shows the void volume (% of total volume) enclosed in the pores corresponding to Kn > 1 and Kn > 10 for all gases and materials, and for the temperatures 250 °C and 600 °C. This gives an overview of the rarefaction effect in various cases. The material a1, as expected, includes almost no pores with Knudsen numbers greater than one, whereas c5 include a large part of the void volume enclosed in pores in transition and Knudsen regimes. These materials depend on the kind of the gas and on the temperature. Material b1 includes no pores in Knudsen regime and has no pores with Knudsen number greater than one at 250 °C. However, while material b1, e.g., filled with krypton at 600 °C shows no Knudsen conduction effect (0 % of pores with Kn > 1), a change of the filling gas to helium brings a large part of the pores of b1 (52 %) into this regime. That implies that increasing the temperature from 250 °C to 600 °C enhances the rarefaction effect, and so the slope of effective thermal conductivity of material b1 versus temperature is smaller for helium than that for argon or krypton. The result of c5 in Table XX shows also an interesting effect: by exchanging the filling gas, the volume of pores in Knudsen conduction as well as of Knudsen regime increased in the order (Kr-Ar-N_2-He). Material c5 filled with helium has 22.2 % and 26.9 % of the void volume in the Knudsen regime at 250 °C and 600 °C, respectively. These are the maxima of all the considered cases (Kn > 10). In this regime, the gas thermal conductivity varies with ($1/\sqrt{T}$) instead of ($\sqrt{T}$), and this effect explains the trend of the effective thermal conductivity curve of material c5 with temperature when filled with helium.

- The change of radiation heat transfer inside the pores. There is actually no direct relation between the conductive and radiative heat transfer. Since the heat transfer through radiation in the applied gases is negligible, thus changing the gas atmosphere does not lead to a change in the radiative properties of the solid material. However, an interaction between these two mechanisms arises from

modifications of the temperature field, i.e. the temperature gradient and subsequently the temperature difference between two opposite sides of the pore. This temperature change is inversely related to a change of λ_{eff}. For example, If λ_{eff} is increased at some constant heat flow rate, we obtain a decrease of the temperature gradient from Fourier´s law. The resulting effect is shown in sample c5 at 600 °C in Figure 68. It is clearly seen that krypton or argon with their small λ_{eff} yield a much higher radiation contribution than helium. The same can be observed for sample b1 at 600 °C and also at 250 °C. However, the relative importance of radiation is different in the various cases. An exact comparison of the effect on materials a1, b1, and c5 is not possible because of the strongly different pore structures.

Table XX: Percentage of void volume enclosed in pores corresponding to Kn > 1 and Kn > 10

Temperature	Filling gas	Mean free Path nm	pore volume					
			Kn > 1			Kn > 10		
			a1 %	b1 %	c5 %	a1 %	b1 %	c5 %
250	Helium	352	1.8	0	**49.6**	0.6	0	**22.2**
	Nitrogen	119	0.7	0	34.6	0.3	0	6.3
	Argon	127	0.8	0	35.4	0.3	0	8.1
	Krypton	94	0.7	0	31.8	0.2	0	2.6
600	Helium	587	2.4	**52**	**58.3**	0.7	0	**26.9**
	Nitrogen	198	0.8	0	41.2	0.5	0	17.1
	Argon	212	0.8	0	42.1	0.5	0	17.8
	Krypton	157	0.8	0	38.1	0.4	0	14.1

As can be seen, the experiments confirm that the change of effective thermal conductivity of porous materials by exchanging the filling gas is dependent mainly on temperature. Figure 69 shows an evaluation of $\Delta\lambda_{eff}$ for all materials over the temperature in case of exchanging the nitrogen by helium. It is obvious that there are two different trends of dependency:

- Increasing the difference of effective thermal conductivity measured in two filling gases (He-N_2) with raising the temperature ($d(\Delta\lambda_{eff})/dt > 0$). This is represented by the materials of group (a). This trend agrees with the dependency of the difference of bulk gas thermal conductivity upon temperature; see the dashed line in Figure 69.

- The other trend of the curves is decreasing the difference of effective thermal conductivity measured in two filling gases (He-N_2) with raising the temperature ($d(\Delta\lambda_{eff})/dt <= 0$). This is found for materials of the two groups (b) and (c). This is a result of combined effect of radiation and Knudsen conduction, as explained above

already. Some materials of these two groups show negligible dependency ($d(\Delta\lambda_{eff})/dt \approx 0$) upon temperature, e.g., see b3 and c4 in Figure 69.

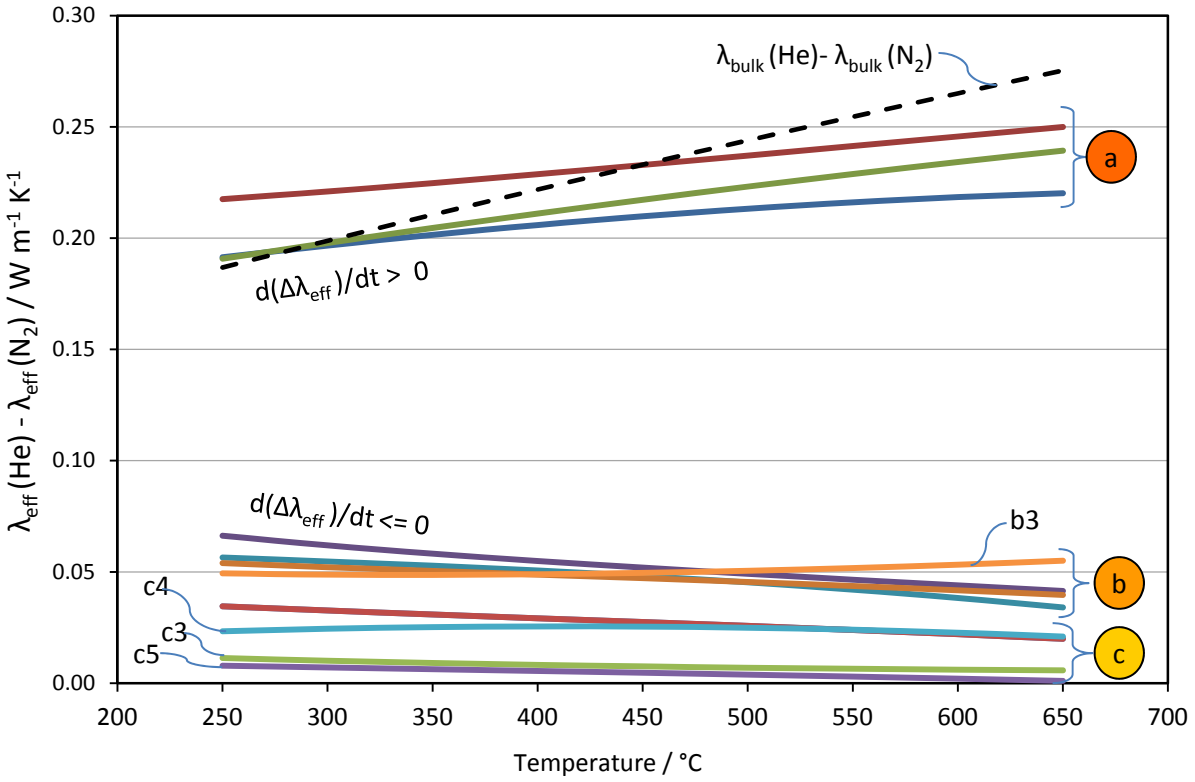

Figure 69: Temperature influence on the differences of the effective thermal conductivities of all materials filled with helium and ones filled with nitrogen

These two trends are also confirmed by comparing the results of thermal diffusivity. It is noticed also that the values of difference $\Delta\lambda_{eff}$ (He-N_2) for materials of group (c) become smaller, and by extrapolating the difference we approach approximately the zero-value, as by c3 and c5 in Figure 69. This is a very important observation. I.e. ***exchanging the filling gas at a defined high temperature in a porous material with pores sized in the nano-range will not change the effective thermal conductivity of this material***. All introduced effects in this chapter should be considered when predicating or modeling the effect of exchanging the filling gas upon the effective thermal conductivity of porous materials.

9 Predicting the Effect of Exchanging the Filling Gas in Porous Media

9.1 General

Industry and researchers are interested in predicting and modeling the change of effective thermal conductivity of porous media by exchanging the filling gas. By modeling and predicting the measured change in effective thermal conductivity of the media, one obtains useful insight and understanding of the characteristics of the porous media. In addition, if the porous media model is accurate in predicting the effective thermal conductivity of the porous media, then one has a verified tool for predicting the behavior of the porous media in other gaseous atmospheres.

Another benefit of this tool is to reduce the burden on the measuring community to test every conceivable change in filling gas. In addition, the understanding of the characteristics of porous media gained from this type of analysis offers the opportunity to the materials scientist to change the structure of the porous media to obtain desired properties, such as higher thermal resistance in a given space. For example, the possibilities include in the walls of refrigerators, or residences, or high temperature furnaces, or for high temperature pipe insulations. The latter can be important to existing petrochemical facilities, where the pipe lines are near each other, and no space exists to add "few centimeters" of material.

Since the major effect is caused by exchanging the filling gas, then the task is to evaluate the change in effective thermal conductivity by exchanging the filling gas. This evaluation has been done using a large number of models for the effective thermal conductivity of porous media. The evaluated results are compared to the experimental results. This chapter concludes also a discussion of the extent of agreement obtained and this has provided a basis for developing a corrected model for evaluation of the effect of exchanging the filling gas.

9.2 Models of Effective Thermal Conductivity:

As mentioned in chapter 3, there are only two different heat transfer mechanisms in the investigated porous media after neglecting the convection, namely, conduction in the solid matrix and filling gas and radiation in the solid and gas. The effective thermal conductivity can be written as:

$$\lambda_{\mathrm{eff}} = f\left(\lambda_{\mathrm{s}}, \lambda_{\mathrm{gas}}, \lambda_{\mathrm{rad}}\right) \tag{63}$$

Many researchers have produced mathematical models to predict the effective thermal conductivity of different porous media. The models differ in the description of the gas and solid contributions and these models are reviewed in Appendix D. For example, the upper and lower limits of the arrangement of the gas and solid contributions are described by the evaluation of a parallel model and a series model. In this work totally twelve models are chosen to evaluate effective thermal conductivity, see Appendix D. Eight of them in equations (67-74) are described based on the coupling in the gas\solid conductions, whereas the other four, see D.3. in Appendix D, involve the heat transfer through radiation. The

choice of models depends on the ability to evaluate the change of λ_{eff} by exchanging the filling gas. The first eight models, which do not consider to radiation, could be expressed as a function of the ratio of gas thermal conductivity to the solid thermal conductivity, see Table XXI, as follows:

$$\frac{\lambda_{\mathrm{eff}}}{\lambda_{\mathrm{s}}} = f\left(\frac{\lambda_{\mathrm{gas}}}{\lambda_{\mathrm{s}}}\right) \tag{64}$$

Figure 70 shows comparison between the models performed through the evaluation of the function in eq. (64) by varying the ratio (λ_{gas}/λ_s) in the range 0.01 - 1 for a defined material with porosity (Ψ) of 90 %. All models except Stark's produce almost the same values of effective thermal conductivity, see section view in Figure 70. Stark's model eq. (74) is developed for fibrous materials with a defined alignment for the fibers (Z_f alignment factor).

Table XXI: List of effective thermal conductivity models

Ref.	Transformed model regards eq. (64)	eq.
Lower Limit (series model)	$\frac{\lambda_{eff}}{\lambda_S} = \frac{1}{(1-\Psi)+\Psi\left(\lambda_{gas}/\lambda_S\right)^{-1}}$	(65)
Upper Limit (parallel model)	$\frac{\lambda_{eff}}{\lambda_S} = \Psi\left(\frac{\lambda_{gas}}{\lambda_S}\right) + (1-\Psi)$	(66)
Eucken 1932	$\frac{\lambda_{eff}}{\lambda_S} = \frac{1+2\,\Psi\frac{1-\left(\lambda_{gas}/\lambda_S\right)^{-1}}{1+2\cdot\left(\lambda_{gas}/\lambda_S\right)^{-1}}}{1-\Psi\frac{1-\left(\lambda_{gas}/\lambda_S\right)^{-1}}{1+2\cdot\left(\lambda_{gas}/\lambda_S\right)^{-1}}}$	(67)
Son Frey 1932	$\frac{\lambda_{eff}}{\lambda_S} = \frac{\left(1-\Psi^{1/3}+\Psi\right)+\left(\lambda_{gas}/\lambda_S\right)^{-1}\left(\Psi^{1/3}-\Psi\right)}{\left(1-\Psi^{1/3}\right)+\left(\lambda_{gas}/\lambda_S\right)^{-1}\left(\Psi^{1/3}\right)}$	(68)
Russell 1935	$\frac{\lambda_{eff}}{\lambda_S} = \frac{\Psi^{2/3}+\left(\lambda_{gas}/\lambda_S\right)^{-1}\left(1-\Psi^{2/3}\right)}{\Psi^{2/3}-\Psi+\left(\lambda_{gas}/\lambda_S\right)^{-1}\left(1-\Psi^{2/3}+\Psi\right)}$	(69)
Maxwell 1954	$\frac{\lambda_{eff}}{\lambda_S} = \frac{\left(\lambda_{gas}/\lambda_S\right)+2-2\Psi\left(1-\left(\lambda_{gas}/\lambda_S\right)\right)}{\left(\lambda_{gas}/\lambda_S\right)+2+\Psi\left(1-\left(\lambda_{gas}/\lambda_S\right)\right)}$	(70)
Traustel et al. 1961	$\frac{\lambda_{eff}}{\lambda_S} = 1-\Psi\left(1-\frac{\lambda_{gas}}{\lambda_S}\right)\left[1+0.35(1-\Psi)\left(1-1.08\frac{\lambda_{gas}}{\lambda_S}\right)\right]$	(71)
Fritz /Kirchner 1973	$\frac{\lambda_{eff}}{\lambda_S} = \frac{2}{3}(1-\Psi)+\frac{\left[\Psi+\frac{1}{3}(1-\Psi)\right]^2}{\Psi\left(\lambda_{gas}/\lambda_S\right)^{-1}+\frac{1}{3}(1-\Psi)}$	(72)
Koglin 1967	$\frac{\lambda_{eff}}{\lambda_S} = \Psi\cdot\frac{\lambda_{gas}}{\lambda_S}+\frac{2}{3}\cdot(1-\Psi)$	(73)
Stark/Fricke 1993	$\frac{\lambda_{eff}}{\lambda_S} = 1-\frac{1-\lambda_{gas}/\lambda_S}{1+\frac{(1-\Psi)}{\Psi}\left(1+Z_f\frac{\left(\lambda_{gas}/\lambda_S\right)-1}{\left(\lambda_{gas}/\lambda_S\right)+1}\right)}$	(74)

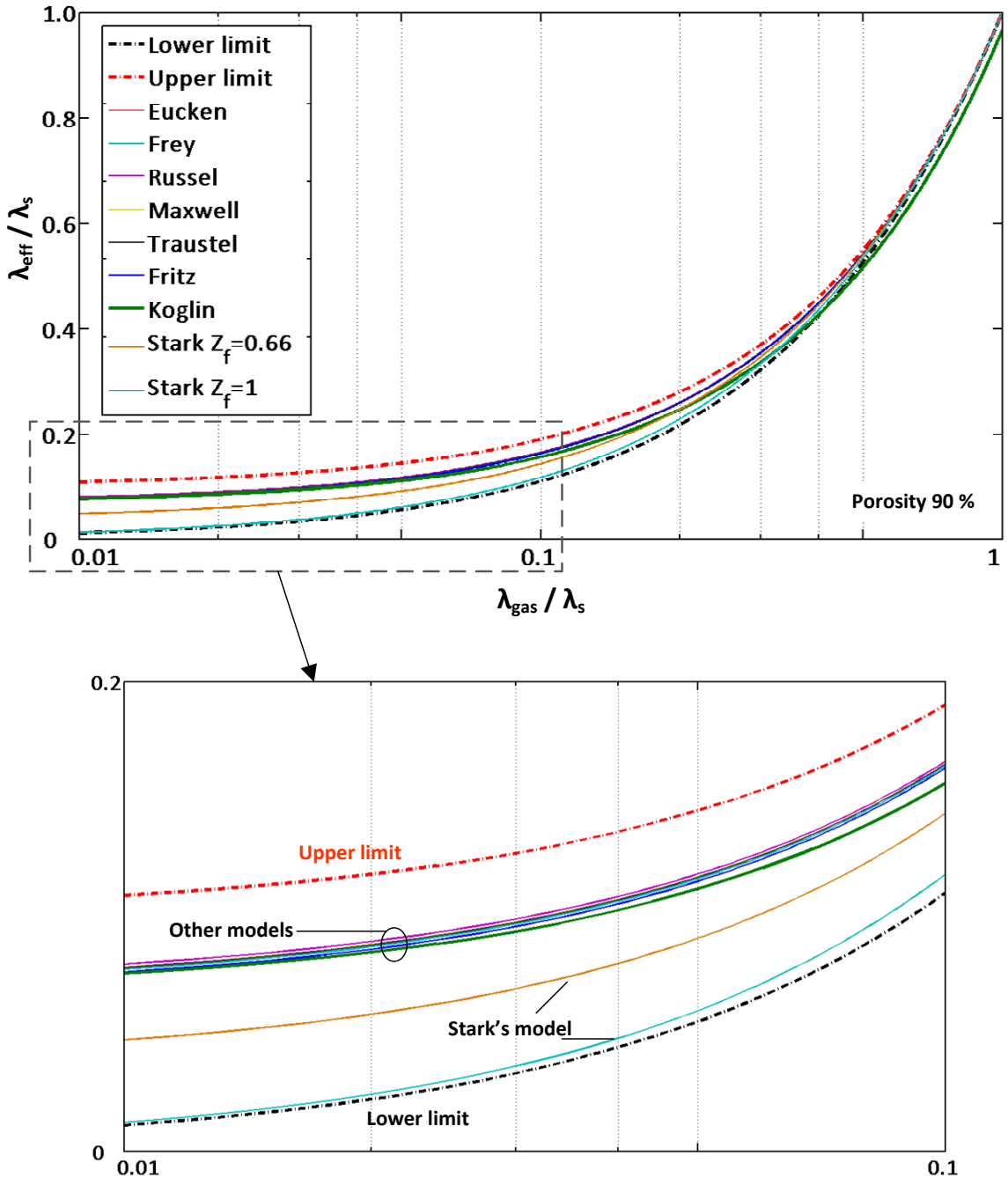

Figure 70: Evaluation of the different models of effective thermal conductivity of porous media

As seen all curves produced by the models fall between the upper and lower limits of effective thermal conductivity. However, Koglin's model eq. (73) goes outside these limits as ($\lambda_{gas}/\lambda_s > 0.5$). This is due to the fact Kolgin's model multiplies the solid contribution with a factor of (2/3), see Table XXI. The trend of all curves produced by the models is almost the same. The curves run flat in the range ($\lambda_{gas}/\lambda_s < 0.1$). They increase with higher slope with increasing the ratio (λ_{gas}/λ_s). The maximum is reached when the gas thermal conductivity equal to the solid thermal conductivity ($\lambda_{gas}/\lambda_s = 1$). The arrangement then consists of one homogenous thermal conductivity and effective thermal conductivity, logically, is equal to the solid thermal conductivity ($\lambda_{eff}/\lambda_s = 1$). Understanding the behavior depicted in Figure 70 explains the coupling effect of the gas and solid contributions. This means by exchanging the

filling gas in the porous media the ratio of the gas thermal conductivity to the solid thermal conductivity is the main parameter and it determines the amount of change in effective thermal conductivity.

By exchanging the gas atmosphere, we actually change the contribution of gas conduction, whereas the contributions of solid conduction and radiation stay constant. Thus, the modification of the effective thermal conductivity ($\Delta\lambda_{eff}$) can be evaluated through applying each model to a defined material using two different gases and then subtracting the results, see Appendix D. As can be seen, the solid thermal conductivity is needed in some models to evaluate $\Delta\lambda_{eff}$. However by five models, which are listed in Table XXII, the $\Delta\lambda_{eff}$ could be expressed as follows:

$$^{gas\,1}\overrightarrow{(\Delta\lambda_{\mathrm{eff}})}^{gas\,2}_{\mathrm{cal}} = f(\psi)\,\Delta\lambda_{\mathrm{gas}} \tag{75}$$

Finding the difference of thermal conductivity between the two filling gases gives the ability to predict how much the effective thermal conductivity changes by exchanging the filling gas. That is actually one of the major objectives of this work. In the next section, various calculations based on different models for gas thermal conductivity will be applied and compared with the experimental results of the investigated materials.

Table XXII: Models for estimation the effect of exchanging the filling gas

respective model	Derived model by exchanging the filling gas regards eq. (75).	Reference	eq.
Koglin's model	$\Delta\lambda_{eff} = \Psi \cdot \Delta\lambda_G$	Koglin, 1967	(76)
Kamiuto's model	$\Delta\lambda_{eff} = \Psi^{1/3} . \Delta\lambda_{gas}$	Kamiuto, et al., 1984	(77)
Rath'model	$\Delta\lambda_{eff} = \Psi . (2 - \Psi) . \Delta\lambda_{gas}$	Rath, et al., 1990	(78)
Verschoor's model	$\Delta\lambda_{eff} = \Psi^{-1} . \Delta\lambda_{gas}$	Verschoor, et al., 1952b	(79)
Litovsky's model	$\Delta\lambda_{eff} = \Psi^{1/4} . \Delta\lambda_{gas}$	Litovsky and Shapiro, 1996	(80)

9.3 Predicating the Effect of Filling Gas Based on Different Models from Literature

Evaluating the effect of the filling gas upon the thermal conductivity of the investigated materials requires estimation of the thermal conductivity of the gas that fills the porous structure. Various models for evaluation of gas thermal conductivity are presented already in a previous chapter, see chapter 3. In this chapter, the change of effective thermal conductivity will be evaluated according to the following models for gas thermal conductivity:

- Bulk gas thermal conductivity
- Single pore model (Kaganer's model) based on
  - Mean pore diameter
  - Most frequent diameter
  - Most probable diameter (inverse evaluation)

Evaluation of these models is performed by comparing the calculated results of these models with the measured results obtained using the RHFA

9.3.1 Validation of the Models through Comparison with Experimental Results

The calculation of the different models of effective thermal conductivity results in the change of effective thermal conductivity $(\Delta\lambda_{eff})_{cal}$ for all twelve materials by exchanging the filling gas. These results will then be compared with the respective experimental results of the change of effective thermal conductivity $(\Delta\lambda_{eff})_{exp}$ at the same temperature with taking into account the uncertainty of the measurements in RHFA. This direct logical comparison could be mathematically expressed as follows

$$^{gas1}\overrightarrow{(\Delta\lambda_{\mathrm{eff}})}^{gas\,2}_{\mathrm{cal}} \gtrless {}^{gas1}\overrightarrow{(\Delta\lambda_{\mathrm{eff}})}^{gas\,2}_{\mathrm{exp}} \pm \sigma_{\Delta\lambda_{\mathrm{eff}}} \tag{81}$$

where $\sigma_{\Delta\lambda_{\mathrm{eff}}}$ is the propagated uncertainty, which results from the uncertainty of the measurements of the effective thermal conductivity in the two gases (gas 1 and gas 2), and can be evaluated as follows

$$\sigma_{\Delta\lambda_{\mathrm{eff}}} = \sqrt{\sigma^2_{\lambda\mathrm{gas}\,1} + \sigma^2_{\lambda\mathrm{gas}2}} \tag{82}$$

An example of propagation of the uncertainty for the material (b1) in case of exchanging Nitrogen by Helium is presented in Table XXIII. The uncertainty of effective thermal conductivity in RHFA averages to 6 % of λ_{eff} measured in each gas. The propagated uncertainty of the change in effective thermal conductivity is around 27 % of $\Delta\lambda_{eff}$ for the material (b1) when exchanging Nitrogen by Helium, and it is around 71 % in when exchanging Krypton by Argon. As can be seen, the propagated uncertainty of $\Delta\lambda_{eff}$ depends mainly on the two different filling gases. The propagated uncertainty of $\Delta\lambda_{eff}$ could be then evaluated for all investigated materials for the different cases of the exchanged filling gases. However, to validate the results that are evaluated by the models the comparison will be performed with the experimental results without taking uncertainty into account.

Table XXIII: Propagation of uncertainty of the change in effective thermal conductivity of material (b1) at 400 °C

σ	$\lambda_{eff} \pm \sigma$	$\lambda_{eff} \pm \sigma$	$\Delta\lambda_{eff}$	$\sigma_{\Delta\lambda_{eff}}$	$\sigma_{\Delta\lambda_{eff}}$
%	W m^{-1} k^{-1}	W m^{-1} k^{-1}	W m^{-1} k^{-1}	W m^{-1} k^{-1}	%
RHFA	exp. with (N_2)	exp. with (He)	(He – N_2)	Eq. (14)	ratio to $\Delta\lambda_{eff}$
6	0.137 ± 0.008	0.188 ± 0.011	0.051	0.0139	27
RHFA	exp. with (Kr)	exp. with (Ar)	(Ar – Kr)	Eq. (14)	ratio to $\Delta\lambda_{eff}$
6	0.107 ± 0.006	0.121 ± 0.007	0.0136	0.0097	71

The reason behind that decision is the variety in the materials and the filling gases. Actually, the propagation of uncertainty depends on the kind of the function, e. g. the previous comparison could be differently expressed as following:

$$(\lambda_{eff}^{gas\ 2})_{cal} \gtrless (\lambda_{eff}^{gas\ 2})_{exp} \pm \sigma_{\lambda_{eff}} \tag{83}$$

The effective thermal conductivity in the new filling gas (gas 2) is calculated from measured thermal conductivity in the filling gas (gas 1) and the evaluated change of thermal conductivity ($\Delta\lambda_{eff}$) from eq. (75) as following:

$$\left(\lambda_{eff}^{gas\ 2}\right)_{cal} = \left(\lambda_{eff}^{gas\ 1}\right)_{exp} \pm \sigma_{\lambda_{eff}} + {}^{gas1}\overrightarrow{(\Delta\lambda_{eff})}_{cal}^{gas\ 2} \tag{84}$$

The new comparison has a maximum uncertainty of $2\sigma_{\lambda_{eff}}$, which is much smaller than the calculated values above.

9.3.2 Evaluation based on Bulk Gas Thermal Conductivity

As a first step, the $\Delta\lambda_{eff}$ of the twelve investigated materials has been evaluated using the derived models equations (76-80) as exchanging the filling gas N2 to He, see Figure 71. The values of bulk gas thermal conductivity are taken from the gas properties in literature (Rohsenow, et al., 1998). As can be seen, the models give good estimation of the experimental results for all materials of group (a). This is obvious by seeing results of models (Kamiuto's model, Litovsky's model and Verschoor's model), whereas material (a2) shows deviation from the experimental results up to 11 %, which is also acceptable considering the uncertainty of the measurements. The results of the other two models (Koglin's model and Verschoor's model) show under-prediction and over-prediction of materials of group (a), respectively. This is because of the difference in the porosity factor f(Ψ) in the models, see Table XXII. These models are created from different parallel-, series-, or complex gas and solid phase distributions of the considered porous media. Thus, it is difficult to decide which model represents the coupling of the gas\solid conduction in the investigated porous materials, since all these materials are different in their microstructure. However, the results of all models for materials of groups (b and c) are strongly over-predicted (400 % - 4000 %), see Figure 71. As an example, evaluation of the models for the materials b3 and b4 resulted in $(\Delta\lambda_{eff})_{cal}$ that ranges between 0.2 W m^{-1} K^{-1} and 0.24 W m^{-1} K^{-1}, whereas $(\Delta\lambda_{eff})_{exp}$ is around 0.05 W m^{-1} K^{-1}. Hence, the results of the models are 400 % to 500 % larger than the experimental ones. This is a confirmation that the Knudsen effect reduces the gas thermal conductivity below the bulk value, as observed in the materials groups (b and c). Consequently, modeling the change of effective thermal conductivity should be based on models of gas thermal conductivity that take Knudsen effect into account.

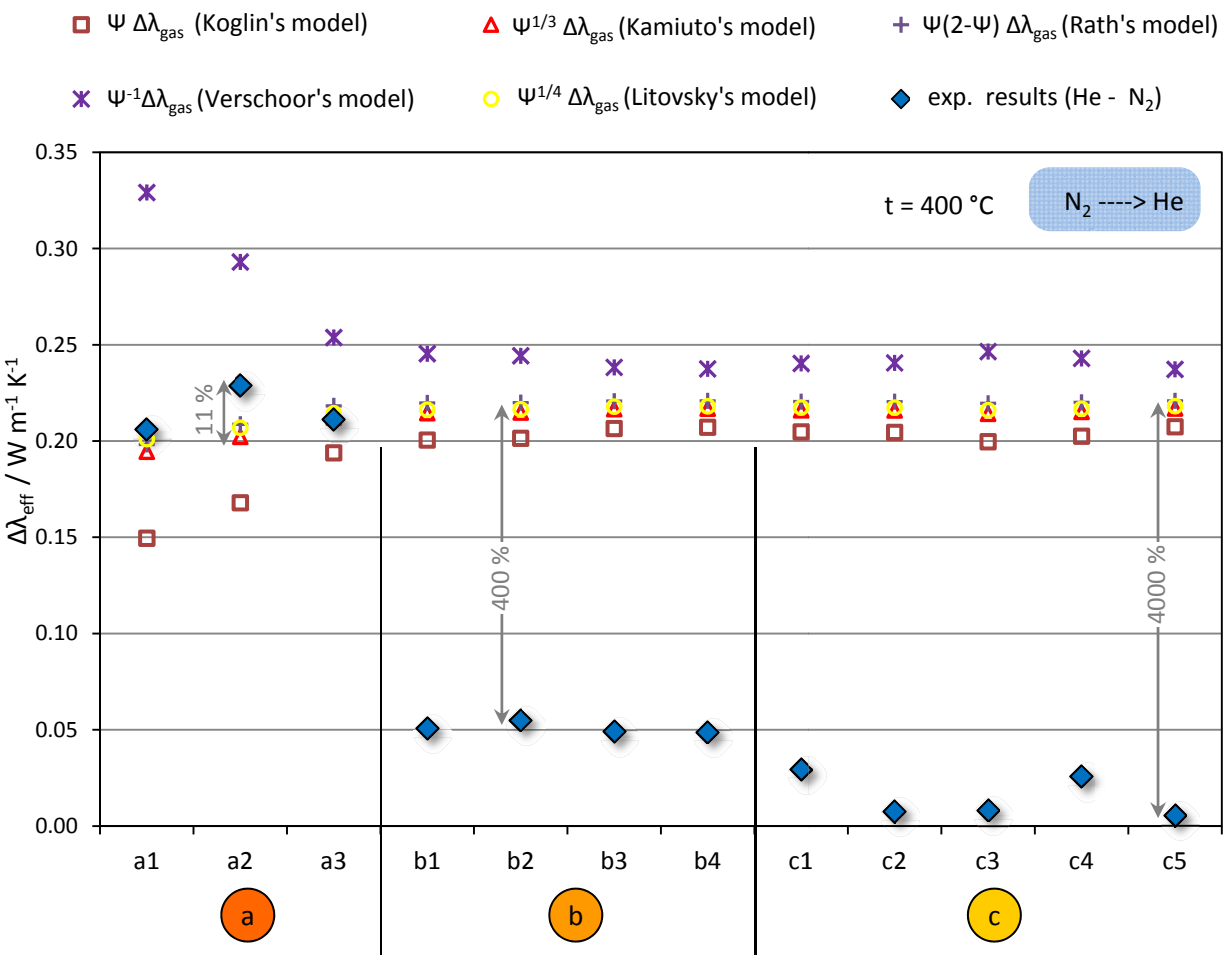

Figure 71: Comparison between the results of the different models with experimental results for all investigated materials at 400 °C

9.3.3 Evaluation based on Single-Pore Model (SPM-Knudsen Effect)

The most used model in the literature for the estimation of effective thermal conductivity of high porously materials is the parallel model, which does not consider any coupling effect between the gas\solid conductions, and it can be expressed as follows:

$$\lambda_{\text{eff}} = f(\lambda_s, \lambda_{\text{rad}}) + \Psi\, \lambda_{\text{gas}} \tag{85}$$

Thus, the effect of the porosity factor f(Ψ) is eliminated. The upcoming predication of the change in λ_{eff} by exchanging the filling gas with regards to the Knudsen effect will be performed according to the following:

$$^{gas\,1}\overrightarrow{(\Delta\lambda_{\text{eff}})}^{gas\,2}_{\text{cal}} = \Psi\, \Delta\lambda_{\text{gas-por}} \tag{86}$$

To model the thermal conductivity of the filling gas in a porous structure ($\lambda_{\text{gas-por}}$), we start with the transfer of Kennard's two parallel-plate system in the free molecule regime to a **S**ingle-**P**ore **M**odel (SPM), see Figure 72. This is achieved through substituting the distance between the plates in the Kennard's model by the characteristic length of porous structure, e.g. the mean pore diameter. The combined model of the Kennard's model (free molecule

regime) and the bulk gas thermal conductivity model (continuum regime) is the Sherman's interpolation, which is valid in the transition regime. This is expressed in eq. (87) as follows:

$$\lambda_{\mathrm{gas-por}}(\mathrm{Sherman}) = \left(\frac{1}{\lambda_{\mathrm{bulk}}} + \frac{1}{\lambda_{\mathrm{Kennard}}}\right)^{-1};$$
$$\lambda_{\mathrm{Kennard}} = \frac{\alpha_{1,2}}{2-\alpha_{1,2}} \frac{\gamma+1}{2} \frac{PC_V}{\sqrt{2\pi RT}} \mathrm{L_{ch}} \tag{87}$$

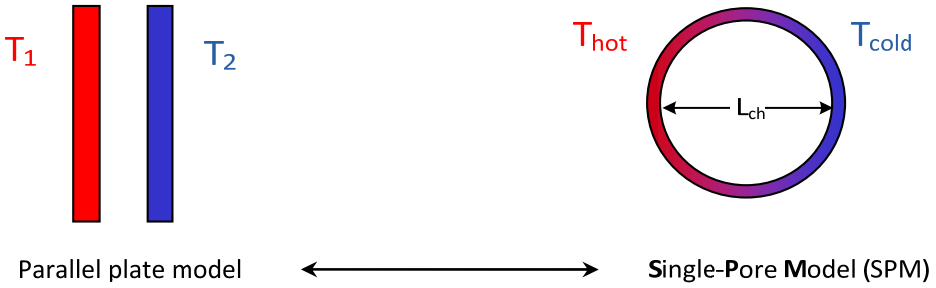

Figure 72: Sketch of the single-pore model

The above mentioned models in eq. (87) have been evaluated for the single-pore model, filled by nitrogen at 25 °C, and assuming the accommodation coefficient to be equal to unity. The pore size has been varied to obtain a Knudsen number in the range $10^{-4} < \mathrm{Kn} < 10^{2}$. The results are plotted in Figure 73 where the Knudsen effect is clearly shown: Downscaling of the pore size brings an increase in the Knudsen number and a decrease in the gas thermal conductivity. This effect starts by the end of the continuum regime at about $\mathrm{Kn} = 10^{-2}$. Sherman's interpolation gives a smooth trend in the transition between the two limiting regimes: the continuum and free-molecule regime, which is reached at about Kn = 10.

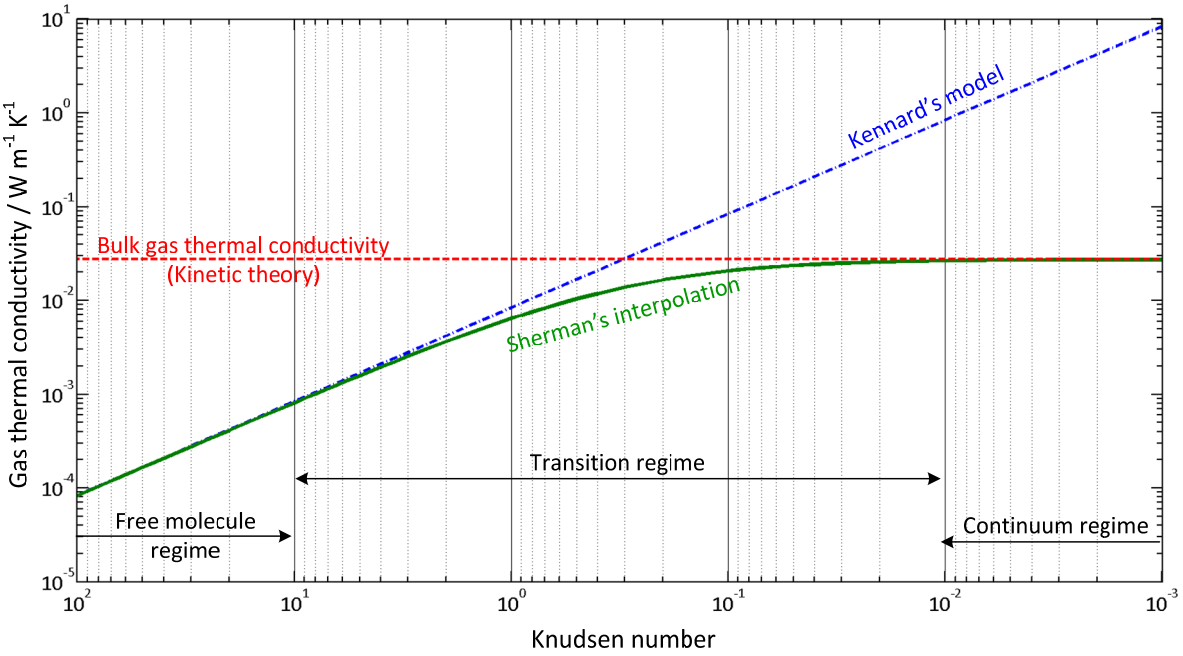

Figure 73: Evaluation of the single-pore model filled with nitrogen at 25 °C

SPM- Mean Pore Diameter as Characteristic Length

Predications of the changes of effective thermal conductivity of the materials in groups (b and c) are executed according to the parallel arrangement model by eq. (87) based on single pore model (SPM). Evaluation of SPM is based on the mean pore diameter as characteristic length. The mean pore diameter is already a known parameter from the structure properties of the investigated materials. Equations (86) and (87) are evaluated for the case of exchanging the filling gas N_2 by He, taking into account the mean pore diameter and porosity of each material and assuming that the accommodation coefficients for both gases and all materials are equal to unity.

SPM- Most Frequent Diameter as Characteristic Length

Similar calculations are performed based on single pore model, however, the most frequent pore diameter is taken to be the characteristic length instead of the mean pore diameter. The results of the evaluation of parallel arrangement model by eq. (87) based on single pore model with both the mean pore diameter and the most frequent diameter are presented in Figure 74 against the experimental results for the materials of the groups (b and c). As shown in the figure, considering the Knudsen effect in the evaluation leads to reduction in the results of the evaluation based on SPM compared to the one based on bulk gas thermal conductivity, see Figure 71.

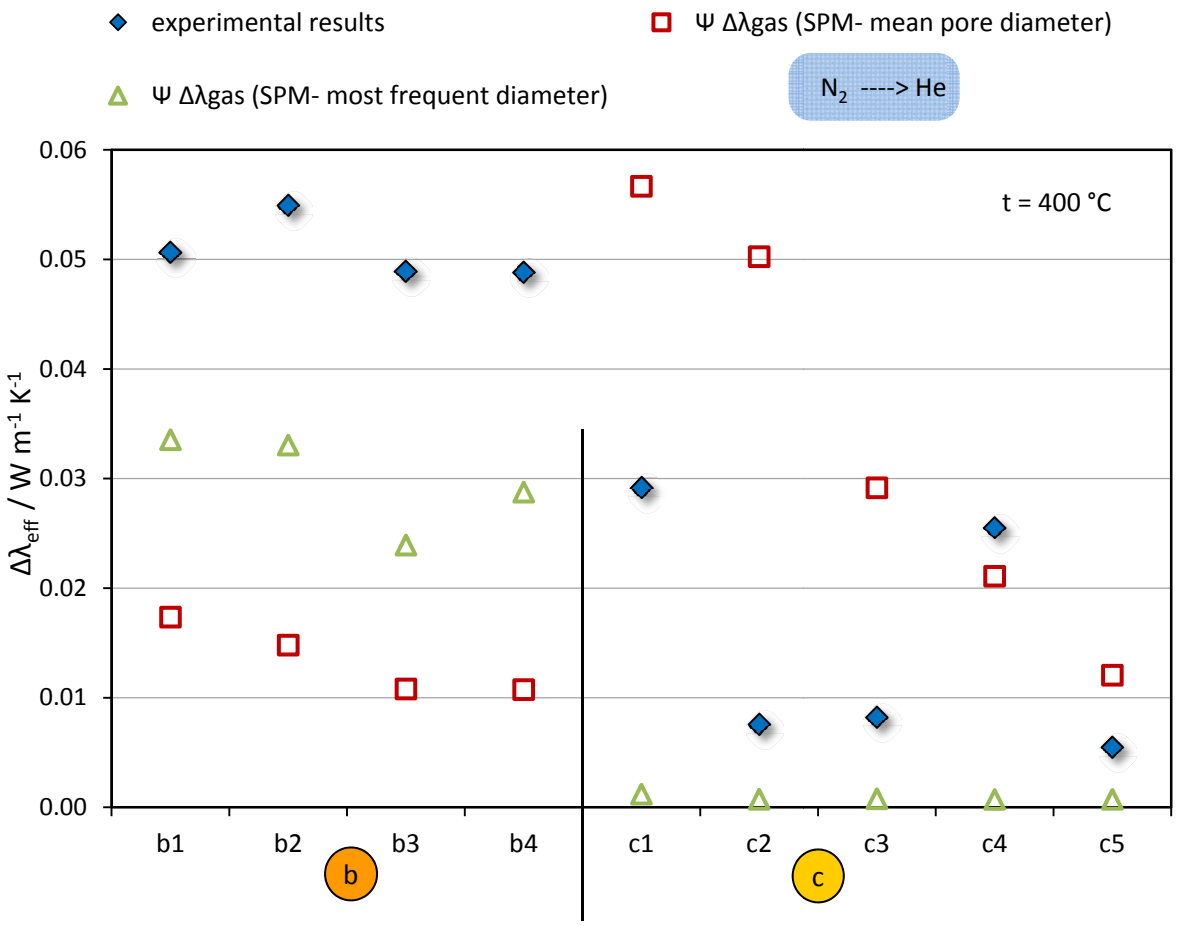

Figure 74: Results of evaluation of parallel arrangement model based on single pore model (Knudsen effect)

It can be noted though that the evaluation based on single pore model fails to predict the change of the effective thermal conductivity by exchanging the filling gas (N_2 to He). By observing the results with the mean pore diameter it is obvious that for the materials of group (b) results of the model show an under-predication, whereas they show an over-predication in the materials of group (c) except c4. The latter have good agreement with experimental results. This could be understood by comparing the mean pore diameter of the materials, see Figure 75. The materials of group (b) have a smaller mean pore diameters comparing with those of materials of group (c). Evaluation based on the most frequent diameter fails also to produce good agreements with experimental results. It shows smaller deviation to the experimental results of the materials of group (b), which could be considered as an improvement compared to that with mean pore diameter. This is due to the fact that the most frequent diameter of each material from group (b) is bigger than the respective mean pore diameter. However, the results of the materials of group (c) are strongly under-predicated with the evaluation based on the most frequent pore diameter. The reason behind this under-estimation is that the materials of group (b) have very small values for the most frequent pore diameter, see Figure 75.

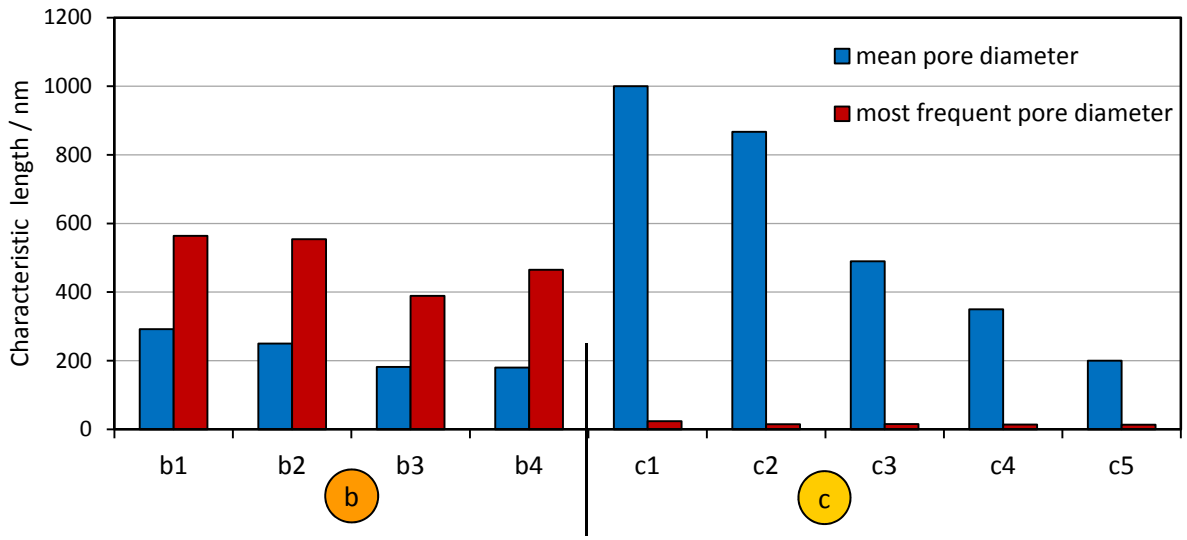

Figure 75: Comparing the characteristic length of the investigated materials

One can observe that the results of evaluation based on the mean pore diameter for materials (b3, b4 and c5) are almost the same $(\Delta\lambda_{eff})_{cal}$ = 0.011, 0.011 and 0.012 W m^{-1} K^{-1}, respectively, see Figure 74. This is because these materials have almost the same mean pore diameter, as seen in Figure 75 (d_{mean}= 182, 180 and 200 nm, respectively) and about the porosity (around 90 %, see Table XVI in chapter 7). Whereas the experimental results of (b3) and (b4) are 10 times larger than that of material (c5). This indicates that ***the mean pore diameter and the most frequent pore diameter are not the parameters that represent the different porous structures of the investigated materials.***

Different Study Cases

The above evaluation is repeated, however, for the case of exchanging Ar by N_2. This is done to confirm the assessment about this kind of evaluation. The results of evaluation are presented in Figure 76 for the materials that are already measured in these two gases (Ar and N_2). In this study case of exchanging the filling gas (Ar to N_2) the comparison of the

results with the measured data shows a small deviation of the two materials (c4 and c5) by the evaluation that is based on the mean pore diameter as characteristic length, whereas all other materials show larger deviation from the measured data. The same effect of shifting in the results is also noticed here by the evaluation based on the most frequent pore diameter.

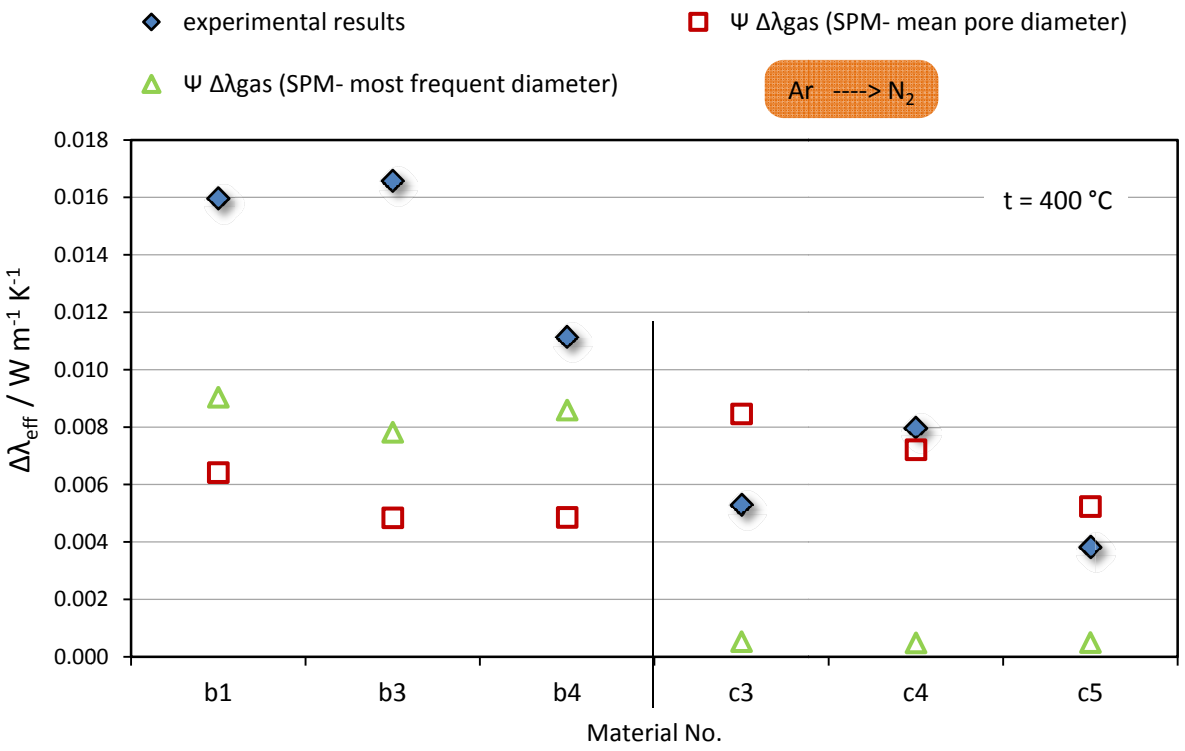

Figure 76: Evaluation based on single pore model (Knudsen effect) for case exchanging the argon by nitrogen

As can be seen, the result of the evaluation based on single pore model depends mainly upon the respective characteristic length (d_{mean}, d_{freq}). This length is the main parameter in evaluating the Knudsen number and thus the ratio of the rarefaction of the filling gas. However, the model does not imply any consideration to the pore size distribution. It is already observed, however, from the evaluation of materials with different pore size distributions that the same mean pore diameter and porosity result in the same change of the effective thermal conductivity by exchanging the filing gas. That increases the need to find a parameter that represents effectively the porous structure and leads to a relatively good estimation of change in the effective thermal conductivity by exchanging the filling gas.

9.3.4 Seeking a Most Probable Pore Diameter

The parallel arrangement model by eq. (87) based on single pore model has been used to find the most probable pore diameter d_{pro} of the various materials at a certain temperature by fitting the measured data. This is actually a kind of an inverse problem: estimation of the input-data (pore diameter) using the known output-data (measured effective thermal conductivity). Implementation of the calculation is performed through using a loop-programming algorithm for the combined models by equations (86) and (87) for the two respective filling gases. The results of the most probable diameter for the materials of group (b and c) in case of exchanging nitrogen by helium at, e.g., 400 °C are presented in Figure 77 in comparison with d_{mean} and d_{freq}. The results for d_{mp} for materials of group (b) show that the most probable diameter is larger than the respective mean pore diameter and even than the most frequent diameter. Whereas for the materials in group (c) the evaluated most probable diameters are smaller than the mean pore diameters, except for material (c4). They are, however, larger than the most frequent diameters. Thus, there is no clear dependency between the evaluated most probable diameter and the known structure properties of the materials.

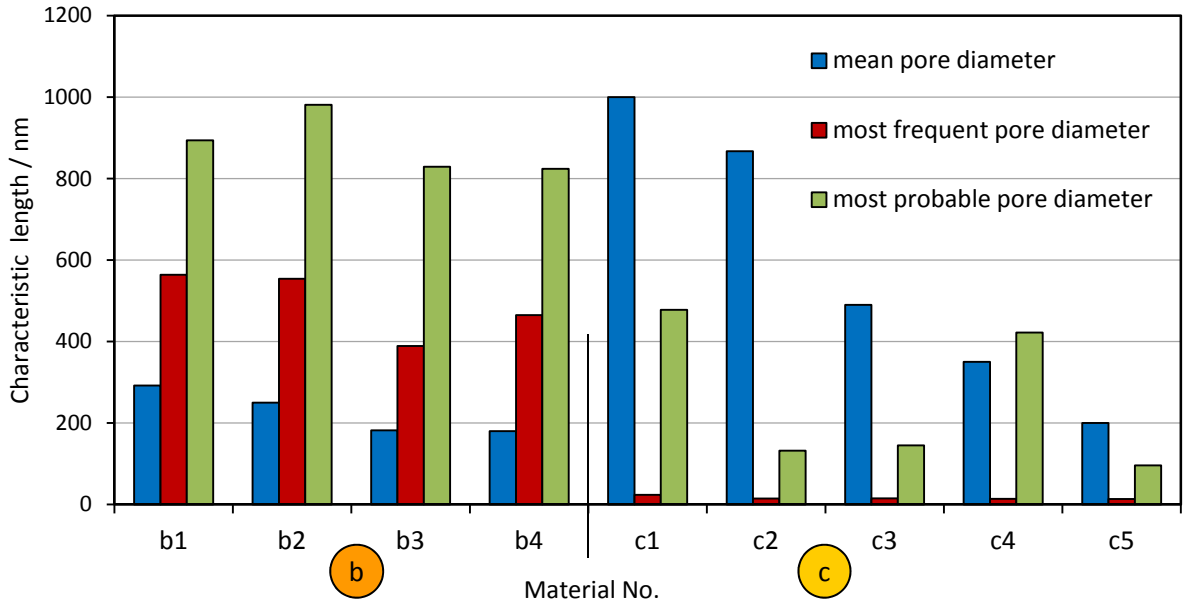

Figure 77: Comparison the most probable pore diameters at 400 °C with the mean pore diameters and with the most frequent diameters

SPM- Most Probable Diameter as Characteristic Length

Evaluation of the change in effective thermal conductivity based on single pore model with the above evaluated most probable pore diameter is performed for the case of exchanging Krypton by Argon for three materials (b1, b4 and c5) over the temperature range (250 °C – 650 °C). The aim of that evaluation is to test the above calculated most probable pore diameter. Comparison between the results of the evaluation and the measured data is presented in Figure 78. The estimated effective thermal conductivity of the three materials filled with Argon is evaluated with regards to equation 16, i.e. from the measured data of the respective material when filled with Krypton and the $(\Delta\lambda_{eff})_{cal}$ that is evaluated with regards to models by equations (86) and (87) based on the above calculated most probable pore diameter.

It can be shown that there is an excellent agreement between the results of the evaluation and measured data with respect the uncertainty of the measurement (± 6 %). Moreover, this is true over the entire temperature range. We have to keep in the mind that this evaluation is based on the most probable diameter, which has been estimated from other experimental results (He and N_2). Actually, the reason behind this inverse calculation and the following tests of the results is to find out the ability of the single pore model (Kennard\Kaganer-model) based on assumed values for to estimate the change in effective thermal conductivity. After observing the results of the evaluation based on the most probable diameter, we can conclude that the single pore model is able to predicate the change of effective thermal conductivity by exchanging the filling gas. However, an improvement is needed to consider the pore size distribution. This will be the focus of the following section.

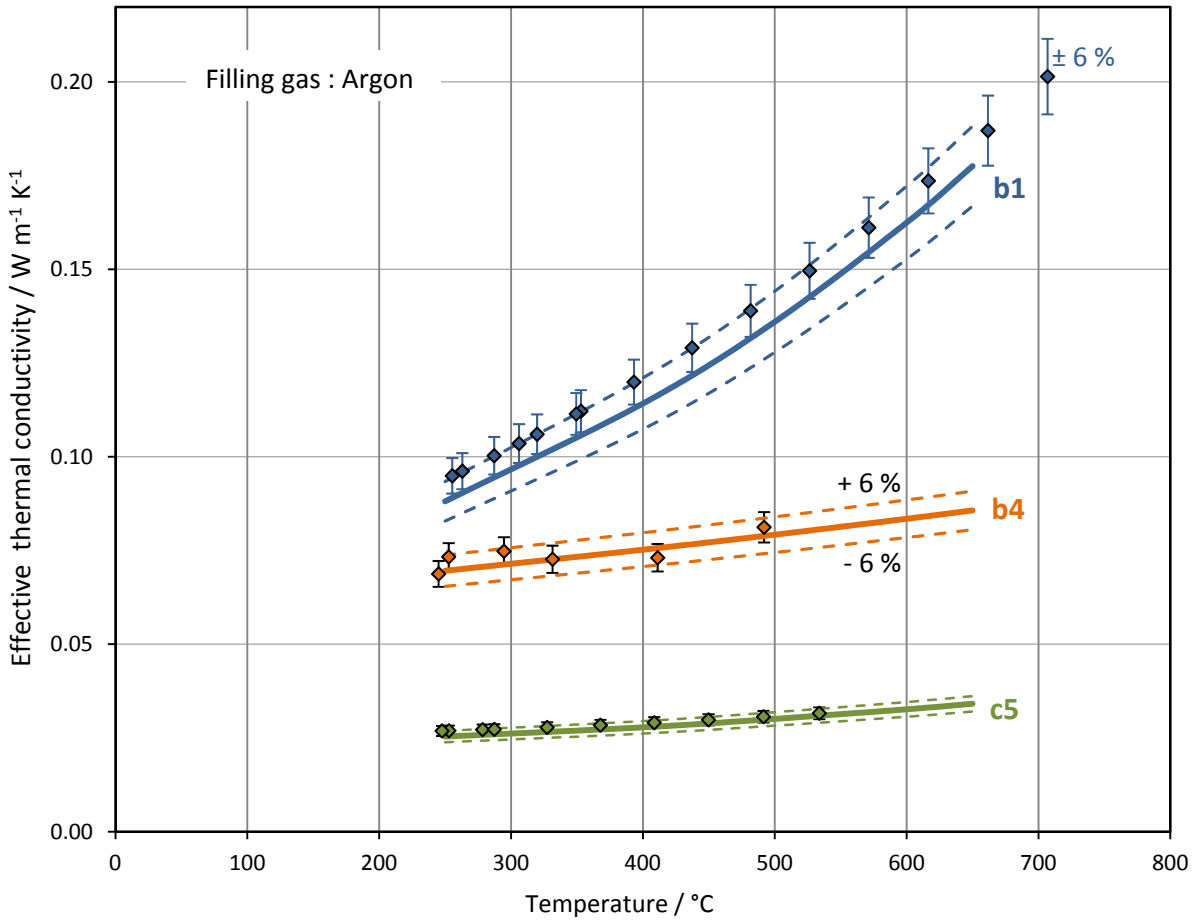

Figure 78: Comparison between the results of evaluation that based on SPM- most probable diameter and the measured data in Argon | lines: estimated regards model by eq. 87, dash-lines: range of uncertainty, points: measured data in RHFA.

9.4 New Improved Model for Estimating the Effect of the Filling Gas

9.4.1 New improved Model for Gas thermal conductivity in the Knudsen's sectors

Only a few porous materials are mono-disperse pore systems, e.g., some kinds of foam. For such systems, we can apply the above mentioned single-pore model for the assessment of the gas thermal conductivity. However, most insulation materials represent bi- or even poly-disperse systems, which makes it more complicated to estimate the gas thermal conductivity

as seen above. The pore-size distributions can be mathematically described through cumulative distribution functions (CDF). These functions are used to subdivide the poly-disperse system into (n) narrow sectors, each of them with a constant mean pore size. The latter can be considered as (*n*) mono-disperse systems, thus we can use the single-pore model to evaluate the gas thermal conductivity in the corresponding Knudsen-number range of the sector (Kn_a - Kn_b):

$$\left(\bar{\lambda}_{gas}|_{Kn_a}^{Kn_b}\right)_i = \lambda_{gas-por}\,(T, \overline{Kn}, \alpha) \tag{88}$$

Partitioning the porous system into sectors depends mainly on the corresponding Kn-number range. The sector can be wide for large pores, i.e. the continuum regime, whereas in the transition and free-molecule regimes the gas thermal conductivity slides are stronger, as seen in Figure 73, and therefore the sectors should be narrow to get correct results.

Exchanging the gas atmosphere, e.g., nitrogen by helium, causes a change in the gas thermal conductivity in any sector (i) of the material corresponding to the Knudsen number (Kn_a - Kn_b), which is evaluated as follows:

$$\left({}^{N_2}\overrightarrow{\Delta\lambda_{gas}}^{He}\right)_i = \bar{\lambda}_{He,i} - \bar{\lambda}_{N_2,i}|_{Kn_a}^{Kn_b} \tag{89}$$

To evaluate the gas thermal conductivity change in the entire porous system, a model based on parallel arrangement for all sectors can be used:

$$\Delta\lambda_{gas} = \sum_{1}^{n} CFD_i^{i+1} \times \left({}^{gas_1}\overrightarrow{\Delta\lambda_{gas}}^{gas_2}\right)_i \tag{90}$$

9.4.2 Improving the Model for Estimation of the Change in Effective Thermal Conductivity Model

To predict the change in the effective thermal conductivity, a final improved model to estimate the effect of the filling gas is expressed as follows:

$${}^{gas_1}\overrightarrow{\Delta\lambda_{eff}}^{gas_2} = \left(\Psi \times \Delta\lambda_{gas}\right)^{\zeta} \tag{91}$$

$\Delta\lambda_{gas}$, the change of the thermal conductivity of the gas, which is filling the respective porous structure, is evaluated with regards to the models described by equations (87-90). The **E**xponential **C**orrection **C**oupling **P**arameter **ECCP** (ζ) reflects mainly two factors: the kind of pore-size distribution (narrow or wide) and the coupling effect between the two phases, namely, gas and solid. This will be noticed later by observing the results of the evaluation.

9.4.3 Calculation Algorithm (overview)

Evaluating the model by equation (91) and comparing with experimental data require some calculations efforts. Implementation of the loops-calculation is performed with the help of matrix-programming software Matlab©. An overview of the calculation algorithm is presented in Figure 79. The main input data are the structure properties of the investigated

material (pore size distribution and porosity), the various properties of the two respective gases and the defined experimental conditions. The output of this calculation is the change of effective thermal conductivity of the respective material by exchanging the filling gas.

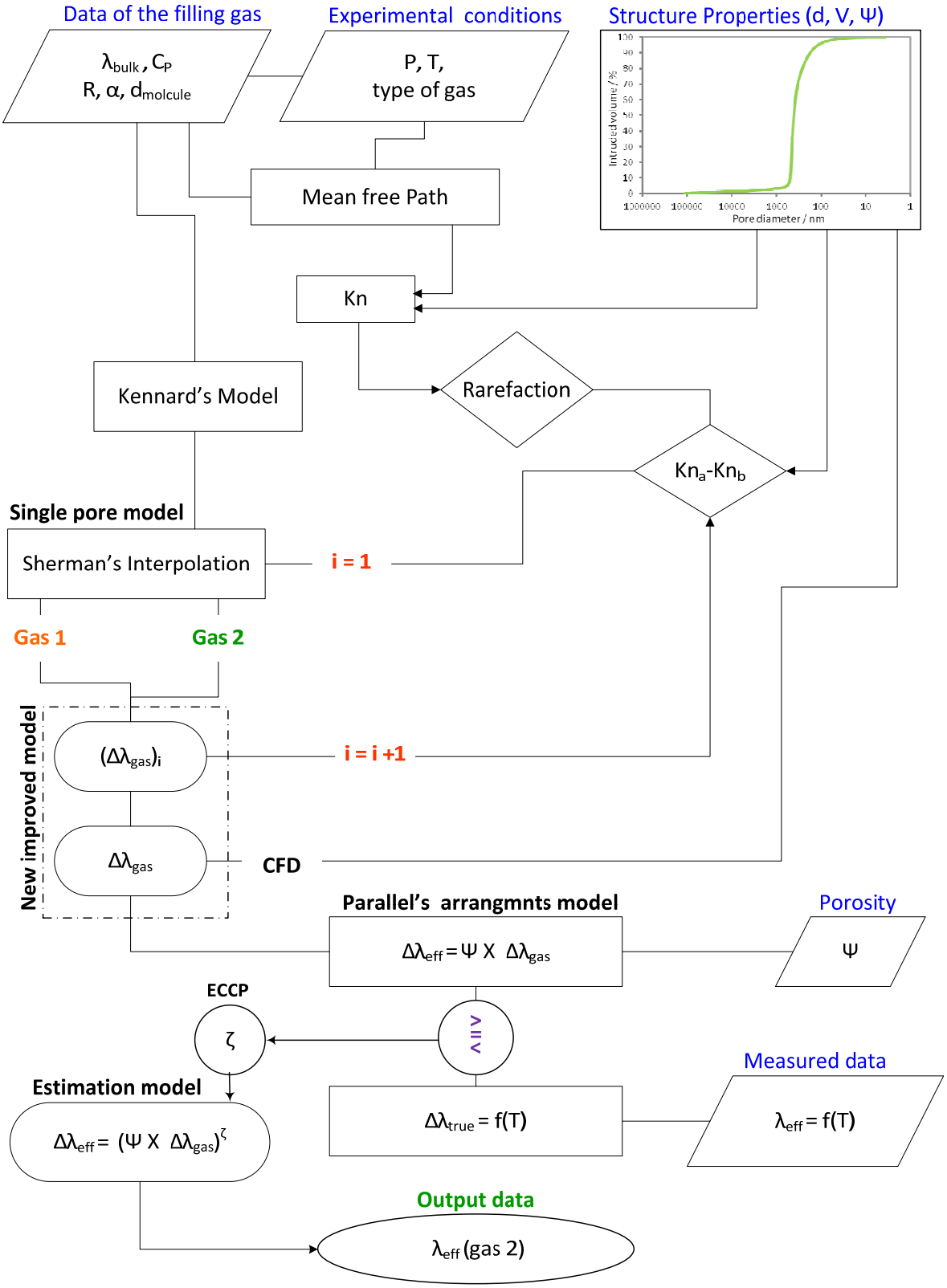

Figure 79: Flowchart of the developed algorithm for calculating the new improved model to estimate the effect of the filling gas

9.4.4 Estimation of the Effect of the Filling Gas using the New Improved Model

The new improved model for gas thermal conductivity eq. (90), and the corrected model for the effective thermal conductivity eq. (91) are evaluated for all investigated materials in order to predict the change of their effective thermal conductivity when exchanging Nitrogen by Helium The results of the new improved model are presented against the experimental results at a temperature of 400 °C, see Figure 80. As can be seen, generally there is a good agreement between experimental data and the results of the new improved model. The new improved model has the ability to estimate the change in effective thermal conductivity of non-Knudsen as well as Knudsen materials, and it considers the pore size distribution as the main input parameter in modeling this change. The model is evaluated for all materials in the group with the same value of the exponential parameter ECCP. However, the results for some materials have a deviation from the experimental ones, as noticed for the materials (a3 and c4), where the first is overestimated by 27 % and the other is underestimated by 41 %, respectively. These could be, however, in the accepted range with regards to the uncertainty. This should be proved later with another kind of comparison where the uncertainty is included. The chosen values for the exponential parameter (ECCP), which is used at this temperature for the calculation, are listed in Table XXIV. These are classified in three ranges. It is noticed also that there is a kind of dependency (inverse relation) between the ECCP and Knudsen ratio.

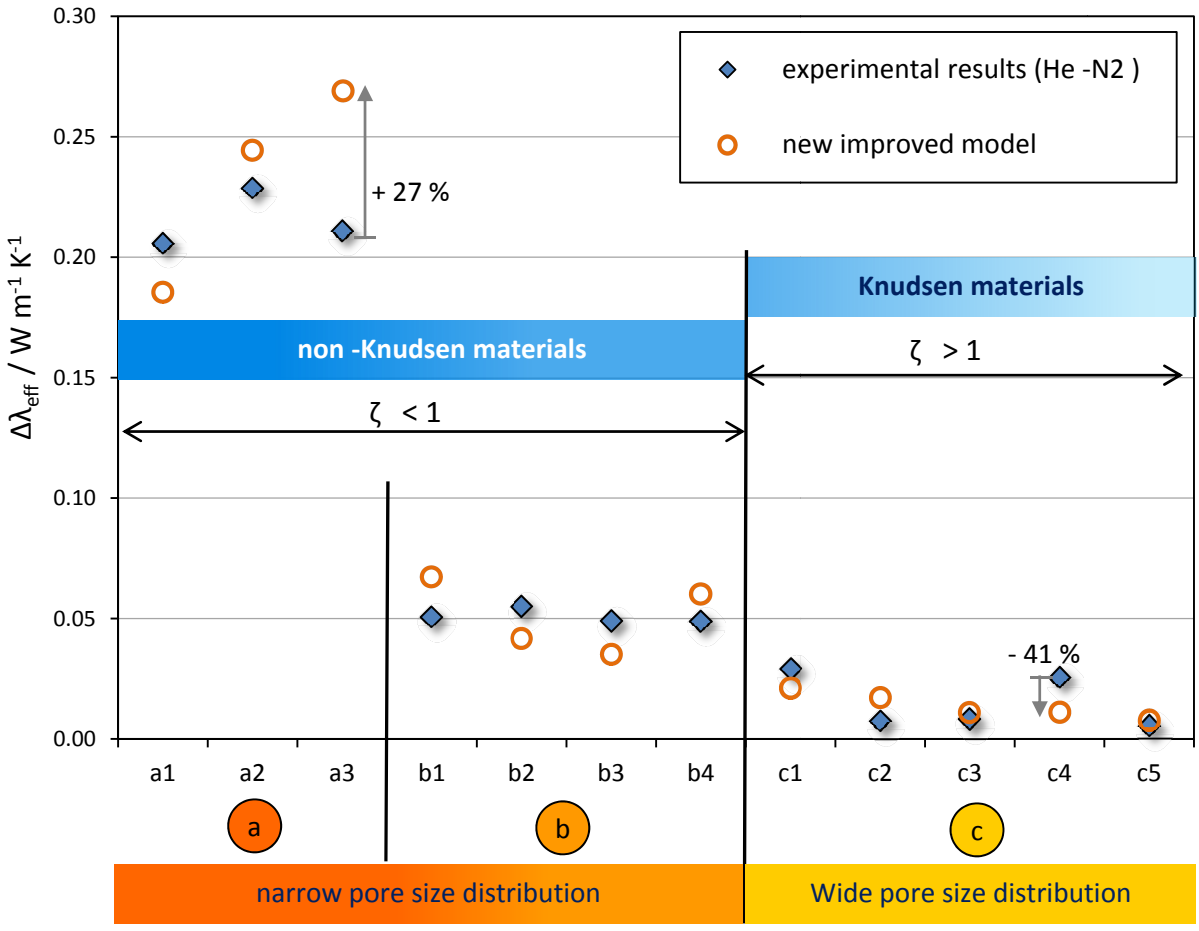

Figure 80: Comparison between the results of evaluation of the new improved model with the experimental results at a temperature of 400 °C

Table XXIV: List of the Exponential Correction Coupling Parameter for all investigated materials

ECCP	Knudsen ratio	Kind of material	Values of Evaluation @ 400 °C
$\zeta < 1$	$\chi_{Kn} > 1$	narrow distributions, non- Knudsen materials	$\zeta \cong 0.74$ for all materials of group (a) $\zeta \cong 0.85$ for all materials of group (b) expect the b4
$\zeta > 1$	$\chi_{Kn} < 1$	wide distributions, Knudsen materials	$\zeta \cong 1.60$ for all materials of group (c)
$\zeta \approx 1$	$\chi_{Kn} \approx 1$	wide-narrow distribution, near Knudsen material	$\zeta \cong 0.99$ for the material (b4)

9.4.5 Validation of the New Improved Model:

New Study Cases:

The above mentioned results were for the study case of exchanging nitrogen by helium at 400 °C. To validate the results of the predictive model, it is important to implement the model to other gases and other temperatures. For example, effective thermal conductivity of three materials (a1, b1 and c5) has been measured when materials were filled with nitrogen. Prediction of the effective thermal conductivity of these materials in krypton atmosphere is done through applying the new improved model with regards to the functions describing their pore size distribution and with the exact same above-assessed values for ECCP. This study case is presented in Figure 81.

As can be seen, there is a very good agreement between the experimental results and the evaluated values with regards to the range of uncertainty. Only for c5 an overestimation is noticed with about 10 - 13 % comparing to the experimental results. Generally, this validates the new improved model in predicting the change due to exchanging the filling gas. Unfortunately, testing the new improved model on experimental results for materials taken from the literature was not possible because all studies in this scope do not analyze or determine the pore size distribution.

Exponential Correction Coupling Parameter (ECCP):

The ECCP is evaluated for all investigated materials over the studied temperature range and for the various study cases, i.e. different pairs of filling gas (e.g. Kr-Ar or N_2-He etc.). Observation of the evaluated ECCP leads to two important notices:

- There is no dependency between the ECCP and the measured temperature as the values of thermal conductivity of the two exchanged filling gases are near to each other. This is the case for example for (Ar to N_2 or Kr to N_2)

- An increase of the ECCP is noticed with increasing the temperature of the Knudsen materials as the values of thermal conductivity of the two exchanged filling gases are far from each other. This is the case for example for (N_2 to He or Kr to He). If we keep in mind that the exponential parameter is larger than one, and the difference

between the thermal conductivity of the applied filling gases is always smaller than the unity, we can conclude that the evaluated change of effective thermal conductivity becomes smaller with increasing temperature. The latter observation reflects actually the coupling effect of conduction\radiation, which is already analyzed in chapter 8.

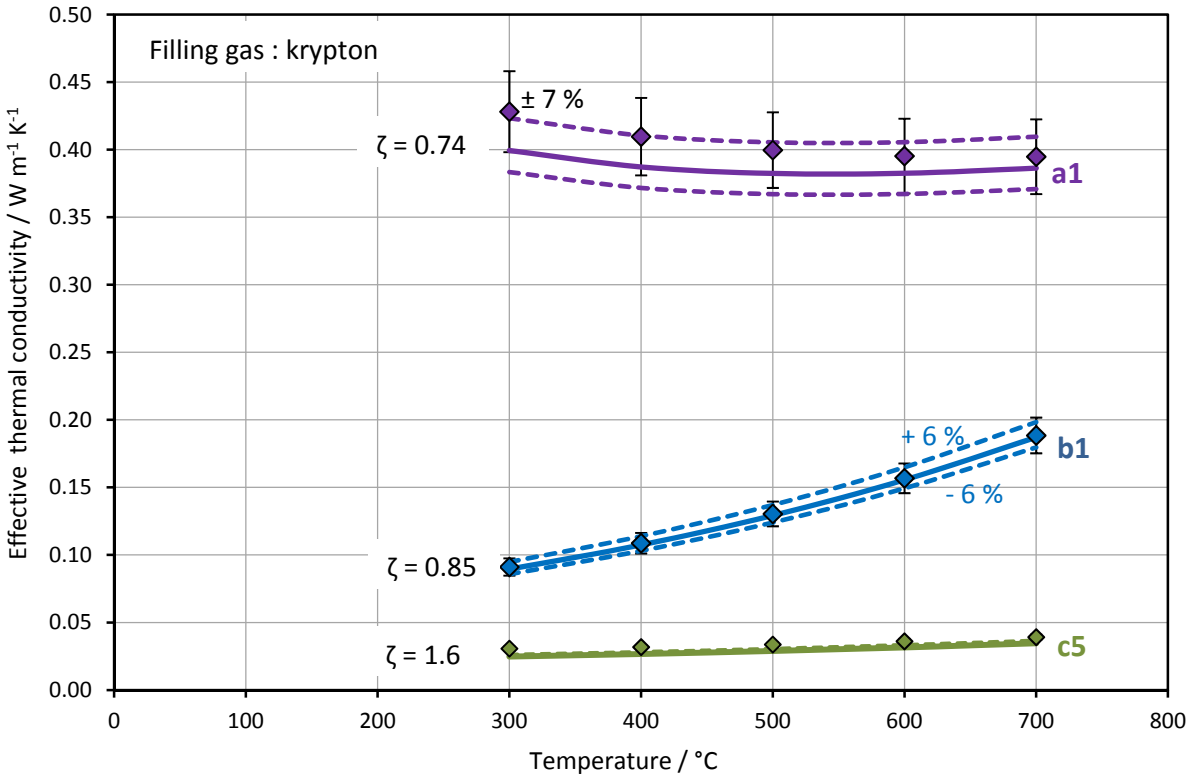

Figure 81: Comparison between the experimental results and the results taken from the evaluation of the new improved model based on measured data in nitrogen,
lines: measured true thermal conductivity, Points: new improved model

9.5 Accommodation Coefficient Effect

By rarefaction of the gas and leaving the continuum regime, molecular collisions with the pore surfaces become more frequent when compared with intermolecular collisions. Subsequently, the accommodation coefficient has an increasing effect on the evaluation of the gas thermal conductivity. The accommodation coefficient is assumed to equal the unity in the above evaluated models for gas thermal conductivity. The accommodation effect can be clearly seen in Figure 82, where results from the single-pore model eq. (87) are plotted versus the Knudsen number. For helium, the accommodation coefficient is decreased from 0.6 to 0.2, and the gas thermal conductivity becomes smaller than that of nitrogen in the range Kn > 0.32, whereas the opposite is true for smaller Knudsen numbers. This leaves no doubt that the influence of the accommodation coefficient in the high Knudsen-number regime is large. However, as mentioned in the background chapter, the sacristy of the data for the accommodation coefficient, especially for the investigated materials, does not allow for a good estimation of thermal conductivity of the filling gas.

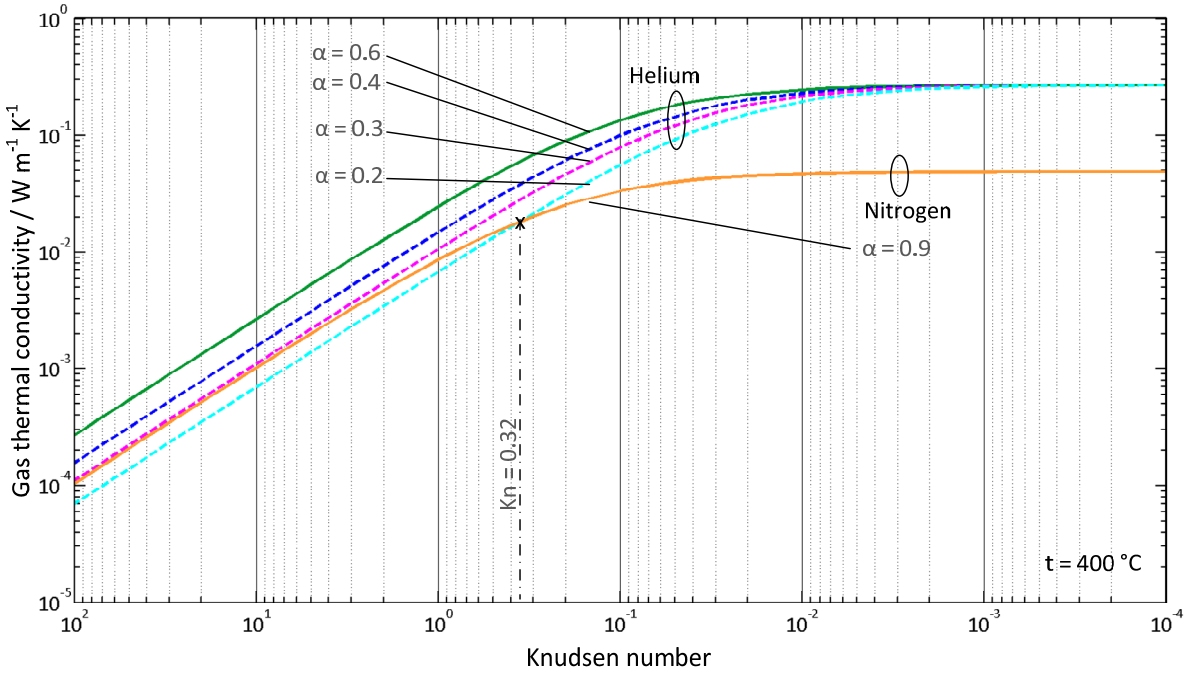

Figure 82: Influence of accommodation coefficient upon the modeling of the gas thermal conductivity regards single pore model

9.6 Discussion

Predicting the change of effective thermal conductivity due to exchanging the filling gas depends on the ratio of thermal conductivity of the filling gas to the thermal conductivity of the material that forms the solid matrix. This dependency is presented in Figure 70, where the results represent evaluation of some models from literature and the upper and lower limits of the solid/gas arrangements. However, calculation of the change of effective thermal conductivity by gas exchange requires the thermal conductivity of the solid materials.

The overall results of evaluation neglecting the coupling effect between gas\solid conduction show that only the materials in group (a) are well represented by the different models based on the bulk gas thermal conductivity, which gives good agreement with the experimental data, see Figure 71.

Single pore model by eq. (87), the most used model in literature for estimation of thermal conductivity of gas, does not take into account the pore-size distribution. Evaluation of this model using the mean pore size gives the following results: materials in groups (b) and (c) show underestimation and overestimation of the thermal conductivity, respectively. Evaluation based on the most frequent diameter instead of the mean pore diameter improves the results in group (b). However, a strong underestimation is found in group (c), see Figure 74. Single pore model is developed to estimate the Knudsen effect. However, in Knudsen regimes it strongly depends on the chosen characteristic length. An inverse calculation aiming to find the most probable pore diameter show that the model is able to predicate the effect of the filling gas, see Figure 78. However, the results of the most probable pore diameter are not related to the investigated porous structure.

The new improved model eq. (90) is introduced for prediction of the effect of the filling gas. This model is based on the parallel arrangement model of gas thermal conductivity with

regards to the different kinds of pore size distribution. The latter is achieved through dividing the porous structure to many Knudsen sectors. Evaluation of the new improved model gives a good estimation of changes in gas thermal conductivity for a poly-disperse porous system. However, deviations in the obtained results from the experimental results could be attributed to two major reasons: the first is the simplification of the conduction model of the two phases, namely, neglecting any coupling between gas and solid; the second is the considered parallel arrangement model for the gas thermal conductivities in the various sectors. These two factors are represented through varying the added Exponential Correction Coupling Parameter. Values for the exponential parameter for the case of exchanging Nitrogen by Helium are listed for all investigated materials. Considering the shape of the pore-size distribution curves and the trend of the exponential parameter, some general conclusions for the range of ECCP can be drawn from this model. Testing these values for a different study case shows a good agreement with the experimental results, see Figure 81.

As a conclusion, it could be say that estimation of the change of effective thermal conductivity of porous materials due to gas exchange needs basically two types of information: the effective thermal conductivity for one gas atmosphere and the kind of pore-size distribution. The new improved model can be then applied with this information and the appropriate exponential parameter.

The increase of ECCP with increasing the temperature reflects indirectly the noticed radiation effect in Knudsen materials.

The strong effects of the accommodation coefficient on estimation of the gas thermal conductivity show the importance to have and to develop a measured database for accommodation coefficients of the various porous insulation materials.

PART IV: CONCLUSION

10 Conclusions and Future Work

10.1 Goals

The study was set out to investigate the effect of exchanging the filling gas on the effective thermal conductivity of various insulation materials. The study has sought to find out how significant the Knudsen effect is in the different kinds of pore size distributions. The general literature on the Knudsen effect is inconclusive about predicting the change in effective thermal conductivity of porous media due to exchanging the filling gas. Besides achieving the objectives of this work, this study has sought to answer three related questions:

1. How to describe the rarefaction of the gas in a *board range pore size system*?
2. How to apply the *laser flash method* to measure thermal diffusivity of the porous media under various gas atmospheres?
3. How to obtain a mathematical description of the pore size distribution to describe a structure controlled parameter for a predictive model to the *effective gas thermal conductivity* in porous media?

In the present work, the influences of exchanging the filling gas accompanied with Knudsen effect on effective thermal conductivity were investigated with experiments and physical mathematical modeling. This work is thought to be the first intensive study in this area of the research, which includes twelve different porous insulation materials. Analysis of the huge number of experimental results leaded to new observations regarding various coupling effects. An improved model for predicting the change in effective thermal conductivity due to exchanging the filling gas has been developed with regards to the Knudsen effect based on models for rarefied gases and parallel arrangements models for effective thermal conductivity.

10.2 Modeling Conclusions

Analysis of the different experimental results of all investigated materials and comparing them to the computational results that emerged through the modeling led to the following general conclusions with regards to the main objectives of this research:

- **Knudsen-Ratio:** Advances in the porous insulation materials are leading to reducing their pore size and thus the Knudsen effect becomes more significant. The Knudsen effect must be consider when studying such materials. It is interesting to notice that some porous systems have wide pore size distribution, i.e. the range of Knudsen numbers is extremely wide. It extends from continuum regime to the free molecules regime in some of these materials that are characterized as board range of pore size. Conventionally in literature, the rarefaction of gas through such porous media is determined through Knudsen number. For better description of the rarefaction of gases in porous materials a new parameter is introduced in this work called “Knudsen ratio”. It emerged from observing the behavior of the various porous systems, especially under various gas atmospheres. The Knudsen ratio is related to the

effective thermal conductivity and the thermal conductivity of the filling gas. According to the Knudsen-Raed ratio, the materials could be subdivided to Knudsen and non- Knudsen materials. Knudsen materials are those materials that rarefy most of the filling gas through their porous structure at normal gas pressure.

- **Non-Linear Effect:** The change in the effective thermal conductivity 'of porous media' due to exchanging the filling gas is found to be large when the two exchanged filling gases have relatively low thermal conductivity, e.g. when exchanging krypton by argon. On the other hand, the change in effective thermal conductivity becomes smaller when the two filling gases have relatively high thermal conductivity. Thus, the slope of change in effective thermal conductivity differs with respect to the thermal conductivity of the filling gas. This contradicts the conclusion by Woodside and Messmer, 1961, who described the change in effective thermal conductivity due to exchanging the filling gas as a linear dependency with one constant slope. Moreover, the newly founded dependency agrees with the results introduced by the study of Abid, 2010. The curve, which described the change of effective thermal conductivity with the thermal conductivity of the filling gas, shows a tendency in high gas thermal conductivity to build up a kind of plateau. This can be physically interpreted as a saturation effect. This is strongly dependent on the ratio of gas to solid conductions. This curve differs for Knudsen materials when the referred values of the filling gas are evaluated taking the Knudsen effect into account.
- **The Pore Size Impact:** The investigated materials have different porous structures that are characterized in a wide or narrow range of pore size distribution. This includes specific pores that sized in macro (bigger than 7 µm), micro (70 nm - 7000 nm) and nano (smaller than 70 nm) ranges. This allows detecting clearly the coupling factor between the Knudsen conduction and the effect of exchanging the filling gas. This coupling is obvious when the exchange of the filling gas by a lower thermal conductivity gas in nano-materials does not give a noticeable decrease in the effective thermal conductivity of the materials. That could be noticed for the Knudsen materials.
- **The Effect on Radiative Heat Transfer**: In the scope of this work, another coupling effect is also analyzed. This is concerned with the coupled Knudsen conduction and radiation effects. In the Knudsen conduction, the dependency on temperature is the inverse of that of free gas conduction. The radiation effect becomes more significant in the high temperature range and overcomes the filling gas effect. That means the effective thermal conductivity of Knudsen materials is independent of the filling gas in the high temperature range. In other words, in such Knudsen materials the chosen filling gas and the pore size distribution effect the temperature dependency of the effective thermal conductivity. For example, effective thermal conductivity of a Knudsen material filled with krypton is increased gradually with raising the temperature, whereas filling the same materials with helium shows constant values for effective thermal conductivity over different temperatures, which implies completely different trend than that of krypton. Through the determination of the true thermal conductivity of the material, the radiation effect arising from exchanging the filling gas has been eliminated. Thus, the change in true thermal conductivity when exchanging the filling gas is caused only by the pure change in gas conduction in the pores.

- **Non-Knudsen Materials:** For the investigated non-Knudsen materials with pore size is in the macro range, many models from literature could predict successfully the change in effective thermal conductivity due to exchanging the filling gas based on the data of the bulk gas thermal conductivity. These models fail by the other two investigated groups of materials i.e. near Knudsen- and Knudsen-materials. Even when the gas thermal conductivity is corrected with respect to the Knudsen effect using a single pore model, because a single pore size does not describe the entire porous structure
- **The new predictive model:** The new predictive model that is presented in this work includes different effects: the pore size distribution, the accommodation coefficient, the radiation effects and any coupling effects. The model illustrates the pore-size distribution effect on the effective thermal conductivity, and based on the kind of cumulative distribution function, the change in the effective thermal conductivity due to exchanging the gas atmosphere is well estimated.
- **Accommodation Coefficient Problems**: One of the most noteworthy issues to consider is the accommodation coefficient. The results show that the effect of the accommodation coefficient increases in the micro- and nano-materials. The lack of experimental data for the accommodation coefficient for the investigated materials imposes large problems for independent comparisons between predicted and measured data.

In modeling of the effective thermal conductivity, more analyses have to be carried out regarding the coupling effect between the gas and solid phases. The investigated porous media consist of different solid materials, thus inter-comparison between the results of the materials in the light of the Knudsen effect should take into account the difference in the solid conduction. More recommendations and plans for future work will be outlined in the next section.

10.3 Conclusions from Tests:

This study has yielded an improved knowledge about the limitations of several test methods when these are applied to porous insulation materials. This knowledge could be summarized by the following conclusions:

- **Pore Size Distribution Tests:** Mercury intrusion porosimetry is a standard method to characterize the pore size distribution of different porous materials. However, applying it to some insulation materials with porous structure that does not have enough resistance to withstand the applied pressure of mercury, e.g. fibrous materials, leads to unreliable data of the measurement and in some cases to the destruction of the inner porous structure. Another limitation to consider is the simplicity of the evaluation model in this method, which considers the pores as spheres, whereas observation of the images of the investigated materials done by the electron microscope shows a more complex porous structure.
- **Radial Heat Flowmeter Apparatus:** Evaluation of the effective thermal conductivity, which was measured in a radial heat flow inward apparatus with a limited narrow mean temperature range, 300 °C to 700 C. This is due to two reasons: the first is the low sensibility of the calorimeter system of the RHFA in the low temperature range, and the second reason is the emerged large temperature difference in the radial

direction of the sample. Heat transfer through radiation dominates in such high temperature differences, which makes the coupling effect with gas conduction more significant. This enhances additionally the transmission part of the radiation, which affects the measurement of the temperature through the thermocouples. Here also the radiative properties of the cylindrical contact surfaces of the sample play an important role. Hence, evaluation of the change in effective thermal conductivity due to the pure effect of exchanging the filling gas included errors with regards to the coupling effect with radiation, even for evaluation based on the true thermal conductivity instead of the effective values. Further correction should be performed to achieve better elimination of the radiation effect.

- **Laser Flash Thermal Diffusivity Method:** Preparation of the samples with surface coating allows applying the laser flash method to some of the investigated porous materials. The spraying of graphite was found to be the best method for the surface coating. However, this was successful with only four materials among twelve investigated porous materials. The samples become transparent in the high temperature range in addition to high fluctuation of the results in this range. The laser flash method is, as known, a transient method and the porous media consist of two phases: on one hand the solid matrix is characterized through relatively high thermal conductivity, on others hand the filling gas has much lower thermal conductivity. This difference between the two phases is not included in the developed evaluation model of laser flash method. That indicates that more investigations are required in this area of research.

10.4 Future Work

The goals of future work in this area of research is to perform an experimental comparison between the materials over an extended temperature range and to develop a method to evaluate the contribution of the radiation coupled to the Knudsen effect in the various gas atmospheres, as well as to estimate the coupling effect of the gas\solid conduction. Additionally, it should aim to develop a benchmark-test- apparatus taking the Knudsen effect into account.

10.4.1 New Guarded Hot Plate Apparatus for Knudsen Effect Investigation

The Knudsen effect has been investigated in this study first through choosing materials with pore size characterized in the nano range, second by exchanging the filling gas, and finally in partial form through performing some measurements of thermal diffusivity under constant vacuum atmosphere. In order to investigate the Knudsen effect on porous material under different levels in vacuum and at high gas pressure as well as in various gas atmospheres, a new guarded hot plate has been developed at the Institute of Thermal Engineering, TU Freiberg, Germany. Choosing the guarded hot plate method as a measurement principle is based on the many advantages of this method comparing to the used radial heat flowmeter. These are: the simplicity in preparation of samples, the accuracy in determining the thickness of the sample as well as the position of the thermocouples, the heat flux being evaluated through measuring the applied electrical power, and the better control over the edge heat losses. Developing the guarded hot plate method for use in extreme surrounding conditions, i.e. at temperatures up to 1000 °C and in gas pressure from 10^{-6} to 100 bar, was accompanied with many difficulties, see the sketch of the new guarded hot plate in Figure 83.

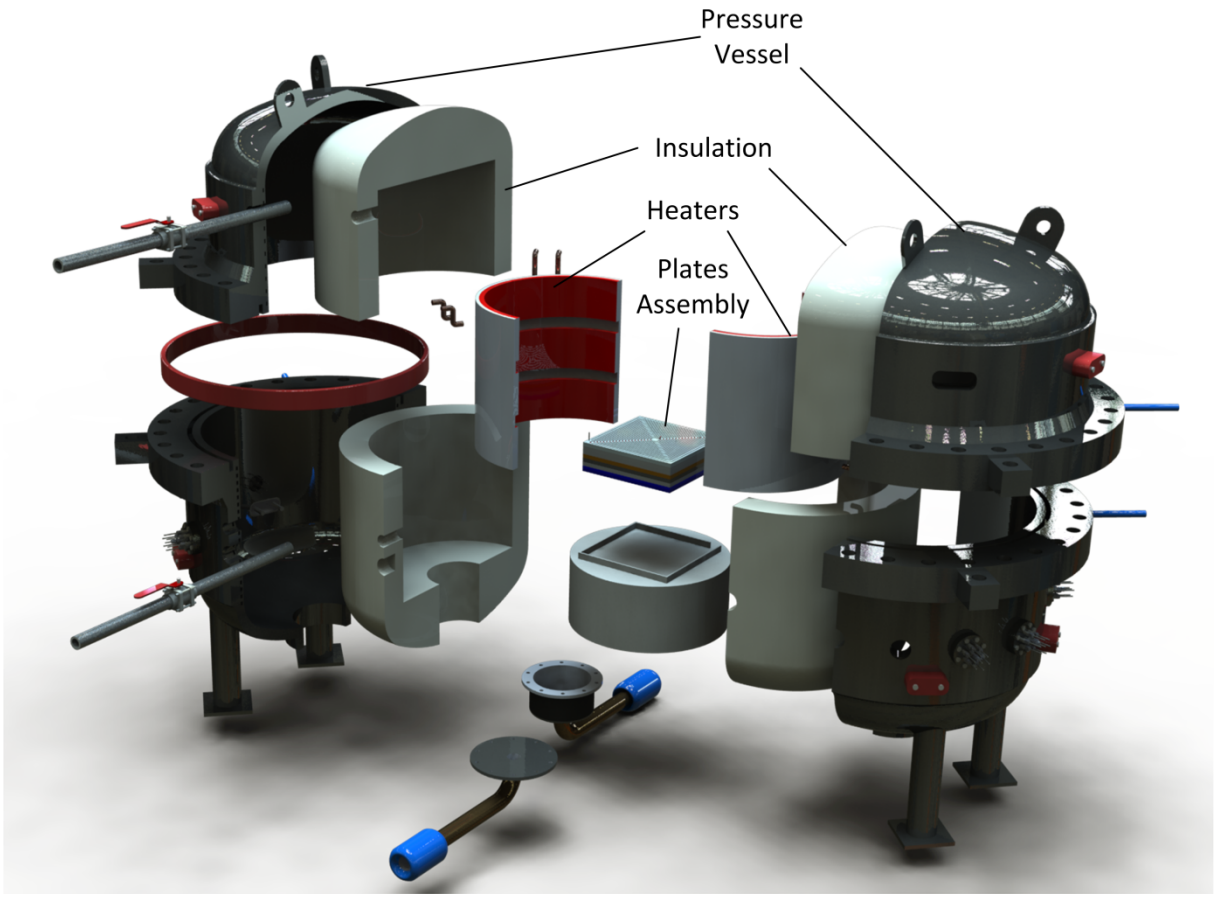

Figure 83: Sketch of the new guarded hot plate developed by K. Raed at Institute of Thermal Engineering, TU Freiberg, Germany

Overcoming these difficulties took more than four years of intensive experimental work and many discussions. Thus, it would take a large part of thesis to present the solutions which is out of the scope of this work. The overall specifications of the new guarded hot plate are listed in Table XXV. The aim after introducing the new apparatus is to show that further experimental investigations are in progress in order to complement the present study about Knudsen effect and effect of the filling gas by considering the pressure effect, which implies a wide change in Knudsen numbers.

Table XXV: Specifications of the new guarded hot plate

Principle	Guarded Hot plate (steady state method)
Specimen geometry	Square 300 X 300 mm
Specimen thickness	15 … 30 mm
Metering section	Ø 130 mm
Range of measurement	0.001 $Wm^{-1}K^{-1}$ – 1 $Wm^{-1}K^{-1}$
Range of temperatures	Room temperature – 1000 °C
Gas pressure	10^{-6}- 100 bar
Gas atmospheres	Air, N_2 and noble gases (Kr, Ar, He)
Uncertainty [10]	approx. 5 % @ 800 °C

[10] Estimated regards to GUM by the first measurements under normal pressure

The new apparatus will be also helpful in validating the experimental results that emerged through the present study. The new apparatus has a controlled hot plate that works from room temperature to 1000 °C, and an additional hot plate on the cold side of the sample to keep the temperature difference over the sample small. These specifications are necessary in order to extend the experimental investigations over the new temperature range.

10.4.2 Recommendations for Further Research

In summary, many coupling effects that play an important role in estimating the effect of the filling gas combined with the Knudsen effect are detected in this study. In this section, various recommendations and plans for further research in this area in order to estimate these coupling effects will be presented in the following points:

- **Uniformity of Solid Conduction:**
  The significance of Knudsen effect and the effect of exchanging the filling gas can be clearly seen and evaluated for different kinds of pore size distribution when they all consist of the same solid material. There are already some experiments in the literature to produce such insulation materials with various pore size distributions, for example through sol-gel process obtaining aerogel based on various narrow pore size distributions, see Ru, et al., 2010. Another example is producing fibrous material based on different fiber diameters, which leads to varying the pore size distribution, see Rutledge, et al., 2009.

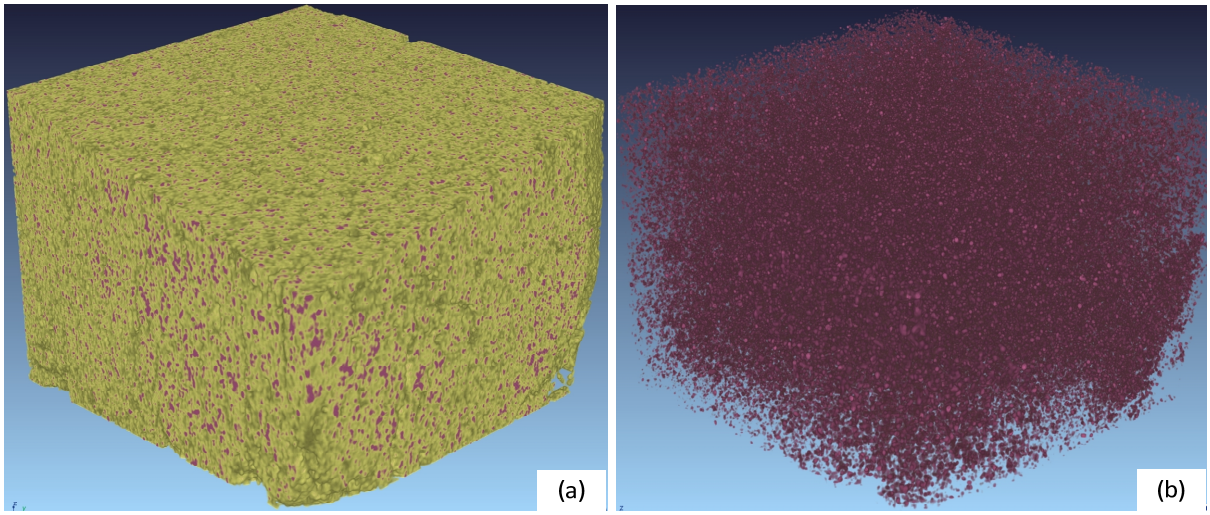

Figure 84: CT-Scan data of one of the investigated materials; (a) representation of two phases: solid and gas (b) representation of the gas that is filled in the solid porous structure

- **Numerical Modeling using the Nano Structure of Insulation Materials :**
  As previously seen, the temperature distribution in the porous media is related to the kind of the filling gas. An exact modeling of the porous structure of such nano- sized porous materials allows to estimate the coupling effect between radiation and Knudsen conduction as well as to predict precisely the effective thermal conductivity through the best arrangement model between solid and gas conduction. Computer tomography, abbreviated as CT, is a commonly used method to produce tomographic

images of the solid matrix, e.g. metallic foam. The image in Figure 84shows the results of CT- data for one of the investigated materials. It can be seen that it is possible to present, with help of evaluation software, the exact distribution between solid and gas phases. However, previous experiments in this field show that CT, even with the highest resolution, is not able to demonstrate insulation materials with nano- sized pores because the contrast between the solid and filling gas in such materials is small. A new idea for further research is to inject a low melting temperature metal into the porous structure. This process would lead to increasing the contrast and improve the performance of CT-scan. The final geometry of the nano- structure emerges through successful CT-scanning data. The obtained geometry is applied to the numerical-modeling of heat transfer process, e.g. applying the Lattice-Boltzmann method

- **Gas Diffusion as a Possible Heat Transfer Mechanism**
  The effective thermal conductivity of the investigated materials is analyzed with respect to the conduction and radiation. The studied porous structures are open pore systems; therefore it is possible due to the large temperature difference over the sample that a drop of pressure emerges. The latter leads to gas diffusion in the direction of the pressure drop. In this case, the heat flux caused by diffusion should be consider and excluded from the total heat flux. This diffusion process depends also on the kind of pore size distribution.

Finally, in spite of the above reported limitations about the experimental facility and the unaccounted factors that affect the measurements, this study outlines complete investigations about the effect of the filling gas with regards to the Knudsen effect on the effective thermal conductivity of widely different porous insulation materials. In the present study, the new improved model that is based on known porous structures could be applied in industry to predict the change in effective thermal conductivity when exchanging the filling gas. The presented different coupling effects are taken into account by applying the Exponential Correction Coupling Parameter in that new prediction model. A new development in producing such insulation materials can be achieved through considering the Knudsen effect with respect to the kind of pore size distribution. Implementation of the above presented recommendations in future research will complement this study and extend it to involve new effects, such as the effect of gas pressure. The newly introduced parameters, definitions and analyzed effects in this study could be considered as a roadmap for further research in this area.

LIST OF SYMBOLS

Roman Letters:

a	mm^2 / s	Thermal diffusivity
$a_R(\Lambda)$	m^{-1}	Rosseland mean extinction coefficient
a, b, c		Coefficients in true thermal conductivity see eq. (51)
A, B, C		Constants in Martin's equation eq.(42)
A_{abs}	m²	Absorption cross-section
b_{struc}		Coefficient dependent on structural elements eq.(24)
C		Constant /Coefficient
C_p	J/kgK	Specific heat of at constant pressure
$C_{p,w}$	J/kgK	Specific heat of water
C_v	J/kg K	Specific heat at constant volume
d	m	Pore size/diameter
d_{freq}	m	Most frequent pore size
d_m	m	Diameter of gas molecule
d_{max}	m	Maximal pore size
d_{mean}	m	Mean pore size
d_{min}	m	Minimal pore size
d_{mp}	m	Most probable pore size
$d_{x,x-1}$	m	Pore sizes at different ranges
Da	-	Darcy-number
e	W/m²	Total hemispherical emissive power
E_Λ	m^{-1}	Real extinction coefficient
E_i	W	Energy of incident gas molecules
E_r	W	Energy of reflected molecules
E_{su}	W	Energy of reflected molecules within thermal
$g_{1,2}$	m	Temperature jump distance
Gr		Grashof-number
h	m	thickness
$\mathrm{I}_\Lambda(0)$		Initial intensity of spectral radiation
$\mathrm{I}_\Lambda(S)$		Intensity of spectral radiation at length S
Kn	-	Knudsen-number
$l\ or\ L$	m	Length/Distance
m_g	kg	Mass of one gas molecule
m_s	kg	Mass of solid atoms/molecules
M	kg/mol	Molar weight
n	molecules/m^3	Density of molecules
Nu	-	Nusselt-number
p	Pa	Pressure
p_0	Pa	Pressure at standard reference conditions
P_e	W	Electrical power
Pr	-	Prandtl-number

$\dot{q}$	W/m²	Heat flux
$\dot{Q}$	W	Heat flow
$\dot{q}_{conv}$	W/m²	Heat flux through convection
$\dot{q}_g$	W/m²	Heat flux through gas
$\dot{q}_{rad}$	W/m²	Heat flux through radiation
$\dot{q}_s$	W/m²	Heat flux through the solid matrix in porous media
r_1	m	Radius at position 1
r_2	m	Radius at position 2
r_a	m	Outer radius
r_i	m	Inner radius
R	kJ/kgK	General gas constant
Ra		Rayleigh-number
S_s	m²	Specific surface area of porous media
S	m	Thickness of specimen
T	K	Absolute temperature
t	°C	temperature
$t_{1/2}$	s	Half time value in laser flash method
$T_{W_{in}}$	K	Temperature of inlet water flow
$T_{W_{out}}$	K	Temperature of outlet water flow
T_0	K	Temperature at standard reference conditions
ΔT	K	Temperature difference
ΔT_∞	K	Maximum Temperature rise in laser flash method
$\dot{V}$	m³/s	Flow rate
V_i	%	Percentage of Intruded Volume of pores with size i
V_{por}	m³	Volume of pore
V_{pores}	m³	Volume of all pores
V_{total}	m³	Total volume of porous media
W	-	Slope of gas thermal conductivity model eq.(43)
Y	-	Exponential constant in Zeng's model eq. (37)
Z	m	Direction/coordinate
Z_f		alignment factor of fiber

Greek letters:

α	-	Thermal accommodation coefficient
β		Gas constant in Kaganer's model eq.(27)
ρ_{bulk}	kg/m³	Bulk density of porous media
ρ_{por}	kg/m³	Density of gas in pore
ρ_s	kg/m³	Density of solid material pore-free
$\kappa_\Lambda(S)$	-	Optical thickness or opacity of material
Λ	m	Mean free path
Λ_0	m	Mean free path in continuum regime
$\Lambda_0{}^* \; or \; \Lambda_{mod}$	m	Modified mean free path
λ	W/mK	Thermal conductivity
λ_0	W/mK	Thermal conductivity of gas at standard reference
λ_{Kn}	W/mK	Knudsen thermal conductivity at microscopic ranges

$\lambda_{bulk,solid}$	W/mK	Thermal conductivity of bulk material
λ_{bulk}	W/mK	Bulk gas thermal conductivity
λ_{conv}	W/mK	Thermal conductivity due to convection
$\bar{\lambda}_{eff}$	W/mK	Mean Thermal conductivity
λ_{evac}	W/mK	Thermal conductivity of gas at lower pressure
λ_{gas}	W/mK	Thermal conductivity of gas
λ_{gas-P}	W/mK	Thermal conductivity of gas in pores
$\lambda_{gas-gap}$	W/mK	Thermal conductivity of gas in gap
λ_{rad}	W/mK	Thermal conductivity due to radiation
λ_s	W/mK	Thermal conductivity of solid matrix
$\sigma_{1,2,3}$		Coefficients dependent on Knudsen-number regards
Γ	m²	Collision cross section
ε	-	Proportional constant in Eucken's equation
ζ	-	Exponential correction coupling coefficient
Θ	°	Contact angle between mercury and solid
μ	-	Ratio of mass of gas to solid
ρ	kg/m³	Density
ρ_w	kg/m³	Density of water
γ	-	Ratio of specific heat at constant pressure and volume
γ_{ten}	dyn/cm	Surface tension of mercury
η	Pa s	Dynamic viscosity of gas
φ		Constant in Praslov's model eq. (34) depending on Kn
$\bar{v}$	m/s	Mean speed of gas molecules
χ		Constant in Praslov's model eq. (34) depending on Kn
χ_{Kn}	-	Knudsen-Raed ratio
χ_{cont}		Coefficient dependent on contact resistance
χ_{geo}		Coefficient dependent on geometry of insulation
ψ *or* Ψ	%	Porosity

Indexes

Ch	characteristic
bulk	Bulk
s	solid
eff	Effective
por	Pore / Porous
true	True/real value
i	Index of sum function
Kn	Knudsen

Constants

Avogadro constant	$N_A = 6.022 \times 10^{23}$ mol^{-1}
Stefan-Boltzmann-constant	$\sigma = 5.67 \times 10^{-8}$ W m^{-2} K^4
Boltzmann-constant	$k = 1.38 \times 10^{-23}$ J K^{-1}

LIST OF ABBREVIATIONS

aka	also known as
ASTM	American Standard for Testing and Materials
CDF	Cumulative Distribution Function
DSC	Differential Scanning Calorimeter
ECCP	Exponential Correction Coupling Parameter
eq.	Equation
FEM	Finite Element Method
FTIR	Fourier Transform Infra Red
GHPA	Guarded Hot Plate Apparatus
IKGB	department of Ceramic, Glass, and Construction Materials, TU Freiberg,
LFA	Laser Flash Apparatus
LFM	Laser Flash Method
MIP	Mercury Intrusion Porosimetry
PSD	Pore-Size Distribution
PTF	Panel Test Facility
RHFA	Radial Heat Flowmeter Apparatus
RHFM	Radial Heat Flowmeter Method
SEM	Scanning Electron Microscope

LIST OF FIGURES

LIST OF TABLES

REFERENCE LIST

ABELL, A. B., WILLIS, K. L., LANGE, D. A., 1999. **MERCURY INTRUSION POROSIMETRY AND IMAGE ANALYSIS OF CEMENT-BASED MATERIALS.** JOURNAL OF COLLOID AND INTERFACE SCIENCE, 39-44

ABERDEEN, J. AND LABY, T. H., 1926. **CONDUCTION OF HEAT THROUGH POWDERS AND ITS DEPENDENCE ON THE PRESSURE AND CONDUCTIVITY OF GASEOUS PHASE**, 459-477

ABID, MUHAMMAD, 2011. **THERMOPHYSICAL PROPERTIES OF A MOIST POROUS MATERIAL**, THESIS, TECHNISCHE UNIVERSITÄT BRAUNSCHWEIG, GERMANY

ASTM 2009, **STANDARD PRACTICE FOR DETERMINATION OF THERMAL RESISTANCE OF ATTIC INSULATION SYSTEMS UNDER SIMULATED WINTER CONDITIONS**, ANNUAL BOOK OF ASTM STANDERS 2009, 788-795

ASTM C177-10, 2010, **STANDARD TEST METHOD FOR STEADY-STATE HEAT FLUX MEASUREMENTS AND THERMAL TRANSMISSION PROPERTIES BY MEANS OF THE GUARDED-HOT-PLATE APPARATUS**

ASTM C201-93, 2009, **STANDART TEST METHOD FOR THERMAL CONDUCTIVITY OF REFRACTORY BRICK**

ASTM C335, 2003, **STANDARD TEST METHOD FOR STEADY-STATE HEAT TRANSFER PROPERTIES OF PIPE INSULATION**

ASTM C1045-07, 2007, **STANDARD PRACTICE FOR CALCULATING THERMAL TRANSMISSION PROPERTIES UNDER STEADY-STATE CONDITIONS**

ASTM D3766, 2008, **STANDARD TERMINOLOGY RELATING TO CATALYSTS AND CATALYSIS**

ASTM D5004, 2009, **STANDARD TEST METHOD FOR REAL DENSITY OF CALCINED PETROLEUM COKE BY XYLENE DISPLACEMENT**

ASTM E 1461, 2007, **STANDARD TEST METHOD FOR THERMAL DIFFUSIVITY BY THE FLASH METHOD**

BAKER, J., CALVERT, M. E., POWER, D. J., CHEN, E. T., RAMALINGAM, M. L., LAMP, T. R, 1996, **ON THE ROLE OF THE KNUDSEN NUMBER WITH RESPECT TO HEAT TRANSFER IN MICRO-SCALE FLOWS,** PROCEEDINGS OF THE 31ST INTERSOCIETY, ENERGY CONVERSION ENGINEERING CONFERENCE, 1396-1401

BALA, KANAN, PRADHAN, PRADEEP R., SAXENA, N. S., SAKSENA, M. P., 1990. **EFFECT OF MEDIUM ON THE EFFECTIVE THERMAL CONDUCTIVITY OF A MACROPOROUS SOLID**, JOURNAL OF PHYSICS D: APPLIED PHYSICS, 748-750

BAULE, B., 1914. **THEORETISCHE BEHANDLUNG DER ERSCHEINUNGEN IN VERDUENNTEN GASEN**, ANN.PHYSIK, 145-176

BLUMM, J. AND OPFERMANN, J., 2002. **IMPROVEMENT OF THE MATHEMATICAL MODELING OF FLASH MEASUREMENTS**, HIGH TEMPERATURES - HIGH PRESSURES, 515-521

BONDARENKO, S. L., LITOVSKY, E. YA., ZVEREVA, M. N., POLONSKII, YU. A., 1989. **EFFECT OF DIFFERENT FACTORS ON THE THERMAL CONDUCTIVITY AND DIFFUSIVITY OF FIBROUS SILICA-BEARING THERMAL INSULATION**, HIGH TEMPERATURE, 864-868

BÜTTNER, D., CAPS, R., HEINEMANN, U., HÜMMER, E., KADUR, A., AND FRICKE, J., 1988, **THERMAL LOSS COEFFICIENT OF LOW-DENSITY SILICA AEROGELS TILES**, 40 SOLAR ENERGY

CAPE, J. A. AND LEHMAN, G. W., 1963. **TEMPERATURE AND FINITE PULSE-TIME EFFECTS IN THE FLASH METHOD FOR MEASURING THERMAL DIFFUSIVITY**, JOURNAL OF APPLIED PHYSICS, 1909-1913

CAPS, R. AND FRICKE, J., 2000, **THERMAL CONDUCTIVITY OF OPACIFIED POWDER FILLER MATERIALS FOR VACUUM INSULATION.** INT.J.OF THERMOPHYSICS, 445-452

CAPS, R. AND FRICKE, J., 2000B. **THERMAL CONDUCTIVITY OF OPACIFIED POWDER FILLER MATERIALS FOR VACUUM INSULATIONS**. INTERNATIONAL JOURNAL OF THERMOPHYSICS, 445-452

CAPS, R., HEINEMANN, U., FRICKE, J., 1997. **THERMAL CONDUCTIVITY OF POLYIMIDE FOAMS**. INTERNATIONAL JOURNAL OF HEAT AND MASS TRANSFER 40: 269-280

CERCIGNANI, C, 2000, **RAREFIED GAS DYNAMICS FROM BASIC CONCEPTS TO ACTUAL CALCULATIONS,** CAMBRIDGE UNIVERSITY PRESS, CAMBRIDGE, USA

CHAURASIA, P. B. LAL, CHAUDHARY, D. R, BHANDARI, R. C, 1978, **EFFECTIVE THERMAL CONDUCTIVITY TO TOW -PHASE SYSTEM,** INDIAN J. OF PURE & APPLIED PHYSICS, 963-967

COQUARD, R., ROCHAIS, D., BAILLIS, D., 2009, **EXPERIMENTAL INVESTIGATIONS OF THE COUPLED CONDUCTIVE AND RADIATIVE HEAT TRANSFER IN METALLIC/CERAMIC FOAMS**, INTERNATIONAL JOURNAL OF HEAT AND MASS TRANSFER, 4907-4918

CORRUCCINI, R. J, 1959, **GASEOUS HEAT CONDUCTION AT LOW PRESSURES AND TEMPERATURES.** VACUUM, 19-29

COWAN, R. D., 1963, **PULSE METHOD OF MEASURING THERMAL DIFFUSIVITY AT HIGH TEMPERATURES**, J. APPL. PHYS. 34:976-977

CUNNINGTON, G. R AND TIEN, C. L, 1977, **HEAT TRANSFER IN MICROSPHERE INSULATION IN THE PRESSURE OF A GAS.** INTERNATIONAL CONFERENCE ON THERMAL CONDUCTIVITY, OTTAWA, 325-333

DABROWSKI, A., ROBENS, E., KLOBES, P., MEYER, K., PODKOCIELNY, P., 2003. **STANDARDIZATION OF METHODS FOR CHARACTERIZING THE SURFACE GEOMETRY OF SOLIDS**, PARTICLE AND PARTICLE SYSTEMS CHARACTERIZATION, 311-322

DARYABEIGI, K., 1999, **ANALYSIS AND TESTING OF HIGH TEMPERATURE FIBROUS INSULATION FOR REUSABLE LAUNCH VEHICLES** , 37TH AIAA AEROSPACE SCIENCES MEETING AND EXHIBIT, RENO, NV

DARYABEIGI, K., 2003, **HEAT TRANSFER IN HIGH-TEMPERATURE FIBROUS INSULATION**. JOURNAL OF THERMOPHYSICS AND HEAT TRANSFER, 10-20

DEISSLER, R. G AND EIAN, C. S, 1952, **INVESTIGATION OF EFFECTIVE THERMAL CONDUCTIVITIES OF POWDERS; NATIONAL ADVISORY COMMITTEE FOR AERONAUTICS REPORT**, REPORT NACA-RM E52CC15.

DEMIREL, Y. AND SAXENA, S. C., 1996, **HEAT TRANSFER IN RAREFIED GAS AT A GAS-SOLID INTERFACE,** ENERGY, 99-103

DENPOH, K., 1998, **MODELING OF RAREFIED GAS HEAT CONDUCTION BETWEEN WAFER AND SUSCEPTOR,** IEEE TRANSACTIONS ON SEMICONDUCTOR MANUFACTURING, 25-29

DIAMOND, S., 2000, **MERCURY POROSIMETRY, AN INAPPROPRIATE METHOD FOR THE MEASUREMENT OF PORE SIZE DISTRIBUTIONS IN CEMENT-BASED MATERIALS**, CEMENT AND CONCRETE RESEARCH, 1517-1525

DIN EN 821-2, 1997, **ADVANCED TECHNICAL CERAMICS- MONOLITHIC CERAMICS- THERMO PHYSICAL PROPERTIES- PART 2: DETERMINATION OF THERMAL DIFFUSIVITY BY THE LASER FLASH METHOD, DEUTSCHE NORM**

DIN EN 993-1, 1995, **PRÜFVERFAHREN FÜR DICHTE GEFORMTE FEUERFESTE ERZEUGNISSE, DEUTSCHE NORM**

DIN EN 12664, 2001, **BESTIMMUNG DES WÄRMEDURCHLASSWIDERSTANDES NACH DEM VERFAHREN MIT DEM PLATTENGERÄT UND DEM WÄRMESTROMMESSPLATTEN-GERÄT, DEUTSCHE NORM**

DOERMANN, D. AND SACADURA, J. F., 1996, **HEAT TRANSFER IN OPEN CELL FOAM INSULATION**, JOURNAL OF HEAT TRANSFER, 88-93

DYBBS, A. AND SPRINGER, G. A., 1965, **HEAT CONDUCTION EXPERIMENTS IN RAREFIED GASES BETWEEN CONCENTRIC CYLINDERS.** THE PHYSICS OF FLUIDS, 1946-1950

ELLISON, A. H., KLEMM, R. B., SCHWARTZ, A. M., GRUBB, L. S., PETRASH, D. A., 1967, **CONTACT ANGLES OF MERCURY ON VARIOUS SURFACES AND THE EFFECT OF TEMPERATURE**, JOURNAL OF CHEMICAL AND ENGINEERING, 607-609

FEDINA, I., LITOVSKY, E., SHAPIRO, M., SHAVIT, A., 1997, **THERMAL CONDUCTIVITY OF PACKED BEDS OF REFRACTORY PARTICLES: EXPERIMENTAL RESULTS**. JOURNAL OF THE AMERICAN CERAMIC SOCIETY, 2100-2108

FINE, H. A., JURY, S. H., YARBROUGH, D. W., MCELROY, D. L., 1980, **ANALYSIS OF HEAT TRANSFER IN BULDING THERMAL INSULATION**, OAK RIDGE NATIONAL LABORATORY REPORT NUMBER ORNL/TM-748

FOURNIER, D. AND KLARSFELD, S., 1974, **SOME RECENT EXPERIMENTAL DATA ON GLASS FIBER INSULATING MATERIALS AND THEIR USE FOR A RELIABLE DESIGN OF INSULATIONS AT LOW TEMPERATURES**, HEAT TRANSMISSION MEASUREMENTS IN THERMAL INSULATIONS, ASTM AMERICAN SOCIETY FOR TESTING AND MATERIALS, 223-242

FRICKE, J., 1992, **ENTWICKLUNG VON WÄRMEDÄMMSTOFFEN UND -SYSTEMEN**, VDI BERICHTE 944:103-115

FRICKE, J. AND CAPS, R., 1988, **HEAT TRANSFER IN THERMAL INSULATIONS - RECENT PROGRESS IN ANALYSIS**, INTERNATIONAL JOURNAL OF THERMOPHYSICS, 885-895

FRICKE, J., LU, X., WANG, P., BÜTTNER, D., HEINEMANN, U., 1991, **OPTIMIZATION OF MONOLITHIC SILICA AEROGEL INSULANTS**, INTERNATIONAL JOURNAL OF HEAT AND MASS TRANSFER 35:2305-2309

FRICKE, J., LU, X., WANG, P., BÜTTNER, D., HEINEMANN, U., 1992, **OPTIMIZATION OF MONOLITHIC SILICA AEROGEL INSULANTS**. INT. J .HEAT MASS TRANSFER, 2305-2309

FRICKE, J., SCHWAB, H., HEINEMANN, U., 2006, **VACUUM INSULATION PANELS - EXCITING THERMAL PROPERTIES AND MOST CHALLENGING APPLICATIONS**, INTERNATIONAL JOURNAL OF THERMOPHYSICS, 1123-1139

FROHN, A AND ANDERS, K, 2002, **WÄRMEÜBERTRAGUNG UND STRÖMUNG IN VERDÜNNTEN GASEN.** 9, VDI WÄRMEATLAS, KAP. MO.

GLICKSMAN, L. R., 1994, **LOW DENSITY CELLULAR PLASTICS,** EDIT BY HILYARAD, N. C. AND CUNNINGHAM, A. CHAPMAN & HALL, LONDON.

GODFREY, T. G., FLUKERSON, W., KOLLIE, T. G., MOORE, J. P., MCELROY, D. L., 1965, **THERMAL CONDUCTIVITY OF URANIUM DIOXIDE FROM -57° TO 1100° C BY A RADIAL HEAT FLOW TECHNIQUE**, JOURNAL OF THE AMERICAN CERAMIC SOCIETY, 207-305

GOMBOSI, T. I, 1994, **GASKINETIC THEORY,** CAMBRIDGE UNIVERSITY PRESS, CAMBRIDGE UK

GOODMAN, F. O., 1968, **CLASSICAL PERTURBATION THEORY OF THE THERMAL ACCOMMODATION COEFFICIENT IN N DIMENSIONS**, SURFACE SCIENCE, 283-316

GOODMAN, F. O., 1980, **THERMAL ACCOMMODATION COEFFICIENTS**, THE JOURNAL OF PHYSICAL CHEMISTRY, 1431-1445

GOODMAN, F. O. AND WACHMAN, H. Y., 1967, **FORMULA FOR THERMAL ACCOMMODATION COEFFICIENTS**, THE JOURNAL OF CHEMICAL PHYSICS, 2376-2386

GOODMAN, O. AND WACHMAN, Y., 1974, **RESTRICTIONS ON THE VALUES OF ENERGY ACCOMMODATION COEFFICIENTS**, SURFACE SCIENCE, 306-308

GORRING, R. L. AND CHRUCHILL, S. W., 1961, **THERMAL CONDUCTIVITY OF HETEROGENEOUS MATERIALS**, CHEMICAL ENGINEERING PROGRESS, 53-59

GÖTZE, P., SKIBINA, V., WULF, R., EMMEL, M., GROSS, U., ANEZIRIS, C., 2012, **DETERMINATION OF EFFECTIVE THERMAL CONDUCTIVITY OF OPEN-CELL FOAM CERAMICS**, INTERNATIONAL SYMPOSIUM ON CERAMIC MATERIALS AND COMPONENTS FOR ENERGY AND ENVIRONMENTAL APPLICATIONS, DRESDEN, GERMANY

GRAVES, R. S., WILKES, K. E., MCELROY, D. L., 1993, **THERMAL RESISTNCE OF ATTIC LOOSE-FILL INSULATIONS DECREASES UNDER SIMULATED WINTER CONDITIONS,** THERMAL CONDUCTIVITY 22TH, ARIZONA, 215-226

GROCHAL, BRUNON J., 1995, **ENERGY TRANSPORT IN TWO-COMPONENT GAS-SOLID MATERIALS AT DECREASING GAS PRESSURE** , ADVANCES IN ENGINEERING HEAT TRANSFER, 277-286

GRUJICIC, M, ZHAO, C. L., BIGGERS, S. B., KENNEDY, M., MORGAN, D. R., 2005, **HEAT TRANSFER AND EFFECTIVE THERMAL CONDUCTIVITY ANALYSES IN CARBON- BASED FOAMS FOR USE IN THERMAL PROTECTION SYSTEM.** PROC. IMECHE VOL. 20 PART L: 1:14

GUSAROV, A. V. AND KOVALEV, E. P., 2009, **MODEL OF THERMAL CONDUCTIVITY IN POWDER BEDS**, PHYSICAL REVIEW B - CONDENSED MATTER AND MATERIALS PHYSICS 80:24202

HAHN, O., RAETHER, F., ARDUINI-SCHUSTER, M. C., FRICKE, J., 1997, **TRANSIENT COUPLED CONDUCTIVE/RADIATIVE HEAT TRANSFER IN ABSORBING, EMITTING AND SCATTERING MEDIA: APPLICATION TO LASER-FLASH MEASUREMENTS ON CERAMIC MATERIALS**, INTERNATIONAL JOURNAL OF HEAT AND MASS TRANSFER, 689-698

HAMAKER, H. C., 1947, **RADIATION AND HEAT CONDUCTION IN LIGHT SCATTERING MATERIALS**, PHILIPS RESEARCH REPORTS 2:55-67

HARDING, G. L AND WINDOW, B., 1981, **FREE MOLECULE THERMAL CONDUCTION IN CONCENTRIC TUBULAR SOLAR COLLECTORS,** SOLAR ENERGY MATERIALS, 265-278

HARPER, JOHN C. AND SAHRIGI, AHMED F. EL, 1964, **THERMAL CONDUCTIVITIES OF GAS-FILLED POROUS SOLIDS**, I & EC FUNDAMENTALS, 319-324

HEINEMANN, U., CAPS, R., FRICKE, J., 1996, **RADIATION-CONDUCTION INTERACTION: AN INVESTIGATION ON SILICA AEROGELS,** INT J HEAT MASS TRANSFER, 2115-2130

HOHENAUER, W. AND LAGER, D., 2010, **FLASH TECHNIQUES TO MEASURE THERMAL DIFFUSIVITY AND THERMAL CONDUCTIVITY OF METAL-FOAM-MATERIALS**, THERMAL CONDUCTIVITY 30TH/THERMAL EXPANSION 18TH, PITTSBURGH, PA, 513-520

ISO 8302, 1991, **THERMAL INSULATION- DETERMINATION OF STEADY-STATE THERMAL RESISTANCE AND RELATED PROPERTIES – GUARDED HOT PLATE APPARATUS**

KAGANER, M. G., 1969, **HEAT TRANSFER BY CONDUCTION IN INSULATION RADIATIVE HEAT TRANSFER IN INSULATION**, THERMAL INSULATIONS IN CRYOGENIC ENGINEERING, 3-47

KAMIUTO, K., MIYOSHI, Y., KINOSHITA, I., HASEGAWA, S., 1984, **COMBINED CONDUCTIVE AND RADIATIVE HEAT TRANSFER**, BULLETIN OF THE JSME, 1136-1143

KANNULUIK, W. G. AND MARTIN, L. H., 1933, **CONDUCTION OF HEAT IN POWDERS**, PROCEEDINGS OF THE ROYAL SOCIETY OF LONDON A141, 144-158

KAUFMANN, J., 2009, **CHARACTERIZATION OF PORE SPACE OF CEMENT-BASED MATERIALS BY COMBINED MERCURY AND WOOD'S METAL INTRUSION**, JOURNAL OF THE AMERICAN CERAMIC SOCIETY, 209-216

KAVIANY, M., 1995. **PRINCIPLES OF HEAT TRANSFER IN POROUS MEDIA**, SPRINGER, NEW YORK

KENNARD, E. H, 1938, **KINETIC THEORY OF GASES,** MCGRAW HILL, NEW YORK, 50-318

KISTLER, S. S, 1935, **THE RELATION BETWEEN HEAT CONDUCTIVITY AND STRUCTURE IN SILICA AEROGEL,** J. PHYSICAL CHEM, 39(1):79-86

KISTLER, S. S, 1941, **THE CALCULATION OF THE SURFACE AREA OF MICROPOROUS SOLIDS FROM MEASUREMENTS OF HEAT SOLID,** 18TH COLLOID SYMPOSIUM, 19-31

KISTLER, S. S., 1931, **COHERENT EXPANDED AEROGELS AND JELLIES**. NATURE, 741-744

KISTLER, S. S. AND CALDWELL, A. G, 1934, **THERMAL CONDUCTIVITY OF SILICA AEROGEL**, INDUSTRIAL AND ENGINEERING CHEMISTRY, 658-662

KLEIBER, M. AND JOH, R., 2006, **BERECHNUNGSMETHODEN FÜR STOFFEIGENSCHAFTEN**, VDI WÄRMEATLAS 10, KAPITAL DA-DC

KONDAPI, P. B., BOOTH, J. R., YARBROUGH, D. W., 2006, **THE LONG-TERM THERMAL PERFORMANCE FOAM HAVING NON-UNIFORM DENSITY** , THERMAL CONDUCTIVITY, DINWIDDIE, RALPH B., WHITE, MARY ANNE, AND MCELROY, D. L.,

KNUDSEN, M, 1911. **DIE MOLEKULARE WÄRMELEITUNG DER GASE UND DER AKKOMMODATIONSKOEFFIZIENT.** ANNALEN DER PHYSIK, 593-656

KNUDSEN, M, 1934, **THE KINETIC THEORY OF GASES**, METHUEN & CO, LTD, LONDON

KOGLIN, B., 1967, **DER WÄRMETRANSPORT IN SCHAUMSTOFFEN**, THESIS IN TU BERLIN, GERMANY

LAL CHAURASIA, P. B., CHAUDHARY, D. R., BHANDARI, R. C., 1978, **EFFECTIVE THERMAL CONDUCTIVITY OF TWO-PHASE SYSTEM**, INDIAN JOURNAL OF PURE AND APPLIED PHYSICS 16:963-967

LE DONNE, M., GORAIEB, A., PIAZZA, G., SORDON, G., 2000, **MEASUREMENTS OF THE EFFECTIVE THERMAL CONDUCTIVITY OF A LI4SIO4 PEBBLE BED**, FUSION ENGINEERING AND DESIGN, 513-519

LEE, DAEHEE, STEVENS, P. C., ZENG, S. Q., HUNT, ARLON J., 1995, **THERMAL CHARACTERIZATION OF CARBON-OPACIFIED SILICA AEROGELS**, JOURNAL OF NON-CRYSTALLINE SOLIDS, 285-290

LEE, OK-JOO, LEE, KUN-HONG, YIM, TAE JIN, KIM, SUN YOUNG, YOO, KI-PUNG, 2002, **DETERMINATION OF MESOPORE SIZE OF AEROGELS FROM THERMAL CONDUCTIVITY MEASUREMENTS**, JOURNAL OF NON-CRYSTALLINE SOLIDS, 287-292

LEE, OK-JOO, LEE, KUN-HONG, YIM, TAE JIN, KIM, SUN YOUNG, YOO, KI-PUNG, 2002, **DETERMINATION OF MESOPORE SIZE OF AEROGELS FROM THERMAL CONDUCTIVITY MEASUREMENTS**, JOURNAL OF NON-CRYSTALLINE SOLIDS, 287-292

LEE, S.-C. AND CUNNINGTON, G. R., 2000, **CONDUCTION AND RADIATION HEAT TRANSFER IN HIGH-POROSITY FIBER THERMAL INSULATION**, JOURNAL OF THERMOPHYSICS AND HEAT TRANSFER, 121-136

LINFORD, R. M. F., SCHMITT, R. J., AND HUGHES, T. A., 1974, **RADIATIVE CONTRIBUTION TO THE THERMAL CONDUCTIVITY OF FIBROUS INSULATIONS**, HEAT TRANSMISSION MEASUREMENTS IN THERMAL INSULATIONS, ASTM, 68-84

LITOVSKY, E. YA. AND SHAPIRO, M., 1992, **GAS PRESSURE AND TEMPERATURE DEPENDENCE OF THERMAL CONDUCTIVITY OF POROUS CERAMIC MATERIALS: PART 1, REFRACTORIES AND CERAMICS WITH POROSITY BELOW 30%**. J. AM. CERAM. SOC., 3425-3439

LITOVSKY, E AND SHAPIRO, M, 1996, **GAS AND TEMPERATURE DEPENDENCE OF THERMAL CONDUCTIVITY OF POROUS MATERIALS: PART 2, REFRACTORIES AND CERAMICS WITH POROSITY EXCEEDING 30%,** J. AM. CERAMICS SOC., 1366-1376

LITOVSKY, E., GAMBARYAN-ROISMAN, T., SHAPIRO, M., SHAVIT, A., 2001, **NOVEL HEAT-TRANSFER MECHANISMS AFFECTING THE THERMAL CONDUCTIVITY OF POROUS CERAMICS**, HIGH TEMPERATURES - HIGH PRESSURES, 27-33

LOEB, A., 1954, **THERMAL CONDUCTIVITY: A THEORY OF THE THERMAL CONDUCTIVITY OF POROUS MATERIALS**, JOURNAL OF THE AMERICAN CERAMIC SOCIETY, 96-99

LOEB, L. B, 1934. **THE KINETIC THEORY OF GASES** , MCGRAW-HILL, NEW YORK, 234-252

LU, X., ARDUINI-SCHUSTER, M. C., KUHN, J, NILSSON, O., FRICKE, J., PEKALA, R. W., 1992, **THERMAL CONDUCTIVITY OF MONOLITHIC ORGANIC AEROGELS.** SCIENCE, 971-972

LU, X., CAPS, R., FRICKE, J., ALVISO, C. T., PEKALA, R. W., 1995. **CORRELATION BETWEEN STRUCTURE AND THERMAL CONDUCTIVITY OF ORGANIC AEROGELS**. JOURNAL OF NON-CRYSTALLINE SOLIDS, 226-234

LU, X., WANG, P., RDUINI-SCHUSTER, M. C., KUHN, J., BÜTTNER, D., NILSSON, O., HEINEMANN, U., FRICKE, J., 1992, **THERMAL TRANSPORT IN ORGANIC AND OPACIFIED SILICA MONOLITHIC AEROGELS**, JOURNAL OF NON-CRYSTALLINE SOLIDS, 207-210

LUIKOV, A. V., SHASHKOV, A. G., VASILIEV, L. L., FRAIMAN, YU. E., 1968, **THERMAL CONDUCTIVITY OF POROUS SYSTEMS**, INTERNATIONAL JOURNAL OF HEAT AND MASS TRANSFER, 117-140

LUU, M., ALLMON, B. A., KNEIDEL, K. E., 1986A, **STUDY OF HEAT TRANSFER IN EVACUATED INSULATIONS AT VARIOUS GAS LOADINGS** , 8TH INTERNATIONAL HEAT CONFERENCE, SAN FRANCISCO, 709-714

MADHUSUDANA, C. V., 1996, **THERMAL CONTACT CONDUCTANCE**, SPRINGER, NEW YORK

MADZHIDOV, KH, ZUBAIDOV, S., SAFAROV, M. M., 1988, **THERMAL CONDUCTIVITY OF ALUMINUM OXIDE IN RELATION TO COBALT CONCENTRATION AND TEMPERATURE IN DIFFERENT GASEOUS MEDIA**, HIGH TEMPERATURE, 513-517

MAILLET, D., MOYNE, C., RÉMY, B., 2000, **EFFECT OF THIN LAYER ON THE MEASUREMENT OF THE THERMAL DIFFUSIVITY OF A MATERIAL BY A FLASH METHOD**, INT J HEAT MASS TRANSFER, 4057-4060

MARSCHALL, J. AND MILOS, F. S., 1997, **THE CALCULATION OF ANISOTROPIC EXTINCTION FOR RADIATION DIFFUSION IN RIGID FIBROUS CERAMIC INSULATIONS**, INT J HEAT MASS TRANSFER 40:627-634

MARTIN, HOLGER, 1980. **WÄRME- UND STOFFÜBERTRAGUNG IN DER WIRBELSCHICHT**. CHEM. ING. TECH., 199-209

MASON, RALPH B., 1933, **THERMAL INSULATION WITH ALUMINUM FOIL**, INDUSTRIAL AND ENGINEERING CHEMISTRY, 245-255

MCCOY, B. J AND CHA, C. Y, 1974, **TRANSPORT PHENOMENA IN THE RAREFIED GAS TRANSITION REGIME.** CHEMICAL ENGINEERING SCIENCE, 381-388

MEHLING, H., HAUTZINGER, G., NILSSON, O., FRICKE, J., HOFMANN, R., HAHN, O., 1998, **THERMAL DIFFUSIVITY OF SEMITRANSPARENT MATERIALS DETERMINED BY THE LASER-FLASH METHOD APPLYING A NEW ANALYTICAL MODEL,** INTERNATIONAL JOURNAL OF THERMOPHYSICS [19], 941-949

MEYER, K., LORENZ, P., RÖHL-KUHN, B., KLOBES, P., 1994, **POROUS SOLIDS AND THEIR CHARACTERIZATION**. CRYSTAL RESEARCH AND TECHNOLOGY, 903-930

MOORE, J. P, DIPPENAAR, R. J., HALL, R. O. A., AND MCELROY, D. L., 1982, **THERMAL CONDUCTIVITY OF POWDER WITH UO_2 OR ThO_2 MICROSPHERES IN VARIOUS GASES FROM 300 TO 1300 K**, ORNL REPORT/TM-8196, WWW.ORNL.GOV

MOORE, J. P., 1984, **ANALYSIS OF APPRATUS WITH RADIAL SYMMETRY FOR STEADY STATE MEASURMENTS OF THERMAL CONDUCTIVITY**, COMPENDIUM OF THERMOPHYSICAL PROPERTY MEASUREMENT METHODS, EDITORS: MAGLIC, K. D., CEZAILIYAN, A., AND PELETSKY, V. E., PLENUM PRESS, NEW YORK, 61-122

NEUBRONNER, M. AND BOECK, T., 2010, **PROPERTIES OF SOLIDS AND SOLID MATERIALS**, VDI- HEAT ATLAS 551-601

NEWMAN, C. R. AND FORCINITI, D., 2001, **MODELING THE ULTRAVIOLET PHOTODEGRADATION OF RIGID POLYURETHANE FOAMS**, INDUSTRIAL AND ENGINEERING CHEMISTRY RESEARCH, 3346-3352

OGNIEWICZ, Y. AND YOVANOVICH, M., 1977, **EFFECTIVE CONDUCTIVITY OF REGULARLY PACKED SPHERES: BASIC CELL MODEL WITH CONSTRICTION.** PRESENTED AT AIAA 15TH AEROSPACE SCIENCE MEETING, LOS ANGELES, USA

PANDE, P. N, SAXENA, N. S, CHAUDHARY, D. R, 1984, **MEASUREMENT OF EFFECTIVE THERMAL CONDUCTIVITY OF BUILDING-CONSTRUCTION MATERIALS AT DIFFERENT INTERSTITIAL AIR PRESSURE,** INDIAN JOURNAL OF TECHNOLOGY, 66-69

PARKER, W. J., JENKINS, R. J., BUTLER, C. P., ABBOTT, G. L., 1961, **FLASH METHOD OF DETERMINING THERMAL DIFFUSIVITY, HEAT CAPACITY, AND THERMAL CONDUCTIVITY** JOURNAL OF APPLIED PHYSICS, 1679-1684

PLACIDO, E., RDUINI-SCHUSTER, M. C., KUHN, J., 2005, **THERMAL PROPERTIES PREDICTIVE MODEL FOR INSULATING FOAMS**, INFRARED PHYSICS AND TECHNOLOGY, 219-231

PRASLOV, R. S., 1961, **GENERALIZATION OF THE EQUATION OF THERMAL CONDUCTIVITY OF GASES**. IZV. VUZ'OV, 132-139

PRATT, A. W., 1969, **HEAT TRANSMISSION IN LOW CONDUCTIVITY MATERIALS**, THERMAL CONDUCTIVITY 1:302-340

RADER, DANIEL J., TROTT, WAYNE M., TORCZYNSKI, JOHN R., CASTANEDA, JAIME N., AND GRASSER, THOMAS W., 2005, **MEASUREMENTS OF THERMAL ACCOMODATION COEFFICIENTS**, U.S.DEPARTMENT OF COMMERCE NATIONAL TECHNICAL INFORMATION SERVICE,

RADER, DANIEL J., TROTT, WAYNE M., TORCZYNSKI, JOHN R., GALLIS, MICHAIL A., CASTANEDA, JAIME N., AND GRASSER, THOMAS W., 2004, **MICROSCALE RAREFIED GAS DYNAMICS AND SURFACE INTERACTIONS FOR EUVL AND MEMS APPLICATIONS**, REPORT OF SANDIA NATIONAL LABORATORIES, SAND 2004-5329

RATH, D., STEIFF, A., WEINSPACH, P.-M., 1990, **ZUR BERECHNUNG DER EFFEKTIVEN WÄRMELEITFÄHIGKEIT VON EVAKUIERTEN DÄMMATERIALIEN**, CHEMIE-INGENEUR-TECHNIK, 956-957

REICH, G., 1990, **DETERMINATION OF THE *(PL)* VALUE BASED ON THE MEASUREMENT OF VISCOSITY AND THERMAL CONDUCTIVITY IN THE TRANSITION REGION**, VACUUM, 2053-2054

ROBENS, E., KREBS, K. F., MEYER, K., UNGER, K. K., DBROWSKI, A., 2002. **PROGRESS IN THE STANDARDISATION OF PARTICLE AND SURFACE CHARACTERISATION**, COLLOIDS AND SURFACES A: PHYSICOCHEMICAL AND ENGINEERING ASPECTS, 253-257

ROHSENOW, W. M., HARTNETT, J. P., AND CHOI, D. H., 1998, **HANDBOOK OF HEAT TRANSFER, THIRD EDITION**, MCGRAW-HILL, MCGRAW-HILL, NEW YORK, NY, USA

RU, Y., GUOQIANG, L., MIN, L., 2010, **ANALYSIS OF THE EFFECT OF DRYING CONDITIONS ON THE STRUCTURAL AND SURFACE HETEROGENEITY OF SILICA AEROGELS AND XEROGEL BY USING CRYOGENIC NITROGEN ADSORPTION CHARACTERIZATION**, MICROPOROUS AND MESOPOROUS MATERIALS, 1-10

RUSSELL, H. W., 1935, **PRINCIPLES OF HEAT FLOW IN POROUS INSULATORS**. JOURNAL OF THE AMERICAN CERAMIC SOCIETY, 1-5

RUTLEDGE, G. C., LOWERY, J. L., PAI, C. L., 2009, **CHARACTERIZATION BY MERCURY POROSIMETRY OF NONWOVEN FIBER MEDIA WITH DEFORMATION**, JOURNAL OF ENGINEERED FIBERS AND FABRICS, 1-13

SAXENA, S. C. AND JOSHI, R. K., 1989, **THERMAL ACCOMMODATION AND ADSORPTION COEFFICIENTS OF GASES,** ED. BY HO, C. Y., HEMISPHERE PUBLISHING CORPORATION, NEW YORK, USA

SCHAAF, S. A. AND CHAMBRE, P. L., 1958, **FLOW OF RAREFIED GASES**, SECTION H VOL. III ''High *Speed Aerodynamics* and Jet Propulsion'' EDIT BY EMMONS, H. W., PRINCETON UNIV. PRESS, NEW JERSEY, 687-739

SCHEUERPFLUG, P., MORPER, H.-J., NEUBERT, G., FRICKE, J., 1991, **LOW-TEMPERATURE THERMAL TRANSPORT IN SILICA AEROGELS**, JOURNAL OF PHYSICS D: APPLIED PHYSICS 24:1395-1403

SHIRTLIFFE, C. J., 1980, **EFFECT OF THICKNESS ON THE THERMAL PROPERTIES OF THICK SPECIMENS OF LOW-DENSITIY THERMAL INSULATION**, THERMAL INSULATION PERFORMANCE EDIT BY MCELROY, D. L. AND TYE, P. , 36-50

SIEGEL, R. AND HOWELL, J. R., 1992, **THERMAL RADIATION HEAT TRANSFER**, TAYLOR & FRANCIS, WASHINGTON, USA

SINGH, R, 2004, **CALCULATION OF EFFECTIVE THERMAL CONDUCTIVITY OF HIGHLY POROUS TWO-PHASE MATERIALS,** APPLIED THERMAL ENGINEERING, 2727-2735

SINGH, R., BENIWAL, R. S., CHAUDHARY, D. R., 1985, **EFFECT OF INTERSTITIAL AIR PRESSURE & PARTICLE SIZE ON THERMAL CONDUCTIVITY THROUGH SOME LOOSE BUILDING MATERIALS,** INDIAN JOURNAL OF PURE & APPLIED PHYSICS, 630-631

SINGH, RAMVIR AND KASANA, H. S., 2004, **COMPUTATIONAL ASPECTS OF EFFECTIVE THERMAL CONDUCTIVITY OF HIGHLY POROUS METAL FOAMS**, APPLIED THERMAL ENGINEERING, 1841-1849

SKOCHDOPOLE, R. E, 1961, **THE THERMAL CONDUCTIVITY OF FOAMED PLASTICS,** CHEMICAL ENGINEERING PROGRESS, 55-59

SMITH, DOUGLAS M., MASKARA, ALOK, ULRICH, BOES, 1998, **AEROGEL-BASED THERMAL INSULATION**, JOURNAL OF NON-CRYSTALLINE SOLIDS, 254-259

SMOLUCHOWSKI, M., 1898, **ÜBER WÄRME IN VERDÜNNTEN GASEN,** ANNALEN DER PHYSIK, 101-130

SMOLUCHOWSKI, M., 1910, "**CONTRIBUTION À LA THÉORIE *DE* L'ENDOSMOSE ÉLECTRIQUE ET *DE* QUELQUES PHÉNOMÈNES CORRÉLATIFS**", BULLETIN INTERNATIONAL DE L'ACADEMIE DES SCIENCES DE CRACOVIE, 129-153

SMOLUCHOWSKI, M, 1911, **ZUR THEORIE DER WÄRMELEITUNG IN VERDÜNNTEN GASEN UND DER DABEI AUFTRETENDEN DRUCKKRÄFTE,** ANNALEN DER PHYSIK, 983-1004

SPRINGER, G. S, 1971, **HEAT TRANSFER IN RAREFIED GASES**, ADVANCES IN HEAT TRANSFER, 163-218

STARK, C. AND FRICKE, J., 1993, **IMPROVED HEAT-TRANSFER MODELS FOR FIBROUS INSULATIONS**. INTERNATIONAL JOURNAL OF HEAT AND MASS TRANSFER, 617-625

STEPHENSON, D. G., 2010, **A NUMERICAL PROCEDURE FOR CALCULATING COMBINED CONDUCTION AND RADIATION HEAT FLUX THROUGH FIBROUS INSULATION**, JOURNAL OF BUILDING PHYSICS, 271-295

STOPS, D. W., 1970, **THE MEAN FREE PATH OF GAS MOLECULES IN THE TRANSITION REGIME.** J. PHYS. D: APPL. PHYS., 685-696

STRONG, H. M, BUNDY, F. P, BOVENKERK, H. P, 1960 **FLAT PANEL VACUUM THERMAL INSULATION.** JOURNAL OF APPLIED PHYSICS, 39-50

SULLINS, A. D. AND DARYABEIGI, K., 2001, **EFFECTIVE THERMAL CONDUCTIVITY OF HIGH POROSITY OPEN CELL NICKEL FOAM** , 35TH AIAA THERMOPHYSICS CONFERENCE, ANAHEIM, CA

SWIFT, D. L., 1966, **THE THERMAL CONDUCTIVITY OF SPHERICAL METAL POWDERS INCLUDING THE EFFECT OF AN OXIDE COATING**, INTERNATIONAL JOURNAL OF HEAT AND MASS TRANSFER, 1061-1074

SWIMM, K., REICHENAUER, G., VIDI, S., EBERT, H. P., 2009, **GAS PRESSURE DEPENDENCE OF THE HEAT TRANSPORT IN POROUS SOLIDS WITH PORES SMALLER THAN 10 μm**, INTERNATIONAL JOURNAL OF THERMOPHYSICS, 1329-1342

SYED, A. M., KOSNY, J. K., YARBROUGH, D. W., WELLS, M., 2008, **INFRARED SPECTROSCOPY OF CELLULOSE INSULATION** , PROCEEDINGS OF THE 29TH INTERNATIONAL THERMAL CONDUCTIVITY CONFERENCE, ITCC 29TH AND ITES 17TH, 56-70

TAO, WEI-HAN, SUNG, WEN-FA, LIN, JIAN-YUAN, 1997, **DEVELOPMENT OF VACUUM INSULATION PANEL SYSTEMS,** JOURNAL OF CELLULAR PLASTICS, 545-556

TAYLOR, R. E. AND MAGLIC, K. D., 1984, **PULSE METHOD FOR THERMAL DIFFUSIVITY MEASURMENT**, COMPENDIUM OF THERMOPHYSICAL PROPERTY MEASUREMENT METHODS MAGLIC, K. D., CEZAILIYAN, A., AND PELETSKY, V. E., PLENUM PRESS.NEW YORK, 305-336

THE ECONOMIST, 2012, **GERMANY'S ENERGY TRANSFORMATION ENERGIEWENDE**, THE ECONOMIST, JULY 2012

TIEN, C. L AND CUNNINGTON, G. R, 1973, **CRYOGENIC INSULATION HEAT TRANSFER,** ADV. HEAT TRANSFER, 349-417

TSENG, C. J., YAMAGUCHI, M., OHMORI, T., 1997, **THERMAL CONDUCTIVITY OF POLYURETHANE FOAMS FROM ROOM TEMPERATURE TO 20 K**, CRYOGENICS, 305-312

TSOTSAS, E. AND MARTIN, H., 1987, **THERMAL CONDUCTIVITY OF PACKED BEDS: A REVIEW**, CHEMICAL ENGINEERING AND PROCESSING, 19-37

VERSCHOOR, J. D., GREEBLER, P., MANVILLE, N. J., 1952, **HEAT TRANSFER BY GAS CONDUCTION AND RADIATION IN FIBROUS INSULATIONS**, TRANS. ASME 74:961-968

VISHNEVSKII, I. I., AKSELROD, E. I., TALYANSKAYA, N. D., MELENTEV, A. D., GLUSHKOVA, D. B., 1975, **THE THERMAL CONDUCTIVITY OF REFRACTORY FIBER PRODUCTS**, REFRACTORIES, 408-413

VLADIMIROV, V., 1998, **INTERPOLATION METHOD FOR DEBYE TEMPERATURE NDT DETERMINATION,** 7TH EUROPEAN CONFERENCE ON NON-DESTRUCTIVE TESTING, COPENHAGEN

VOZÁR, L. AND HOHENAUER, W., 2003, **FLASH METHOD OF MEASURING THE THERMAL DIFFUSIVITY A REVIEW**, HIGH TEMPERATURES - HIGH PRESSURES, 253-264

WACHMAN,Y., 1962, **THE THERMAL ACCOMMODATION COEFFICIENT: A CRITICAL SURVEY**, ARS JOURNAL, 2-12

WAKAO, N. AND KAGNEI, S., 1982, **HEAT AND MASS TRANSFER IN PACKED BEDS**, GORDON AND BREACH SCIENCE, LONDON, 161-205

WAKAO, N. AND VORTMEYER, D., 1971, **PRESSURE DEPENDENCY OF EFFECTIVE THERMAL CONDUCTIVITY OF PACKED BEDS**, CHEMICAL ENGINEERING SCIENCE, 1753-1765

WANG, C. M., LIN, S. Y., KAO, K. S., CHEN, Y. C., WENG, S. C., 2010, **MICROSTRUCTURAL AND ELECTRICAL PROPERTIES OF CATIO3-CACU3TI4O12 CERAMICS**, JOURNAL OF ALLOYS AND COMPOUNDS, 423-430

WANG, L., ZHOU, X., WEI, X., 2008. **HEAT CONDUCTION**, SPRINGER, BERLIN,

WAWRYK, R. AND RAFALOWICZ, J., 1988, **THE INFLUENCE OF RESIDUAL GAS PRESSURE ON THE THERMAL CONDUCTIVITY OF MICROSPHERE INSULATIONS**, INTERNATIONAL JOURNAL OF THERMOPHYSICS 9:611-625

WEBB, PAUL A., 2001, **VOLUME AND DENSITY DETERMINATIONS FOR PARTICLE TECHNOLOGISTS**, MICROMERITICS INSTRUMENT CORP. 2/16/01, WWW.MICROMERITICS.COM

WEI, G., ZHANG, X., YU, F., CHEN, K., 2006, **THERMAL DIFFUSIVITY MEASUREMENTS ON INSULATION MATERIALS WITH THE LASER FLASH METHOD**, INTERNATIONAL JOURNAL OF THERMOPHYSICS, 235-243

WILKES, K. E., WENDT, R. L., DELMAS, A., AND CHILDS, P. W., 1993, **THERMAL PERFORMANCE OF ONE LOOSE-FILL FIBERGLASS ATTIC INSULATION**, INUSLATION MATERIALS: TESTING AND APPLICATIONS, 2ND VOLUME EDIT BY GRAVES, R. S. AND WYSOCKI, D. C., 275-291

WOLF, J. R AND STRIEDER, WILLIAM C., 1994, **PRESSURE-DEPENDENT GAS HEAT TRANSPORT IN A SPHERICAL PORE,** AICHE JOURNAL, 1287-1296

WONCHALA, E. P. AND WYNNYCKJI, 1984, **THE EFFECTIVE THERMAL CONDUCTIVITY OF SOLIDS WITH COMPLEX PORES IN THE TRANSITION AND KNUDSEN REGIONS,** THE CANADIAN JOURNAL OF CHEMICAL ENGINEERING, 719-722

WONCHALA, E. P. AND WYNNYCKYJ, J. R., 1984, **THE EFFECTIVE THERMAL CONDUCTIVITY OF SOLIDS WITH COMPLEX PORES IN THE TRANSITION AND KNUDSEN REGIONS**, THE CANADIAN JOURNAL OF CHEMICAL ENGINEERING 62:719-722

WOODSIDE, W AND MESSMER, J. H, 1960, **MOLECULAR EFFECTS IN HEAT CONDUCTION THROUGH POROUS ROCKS**, JOURNAL OF GEOPHYSICAL RESEARCH, 3481-3485

WOODSIDE, W AND MESSMER, J. H, 1961, **THERMAL CONDUCTIVITY OF POROUS MEDIA. I. UNCONSOLIDATED SANDS, II. CONSOLIDATED SANDS,** JOURNAL OF APPLIED PHYSICS, 1688-1706

WU, J.-W., SUNG, W.-F., CHU, H.-S., 1999, **THERMAL CONDUCTIVITY OF POLYURETHANE FOAMS**, INTERNATIONAL JOURNAL OF HEAT AND MASS TRANSFER 42:2211-2217

WULF, R., 2009, **WÄRMELEITFÄHIGKEIT VON HITZEBESTÄNDIGEN UND FEUERFESTEN DÄMMSTOFFEN – UNTERSUCHUNGEN ZU URSACHEN FÜR UNTERSCHIEDLICHE MESSERGEBNISSE BEI VERWENDUNG VERSCHIEDENER MESSVERFAHREN**, THESIS IN TECHNISCHE UNIVERSITÄT FREIBERG, GERMANY

WULF, R., BARTH, G., GROSS, U., 2007, **INTERCOMPARISON OF INSULATION THERMAL CONDUCTIVITIES MEASURED BY VARIOUS METHODS**, INT. J. THERMOPHYSICS, 1679-1692

YE, G., 2003, **EXPERIMENTAL STUDY AND NUMERICAL SIMULATION OF THE DEVELOPMENT OF THE MICROSTRUCTURE AND PERMEABILITY OF CEMENTITIOUS MATERIALS**, THESIS IN DELFT UNIVERSITY PRESS

ZENG, S. Q, HUNT, A, GREIF, R, 1995, **MEAN FREE PATH AND APPARENT THERMAL CONDUCTIVITY OF A GAS IN A POROUS MEDIUM,** TRANS. ASME, 758-761

ZENG, S. Q, HUNT, A. J., CAO, W., GREIF, R., 1994, **PORE SIZE DISTRIBUTION AND APPARENT GAS THERMAL CONDUCTIVITY OF SILICA AEROGEL**, TRANS. ASME: JOURNAL OF HEAT TRANSFER, 756-759

ZENG, S. Q., HUNT, A., GREIF, R., 1995, **THEORETICAL MODELING OF CARBON CONTENT TO MINIMIZE HEAT TRANSFER IN SILICA AEROGEL**, JOURNAL OF NON-CRYSTALLINE SOLIDS, 271-277

ZENG, S. Q., HUNT, A., GREIF, R., 1995, **TRANSPORT PROPERTIES OF GAS IN SILICA AEROGEL**. JOURNAL OF NON-CRYSTALLINE SOLIDS 186:264-270

ZHANG, HUI, WANG, JUE, DENG, SHENG ZHONG, ZHOU, BIN, 1999, **GAS THERMAL CONDUCTION OF NANO-POROUS SLICA AEROGELS,** JOURNAL OF TONGJI UNIVERSITY, 541-544

ZHENG, LEI AND STRIEDER, WILLIAM, 1994, **KNUDSEN VOID GAS HEAT TRANSPORT IN FIBROUS MEDIA,** INT. J. HEAT MASS TRANSFER, 1433-1440

ZHOU, J., YE, G., VAN BREUGEL, K., 2010, **CHARACTERIZATION OF PORE STRUCTURE IN CEMENT-BASED MATERIALS USING PRESSURIZATION-DEPRESSURIZATION CYCLING MERCURY INTRUSION POROSIMETRY**, CEMENT AND CONCRETE RESEARCH, 1120-1128

ZIEGENBEIN, B., 1983, **EVACUATED HIGH-TEMPERATURE INSULATIONS FOR ELECTROCHEMICAL BATTERIES.** HIGH TEMPERATURE- HIGH PRESSURE, 329-334

List of Appendixes

APPENDIX A: DATA SHEETS OF SUPER-INSULATION (EXAMPLES FOR KNUDSEN MATERIALS)

Appendix A: Data sheets of Super-Insulation (Knudsen Materials)

A.1. Data Sheets of Material WDS® Ultra produced by Porextherm©

http://www.porextherm.com/

A.2. Data Sheets of Material Silcapor high® produced by Silca©

For download on http://www.silca-online.de/

A.3. Data Sheets of Microtherm® Ultra produced by Microtherm nv©

http://www.microthermgroup.com/

WDS® Ultra

Characteristics

WDS® Ultra is a microporous insulation material with an extremely low coefficient of thermal conductivity, i.e. with very good insulating properties.

WDS® Ultra consists of inorganic silicates. The main constituent is fumed silica, the other components are opacifiers for minimizing infrared radiation.

WDS® Ultra is not flammable and meets the requirements acc. to DIN ISO 4102 for fire protection class A1.

Application

Tried and tested applications for WDS® Ultra include insulation for heat-treatment furnaces in the aluminum industry, or back-up insulation in the industrial furnace industry.

In these applications, WDS® Ultra fulfills several functions, such as:

- Precisely controlled energy emission
- Reduction of weight and volume
- Increase of heat retention
- Increased effective volume

WDS® Ultra is also successfully used as insulation material in the following areas:

- Heat treatment systems for glass
- Fire protection equipment
- Electronic devices
- Measurement equipment
- Plant construction parts
- Chimneys, pipes

Form of delivery

1. **Standard sizes:**
   - 1000 mm x 650 mm x **X**
   - 650 mm x 500 x X
2. **Standard thicknesses (X):**
   - 10 mm, 15 mm, 20 mm, 25 mm, 30 mm, 35 mm, 40 mm, 45 mm, 50 mm
   - Tolerances acc. to DIN ISO 2768 → Tolerance class “c”, coarse for length, breadth, for thickness ±1mm.
   - also available in customized panel forms
   - max. Size 1320 mm x 1000 mm x thickness

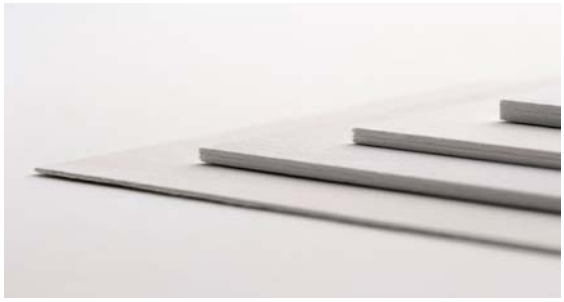

Restrictions on application

WDS® Ultra is sensitive to all liquids that can wet it, such as water, oil, petroleum spirit, since they can destroy the nanoporous structure.

The moisture sensitivity of WDS® Ultra can be greatly improved or eliminated altogether by suitable surfact treatment (e.g. PE film, aluminum foil, or liquid coatings)

Shelf life

WDS® Ultra has an unlimited shelf life. WDS® Ultra must be handled and stored in dry conditions. WDS® Ultra is resistant to diffusion by atmospheric humidity (water vapor).

Composition

Silicon dioxide	SiO_2	approx. 80%
Silicon carbide	SiC	approx. 15%
Others		approx. 5%.

Electrical resistance

Panel unhardened	
Stored under dry conditions	> 2000 MΩ

Thermal shock resistance

WDS® Ultra is insensitive to high and low temperature thermal shocks.

Product data

Physical properties			Standards	Units	Values
Color					Grey
Bulk density				kg / m³	230 ± 10%
Max. application temperature				°C	950
Low-temp. flexural strength			DIN 53423	N / mm²	0.16
Shrinkage	Temperature applied to one side			0.5% at 1000 °C / 12h	
Linear shrinkage / long term	Temperature at all sides			800 °C	1.0%
				1000 °C	4.8%
Compression		400 °C	800 °C		
	1 %	0.090 MPa	0.117 MPa		
	3 %	0.288 MPa	0.364 MPa		
	5 %	0.494 MPa	0.617 MPa		
	10 %	1.029 MPa	1.263 MPa		
Thermal conductivity			DIN 51046		
		50 °C		W / mK	0.018
		100 °C		W / mK	0.019
		200 °C		W / mK	0.020
		300 °C		W / mK	0.022
		400 °C		W / mK	0.024
		500 °C		W / mK	0.027
		600 °C		W / mK	0.031
		700 °C		W / mK	0.035
		800 °C		W / mK	0.040

Thermal conductivity as a function of mean temperature (DIN 52612)

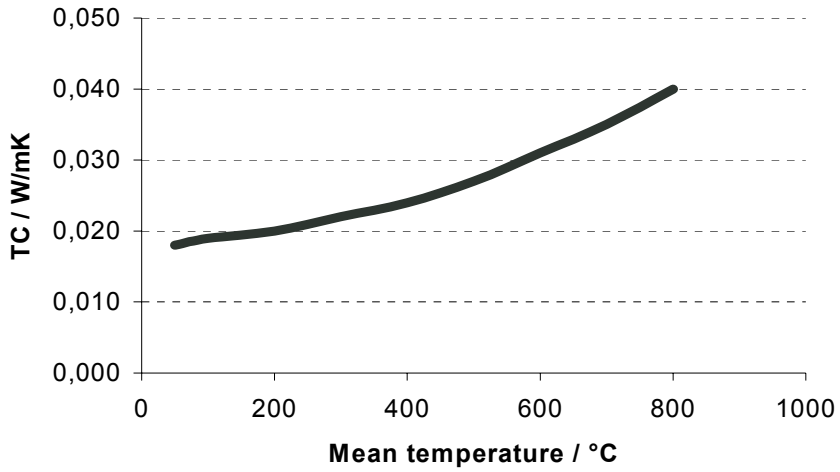

Compression behavior

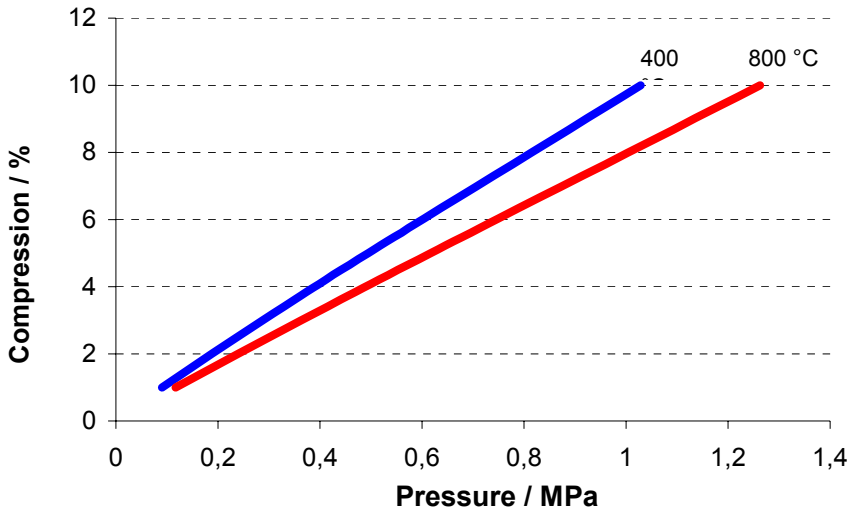

Safety directions

WDS® Ultra is not a hazardous material as defined in EU directive 2006/1907/EEC.
The fibers used for mechanical reinforcement of WDS® Ultra are not respirable as defined by WHO.
WDS® Ultra does not liberate hazardous decomposition products and, as far as is known at present, does not cause any problems to human health.

Please address all technical questions that affect quality and product safety to:

Porextherm Dämmstoffe GmbH
Heisingerstrasse 8/10
D-87437 Kempten

www.porextherm.com
info@porextherm.com

Microtherm®

Insulation for Hot Metals Applications

Thinnest insulation systems for steel and non-ferrous manufacture

MICROTHERM® IS USED EXTENSIVELY IN THE PROCESSING OF STEEL AND NON-FERROUS METALS.

LADLES

Microtherm® brings proven benefits – reduction of heat loss, increased capacity and possible longer lining life in steel ladles with sizes ranging from 20 up to around 350 tonnes.

TORPEDO LADLES

Reduction in heat loss from the shell of a well insulated torpedo ladle can result in hotter metal arriving at the steel plant, maybe up to 40 °C (around 100 °F) hotter. Using Microtherm helps to maintain a constant energy level necessary to conduct secondary metallurgy processes.

TUNDISHES

Problems can occur in continuous casting of steel because of inappropriate liquid steel temperatures in the tundish. The use of Microtherm® to insulate the tundish can aid in maintaining consistent steel temperature and viscosity. Other advantages can be increase of capacity and safety issues like longer process times at tower position.

Microtherm® - cool answers to hot problems

MICROTHERM
THERMAL INSULATION SOLUTIONS

Microtherm® product range for Steel applications

A/ Microtherm® Super G/SGHY Panels

- Up to 1000 °C (24mW/mK @ 400 °C)
- Hydrophobic grade (up to 250°C) available
- Density 200 – 400 kg/m^3
- Thickness: 3/5/7/10mm

B/ Microtherm Steelflex® Panels

- Up to 1000 °C (24mW/mK @ 400 °C)
- Cost effective water repellent plastic film
- Density 290 – 300 kg/m^3
- Thickness: 5/7/10mm

C/ Microtherm SteelflexPlus® Panels

- Up to 1050 °C (38mW/mK @ 400 °C) with reduced shrinkage
- Multi layer PE water repellent barrier film
- Nominal density > 430 kg/m^3 with superior resistance to pressure
- Thickness: 5/6/7mm

D/ Microtherm® Super A Panels

- Up to 1200 °C (33mW/mK @ 400 °C)
- Density 350 – 400 kg/m^3
- Thickness: 3/5/6/7mm

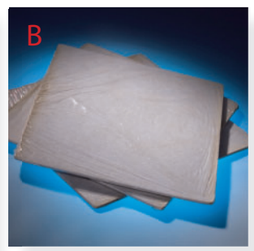

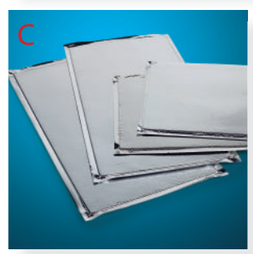

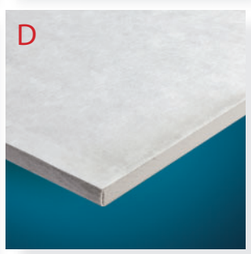

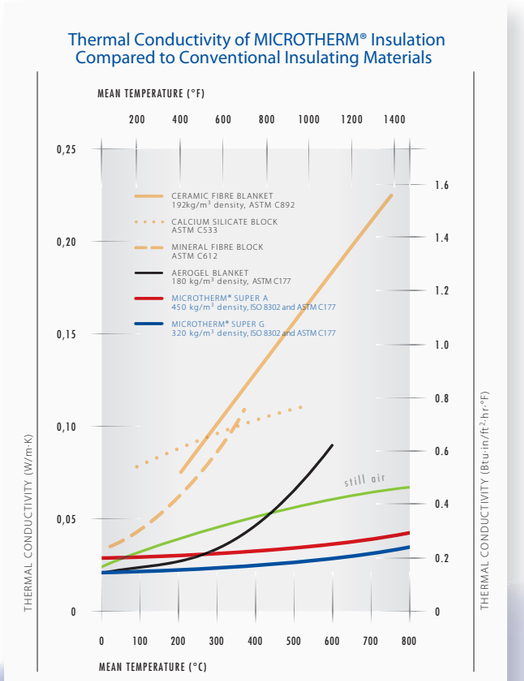

Properties

- Formulation based on opacified pyrogenic silica with glass filament reinforcement.
- Capable of continuous exposure to 1000 °C (1832 °F), Steelflex+ to 1050 °C (1922 °F).
- Microtherm Super A capable of use up to 1200 °C (2192 °F).
- No known health hazards when used within prescribed working temperature limits.
- Non-combustible & environmentally safe.
- Products enclosed for dust free handling during fitting.
- Easily fitted during installation.

Benefits

- Only around one quarter the thickness of conventional insulations at high temperature. Thinnest insulation available.
- Lightweight but load bearing insulation systems.
- Simple pin mounting for tundish application.
- Possible increase of internal capacity.
- Can be supplied pre-formed. Glass cloth covered panels can be easily shaped and fitted during assembly.
- Hydrophobic grades are available for installation behind castable cement.
- Microtherm® Steelflex® range with water resistant barrier film provide an alternative solution where water may be encountered.

Microtherm® in steel and non-ferrous metals manufacture

Steel ladles

Benefits from Microtherm®

- Reduction of heat loss through the shell
- A cooler shell expands less giving a tighter lining.
- Less thermal shock in bricks result in:
  - More uniform expansion
  - Fewer gaps between bricks
  - Less tendency to pinch
  - Better resistance to penetration of molten steel

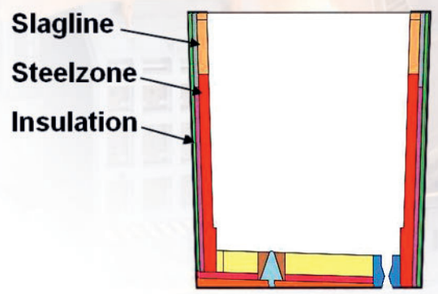

Tundishes

- The use of Microtherm® to insulate the tundish can aid in maintaining consistent steel temperature and viscosity.
- Accurate temperature / flow control is essential to assist the multiple metallurgical operations and homogenisation that occur within the tundish flow.

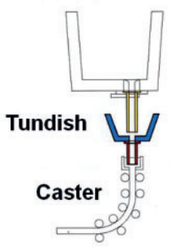

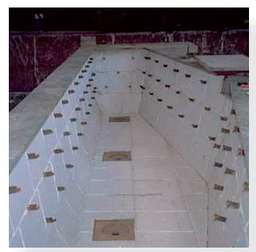

Torpedo ladles

- The transfer of molten iron from blast furnace to steel plant by means of torpedo ladles can often involve long holdingtimes and distances of travel.

- Improving the insulation level by using Microtherm® allows a much thinner lining thickness overall with no loss in thermal efficiency - still producing benefits of increased ladle capacity.

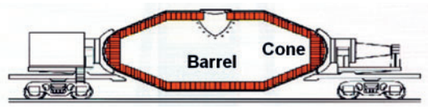

Some other applications

- Electric Arc Furnace
- Blast furnaces:
  - Hot wind pipe sections
  - Hot wind valves
  - Hot wind bellows & elbows
- Launder & Launder cover
- RH Degasser
- Annealing lines
- Cokes Batteries

MICROTHERM
THERMAL INSULATION SOLUTIONS

Microtherm® - the complete service package

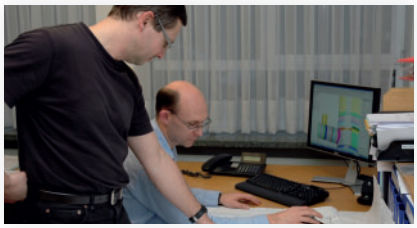

- Problem analysis
- Thermal calculations
- Full system design
- Performance testing – in-house speciality fire testing
- Performance verification with thermography
- Installation support and co-ordination

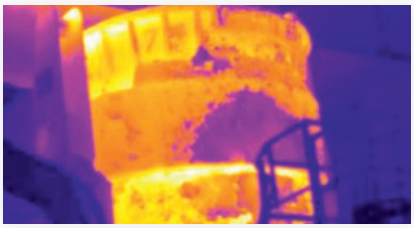

Our innovative insulation solutions continue to evolve. This brochure outlines our capabilities.
If you have a special need that is particularly challenging, why not contact our Design Team for advice.

The Microtherm Group - truly global service of the highest standard

Microtherm Inc.
3269 Regal Drive
Alcoa, Tennessee 37701
USA
T. (+1) (865) 681 0155
F. (+1) (865) 681 0016
E. sales@microtherm.us

Microtherm N.V.
Industriepark Noord 1
9100 Sint-Niklaas
Belgium
T. (+32) 3 760 19 80
F. (+32) 3 760 19 99
E. info@microthermgroup.com

Nippon Microtherm Co., Ltd.
Korakuen Shinjuku Bldg,
4-15-7, Nishi-shinjuku
Shinjuku-ku, Tokyo 160-0023, Japan
T. (+81) 3 3377 2821
F. (+81) 3 3378 2821
E. sales@microtherm.co.jp

www.microthermgroup.com

Issue ref.221110/01

MICROTHERM
THERMAL INSULATION SOLUTIONS

APPENDIX B: LIST OF GAS PROPERTIES

B.1 Thermal Properties of Selective Gases in this Study

Krypton

Molecule diameter = 4.04×10^{-10} m , P = 1 bar

T K	Bulk gas Thermal conductivity* W m^{-1} K^{-1}	Mean Free Path† µm	Cp‡ J Kg^{-1} K^{-1}
300	0.0096	0.0571	0.2481
400	0.0123	0.0762	0.2481
500	0.0148	0.0952	0.2481
600	0.0171	0.1142	0.2481
700	0.0192	0.1333	0.2481
800	0.0211	0.1523	0.2481
900	0.023	0.1714	0.2481
1000	0.0247	0.1904	0.2481
1100	0.0263	0.2094	0.2481
1200	0.0279	0.2285	0.2841

Argon

Molecule diameter = 3.58×10^{-10} m , P = 1 bar

T K	Bulk gas Thermal conductivity W m^{-1} K^{-1}	Mean Free Path µm	Cp J Kg^{-1} K^{-1}
300	0.0177	0.0727	0.5203
400	0.0219	0.097	0.5203
500	0.0259	0.1212	0.5203
600	0.0297	0.1455	0.5203
700	0.0334	0.1697	0.5203
800	0.0369	0.194	0.5203
900	0.0403	0.2182	0.5203
1000	0.0435	0.2425	0.5203
1100	0.0466	0.2667	0.5203
1200	0.0495	0.291	0.5203

* calculated for all gases using interpolation function published in VDI Heat Atlas, 2006

† KENNARD, E. H, 1938, KINETIC THEORY OF GASES, MCGRAW HILL, NEW YORK

‡ calculated using interpolation function published from ROHSENOW, W. M., HARTNETT, J. P., AND CHOI, D. H., 1998, HANDBOOK OF HEAT TRANSFER, MCGRAW HILL, NEW YORK

Nitrogen

Molecule diameter = 3.7×10^{-10} m, P = 1 bar

T K	Bulk gas Thermal conductivity W m^{-1} K^{-1}	Mean Free Path µm	Cp J Kg^{-1} K^{-1}
300	0.0256	0.0681	1.0391
400	0.0325	0.0908	1.044
500	0.039	0.1135	1.0566
600	0.045	0.1362	1.0753
700	0.0507	0.1589	1.0976
800	0.0562	0.1816	1.1213
900	0.0615	0.2043	1.1446
1000	0.0667	0.227	1.1667
1100	0.0719	0.2497	1.1868
1200	0.0771	0.2724	1.2048

Helium

Molecule diameter[4] =2.15×10^{-10} m, P = 1 bar

T K	Bulk gas Thermal conductivity W m^{-1} K^{-1}	Mean Free Path µm	Cp J Kg^{-1} K^{-1}
300	0.1543	0.2017	5.1932
400	0.1884	0.2689	5.1932
500	0.2202	0.3361	5.1932
600	0.2501	0.4034	5.1932
700	0.2786	0.4706	5.1932
800	0.3058	0.5378	5.1932
900	0.3321	0.605	5.1932
1000	0.3577	0.6723	5.1932
1100	0.3827	0.7395	5.1932
1200	0.4073	0.8067	5.1932

[4] Data for molecule diameters are taken from the 85th edition of CRC Handbook of Chemistry and Physics, 2004, Edited David R. Lide, published by CRC Press

B.2 Comparison of Thermal Conductivity of Gases

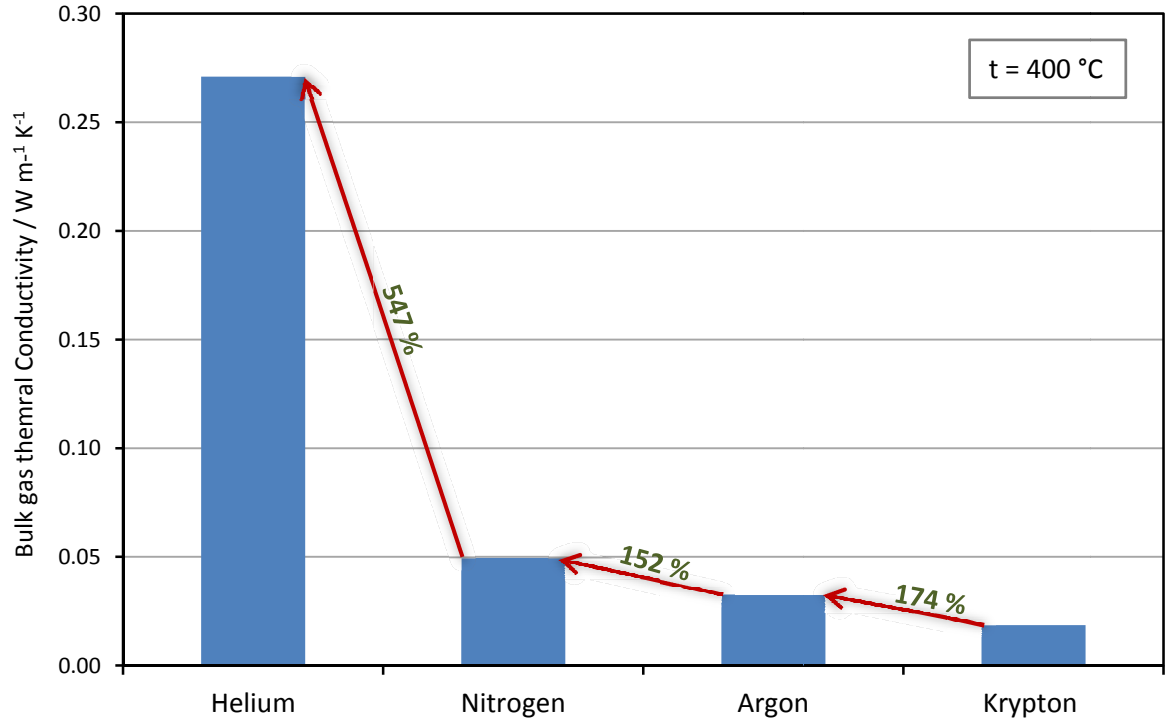

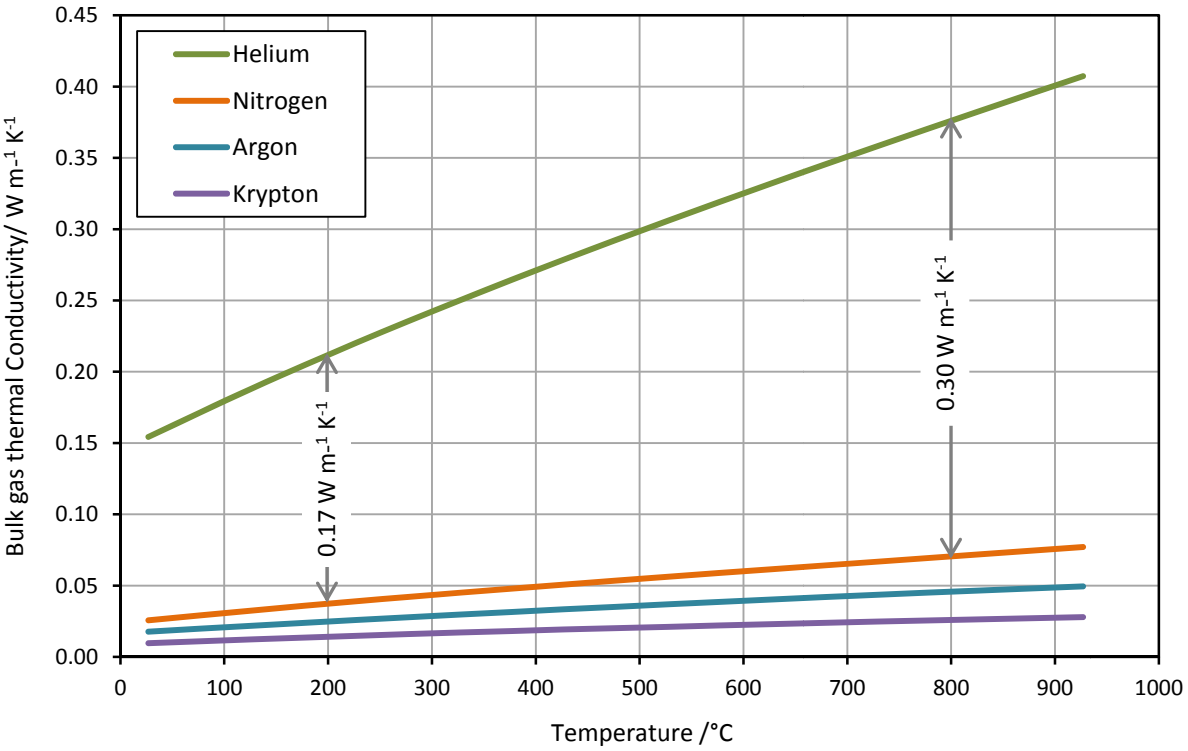

APPENDIX C: RESULTS OF EFFECTIVE THERMAL CONDUCTIVITY OF ALL INVESTIGATED MATERIALS

Results of effective thermal conductivity measurements by radial heat flowmeter apparatus for all materials are presented versus the temperature in Appendix C. For the next twelve diagrams: Points are experimental results. True thermal conductivity that evaluated using eq. (51) is presented as line in each gas atmosphere.

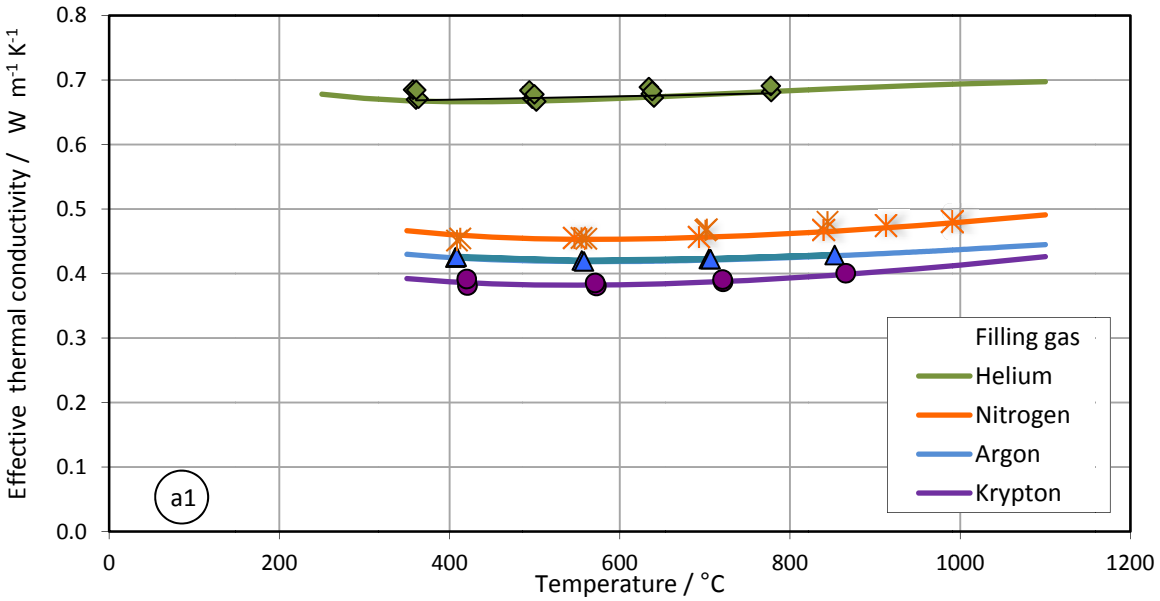

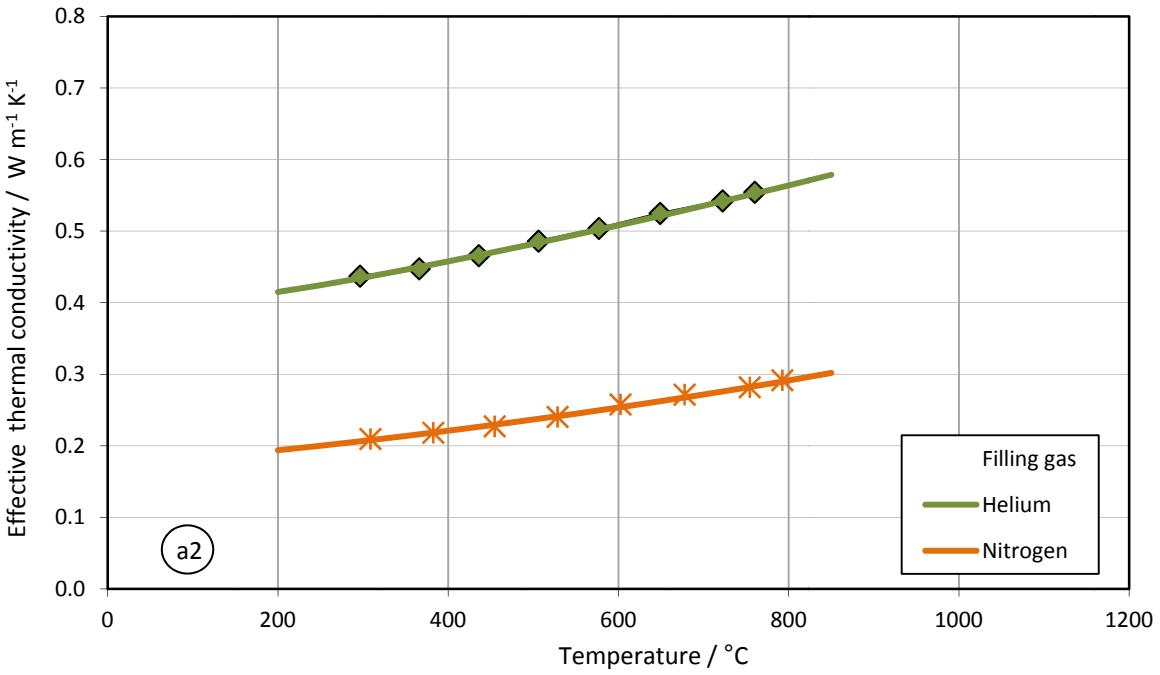

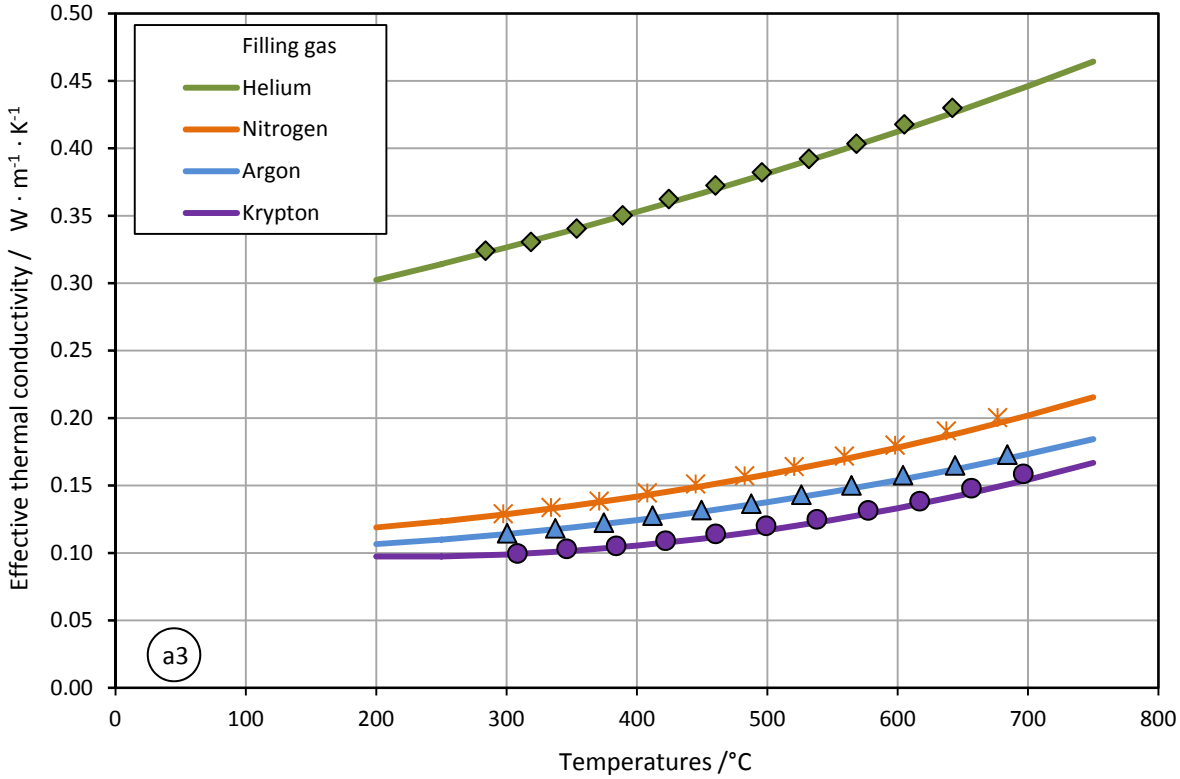
Filling gas
Helium
Nitrogen
Argon
Krypton
a3
Effective thermal conductivity / W · m⁻¹ · K⁻¹
Temperatures /°C
0.00
0.05
0.10
0.15
0.20
0.25
0.30
0.35
0.40
0.45
0.50
0
100
200
300
400
500
600
700
800

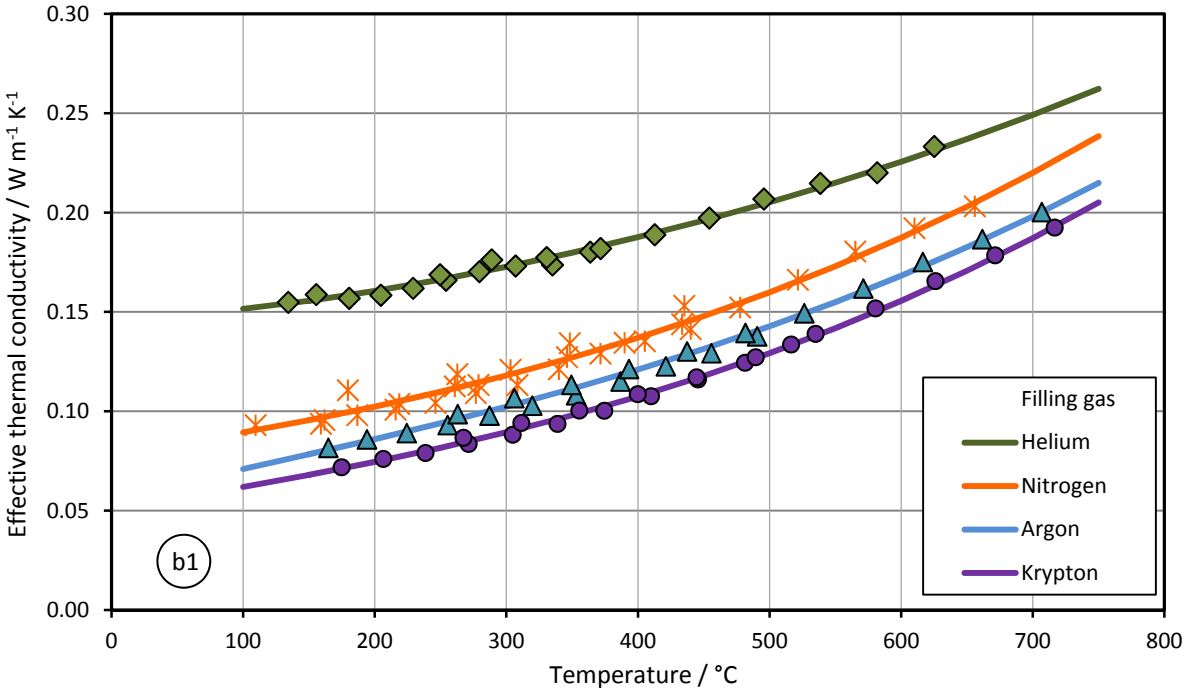
Filling gas
Helium
Nitrogen
Argon
Krypton
b1
Effective thermal conductivity / W m⁻¹ K⁻¹
Temperature / °C
0.00
0.05
0.10
0.15
0.20
0.25
0.30
0
100
200
300
400
500
600
700
800

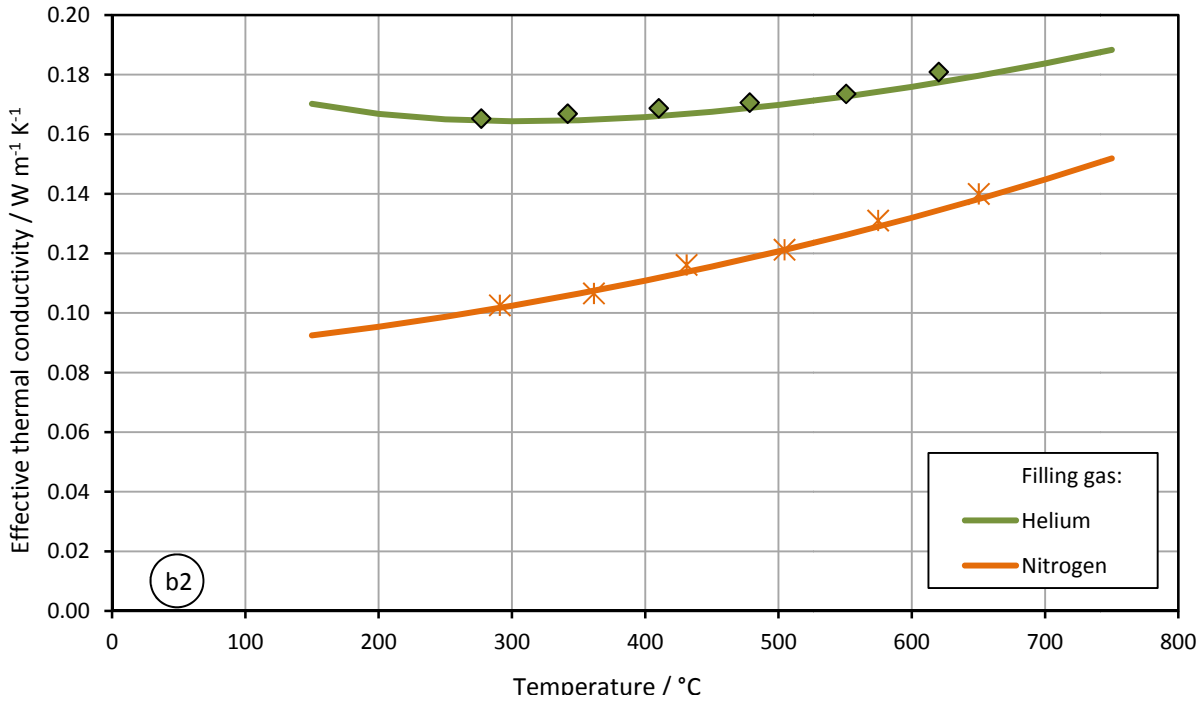
Effective thermal conductivity / W m-1 K-1
0.20
0.18
0.16
0.14
0.12
0.10
0.08
0.06
0.04
0.02
0.00
0
100
200
300
400
500
600
700
800
Temperature / °C
Filling gas:
Helium
Nitrogen
b2

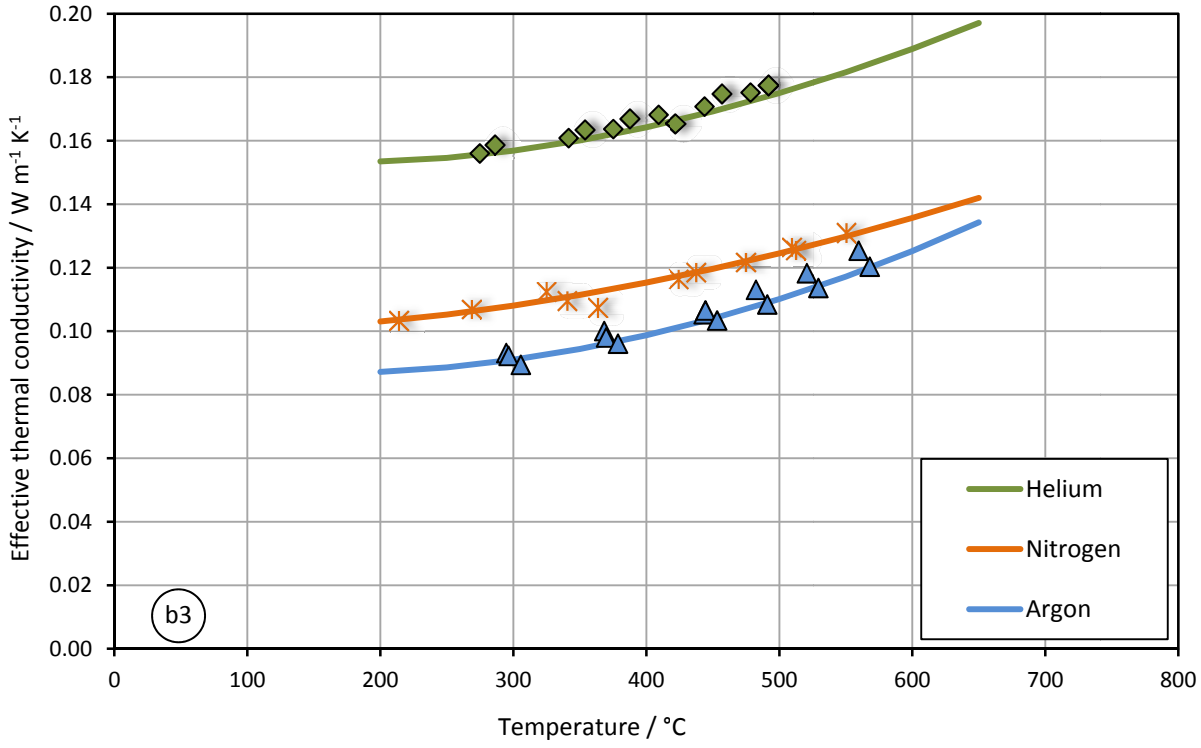
Effective thermal conductivity / W m-1 K-1
0.20
0.18
0.16
0.14
0.12
0.10
0.08
0.06
0.04
0.02
0.00
0
100
200
300
400
500
600
700
800
Temperature / °C
Helium
Nitrogen
Argon
b3

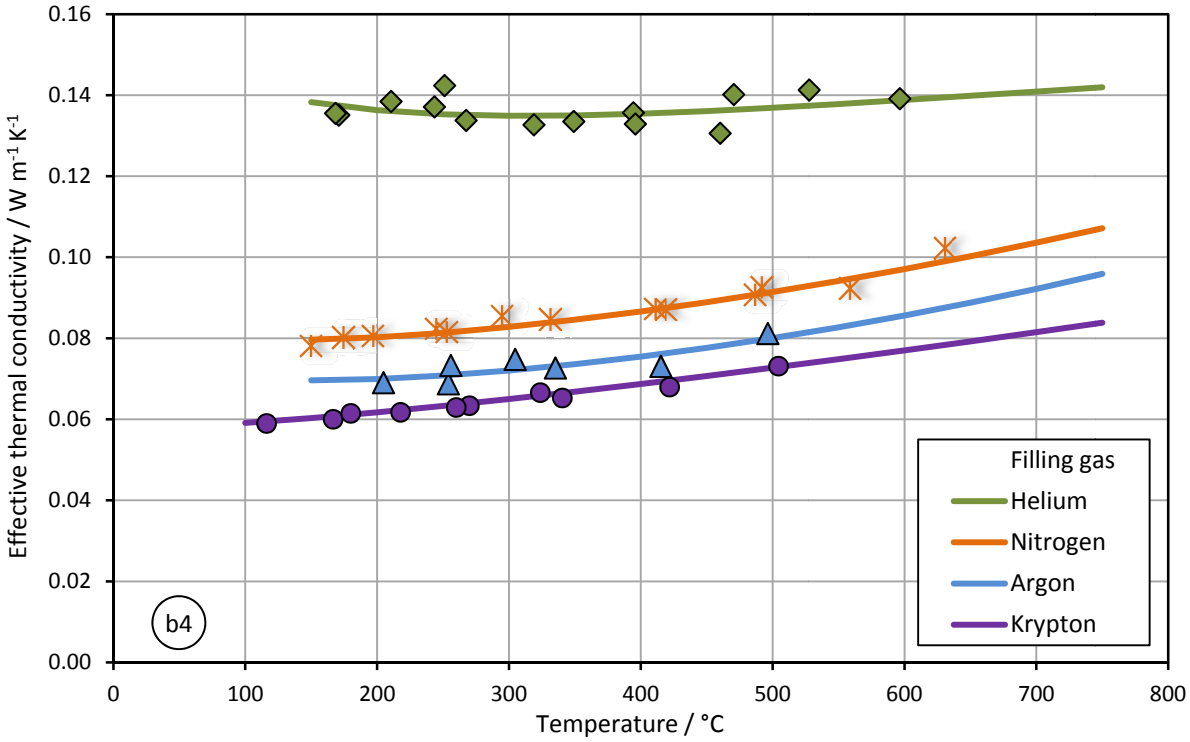
Effective thermal conductivity / W m-1 K-1
0.16
0.14
0.12
0.10
0.08
0.06
0.04
0.02
0.00
0
100
200
300
400
500
600
700
800
Temperature / °C
Filling gas
Helium
Nitrogen
Argon
Krypton
b4

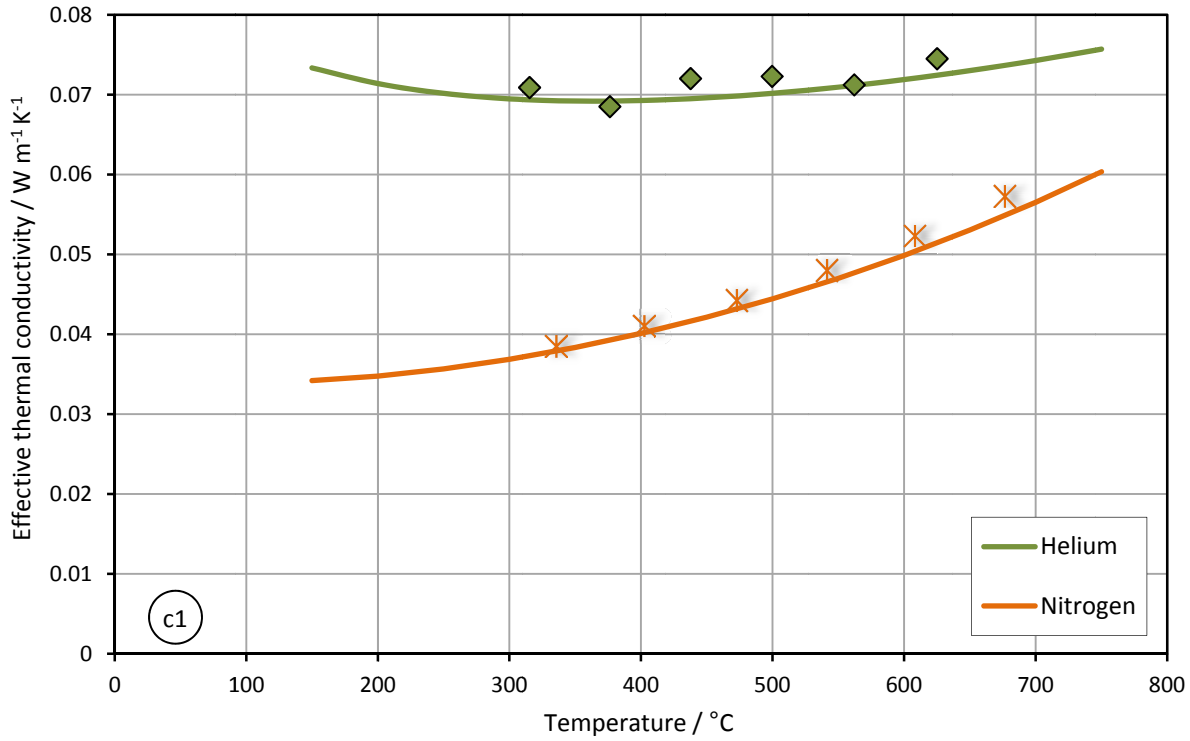
Effective thermal conductivity / W m-1 K-1
0.08
0.07
0.06
0.05
0.04
0.03
0.02
0.01
0
0
100
200
300
400
500
600
700
800
Temperature / °C
Helium
Nitrogen
c1

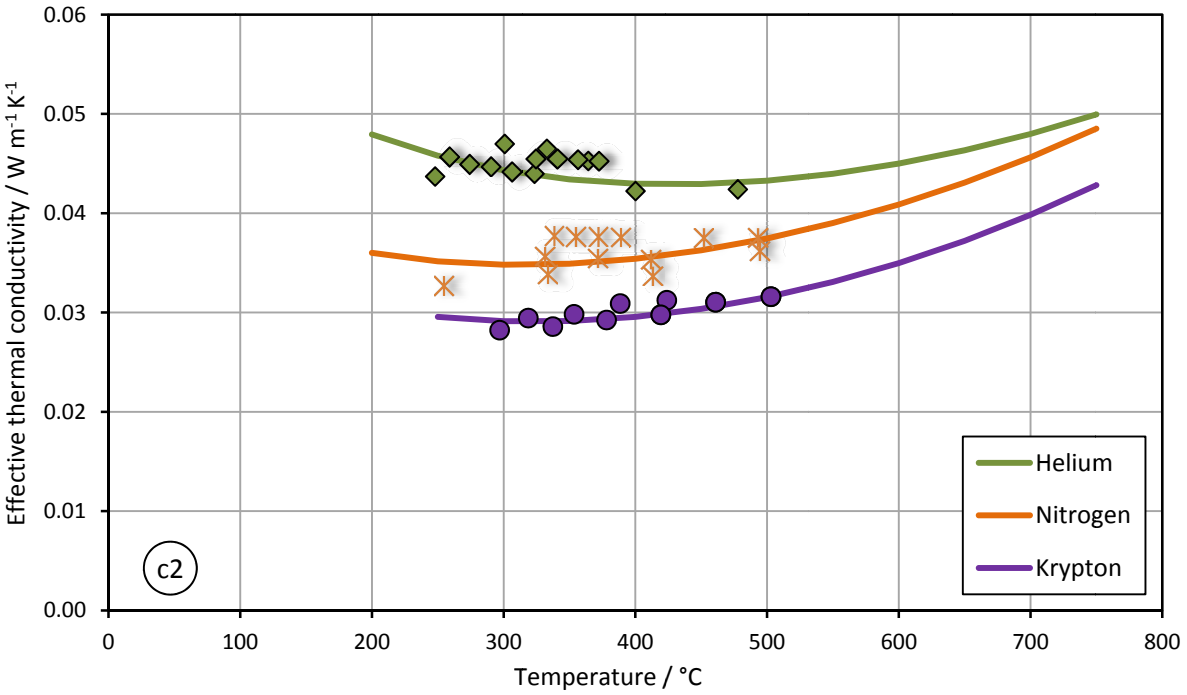
Effective thermal conductivity / W m-1 K-1
0.06
0.05
0.04
0.03
0.02
0.01
0.00
0
100
200
300
400
500
600
700
800
Temperature / °C
c2
Helium
Nitrogen
Krypton

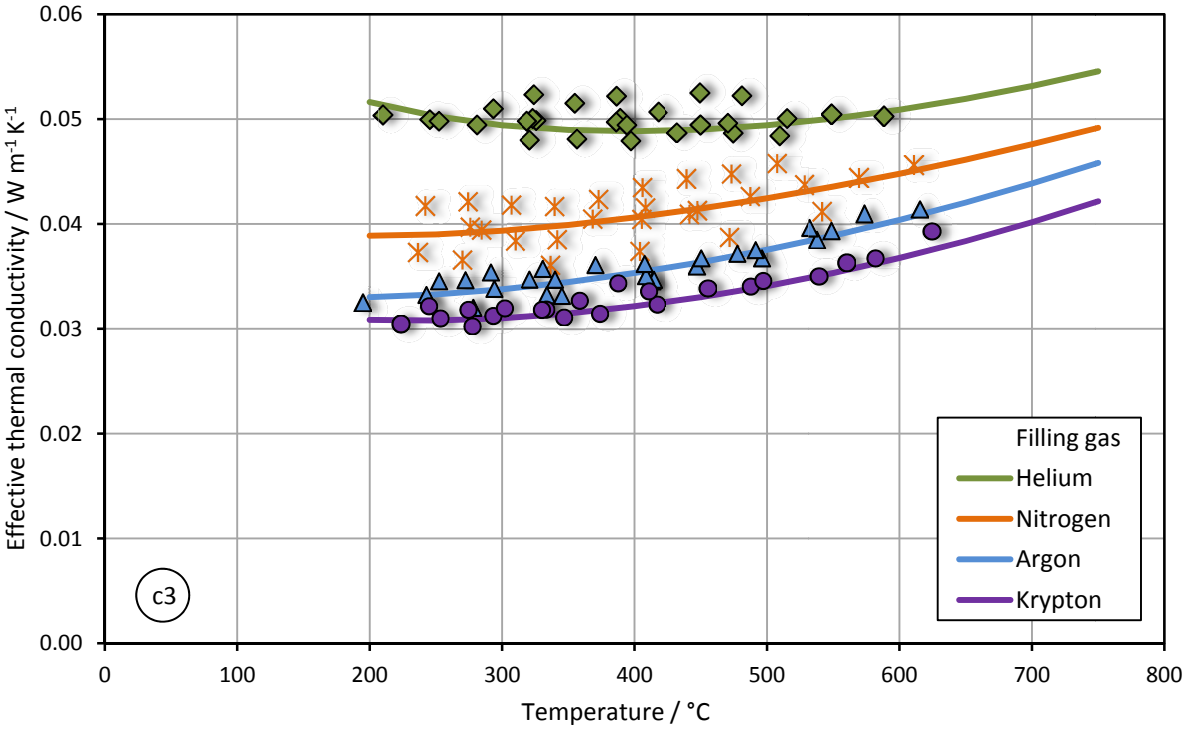
Effective thermal conductivity / W m-1 K-1
0.06
0.05
0.04
0.03
0.02
0.01
0.00
0
100
200
300
400
500
600
700
800
Temperature / °C
c3
Filling gas
Helium
Nitrogen
Argon
Krypton

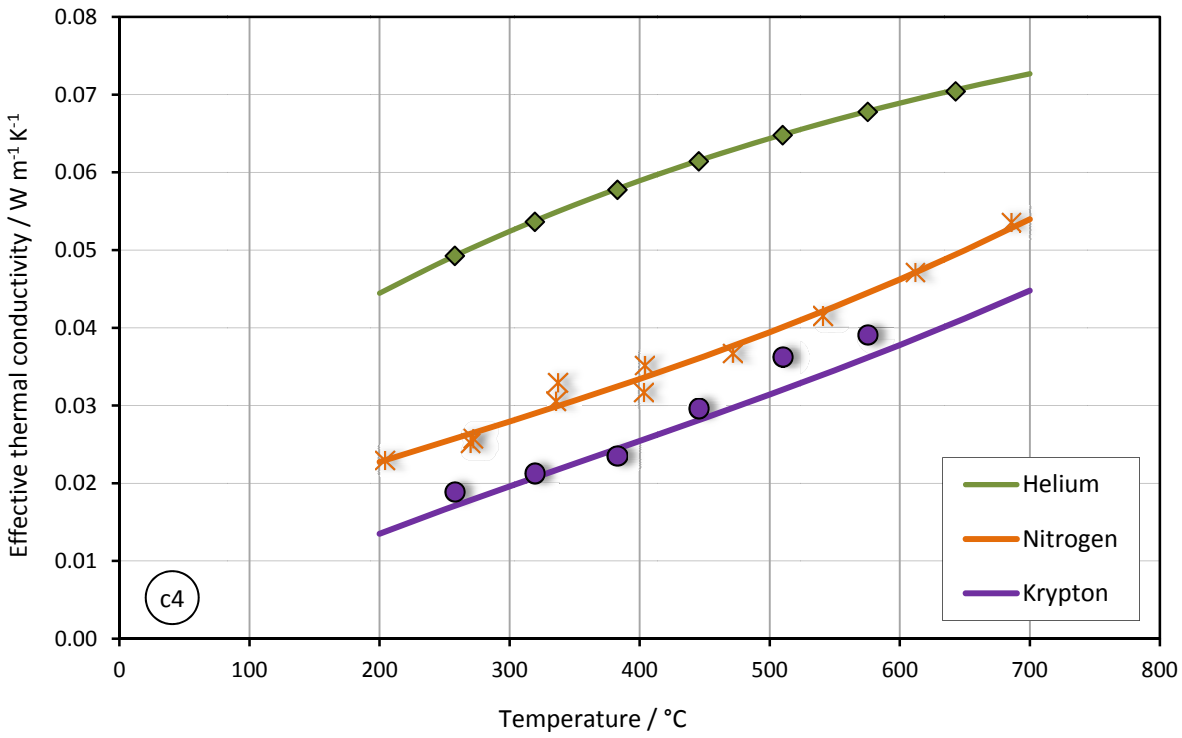
Effective thermal conductivity / W m-1 K-1
0.08
0.07
0.06
0.05
0.04
0.03
0.02
0.01
0.00
0
100
200
300
400
500
600
700
800
Temperature / °C
c4
Helium
Nitrogen
Krypton

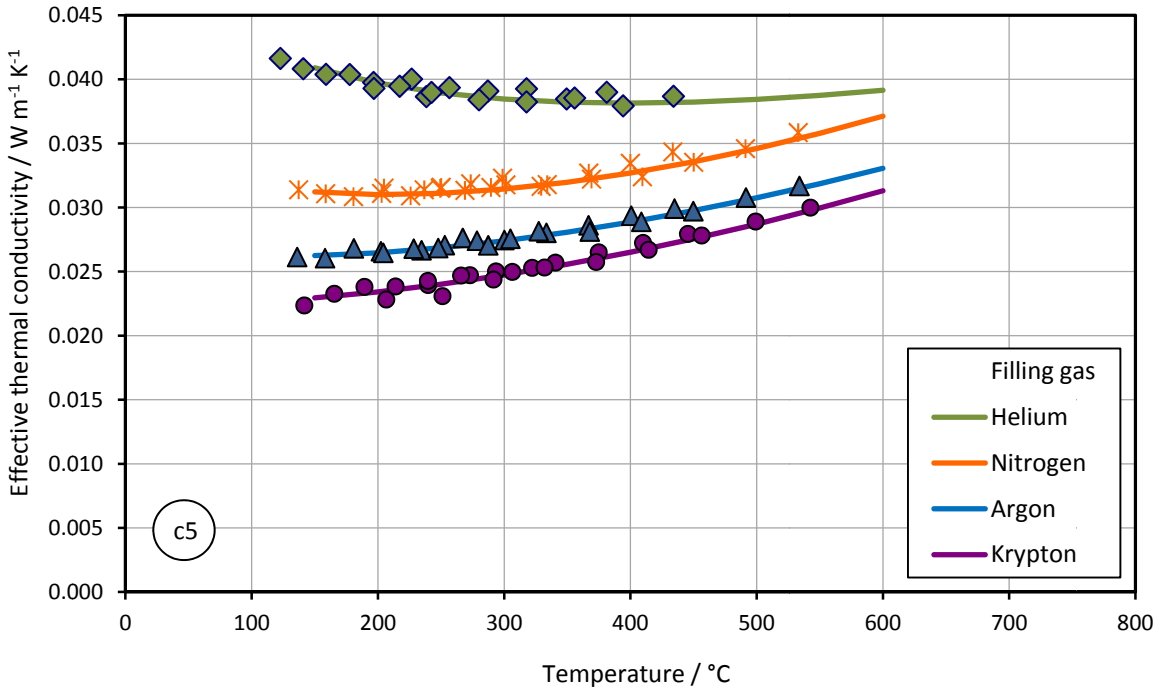
Effective thermal conductivity / W m-1 K-1
0.045
0.040
0.035
0.030
0.025
0.020
0.015
0.010
0.005
0.000
0
100
200
300
400
500
600
700
800
Temperature / °C
c5
Filling gas
Helium
Nitrogen
Argon
Krypton

APPENDIX D: REVIEW OF SOME MODELS FOR ESTIMATION OF EFFECTIVE THERMAL CONDUCTIVITY OF POROUS MEDIA

D.1. Models of Effective Thermal Conductivity with consider to Porosity as single Characteristic Parameter (no contribution of radiation)

Ref.	Model
Lower Limit (series model)	$\lambda_{eff,min} = \left(\frac{\Psi}{\lambda_{gas}} + \frac{(1-\Psi)}{\lambda_s}\right)^{-1}$
Upper Limit (parallel model)	$\lambda_{eff,max=} \Psi.\lambda_{gas} + (1-\Psi).\lambda_S$
Eucken 1932	$\lambda_{eff} = \lambda_s \frac{1 + 2\,\Psi \frac{1-\lambda_s/\lambda_{gas}}{1+2\cdot\lambda_s/\lambda_{gas}}}{1 - \Psi \frac{1-\lambda_s/\lambda_{gas}}{1+2\cdot\lambda_s/\lambda_{gas}}}$
Son Frey 1932	$\lambda_{eff} = \lambda_s \left(\frac{\left(1-\Psi^{1/3}+\Psi\right) + \lambda_s/\lambda_{gas}\left(\Psi^{1/3}-\Psi\right)}{(1-\Psi^{1/3}) + \lambda_s/\lambda_{gas}(\Psi^{1/3})}\right)$
Russell 1935	$\lambda_{eff} = \lambda_s \left(\frac{\Psi^{2/3} + \lambda_s/\lambda_{gas}\left(1-\Psi^{2/3}\right)}{\Psi^{2/3} - \Psi + \lambda_s/\lambda_{gas}(1-\Psi^{2/3}+\Psi)}\right)$
Maxwell 1954	$\lambda_{eff} = \lambda_s \left(\frac{\lambda_{gas} + 2\lambda_s - 2\Psi\left(\lambda_s - \lambda_{gas}\right)}{\lambda_{gas} + 2\lambda_s + \Psi\left(\lambda_s - \lambda_{gas}\right)}\right)$
Traustel et al. 1961	$\frac{\lambda_{eff}}{\lambda_S} = 1 - \Psi\left(1 - \frac{\lambda_{gas}}{\lambda_S}\right)\left[1 + 0.35(1-\Psi)\left(1 - 1.08\frac{\lambda_{gas}}{\lambda_S}\right)\right]$
Fritz /Kirchner 1973	$\lambda_{eff} = \lambda_S \left(\frac{2}{3}(1-\Psi) + \frac{\left[\Psi + \frac{1}{3}(1-\Psi)\right]^2}{\Psi\left(\lambda_S/\lambda_{gas}\right) + \frac{1}{3}(1-\Psi)}\right)$
Koglin 1967	$\lambda_{eff} = \Psi\,\lambda_{gas} + \frac{2}{3}\,(1-\Psi)\lambda_S$
Lichtenecker 1924	$\lambda_{eff} = \lambda_{gas}^{\Psi}\,\lambda_S^{(1-\Psi)}$

D.2. Models of Effective Thermal Conductivity with Consider to the Distribution of Solid\Gas Phases (no contribution of radiation)

Ref.	Model	Feature
Krischer 1956	$\lambda_{eff} = -\frac{\lambda_{gas}\,\lambda_S\left[\Psi\lambda_{gas} + (1-\Psi)\lambda_S\right]}{a\,\Psi(\Psi-1)\left(\lambda_{gas}-\lambda_S\right)^2 - \lambda_{gas}\,\lambda_S}$	(a) direction factor that represents the kind of distribution between series and parallel arrangements
Singh 2004	$\lambda_{eff} = \lambda_{\parallel}^{K}\,\lambda_{\perp}^{(1-K)}$ $K = \frac{\ln\left[\Psi\frac{\lambda_{eff}}{\lambda_{gas}} + (1-\Psi)\frac{\lambda_{eff}}{\lambda_{gas}}\right]}{\ln\left[1+\Psi(1-\Psi)\left(\frac{\lambda_{gas}}{\lambda_S}+\frac{\lambda_S}{\lambda_{gas}}-2\right)\right]}$	Estimation of (*K)* through experimental results
Harper/Sahrigi 1964	$\lambda_{eff} = \left(a_s + f_1 a_{s-gas} l_s\right)\lambda_S + \left(a_{gas} + f_2 a_{s-gas} l_G\right)\lambda_G + \frac{f_3 a_{s-gas}}{\frac{l_s}{\lambda_S}+\frac{l_{gas}}{\lambda_{gas}}}$	$f_{1,2,3}$ empirics factors, $a_{s-gas}, a_s,$ a_{gas}, l_s, L_{gas} are geometric parameters
Stark/Fricke 1993	$\lambda_{eff} = \lambda_S\left[1 - \frac{1-\lambda_{gas}/\lambda_S}{1+\frac{(1-\Psi)}{\Psi}\left(1+Z_f\frac{(\lambda_{gas}/\lambda_S)-1}{(\lambda_{gas}/\lambda_S)+1}\right)}\right]$	Z_f , fiber alignment factor
Jefferson et al. 1958	$\lambda_{eff} = \lambda_s\left(1-\frac{\pi}{4(1+2S)^2}\right) + \frac{\pi}{4(1+2S)^2}\left(\frac{(0{,}5+S)\lambda_H\lambda_S}{0{,}5\lambda_S + S\cdot\lambda_H}\right)$ $\lambda_H = \lambda_S\lambda_{gas}\left(\frac{2\lambda_{gas}}{\left(\lambda_{gas}-\lambda_S\right)^2}\ln\left(\frac{\lambda_{gas}}{\lambda_S}\right) - \frac{2}{\left(\lambda_{gas}-\lambda_S\right)}\right)$ $S = 0.403\cdot\Psi^{-1/3} - 0.500$	
Chaurasia/ Chaudhary/ Bhandari 1978	$\lambda_{eff} = (d\cdot\lambda_G + b\cdot\lambda_S)^n\left(\frac{\lambda_G\lambda_S}{c\cdot\lambda_S + a\cdot\lambda_G}\right)^{1-n}$	(a, d, b, c) are model elements; (n) weighting factor

D.3. Models of Effective Thermal Conductivity with Consider to the Contribution of Radiation (λ_{rad})

Ref.	Model
Verschoor et al. (1952)	$\lambda_{eff} = \frac{\lambda_{gas} + \lambda_{conv} + \lambda_{rad}}{\Psi} + \lambda_s$
Bolt 1986	$\lambda_{eff} = \left(\left(1 - \Psi^{2/3}\right)\lambda_S + \frac{\Psi^{2/3}}{\frac{(1-\Psi^{1/3})}{\lambda_S} + \frac{\Psi^{1/3}}{\lambda_{gas} + \lambda_{rad}}} \right) e^{\left(\Psi L\left(1-\Psi^{1/3}\right)\right)}$
Rath et al. 1990	$\lambda_{eff} = (1-\Psi)^2 . \lambda_{solid} + \Psi . (2-\Psi) . \left(\lambda_{gas} - \lambda_{rad}\right)$
Litovsky/ Shapiro 1996	$\lambda_{eff} = \lambda_s . M(1-\Psi)^{3/2} + \lambda_{gas}\Psi^{1/4} + \lambda_{conv} + \lambda_{rad}$

APPENDIX E: PUBLICATIONS RELATED TO THIS RESEARCH

K. Raed, U. Gross
New Guarded Hot Plate Facility for Temperatures up to 1000 °C and Pressures from 10^{-8} to 10^{+2} bar
31th Int. Thermal Conductivity Conference &
19th Int. Thermal Expansion Symposium, June 26–30, 2011, Saguenay, Quebec, Canada

K. Raed, U. Gross
Application of Laser-Flash Method to Porous Media – Problems and Challenges
31th Int. Thermal Conductivity Conf. & 19th Int. Thermal Expansion Symposium, June 26–30, 2011, Saguenay, Quebec, Canada

U. Gross, K. Raed
Study on the Effective Thermal Conductivity of Macro, Micro and Nano Porous Materials in the Light of Knudsen Conduction/ Radiation Coupling Effect
Proc. of Int. Heat Transfer Conf., IHTC14, August 8-13, 2010, Washington, DC, USA

K. Raed, U. Gross
Modeling of Influence of Gas-Atmosphere and Pore Size Distribution on the Effective Thermal Conductivity of Knudsen and non-Knudsen Porous Materials
Int. J. Thermophysics 30 (2009) 4, 1343-1356

K. Raed, U. Gross
Review on Gas Thermal Conductivity in Porous Materials and Knudsen Effect. Thermal Conductivity 29, DEStech Publ., Lancester, Pennsylvania, USA, ISBN No. 978-1-932078-72-5, 2008, 357-373

K. Raed, G. Barth, R. Wulf, U. Gross
Gas Atmosphere and Pore Size Distribution Effects on the Effective Thermal Conductivity of Nano-Scaled Insulations. Proceeding of 17th Europe an Conference on Thermophysical Properties, September 5th to 8th 2005, Bratislava, Slovakia